Bioprocess Intensification: A Study of Rotating Packed Bed Porous Mesh Impellers for Enhancement of Aerobic Fermentation Processes

Craig D Cartwright BSc (Hons)

Thesis submitted for the Degree of Doctor of Philosophy, Faculty of SAGE, Newcastle University, Newcastle upon Tyne

January 2011

School of Chemical Engineering and Advanced Materials
Newcastle University

Newcastle upon Tyne

NE1 7RU

Contents

Abstract

Oxygen transfer can be a rate limiting factor in aerobic fermentation systems. If oxygen concentration becomes insufficient productivity will decrease and the culture will ultimately die. Novel reactor technology such as the Rotating Packed Bed Reactor (RPB) may overcome this traditional limitation. The exploitation of high centripetal forces and highly porous packing material in the RPB in gas-liquid processes is proposed to enhance oxygen transfer by production of fine bubbles. The aim of the enhancement is to ensure that the Dissolved Oxygen (DO) concentration exceeds the demand of the microbial culture utilised.

The purpose of the thesis is the development and characterisation of a new HiGEE Bioreactor (HBR) for application to fermentation systems. The work was undertaken in three stages. Initial experiments focused on the mass transfer characterisation of several porous packings intended for use in the HBR. The performance of the packings was evaluated by measuring their oxygen transfer capability, power input and air bubble size produced when employed as impellers in a conventional gas-liquid stirred tank reactor (STR). It was observed that the 11 cm stainless steel Knitted Wire mesh impeller (at a fixed airflow rate of 1.0 vvm, and agitation rate of 400 rpm) produced a K_La value of 0.0312 s^{-1} compared to K_La of 0.0334 s^{-1} for the double Rushton turbine at an agitation rate of 1000 rpm and aeration rate of 1.0 vvm but with a significant decrease of about 7000 W m^{-3} in power. Similarly in the bubble experiments performed, the 11 cm knitted wire impeller could produce bubble diameters as low as 0.15 cm compared to 0.28 cm for the Rushton impeller. Two fermentation systems studied (oxygen transfer optimisation with *Escherichia coli* K12, and product optimisation with *Pseudomonas putida* KT2442) further demonstrated that the knitted wire mesh packing could produce a higher biomass concentration due to the enhanced oxygen transfer rate.

In the final set of experiments a new HBR was designed and commissioned. A set of hydrodynamic experiments focused on the flooding conditions and bubble sizes produced within the reactor. For both experiments the packing had a profound influence on the results, producing a very fine bubble diameter of 0.361 mm at 1200 rpm with packing compared to 2.50 mm at 1200 rpm without packing whilst also allowing higher throughputs of liquid and gas before flooding occurred. A series of transfer studies also illustrated the effect of packing, with a K_La value of 0.0025 s^{-1} (no packing) and 0.0030 s^{-1} (with packing) achieved for an experiment at 1200 rpm. The RPB was then tested to be utilised as a bioreactor by studying the fermentation of *P.putida* KT2442 to produce polyhydroxyalkonates (PHA).

Keywords: Bioprocess Intensification; oxygen transfer; aerobic fermentation; HiGEE Bioreactor, Knitted Wire mesh packing

Acknowledgements

I would like to take the opportunity to express my sincere thanks to all those people who have given me support and guidance during my PhD. Without them this thesis would not exist!

Firstly I would like to thank my supervisory team. Firstly to my main supervisor Dr Kamelia Boodhoo who has been a very able and dedicated supervisor throughout my PhD. I would like to thank my second supervisor Dr Jarka Glassey whose sound advice and guidance has been regularly sought. I would also like to thank Prof Colin Harwood and Dr Richard Daniel from Microbiology for their help during the fermentation work conducted. Thanks also go to Dr Jerry Cooper at CPI and Drs Auxi Prieto and Marta Tortajada for their help and support during the work conducted as part of the E.U project. I would like to thank the dedicated technical support team under Mr Stewart Latimer for their able assistance at all times during the project. Especially I would like to thank Mr Brian Grover whose expertise and support led to the fabrication of the RPB reactor described in this work. I would also like to thank my friends at Newcastle University, especially to Dr Edward McCarthy, Dr Chris O'Malley, Miss Lisa Sanderson, Mr Peter Smith, Miss Claudia Troeger, and Mr Rob Worth.

Secondly I would like to thank people back home for their great support during my PhD. Without them I would not be here now. I would especially like to thank my Mam for all her support and constant reassurance, and to my friends Mr Liam Booth, Mr Craig "Crouch" Cullinan, Mr Will Gardner, and Mr Adam Shaw. I especially would like to thank Miss Helen Evans, Mr Ben Lambert, and Mr James "Smurf" Smith for their constant support, guidance and reassurance throughout my PhD.

I also extend my thanks to Mrs Alison Lambert who volunteered to proof read my thesis for spelling and grammar which was of a great assistance!

Finally my thanks go to the EPSRC for the funding of this work, as well as the EPSRC Instrument Pool for the loan of the high speed digital camera for the bubble study conducted with the new RPB reactor.

Dedication

The work in this thesis is dedicated to two people. First it is dedicated to Prof Rob Cumming from the University of Teesside who inspired me to read for my BSc (Hons) in Microbiology. Secondly it is dedicated to Mr Nick Veuger who was a good friend and colleague during my time at Newcastle University. I hope the work contained as part of this thesis honours their memory.

Nomenclature

Acronyms

DCW	Dry Cell Weight (g l^{-1})
DO	Dissolved Oxygen
CPI	Centre for Process Innovation
EU	European Union
LB	Luria-Bertani Medium
OD	Optical Density
SCEAM	School of Chemical Engineering and Advanced Materials
SMS	Spitzens Minimal Media
TVC	Total Viable Count (CFU)

Variables

a	Gas/Liquid Interface area per liquid volume (cm^2 cm^{-3})
A_b	Bubble Area (cm^2)
BF	Buoyancy Force
B_D	Bubble Diameter (cm or mm)
C_L	Dissolved Oxygen Concentration in Bulk Liquid Phase (% sat)
C*	Dissolved Oxygen Saturated Concentration (% Sat)
C_{crit}	Critical DO Concentration (% Sat)
C_S	Residual Substrate Concentration (g)
$d_{b,i}$	Initial Bubble Diameter (either cm or mm)
d_o	Bubble diameter at the orifice (either cm or mm)
G	Gas mass flowrate (kg/s)
G_{in}	Gas flowrate in (mol/s)
Gm	Gas molar flowrate (mol/s)
H	Axial height of packed bed (m)
H	Henry's constant (atm)

H_G	Average Fractional Gas Hold Up
g	Acceleration due to gravity ($\equiv 9.81$ m s^{-2})
Ja	Generic Transfer
K_L	Mass Transfer Coefficient (cm h^{-1})
k_l	Individual Cell Mass Transfer Coefficient (cm h^{-1})
k_p	Probe Sensitivity (s)
K_S	Substrate Concentration (mol.)
L	Liquid mass flowrate (kg/s)
Lm	Liquid molar flowrate (mol/s)
m	Viscosity of the fluid studied (mPa s)
m_w	Viscosity of Water (mPa s)
N_O	Original number of microbes
N_T	Number of microbes at time = t
NTU	Number of Transfer Units
OTR	Oxygen Transfer Rate (mol l^{-1} h^{-1})
OUR	Oxygen Uptake Rate for a microbial culture (mol l^{-1} h^{-1})
(P_g/V)	Power Input per Unit Reactor Volume (W m^{-3})
Q_{O_2}	Specific Respiration Rate of a microbial culture (mol l^{-1} g^{-1} h^{-1})
q_s/V	Oxygen Absorption Rate per unit volume
Re_m	Reynolds Number for Mixing
ST	Surface Tension
t	Time (either hours or seconds)
t_m	Mixing Time
U_s	Superficial air velocity (m s^{-1})
t_m	Mass Transfer Time (s^{-1})
x	Total Biomass Concentration (g)

x_O	Original Biomass Concentration (g)
x_t	Biomass Concentration at time = t (g)
V_L	Liquid Volume (m^3)
Z_F	Height of aerated liquid
Z_L	Height of unaerated liquid

Greek Letters

γ	Shear Rate (s^{-1})
σ	Surface Tension (N m^{-1})
ε_G	Gas Hold Up
ρ	Density (kg m^{-3})
ρ_L	Density of the Liquid Phase (kg m^{-3})
ρ_G	Density of the Gas Phase (kg m^{-3})
ρ_{O2}	Density of Oxygen (kg m^{-3})
τ	Probe Response
μ	Specific Growth Rate of a microbial culture (Hours $^{-1}$)
μ_{max}	Maximum Specific Growth Rate of a microbial culture (Hours^{-1})

Chapter 1: Introduction

1.1 Background

Aerobic fermentations are important biological reactions, producing many novel and important compounds such as antibiotics, therapeutic proteins and insulin (Stanbury *et al* 2000). Some products, such as polymers and other bulk chemical compounds, which are traditionally produced by synthetic chemical reactions, can be made via fermentation routes. Such biological pathways are usually more environmentally sustainable as they rely on renewable resources rather than non-renewable fossil resources. Achieving high productivity in bioprocesses is often a major challenge in comparison to the chemical processing route. This is because products are produced in low concentration in generally slow biotransformation processes which are affected by a number of operating conditions such as temperature, pH, Dissolved Oxygen (DO) concentration and substrate concentration, all of which have a significant impact on the growth of the biological culture. To ensure that maximum productivity is maintained, transfer processes and nutrients need to be provided at a sufficient level to sustain microbial growth (Madigan *et al* 2006). Traditionally aerobic fermentations tend to become rate-limited by oxygen transfer, restricting the growth of the culture. If the dissolved oxygen (DO) level in the medium is less than the microbe's requirements, this will ultimately lead to the non-viability of the culture (Stanbury *et al* 2000). Growth of a microbial culture can be further restricted by substrate limitation, accumulation of a toxic product, shear damage to cells, and at a larger scale poor mixing of the reactor contents. As competition within industry increases, combined with economic and environmental concerns, the need for bioprocess intensification to enhance oxygen transfer has become an important concern in order to eliminate mass transfer limitations and intensify production (Boodhoo *et al* 2008).

Process intensification (PI) is a philosophy of engineering, which began in the late 1970s at ICI. In its original concept devised by Ramshaw, PI goals were adopted to cut the size and capital costs for a given equipment (Ramshaw 1985). Ultimately, the goal was to dramatically reduce the capital cost of the whole plant by reducing not only the cost of process equipment but also the associated piping and civil engineering costs, which

represented a significant proportion of the total plant costs, as illustrated in Table 1.1 for a typical Penicillin plant.

Table 1.1: Capital cost breakdown for a Penicillin fermentation process (adapted from Stanbury *et al* 2000)

Item	% of Total Cost
Process Equipment	23.6
Installation	5.2
Insulation	1.9
Instruments	2.7
Piping	11.8
Electrical	15..8
Building	11.3
Utilities	21.3
Site	2.4
Laboratory Equipment	3.8
Spare Parts	0.5

In many cases, PI was achieved by the use of novel technology, enabling a reduction of costs by a factor of 10 or greater. Integration of reactor/separator into one unit allows the number of processes within a system to be cut, leading to PI As PI principles were being applied through research in the chemical industry it rapidly became apparent there were a number of additional benefits to be gained other than reducing capital costs. Benefits such as enhanced safety, improved efficiency, reduced energy consumption and decreasing environmental impact have become evident (Reay *et al* 2008). Many of these achievements were due in part to the smaller volumes and low residence time which feature as part of the novel reactor technologies developed under the PI theme. Novel reactors under investigation at Newcastle University include the Oscillatory Flow Reactor (OFR) (Troeger *et al* 2008), Rotating Packed Beds (RPB or HiGEE) (Peel 1995), Spinning Disc Reactors (SDR) (Vicevic *et al* 2007), and narrow channel reactors (McCarthy *et al* 2007). In order to be viable, P.I procedures need to be applied plant wide and not just to the reaction part of the process.

The same goals and principles as described above apply to Bioprocess Intensification, but with the aim of intensifying fermentation or other biological reactions. For the purpose of Bioprocess Intensification, enhancement of oxygen transfer in aerobic fermentations is one of the desirable objectives. An oxygen transfer rate (OTR) which exceeds the oxygen demand of the microbe allows growth at or close to the maximum specific growth rate. Any

enhancement therefore will seek to ensure that the OTR remains above the oxygen demand of the culture, regardless of the biomass concentration present. Previous research in this area has focused on the use of producing smaller bubbles, having a greater surface area for transfer to occur (Martin *et al* 2008). This has been demonstrated with novel reactor technology such as airlift columns (Chisti 2006). Further improvements have been made to the design with the addition of porous packing material (Nikakhtari *et al* 2005A).

Comparable material has also been exploited as the packing in Rotating Packed Bed (RPB) reactors, also commonly referred to as HiGEE reactors (Lin *et al* 2007). As with the airlift design, enhancement of gas-liquid transfer occurs by producing bubble sizes of less than 1 mm. The reduction of bubble size is both due to the action of the packing (acting in a similar manner to the packing in an airlift reactor) and the high gravity environment induced by the high centrifugal force applied (around 1000*g*). Both factors have been shown to significantly enhance transport processes (Wang *et al* 2008). The enhancements provided by the RPB could be exploited in aerobic fermentation systems to overcome oxygen transfer limitations, especially under conditions of high cell densities and/or highly viscous media. High cell density fermentations have an oxygen demand which quickly outstrips the transfer rate where as highly viscous fermentations suffer from decreasing oxygen solubility due to the rise in viscosity. In both scenarios, the balance between oxygen transfer and oxygen demand is crucial to the performance of the reactor. In addition the unique mixing characteristics of the reactor could potentially reduce the effects of substrate limitation providing further enhancement.

1.2 Aim and novelty of the present work

The intention of the present project is to exploit the high gravity environment and porous packing of a newly fabricated bioreactor (henceforth referred to as a HiGEE bioreactor (HBR)) in order to enhance the oxygen transfer rate in an aerobic fermentation. There appears to be limited research reported in the literature on fermentation and other biological processes in rotating packed bed type reactors (Hoffmeister 2007; Yang *et al* 1996). The latter did not, however, involve solid body rotation of the packed reactor chamber as a whole as is being proposed here but rather rotation of the packed bed within the static walls of a conventional stirred tank vessel.

The research will be carried out in a number of stages (for a detailed overview see Chapter 3), which will firstly investigate the oxygen transfer potential of the porous packing material to be used as impellers in a conventional stirred tank reactor (STR) in relation to their power consumption, followed by a study on bubble size using these impellers. Two aerobic fermentation systems will then be employed to investigate whether the packing material can support the growth of a microbial community in the STR. Mass transfer characterisation of the newly built HBR will then be studied followed by an investigation into whether the high gravity environment within the HBR packed with the aforementioned porous elements can lead to an enhancement of biomass concentration when compared to standard reactor technology available.

The current research builds upon previous work conducted by Toogood (2005) at Newcastle University whereby the oxygen transfer capability and power consumption of a set of 11 cm diameter porous mesh impellers were evaluated in a conventional stirred tank reactor (STR) and compared to a standard Rushton impeller mainly in water. The performance of a selected porous impeller (knitted wire mesh) in an *E.coli* fermentation process was also tested in a preliminary study by Ndlovu (2004). The present work intends to expand on the previously conducted studies in a number of different ways to produce a more comprehensive set of reliable data, as described in further detail in Chapter 3.

Chapter 2: Literature Review

The literature review provides the foundation and basis for the research to be undertaken. It will consider the principles of fermentation, microbial growth, and how this can be impacted by oxygen mass transfer. The review also focuses on the principles of Process Intensification (PI) and ultimately how PI techniques can be adapted for the improvement of fermentation systems.

2.1 The Development of the Modern Fermentation Process

2.1.1 Introduction

The goal of fermentation is to induce a mass culture of cells to produce commercial products. Cells used have traditionally been bacteria, fungi, or yeasts and in recent years have expanded to included mammalian or plant cells.

The word "Fermentation" originally derives from the Latin "*fervere*" which translates as "To Boil". This was based on the observation of bubbles formed by the action of yeast on fruit or malted grain. The bubbles noted are in fact CO_2 bubbles produced during anaerobic catabolism of the sugar present in the malt or grain (Stanbury *et al.* 2000). A traditional biochemical view of fermentation is one that occurs without oxygen, leading Louis Pasteur to describe the process as "La *vie sans air"* or "Life without air". Fermentation was traditionally defined as an anaerobic process for the production of lactic acid or alcohol from glucose (Lee 1992). Modern Biochemical Engineering definitions incorporate processes that use air or oxygen alongside the more traditional view of fermentation.

Currently four commercially important groups of fermentation are exploited industrially (Bailey *et al* 1987):

1. Production of Microbial Cells (e.g. Bakers yeast, Quorn)
2. Production of Microbial Enzymes (e.g. Proteases, Lipases)
3. Production of Microbial Metabolites (e.g. Ethanol, Penicillin, Citric Acid)

4. Modification of a compound added to a Fermentation (Biotransformation, e.g. Steroids)

There are a number of advantages that fermentation processes have over traditional chemical reactions which are noted as follows:

1. Mild Reaction Conditions—Fermentation processes occur at atmospheric pressure, room temperature and a pH that is fairly neutral. Operation is therefore less hazardous and as a result the manufacturing facilities are less complex compared to those for a chemical plant.

2. Specificity—Enzymes are highly selective and are able to catalyse one or a small number of chemical reactions

3. Effectiveness—The rate of an enzyme catalysed reaction is generally faster than ones controlled by a catalyst. Only a small amount of enzyme is needed.

4. Renewable Resources—Major raw material for bioprocesses are biomass providing both carbon skeleton and energy for synthesis of organic chemicals.

5. Recombinant DNA Technology—Have the potential to improve biological processes. New cell lines can be produced which can produce new products.

Products which traditionally have been difficult to generate by chemical means can be produced much more readily in some instances by fermentation. Fermentations could also provide a more environmentally friendly way of generating plastics (such as polyhydroxyalkanoates) and biofuels to replace those created from fossil fuels (Hallenbeck and Ghosh 2009).

Despite the advantages that fermentation processes offer, there are a number of disadvantages that must be considered which are as follows:

1. Complex Product Mixtures—Cell requires multiple enzyme reactions to occur in sequence or parallel, the final product mixture contains cell mass, many metabolic by-products and a remnant of the original nutrients. Cell mass contains various cell components.

2. Dilute Aqueous Environments—A number of products exploited commercially are produced in small amounts of aqueous medium making separation expensive. As a number of fermentation products are heat sensitive, traditional separation techniques cannot be employed.
3. Contamination—Fermentation system can easily become contaminated because a number of environmental microbes can grow well in most medium employed in fermenters. Problem is exacerbated in systems containing animal or plant cells where growth rates are generally slower.
4. Variability—Cells have a tendency to mutate due to the changing environment of the fermenter and therefore may lose some characteristics which are vital for that fermentation. Compared to a catalyst enzymes are quite sensitive and due to their highly selective nature must be used with care.

2.1.2 The Modern Fermentation Process

The development of the modern fermentation process is outlined in table 2.1 which begins prior to the start of the twentieth century. The vast majority of development has occurred within the last century, advances being spurned by the discovery of antibiotics and the need for mass production during the Second World War. As more sophisticated technology has become available, the number of products produced by fermentation has increased.

Table 2.1: The History of Modern Fermentation (Stanbury *et al* 2000)

Stage	Main Products	Developments
1 Pre 1900s	Alcohol, Vinegar	Pure Cultures (e.g. *Streptomyces carlsbergensis)*

		produced by Carlsberg Brewery in 1896.
2 1900-1940	Bakers yeast, Glycerol, Citric Acid, Lactic Acid, Acetone/Butanol	Enclosed STR, Air sparging, Sterilisation, Temperature Control, Fed Batch
3 1940-Present	Penicillin and antibiotics, Amino acids, Enzymes, Biotransformations	Mutation and strain selection, Mechanically agitated vessels, Aseptic conditions, pH and O2 electrodes (sterile), control loops
4 1960-Present	Single Cell Protein	Genetic Engineering, Airlift Reactors, Computer Control (control loops etc), continuous culture (e.g. chemostat),Novel Feedstock's (Hydrocarbons)
5 1979-Present	Foreign Compounds (Insulin, Human Growth Hormone, Interferon)	Insertion of new genetic material into microbial DNA, Animal and Plant Cell Cultures, Novel Reactor Designs, Sophisticated Computer Control, Novel Sensors

2.1.3 Microbial Growth Kinetics in Batch Culture

Central to the performance of a bioreactor is the growth kinetics of the microbe. General parameters exist governing microbial growth, alongside many specific requirements particular to each individual culture which must be observed. Batch fermentations are a closed culture system, containing the prerequisites necessary for growth (Stanbury *et al* 2000). Once the culture is inoculated into the reactor, several distinct growth phases are observed. After inoculation, the microbe utilises the ingredients in the medium for growth, including replication of its DNA, synthesis of new cellular material and preparation for its own replication. This growth is characterised by a distinct growth curve, shown in figure 2.1

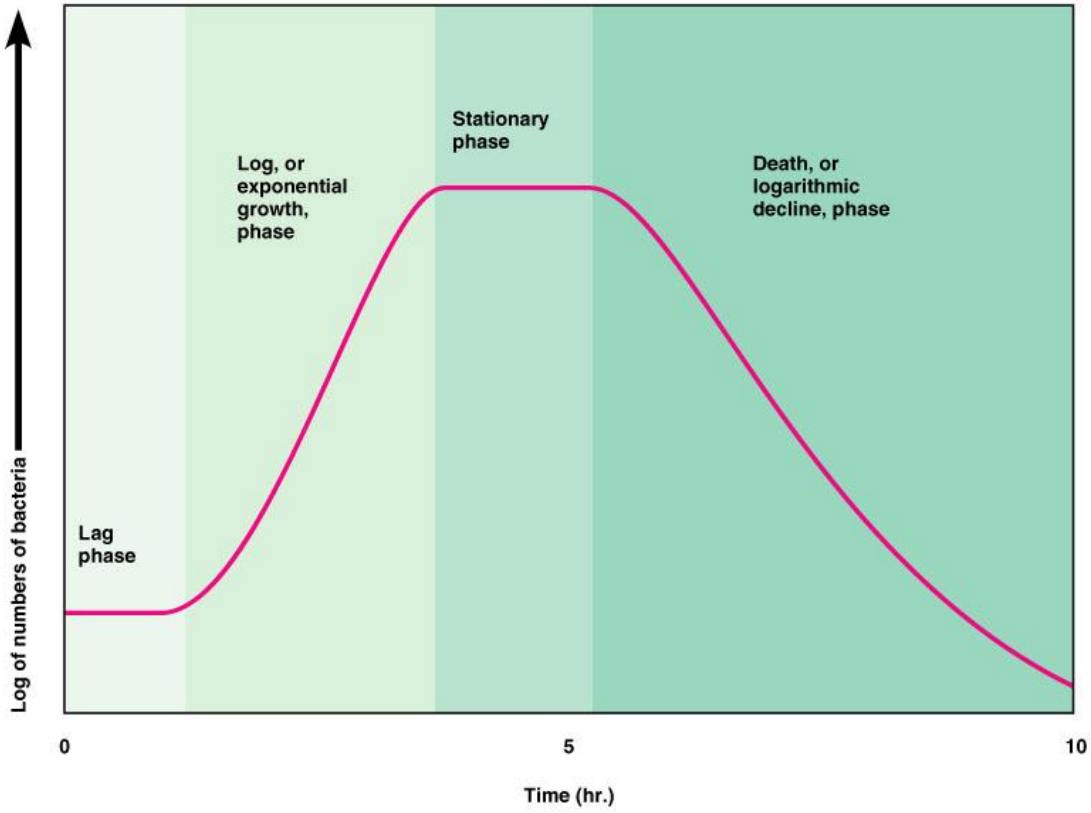

Figure 2.1: The Microbial Growth Curve for Batch Growth (Decker 2005).

The lag phase is the first growth phase during which little growth actually occurs. The length of the lag phase itself is unique to the culture and the fermentation being conducted. This phase of growth has been described as a balance between the amount of work needed to be completed by the cell to adapt to a new environment and the rate at which this is accomplished (Robinson *et al* 1998) The length of the lag phase can be shortened by the use of fresh medium and/or culture, and the use of the same medium for both the initial culturing and for the reactor phase (Nicklin 2003). The term lag phase encompasses two different types of lag; initial lag describes the initial inoculation movement (i.e. from the shake flask to the reactor) under constant environmental conditions whilst the intermediate lag arises from sudden changes in the microbe's environment (i.e. temperature, pH changes for example). Both instances see the microbe move from one environment to another and so for that reason both the initial and intermediate lag phases can be considered the same (Swinnen *et al* 2004)

Cell adaption to their new environment will include the synthesis of new enzymes whilst other enzymes are suppressed, which is dependent on the nutrients available in the culture

medium. In the lag phase cell mass can increase by a small amount, but without a corresponding increase in cell number density. Low concentration of critical nutrients will cause a longer lag time than expected. A number of lag phases may be noted if a second carbon source is present in the medium. This phenomenon is known as diauxic growth, and occurs when a second substrate is utilised after the first source has been exhausted. If glucose and lactose are present, the first lag phase will correspond with glucose uptake. Only when the glucose supply has been exhausted will lactose be used, therefore leading to a second lag phase developing. The second lag phase arises whilst new enzymes are synthesised to enable the microbe to utilise the second carbon source. Actual fermentation processes may rely on multiple carbon sources, with possible multiple lag phases occurring, as a result modelling of the system can become a challenge. Models have been developed which illustrate use of multiple carbon sources which closely follow experimental data (Doshi and Venkatesh 1998).

Mathematically, the lag phase can be modelled by extrapolating the straight line of the growth curve (i.e. the start of the exponential phase when plotted as a log scale). This produces a rough indication of the lag time for the fermentation which incorporates the acceleration of growth into the exponential stage of growth. Ginovart *et al* (2010) explored the age and size of an inoculum on the lag phase of a beer fermentation. This was performed using a computer simulation (using IDISM YEAST) to model the effect to the lag phase. The study found that the shortest lag phase was achieved with the largest amount of inoculum and youngest yeast cells available (Ginovart *et al* 2010).

Immediately after the lag phase, the exponential phase of the growth curve is reached. This phase of growth is characterised by rapid cellular growth rate and is illustrated by equation 2.1. Subsequent integration and taking natural logarithms yields equations 2.2 and 2.3. A plot of the natural logarithm of the biomass concentration (y axis) against time (x axis) generates a straight line graph with a gradient equal to the specific growth rate (μ).

$$\frac{dx}{dt} = \mu x \qquad (2.1)$$

$$x_t = x_0 e^{\mu t} \qquad (2.2)$$

$$\ln x_t = \ln x_0 + \mu t \qquad (2.3)$$

Equations 2.1-2.3 describing exponential growth predicts that this growth pattern will continue indefinitely. This assumption is made on the basis that nutrients will always be available in the system to fuel this growth. In reality this is not the case, as the culture grows the nutrients present are consumed. Therefore after a certain length of the time, the rate of growth slows until growth ceases. The cessation of growth can be due to depletion of a critical nutrient (substrate limitation) or by the accumulation of an autotoxic product (toxic limitation). The effect of substrate limitation on the overall growth rate can be expressed by the relationship between μ and the residual growth limiting substrate as in equation 2.4 and figure 2.2 (Nielsen 2006; Doran 1999). Both equation 2.4 and figure 2.2 are expressions of the Monod model of microbial growth kinetics which is quintessentially the same as the Michaelis-Menten model for enzyme kinetics.

$$m = m_{\max} \frac{c_s}{K_s + c_s} \qquad (2.4)$$

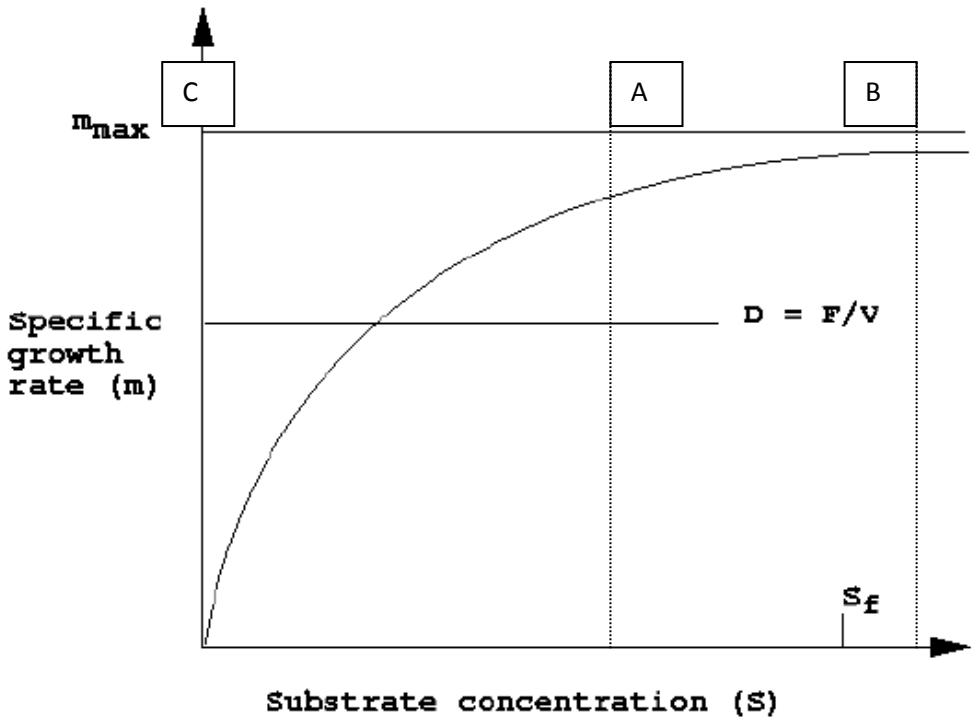

Figure 2.2: Effect of residual limiting substrate concentration on the specific growth rate of a bacterial population described by the Monod Model (Adapted from Doran 1999)

Section A-B in figure 2.2 is equivalent to the exponential section of growth in figure 2.1, section C-A corresponds to the deceleration phase of microbial growth. This is when the growth of the microbial culture has resulted in the depletion of the substrate to a concentration which can no longer sustain the cultures growth. If the microbial culture has a low K_S value (a high affinity for the limiting substrate), growth is not affected until the substrate is very low in concentration, and the deceleration phase for such growth is usually quite short. Conversely if the K_S value is high (low affinity for the limiting substrate) growth is affected at a higher level of substrate concentration; therefore the deceleration phase will be longer (Lee *et al* 1999). The highest biomass concentration occurs towards the end of the exponential phase; consumption of the substrate occurs rapidly at this stage.

In order for the cessation of growth to be taken into account, equation 2.1 can be modified with an inhibition term. This then correctly predicts the entry into the stationary phase and is presented in equation 2.5. The assumption is that inhibition to growth is proportional to the concentration of the culture squared. Equation 2.6 (the logistic equation) is yielded by integration of equation 2.5. Plotting of x against t yields a sigmoidal curve as shown in figure 2.3. At low values of t, the curve is almost exponential with the sigmoidal shape becoming more prominent as the value of t increases.

$$\frac{dx}{dt} = kx - k\gamma x^2 \qquad (2.5)$$

$$x = \frac{x_0 e^{kt}}{1 - \gamma x_0 (1 - e^{kt})} \qquad (2.6)$$

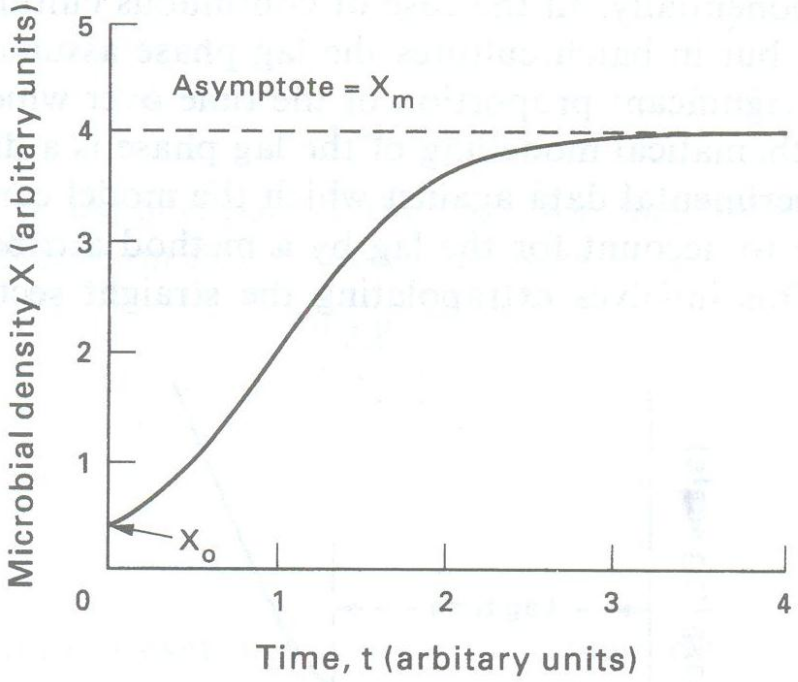

Figure 2.3: Logisitic Equation (Richardson *et al* 2005)

For fed-batch fermentation systems, the exponetial phase of growth can be controlled by addition of substrate using computer control. Lee *et al* (1999) explored the control of the exponetial phase in different fermentation systems using fuzzy logic or neural networks. The authors found that the advanced control systems held a great deal of promise for control of the exponential phase in complicated fermentation systems (Lee J *et al* 1999). Although adding substrate to control the exponential phase is desirable, it needs to be carefully balanced against any catabolite repression that may occur in the system.

Deceleration of growth immediately follows exponential growth, which can be due to the depletion of a critical nutrient (known as substrate inhibition) or a toxic product (toxic inhibition). In the case of *E.coli* growth can be inhibited by production of acetone when glucose is present in excess, which is known as the Crabtree effect (Luli and Strohl 1990). For any prokaryote the onset of inhibition is swift, resulting in unbalanced growth. The cell restructures itself following onset of inhibition allowing it to survive in a hostile environment. Molecular mechanisms lead to repression of growth in preparation for the stationary phase. A study by Merico *et al* (2003) studied the Crabtree effect with the yeast *Zygosaccharomyces bailii*. The authors noted that the effect is strongly linked to the carbon source utilised by the yeast so that when fructose was present in limiting conditions a larger amount of ethanol was produced compared to when glucose was present in limiting conditions (Merico *et al* 2003).

Once the growth rate has declined to zero, the culture enters what is defined as the stationary phase. The culture exists in a dynamic equilibrium whereby the death of a microbial cell releases nutrients to allow new cells to grow. During this period although net growth is zero, cells are metabolically active and produce secondary metabolites. When the number of cells dying start to exceed the new cells being produced, the culture is said to be dying. The number of viable cells drops considerably.

The importance of the stationary phase in microbial growth was noted by Manginot *et al.* (1998) during a study with different industrial yeast strains. In part of the experiment during the stationary phase different nitrogen feeding strategies were employed to investigate the yeasts behaviour during the stationary growth phase. It was noted that differences between different strains of yeast required different amounts of nitrogen feeding but this did not become apparent until the stationary phase was reached (Manginot *et al.* 1998). During the production of polyhydroxyalkanoates (PHA) the stationary phase is an important part of the growth cycle as if there is insufficient substrate in the system then the PHA (which is used as a carbon store) will be utilised for growth by the microbe (Tortajada *et al* 2008).

Amongst the various models exist that describe microbial growth, the Monod model provides a robust description of the growth cycle. The model is however unable to predict the lag phase in its basic form (equation 2.4). equation 2.7 is the modified version of equation 2.4 which takes the lag phase into account.

$$\mu = \mu_m \frac{S}{Ks + S} - \kappa_d \qquad (2.7)$$

For growth under batch conditions, k_d has little effect on biomass formation when the growth rate of the cells is high and therefore the basic form of the Monod model, as expressed in equation 2.4, is sufficient to describe growth (Richardson *et al* 2006) For continuous growth conditions, k_d becomes important when nutrient levels are low and so the model proposed in equation 2.7 is used.

2.1.4 Factors affecting microbial growth

A number of physio-chemical factors have a profound impact upon microbial growth. Different microbes react differently to changes which occur in their environment, so that conditions in which one microbial species may flourish can at the same time be detrimental to another microbial. A few of the different environmental factors which can effect microbial growth are further explored below.

2.1.4.1 Effect of pH

A great number of microbial cultures have an optimum pH of 6-7. Some archea and bacteria live in more extreme environments in which their optimum pH is either highly acidic or alkaline. The specific growth rate of a microbe is affected by pH in much the same way as product inhibition effects growth rate. Figure 2.4 illustrates the effect of pH on the specific growth rate of a typical microbe (growing at neutral pH).

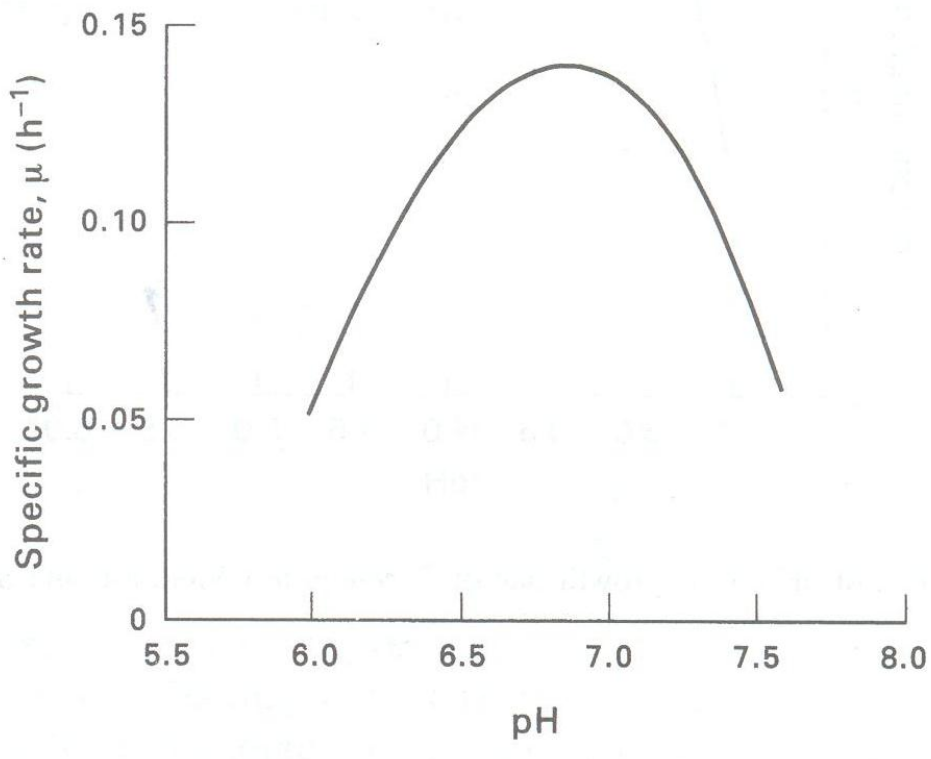

Figure 2.4: The effect of pH of the specific growth rate of a bacterial culture (Richardson *et al* 2006)

Most microbial species have very well defined range of pH. Given that pH is determined from the log of the hydrogen ion concentration (or H_30^+) any small change in pH has a profound effect on microbial growth. Acidophiles have an optimum pH of around 1-5.5, of which fungi tend to be more tolerant to acidic conditions than bacteria (Nicklin 2003). They accomplish this by having a mechanism which excludes proteins allowing the internal pH to stay at a higher level than its outside environment.

The ranges of pH described above apply only to the external pH of the environment the microbe is a part of. The internal pH must remain near neutral to ensure that certain macro molecules are not destroyed by either extreme low or high pH levels.

2.1.4.2 Effect of Temperature

There is a large variation in the optimum and tolerance to different temperature ranges between different microbial species. Three broad categories have been defined (Madigan *et al* 2009):

Psychrophiles—Temperature optimum of below 20 ^oC. These bacteria can be killed at room temperature. They can function at low temperatures as their membranes hold a high proportion of unsaturated fatty acids. These fatty acids hold their fluidity together at a much lower temperature

- Mesophiles—Temperature optimum of 20-45 ^oC. This includes stenophiles (microbes which grow at a temperature range of about 30 ^oC)
- Thermophiles—Temperature optimum of above 45 ^oC. Only certain species are true thermophiles, known as hyper-thermophiles these microbes can grow at temperatures of over 100 ^oC

The rate at which chemical reactions occurs increases with increasing temperature (Postgate 2000). A temperature increase of 10 ^oC in some instances doubles the rate of reaction (Shuler *et al* 2002). As a result of this rate increase cell growth will become faster. There is a limit to how fast cells can divide and also several compounds have temperature limits under which they perform (such as proteins, lipids and nucleic acids). If the temperature exceeds their maximum tolerance, they will be permanently denatured and therefore will be rendered non viable. Conversely there is also a lower limit to temperature, if the molecule is brought below

this point it will not be fluidic enough to function properly. For bacterial strains that can produce spores, these are generally able to withstand higher/lower temperatures in a spore form than when the bacteria are present in its viable form.

2.1.4.3 Osmotic Effect (Water Activity)

Water activity (a_w) is defined as the ratio of the vapour pressure of pure water to the vapour pressure of water surrounding the microbe. It is in essence a measure of the availability of water in an environment, expressed in equation 2.8

$$a_w = \frac{P_{soln}}{P_{water}} \qquad (2.8)$$

The water activity in a microbe ranges from 0-1, water activity is lowered as the amount of solutes in a mixture increase. In a similar manner to the effect of temperature, microbes vary a great deal in their tolerance to dry or high osmotic strength environments. If a microbial cell (composed of rigid cell walls) is placed in an environment with hypotonic conditions, the cells will rapidly take up water to restore the osmotic balance. These cells then become turgid. If a cell without such a wall structure attempts the same procedure, the cell wall will swell, ultimately killing the microbe when the walls burst due to the excess water (Madigan *et al* 2009). Such microbes therefore have a problem with uptake and retention of water in dry or hypertonic environments. Although by definition hypertonic environments contain a large amount of water, this may not always be available to the microbe. In some cases due to the lack of water being available and the high level of solutes present, water can flow in the opposite direction (i.e. from the cell to the outside environment) in effect halting growth. A microbe's water activity can therefore be used to determine if a microbe can survive in the environment it currently inhabits. Only a few bacteria can survive in an environment with a water activity of less than 0.9. This provides excellent conditions in which food can be preserved free from microbial contamination.

Lin *et al* (1991) investigated the a_w value and the effect this had on ethanol production during a fermentation with the yeast *Zymomonas mobilis*. It was noted by the authors that decreasing the a_w value (in other words increasing the osmolality of the fermentation broth) caused a drop in cell numbers and ethanol production. Eventually the decrease in the a_w value reached

a point where cell growth and production of ethanol became severely limited. Similar results were obtained for cells that were either free or immobilised (Lin *et al* 1991).

2.1.4.4 Effect of Oxygen

Microbes vary in their requirements (or lack) of oxygen during their growth. There are four broad groups to which microbes tolerate oxygen

1. Aerobes: Can grow at full oxygen tolerance, some can tolerate higher (greater than 21 %) levels of oxygen. Oxygen is used as the terminal electron acceptor.
2. Microaerophiles: Grow with the need for some oxygen to enable the biosynthesis of several important compounds. They can not target at normal oxygen concentrations, having levels of around 2-10 % (v/v)
3. Facultative organisms: Can grow with or without the need for oxygen given the appropriate medium and culturing conditions. For some facultative organisms growth is more efficient in the presence of oxygen.
4. Anaerobes: Organisms which lack a respiratory system and therefore can not use oxygen as the terminal electron acceptor. Aerotolerant anaerobes grow without the need for oxygen but survive if oxygen is present where as obligate anaerobes can not tolerate any oxygen present.

2.1.4.5 Effect of Radiation

Visible and ultra violet (UV) radiation potentially can damage a microbial cell (including the blue and more violet parts of visible light). UV radiation is most harmful when encountered at around 260 nm causing damage to microbial DNA particularly the thymine dimmers (Madigan *et al* 2009). Other damage caused may be the production of singlet oxygen which is known to be a powerful oxidising agent. This can cause significant damage to many cellular components, and it some cases will lead to the death of the microbe.

Some bacteria may have defences against radiation damage. In particular *Saccharomyces cerevisiae* and *E.coli* have methods which can be utilised to repair their DNA if it becomes damaged or mutated (Stanbury *et al* 2000). Studies have also shown that anaerobic bacteria and those that can survive without oxygen are less prone to radiation damage. The reason for this is believed to be due to reducing agents and other compounds produced during anaerobic respiration which effectively shields the microbe from harm.

2.1.5 Determination of Biomass Concentration

The kinetics and stoichiometry of a microbial culture can be calculated by knowing the cell concentration that exists in the system. Although direct and indirect methods are available, direct methods are often not appropriate because of suspended solids present.

In a biological system growth is described as the orderly increase of all chemical components. Increase of mass in reality may not adequately reflect growth as the microbe may be increasing their content of storage products such as glycogen. Balanced growth is therefore defined as the doubling of the biomass which is accompanied by the doubling of all the other measurable properties of the microbial population such as protein, DNA and so on. Balanced growth is concerned with the growth of a culture whose growth maintains a constant chemical composition. The number of cells in a population can be measured under a microscope using a special chamber. For microbial cells the following are desirable features of direct counting methods are:

1. Minimum equipment required
2. Results rapidly obtained
3. Morphological characteristics of the microbe are observable.

Despite these advantages there are also disadvantages to this approach which are as follows:

1. Non-viable cells are not distinguishable from viable cells
2. For low cell numbers the method is not practical
3. Small cells can be missed as they are hard to spot under the microscope.
4. Method not suitable for highly flocculating cells

One set of methods focuses on establishing cell number, often by using a Pertroff-Hausser slide (Lee *et al* 1992). The slide has a grid which has been calibrated which is then used to count the number of cells in a sample which has been placed in the culture chamber. The cells are counted using microscopy and to ensure accuracy usually around 20 grids are counted. If a count between live and dead cells is wanted, a stain will need to be applied which makes this distinction. Total Viable Count (TVC) method can be used to count live cells only. In this procedure a known amount of sample is diluted via serial dilution series (using a buffer to

prevent growth) and placed onto an agar plate which is then incubated at an appropriate temperature/time (Kennedy *et al* 1992). Once ready any colonies that have grown on the plate represent the number of viable organisms at the time the sample was taken. These are then counted and back calculated to denote the number of colonies viable in the original sample. The unit used to report the result is 'x' CFU (CFU = colony forming units). For the method to be statistically reliable, a number of cells need to be counted, around 30-300 is the norm (Madigan *et al* 2009). One of the major disadvantages for the method is the time needed to obtain a result, which can be a day or more. The time will depend on the medium and/or the culture used.

A second set of methods calculates cell concentration rather than number, which can again be divided into direct and indirect methods. One direct method involves the calculation of the microbe's dry cell weight (DCW), but is only appropriate in a medium free from any other solids. Different variations exist for this method, the basics are that a sample of the desired culture is spun down in a centrifuge, and dried in an oven until constant weight has been achieved (Hashemi *et al* 2011). In some cases the sample is placed in a pre-weighed eppindorf and others a pre-weighed filter paper. Either way the results are usually reported as 'x' DCWg l^{-1} (DCW = Dry Cell Weight). The downside of the method is the time needed to get the sample of a constant weight, which in a normal oven can be up to 3 days. The bacterial growth can be based on the variability of the dry cell weight if so desired (either experimentally or by modelling). This approach was utilised by Hashemi *et al* (2011) to model the growth of a *Bacillus* sp and the production of α-amylase.

Optical density (OD) is a much more rapid method of determining cell concentration (Madigan *et al* 2009, Blanch *et al* 1997). The method measures the turbidity of a sample, which the greater the microbial content the greater the turbidity. Light scatter is used to determine the turbidity of a sample, the greater the light scatter the greater the turbidity. The amount of scatter in a system can be read using a spectrophotometer, the amount of absorbed light by the culture is related to the cell density. To negate the effect of background absorption by the media, the blank sample is usually the media without the culture present. Further measures to prevent media components being detected include using a wavelength of around 600-700 nm (Doran 1999, Kennedy *et al* 1992). A calibration curve can be established using the dry cell weight and OD of the system. A number of different research

papers have noted the use of O.D. to investigate cell growth (Adsul *et* al 2011, Heinz-Kroner *et* al 1984, Kennedy *et* al 1992, Kang *et al* 2010).

2.1.6 The Fermentation Process: Upstream Processing

Upstream Processing (USP) invariably involves the selection of the strain of microbe to be used and the medium in which growth will occur. The design of the process from the initial USP to the final part of product recovery needs to be taken into account with the first stages of the USP. The microbial strain maybe a wild type which naturally produces the product of choice (such as *Pseudomonas* species producing PHA) or a recombinant strain which was foreign genetic material inserted to produce the product (such as recombinant *E.coli* strains producing insulin). Work with recombinant strains will typically involve the use of plasmids bearing the required genetic material. This plasmid will then be incorporated into the host microorganism (such as *E.coli*).

The vast majority of fermentations (including solid substrate) require liquid medium (referred to as broth) in order to grow (Blanch *et al* 1997). Broth provides the culture with all its nutritional requirements. Composition of the broth varies upon its intended application and factors such as cost, handling and safety will also contribute to the final make up. In many lab and pilot scale reactors a defined chemical medium will be used. In essence this medium is a series of dissolved salts in purified water. Each batch has the same amount of ingredients, and is usually supplemented by a carbon source and a Trace Element Solution (TES). The consistency of the medium can be guaranteed in each batch produced. For larger scale pilot plant and industrial scale reactors defined medium can become too expensive, therefore a complex medium such as Luria Bertani (LB) is utilised (Stanbury *et al* 2000). The nutrients in the medium are used by the microbe for biosynthesis, energy production, and product formation which results in the increase of microbial concentration (Shuler *et al* 2002). The carbon source is used as part of the cells biosynthesis pathway leading to reproduction and growth.

Traditionally the microbe is then grown in shaker flasks to ensure that good growth will occur in the medium chosen. It also allows for the tweaking of substrate and other nutrient levels to allow for optimum growth. This can be quite a time consuming task, especially if a number of different experiments are needed to produce a good growth curve. High throughput screening of cultures can be used to speed up this process. Work carried out at

University College London (UCL) has involved the use of a miniature stirred bioreactor, allowing a number of small scale fermentations (4-16) to be conducted in parallel (Gill *et al* 2008A). The research conducted by Gill *et al* (2008) utilised the system to conduct reproducible fermentations with both *E.coli* and *Bacillus subtillis*. The research reported both good growth of the organism and good oxygen transfer into the system. The results could then allow scale up from this to a larger lab scale fermenter (Gill *et al* 2008). Other methods of high throughput processing (such as microtitre) can be used to decrease the amount of time it takes for products to be produced and get to market (Chhatre C *et al* 2009, Zhang *et al* 2008, Duetz *et al* 2007). Once USP protocols have established growth of the organism, the main fermentation occurs. For batch systems this is as described in section 2.1.2.

2.1.7 The Fermentation Process: The Stirred Tank Reactor

Traditionally the STR design has been used, due to its high flexibility and high mass and heat transfer. The STR is a cylindrical type reactor, which has the ability to aerate and agitate the vessel. A typical STR is shown in figure 2.5. The STR is considered an idealised form of fermenter as it can serve as a design platform for other vessels and has been utilised in many different areas of research (Ford *et al* 2008, Conway *et al* 2002). The reactor can be operated on its own, or as part of a series. Due to the cost of commissioning a novel bioreactor on an industrial scale, the industry as a whole likes to modify existing designs which proves to be less costly. The STR design was first used at an industrial scale for the fermentation of penicillin (Stanbury *et al* 2000).

Control of temperature in smaller STR is achieved by use of a heating/cooling jacket. In larger scale systems internal or external loops may be used, although extra internal equipment can pose a problem for sterilisation (Madigan *et al* 2009). Aeration of the vessel is accomplished by the use of a sparger, placed at the lower end of the reactor underneath the bottom impeller. The design of the sparger is varied, some being a ring design with multiple holes, others simply being a tube with one hole. The mechanical impeller system is used to mix the system. In aerated fermentations the impeller system also ensures the rapid breakup of air bubbles in the system to ensure maximum transfer. The vast majority of STR units have baffles, which direct the flow and ensure that the system is adequately mixed (Chisti and Moo-Young 1996). Baffles are also present to prevent vortex formation occurring, which occurs due to the centrifugal forces induced by the impellers. Vortex formation usually

results in a decreased transfer rate being observed. Mixing of the system occurs via a mechanical agitation system (also known as the impellers). The liquid volume usually dictates the number of impellers required. Impellers such as the Rushton turbine design will have blades, generally 2-6 in number. A large number of STRs also have a conical base, which also aids in mixing the fluid present.

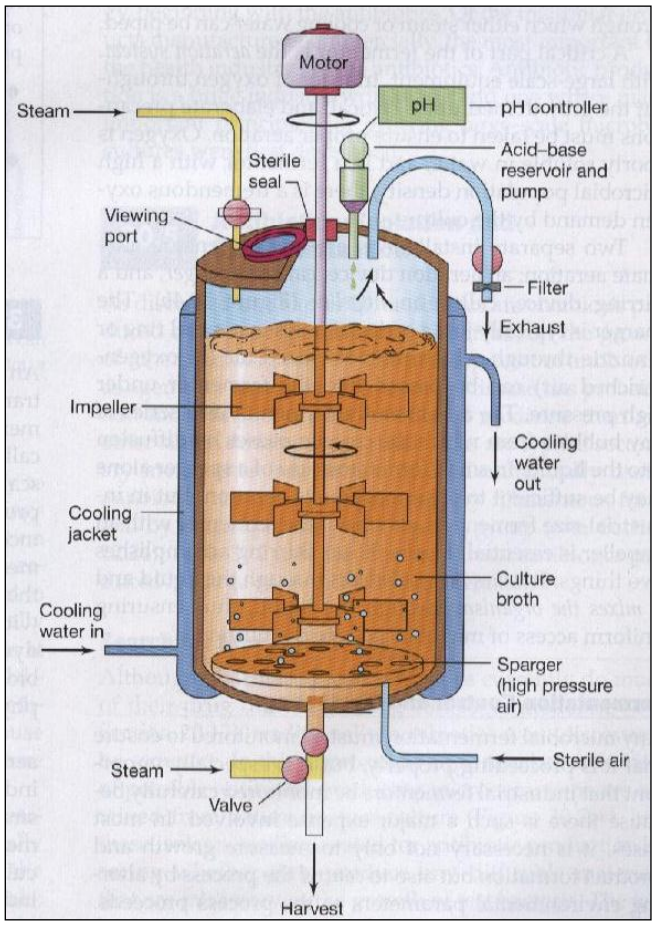

Figure 2.5: A Typical STR in use for a Fermentation System (Madigan *et al* 2006)

2.1.8 The Fermentation Process: Downstream Processing

Immediately following fermentation, purification and recovery of the product follows which is generally known as Downstream Processing (DSP). In some cases the microbe may be the product, whilst the product may be an intracellular product so that the host cell needs to be disrupted before recovery can begin (Ottens *et al* 2006). Table 2.2 illustrates some of the methods used in previous fermentations.

Table 2.2: Examples of DSP Techniques (adapted from Ottens *et al* 2006)

Process	Description	Examples
Cell Disruption	Breaking apart of cell wall to release product.	Non mechanical (small scale) examples include drying, osmotic shock, temperature shock and chemolysis. Mechanical shock (large scale) includes ultrasonic disrupters, bead mills, and homogenisers.
Clarification	Removal of cell or cell debris prior to concentration and purification of product.	Two main techniques are centrifugation and filtration. Large agglomerates can be removed by sedimentation
Concentration	Dilute product is concentration prior to purification, usually involves the removal of water. In some instances this can produce the final pure product.	Evaporation, precipitation, and ultra filtration are the main examples
Purification	Concentrated product has contaminants and impurities present which need to be removed.	For bulk products liquid-liquid extraction (with solvents such as chloroform) can be used in single or multiple stages.

It should be noted that in table 2.2 the examples in the purification section are for bulk products such as citric acid where extreme purity is not needed (Ottens *et al* 2006). Where the purification requirements of the product are extremely high (such as for intravenous pharmaceuticals) then ultrapurification will be required (Ottens *et al* 2006).

In the vast majority of instances a combination of techniques from the above table will be utilised to produce a highly pure product. As many fermentations contain a complex broth the purification steps can represent a higher cost than that to produce the product in the first place, and can account for around 50% of the total manufacturing costs (Schuler *et al* 2002). Generally as the number of DSP units rise, although the purity of the product rises, so do the costs and the amount of product when complete. For example only a few DSP units are required for citric acid production (at concentration 100 g l^{-1}) as it sells for 1-2 \$ kg^{-1}, whilst some therapeutic proteins (at concentration 0.00001 g l^{-1}) can sell for 100,000,000 \$ kg^{-1} (Schuler *et al.* 2002). It seems reasonable therefore that the number of DSP units will be higher for the protein fermentation to ensure a highly pure product is extracted.

2.1.9 The Fermentation Process: Scale Up Procedure

Once the lab scale or pilot plant fermentation has shown to be successful, scale up to pilot/industrial scale is in most cases desirable in order to produce a higher volume of product. As a rule of thumb the ratio of the height to the diameter of a fermenter (at any scale) is roughly 2:1 or 3:1 (Schuler *et al* 2002). However because this ratio is maintained, the surface area to volume ratio then decreases. The change in ratio therefore affects the absorption of oxygen into the media, and also the release of carbon dioxide from the media. For a shear sensitive culture, this has an important effect on the cultures growth because of restrictions on the agitation rate of the system. Traditional scale up tends to be a highly empirical exercise, and will work only when no change occurs in the controlling regime. For a modern fermenter that is fully agitated and controlled, practical boundaries can be applied (shown in figure 2.6). The placement of the boundary will depend on whether scale up or scale down is occurring, and also on the system studied. It should be noted that the boundaries for any given system are not clear and constant, but rather blurred and can change as the fermentation develops (Stanbury *et al* 2000).

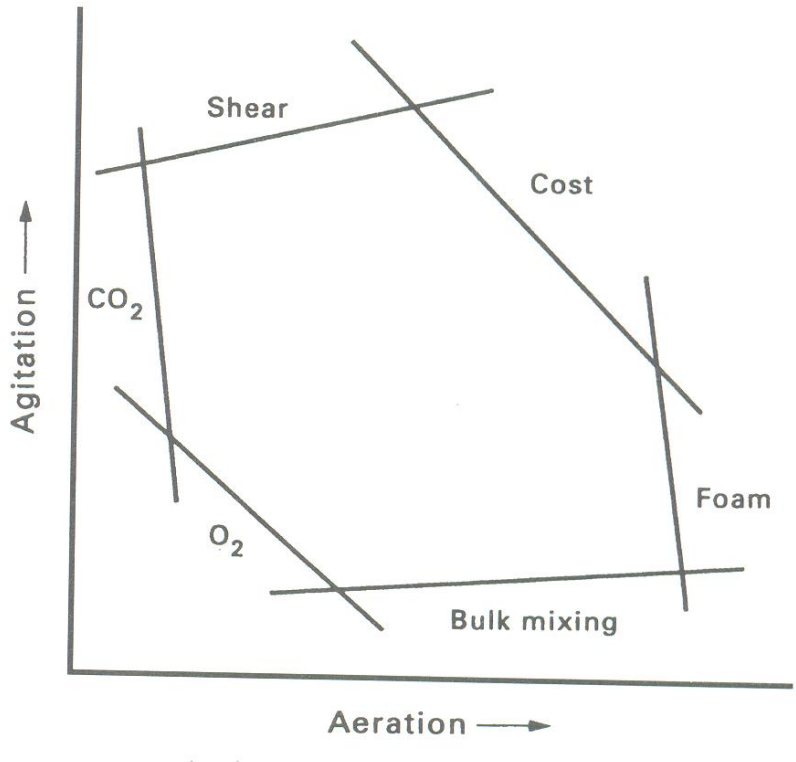

Figure 2.6: Practical Boundaries for Scale up (Stanbury *et al* 2000)

One of the major problems during scale up is that conditions in the shake flask/lab scale reactor can never be fully be duplicated at the pilot/industrial scale fully. This is the case even if the same manufacturer is used for all reactors, and that geometrically similarity is maintained (Stanbury *et al* 2000). In a large number of cases problems during scale up relate to transfer processes. Factors such as mixing time become important when considering how efficiently mixed a reactor is, and how this will be effected during scale up. When moving to a larger reactor system suddenly transfer process limitations (such as oxygen transfer) control the fermentation, where this does not occur in the smaller system. If such a change in the controlling regime occurs, then the small scale study becomes dubious when trying to model how the system when scaled up (Schuler *et al* 2002).

In larger reactors mixing becomes less efficient with size, and therefore great variability in the level of oxygen concentration will exist. This has been confirmed with placing DO probes in different locations within the reactor. This high level of heterogeneity in a reactor may mean that cells may pass into anaerobic regions, which would alter cell metabolism to

compensate for this. If this is occurring frequently, cellular metabolism may be constantly altering which leads to a drop in product formation (Schuler *et al* 2002).

Rules that are commonly encountered during scale up include constant power/volume ratio, constant tip speed of the impeller, constant K_La value, constant substrate or product level (such as DO concentration), or constant mixing time/Reynolds number (Shuler *et al* 2002) . All of these rules have been applied to different fermentation systems with different results obtained. Failure of a rule in scale up is usually due to the change of the controlling regime (as noted earlier). More advanced models are now available which predict what will happen to important factors (such as dispersion of gas, mixing time etc) upon scale up, which will provide more accurate scale up results. For example for fermenters of around 0.1-100 m^3, the mixing time can be shown to be related to the volume of the reactor by equation 2.9 (from Shuler *et al* 2002)

$$t_m = T_\kappa V^{0.3} \qquad (2.9)$$

In Equation 2.9 T_k is dependent upon the type of impeller used, the design of the vessel the impeller is in, and where the impeller is placed within it. The assumption is that multiple Rushton impellers are used, and therefore has been built upon data from multiple fermenters at different scales with different sized Rushton impellers. This may mean that the equation would not necessarily be correct if applied to fermenters where a different impeller where to be used.

2.1.10 The Fermentation Process: Scale Down Procedure

Scale down does the exact opposite of scale up, in that reactor conditions in a larger reactor are mimicked on a smaller scale (Schuler *et al* 2002). Miniature bioreactors have been used by researchers at UCL which allow for the investigation of multiple interacting variables (Gill *et al* 2008A). One of the purposes of scale down is to investigate if there any limitations on a fermentation system that is being studied. In this case far fewer raw materials are needed to complete the study, and in the case of a limitation this would be found faster at a smaller scale. As noted previously a smaller scaled down system can be used to rapidly screen proposed system changes before applying the successful version at lab/pilot scale (Schuler *et al* 2002). The idea is that the scaled down version will be able to mimic a known piece of process equipment. The smaller version of the system can then be used to estimate the

response of the system (such as microbial growth rate, biomass concentration) to changes in the composition of medium and other variables (such as substrate concentration, pH). Many scaled down reactors therefore can complement mathematical models.

Due to the size of scale down equipment, high throughput fermentation is therefore possible. The research conducted by Gill (2008B) has been previously mentioned in relation to rapid screening of strains and medium for use in USP operations. The same research is also an example of scale down fermentation equipment which can be used for rapid screening of different variables (agitation rate, oxygen transfer) (Gill *et al* 2008A).

2.1.11 Maintenance of Sterility: Reactor and Medium

Sterilisation of a fermenter prior to use is vitally important. It ensures that no unexpected microorganisms or any other contaminant are present which could alter the properties of the final product. For small scale fermenters (such as those on a lab scale) the chosen media is placed in the reactor which is then placed in an autoclave. In such an operation pressurised steam is taken to 121 ^{o}C for around 15 minutes. For larger operations (such as pilot plant and industrial scale) *in situ* sterilisation occurs. This occurs with either the media present (the two sterilised together) or the reactor and media are sterilised separately. During the procedure steam is passed through the vessel jacket, internals and also the headspace. Although cheaper than dry heat sterilisation, steam sterilisation can affect the contents of the media, as some of the ingredients (such as glucose) are sensitive to sterilisation, and therefore may need to be filter sterilised instead. The temperature of the steam and the time needed for the sterilisation is usually different to lab scale, as a more rigorous sterilisation procedure is required (i.e. longer time and higher temperature). The normal standard of sterilisation at this level is to provide a probability of microbial contamination of 0.1 %. When carrying out sterilisation if the original number of microbes are known, the Del Factor can be then calculated with use of equation 2.10 (Stanbury *et al* 2000)

$$\nabla = \ln \frac{N_O}{N_t} \qquad (2.10)$$

The Del factor relates a particular heat and temperature profile to the number of viable organisms it is able to reduce. Therefore a large Del factor will signify the greater sterilisation protocol that would be needed to be applied. For a contamination event of 0.1 %, the value of N_t will be 10^{-3}. Death of the microbial cells occurs during both the heating and

cooling phase, and the Del factor is usually expressed as the Overall Del factor which is derived from equation 2.11 (Stanbury *et al* 2000).

$$\nabla_{total} = \nabla_{heating} + \nabla_{holding} + \nabla_{cooling} \qquad (2.11)$$

If both the heating and cooling figures are known, the holding time can be correctly calculated.

2.1.12 Maintenance of Sterility: Gas Supply

For aerobic fermentations, the gas supply is usually compressed air. This without any sterilisation would carry into the sterilised vessel unwanted microbes which would contaminate the vessel and cause changes to the system. To prevent this contamination and prevent contamination by aerosols formed during fermentation, air filters are attached to both inlet and outlet ports. The filters are usually composed of either fibres (glass or mineral) are a polymer (such as PVC or PTFE). There purpose is to ensure that no unwanted microbes get across the sterile barrier by trapping and then containing any unwanted microbes in the filter. As with the rest of the fermenter the filters need to be able to withstand steam sterilisation.

Whatever the material used as the filter is important, the testing of the integrity of the filter is vitally important to ensure that no contamination occurs via the gas flow. One such test uses pressure drop versus the flow rate of the gas. In this case any defect is detected in the membrane itself. Other tests may include using an aerosol of corn oil which has been nebulised in air to a concentration of 1.0 mg/ l (air). Oil particles in the aerosol are general of the size of around 0.1-1.0 μm, and therefore should be trapped by the filter. Any droplets emerging from the sterile end of the filter can de detected by use of a photometer (Schuler *et al* 2002).

2.1.13 Aeration and Agitation

For aerobic fermentations, oxygen is a key requirement for a microbe's metabolism. The oxygen demand of a fermentation can be demonstrated by the stoichiometry of the system. This does not give the full picture, as there is no account how fast this oxygen is taken up by the cells. As oxygen is dissolved into the medium, the specific oxygen uptake rate (q_{O2}) also

increases. As the D.O level rises further, a limit is reached whereby the microbe is consuming the maximum amount of oxygen it can. At this point although the D.O level may rise further, the q_{O2} does not. This point is known as the C_{crit} level and is unique to each microbial species. This is graphically displayed in figure 2.7

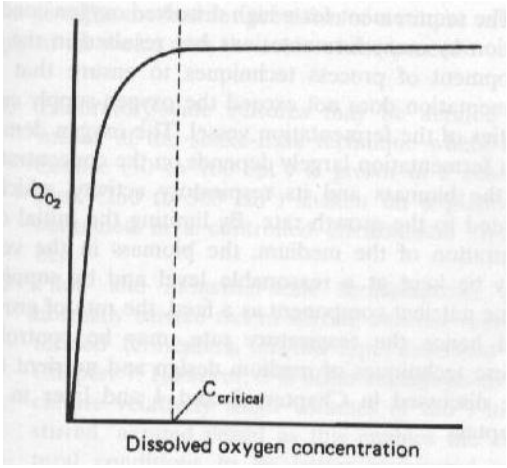

Figure 2.7: Effect of DO Concentration on the q_{O2} of a microbial culture (Schuler *et al* 2002)

Oxygen is supplied in the cheapest form available, namely air. Air is usually provided as part of a compressed air line, which is released into the reactor via a sparger type delivery system (see section 2.1.5).

Once the air has passed into the reactor, it must be fully mixed throughout the system. Traditionally in an STR design, this has been the job of a mechanical agitation system known as the impellers. The impeller system ensures the rapid break up of gas bubbles, and to that the reactor is well mixed. Apart from this they attempt to form a homogenous environment is maintained within the reactor (such as temperature and viscosity). One of the first designs, the Rushton impeller (1940s) can be used either as a single, double or triplicate impeller system (dependant on the size of the reactor). The design features a number of blades (6-8) located on the edge of the impeller, which allows fluid to be pumped in a radial manner. The impeller can also cope well with fast gas streams, not allowing flooding to occur. Flooding occurs when the impeller speed is not sufficient to disperse gas bubbles through the reactor, a central gas plume through the reactor results. This will lead to a drop in the mass transfer capability of the system. A typical example of a Rushton impeller is shown in figure 2.8

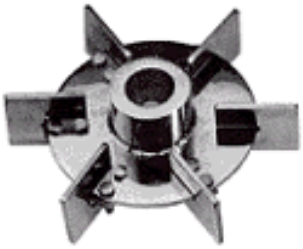

Figure 2.8: A typical 6 blade Rushton Impeller

Although the design adequately mixes the vessel and provides rapid bubble breakage, it consumes a great deal of power. In recent years different designs have evolved to lower this energy consumption for the same oxygen transfer capability. Axial impeller systems, which pump fluid in an axial manner, have been shown to produce a similar oxygen transfer to Rushton impellers whilst using less power. Some systems use a combination of both systems thereby providing mixing in two different forms. For fermentation, considerations of shear stress may need to be considered when using impellers.

Gas hold up is a useful parameter to characterise the hydrodynamics in a fermenter. The gas hold up of a fermenter depends mainly on the superficial gas velocity and the power consumption making it sensitive to the physical properties of the fluid (Ford *et al* 2008). Gas hold up can be determined by measuring the level of aerated liquid (Z_F) against that of the unaerated liquid (Z_L). Therefore the average fractional gas hold up (H_G) is given as equation 2.12

$$H_G = \frac{Z_F - Z_L}{Z_F} \qquad (2.12)$$

Calderbank (1958) correlated gas hold up for gas-liquid dispersion agitated by a flat blade disk impeller as follows in Equation 2.13:

$$H_G = \frac{V_S H}{V_t} + 2.16 \times 10^{-4}\left[\frac{(P_m/V)^{0.4}\rho_c^{0.2}}{\sigma^{0.6}}\right]\left(\frac{V_S}{V_t}\right)^{1/2} \qquad (2.13)$$

The 2.16×10^{-4} coefficient in the above equation is in metres and Vt = 0.265 m/s when the bubble size is in the range of 2-5 mm diameter.

The oxygen absorption rate per unit volume q_s/v can be estimated by Equation 2.14

$$\frac{q_s}{v} = K_L a(C^* - C_L) = k_L a(C^* - C_L) \quad (2.14)$$

Since oxygen is a sparingly soluble gas the overall mass transfer coefficient K_L is equal to the individual mass transfer coefficient k_L. The ideal design objective for a fermenter is to maximise the oxygen mass transfer rate with the minimum power consumption necessary to agitate the medium alongside the minimum airflow rate. To maximise the oxygen absorption rate k_L, a, and C^*-C_L need to be maximised. The concentration difference is usually quite limited to control because C^* is limited by its maximum solubility (which is relatively low). As a result the main parameters of interest in the design are the mass transfer coefficient and the interfacial area.

Mechanically agitated reactors (such as the STR) are very effective in the mixing of a fermenter, the suspension of microbes, break up of air bubbles (for enhanced oxygen mass transfer) and prevention of large cell aggregates forming (Ford *et al* 2008). However the shear generated by the agitator can disrupt the cell membrane and eventually kill some organisms (Middler and Fin 1966). Shear also plays a role in the deactivation of enzymes (Hooker *et al* 1988).

In the laminar flow region of a Newtonian fluid, shear stress (τ) is equal to the viscosity (μ) times the velocity gradient (du/dy) as noted in equation 2.15

$$\tau = -\mu \frac{du}{dy} \quad (2.15)$$

The μ in equation 2.15 is known as the eddy viscosity which is not only dependant on the physical property of the fluid but the operational conditions of the reactor too. As a result to estimate shear in a turbulent system (such as an agitated fermenter) it is easier to estimate shear rate (du/dy) instead of shear stress.

In an agitated system the determination of shear rate can be quite difficult due to the complicated nature of the fluid dynamics generated. A fluid element within an agitated reactor will go through a wide range of shear rates-maximum shear when it passes through

the impeller region to minimum shear when it passes close to the vessel wall. Metzner and Otto (1957) developed a general correlation which described the average shear rate generated by a flat blade disk impeller based on power measurements in Non-Newtonian liquids noted in Equation 2.16

$$(-\frac{du}{dy})_{av} = 13N \quad (2.16)$$

For $N_{Rei} < 20$

Actual shear generated by an impeller can be estimated from velocity profile data using photography hot wire or laser anemometry or a pitot tube. Bowen (1986) developed correlations for the average and maximum shear rates for the flat-blade disk turbine as shown in Equations 2.17 and 2.18

$$(-\frac{du}{dy})_{av} = 4.2N(\frac{D_I}{D_T})^{0.3}(\frac{D_W}{D_I})^{-1} \quad (2.17)$$

$$(-\frac{du}{dy})_{max} = 9.7N(\frac{D_I}{D_T})^{0.3}(\frac{D_W}{D_I})^{-1} \quad (2.18)$$

Equations above were based on data with the range of Re numbers between 14,000-110,000. The average shear rate for a typical blade arrangement (D_I/D_T = 0.33 and D_W/D_I = 0.2) is about 15N with a maximum shear rate of 35N. The equations predict that increasing the blade width will decrease the shear rate.

The equations do not however take into account trailing vortices that develop behind the blades of the impeller. The rotational vortex motion results in an additional shear field due to the differences in angular velocity. The shear stress due to this vortex can be calculated from Equation 2.19

$$\tau_{r\phi} = -\mu r \frac{dw}{dr} \quad (2.19)$$

2.1.14 Measurement and Control in Fermentation Systems

Measurement and control of a bioprocess such as fermentation would appear to be like any chemical process system. Factors such as temperature, pH are important parameters in both reactor systems. For biochemical processes, there are additional parameters such as cell

growth which need additionally to be taken into account. This can be difficult to perform on a large scale reactor online.

Measurement of a variable in any reactor is to give information on what is going on. It provides information on how close the variable is to its set point, how fast it moves away from the set point, and how the variable tends to drift round this value. Factors such as reliability, accuracy, reproducibility, response times, and cost all will play a part if choosing a sensor to measure a particular variable. Typical measurements for a fermenter will include a measure of the oxygen (dissolved oxygen by probe or mass spectrometry), mixing (usually the speed or energy consumed), temperature, pH and in some cases foam level. Measurement of these variables is usually achieved by means of a sensor which is connected to a data logger. A summary of possible sensors is given in table 2.3

Table 2.3: Sensors for monitoring and control of Fermentations (from Waites *et al* 2001)

Sensor	Physical Measurement	Chemical Measurement	Biological Measurement
Electrodes	Temperature (thermistor, resistance thermometer, thermometer)	Dissolved Oxygen, Dissolved Carbon Dioxide, Nutrients, pH, metal ions, Foam Level	Biologically active products via biosensors
Meters	Airflow Rate (In/Out), Agitation Shaft Power, Speed of agitation (Impeller Tachometer)	Acid/Alkali Addition	n/a
Transducers	Pressure, Liquid Flow	n/a	n/a
Mass Spectra	n/a	Direct on-line/off-line nutrients and in-flow and exhaust	Products

		gasses	
Spectrophotometers (on or offline)	n/a	n/a	Biomass

Sterility control in a fermenter limits the number of online probes during a fermentation cycle. This is because no matter where the probe is located in the vessel, it penetrates the sterile barrier to be able to come into contact with the inner reactor contents. Each of these breaches increases the likely hood of a foreign organism contaminating the medium. Therefore a balance must be maintained for a fermentation run between the number of parameters monitored and the increased contamination event from having further probes installed. The probes when inserted must be able to withstand steam sterilisation at high temperature and humidity (usually around 121 ^{o}C and 100 % humidity). New probes are being designed enabling a wider range of factors to be monitored online. A NIR probe could be used to provide spectroscopic data, leading to the monitoring of cell growth online. On line NMR for small scale systems could give important information on a microbe's intracellular metabolism. This could be combined with FTIR spectra analysis online which provides information on solutes with a cell.

In a small scale fermenter probe placement is not much of an issue. However as the size of the reactor increases towards industrial scale, probe placement needs to be carefully thought about. As the mixing of a vessel becomes less effective as size increases, the readings of the DO probe (and possibly pH) provides will be different dependant on where the probe is placed. Usually the middle of the reactor is thought to be where the average readings will be obtained; constraints on some systems (such as mechanical ones) will mean that probes will have to be placed elsewhere. Fouling of the probe will also dictate that the probe be placed with a sufficient turbulent region so that the probe tip is kept clean by fluid moving across it. Some probe designs will include back flushing designs which allow the probe to be kept clean, and remove microbes from the surface of the tip. The vast majority of fermentations are long residence time reactions, many lasting for several days. In this case probes used must be able to withstand continuous use for long periods without drift. As has been noted with many fermentations the quality of the information gained from the probes decreases as the fermentation time increases. Therefore the less drift a probe has, the better the quality of data

will be obtained. If online analysis is either not available or not deemed appropriate then at line or off line measurements maybe performed. Traditionally cell growth within the reactor can be monitored via spectrophotometeric measurements to give OD readings. Offline measurements of the exit gas can be analysed using a mass spectrometer, although only volatile species can be analysed.

2.1.15 Modelling of Fermentations

Modelling of a fermentation system allows its behaviour to be predicted. This is achieved by solving calculations for the factors being measured and controlled. In the process some assumptions and simplifications will be made, this will inevitably effect how reliable the model is (Mulchandani and Bassi 1995). The majority of models in use for the reactor are physical ones which will describe mass and heat transfer, mixing, and foaming. Overall simplification occurs by ignoring effects such as rheological effects (in the broth). Process control models are limited to variables which can be reliably measured on line (such as pH, D.O for example). Factors such as heat transfer are important when the design of a reactor is considered.

As oxygen transfer into aerobic fermentations is usually a major rate limiting factor, modelling of the transfer process in a reactor is key to understanding how it can be improved. The poor solubility of oxygen into a liquid medium is only one consideration, the surface area of the reactor also effects transfer. Generally as scale up of a STR occurs, the surface area decreases. Due to less surface area being present there is less surface area available for oxygen transfer to occur. Due to the majority of resistance to mass transfer occurring at the liquid film of the gas-liquid boundary layer, mass transfer can be modelled as the liquid film $K_L a$.

As discussed earlier DOis measured in the vast majority of cases by a probe. Assuming the greatest resistance to transfer is at the gas-liquid boundary layer, C* can be obtained by assumption that the liquid (within the gas-liquid interface) is in steady state with the gas phase. When using a polarographic D.O probe, Equation 2.21 is the result

$$OUR = \frac{G_{in}}{100}(\%O_2^{in} - \%O_2^{out} x \frac{\%N_2^{in}}{\%N_2^{out}}) = (K_L a)_{O_2} xVx(\frac{P_{O_2}}{H_{O_2}} - \frac{\%DO}{100} x \frac{P_2^{cal}}{H_{O_2}}) \qquad (2.21)$$

2.2 Oxygen Mass Transfer in Fermentation Systems

For aerobic fermentation systems, oxygen mass transfer is a crucial process to ensure healthy growth of the organism. If the transfer of oxygen is not fast enough from the bubbles cell growth becomes dependent upon the supply of oxygen from the gas phase (Doran 1999). Oxygen concentration tends to be higher at the surface of the air bubbles in comparison to the rest of the medium and it is this concentration gradient that promotes the transfer of oxygen from the air bubble into the fermentation medium. Oxygen mass transfer, like a large majority of mass transfer systems involves a moving fluid (in turbulent flow), in which mass transfer occurs via molecular motion (supplemented by convective transfer). This section of the literature review considers how oxygen is moved by these processes from the air bubble to the microbe.

In order to travel from the air bubble to the microbe, oxygen molecules must overcome a series of transport limitations which are illustrated in figure 2.10. The limitations arise from a combination of the following resistances to the transfer process, summarised as follows (Bailey *et al* 1987):

1. Diffusion from the bulk gas to the gas-liquid interface
2. Movement across the gas-liquid interface
3. Diffusion of the solute through the stagnant liquid region (adjacent to the bubble in the well mixed bulk fluid)
4. Movement/transport of the solute through the bulk liquid to a second relatively unmixed layer of liquid surrounding the microbial cells
5. Transport through this layer of fluid into the microbial cell
6. Diffusion through the solid to the individual cell (if the cells are in a floc, clump or solid particle)
7. Transport through the cytoplasm to the intracellular reaction site.

If oxygen mass transfer is occurring to individual microbial cells then the sixth resistance noted above does not apply. Liquid film resistance dominates liquid-gas mass transfer, and although resistance due to the gas boundary layer does exist it is not usually considered due to its very low impact on the transport process.

There are various factors which play a role in the magnitude of the different oxygen mass transfer resistances encountered. Factors documented include mixing intensity, bubble size, rheological and composition of the medium and interfacial adsorption characteristics to name but a few (Doran 1999). When considering oxygen mass transfer in a well-mixed bioreactor, the following statements can be considered applicable:

1. Transfer of oxygen through the bulk gas phase in the bubble is relatively fast
2. The gas-liquid interface is considered to carry negligible resistance (as noted previously)
3. The liquid film surrounding the bubbles is considered the major source of resistance to the transfer process
4. Concentration gradients in the bulk liquid are minimised in a well-mixed bioreactor. As a result resistance to mass transfer is considered small. In viscous fermentation systems fast mixing may be difficult leading to oxygen transfer resistance in the bulk liquid becoming an important consideration.
5. For single microbial cells the liquid film surrounding them is much smaller than the liquid film surrounding the bubble. In this instance its effect on mass transfer can therefore be neglected. In the case of a biofilm or a large clump of cells liquid film resistance can become significant.
6. Resistance due to the microbial cell-liquid interface is small enough to not be considered
7. Due to the small distances involved, intracellular oxygen mass transfer resistance is usually not considered.

Within in a well-mixed bioreactor (with the microbial cells dispersed throughout the fermentation medium) the liquid film surrounding the bubble is considered as the rate limiting step to the transport process and tends to control the overall mass transfer rate. The oxygen mass transfer rate can be calculated by use of equation 2.20

$$\frac{dC_L}{dt} = K_L a(C^* - C_L) \qquad (2.20)$$

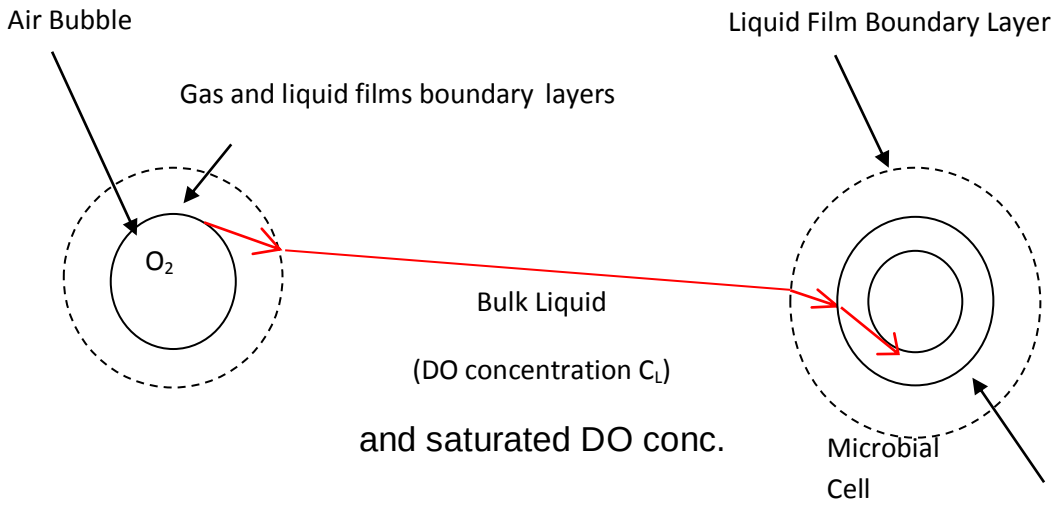

Figure 2.10: The process of oxygen mass transfer

Transfer of oxygen across the cell wall can be rate limiting, but not to the same degree as that noted at the gas-liquid boundary layer. The level of resistance generated by the cell wall depends upon the size of the microbe and physical properties of the cell (such as electrical charge, gram status). Once inside the cell, diffusion of oxygen is quite rapid due to the microbes size (around 1-5 µm). The transport rate of oxygen round the cell is usually higher than demand; therefore growth would not be limited by this stage

2.2.1 The Two Film Theory of Oxygen Transfer

The two film theory is one model which is used to explain how oxygen transfer occurs. For transfer between gas-liquid and liquid-solid the two film theory has generally been used to describe this process. In this theory although transfer across the film is determined overall by two steps, the mass flux must be described separately for each phase. In the case of gas-liquid transfer, the mass flux for each phase can be written as follows (Noorman *et al* 2006)

$$J_g = k_g(p - p_i) \qquad (2.21)$$

$$J_l = k_l(C_i - C_L) \qquad (2.22)$$

Equation 2.21 describes the mass flux in the gas phase, and 2.22 describes the mass flux in the liquid phase. The values of C_i and P_i (i.e. the concentrations at either side of the transfer interface) are related via the Henry co-efficient (H) (Noorman *et al* 2006)

$$P_i = HC_i \qquad (2.23)$$

The overall mass flux can be estimated solely on the basis of equation (2.22) considering that most of the resistance to mass transfer is in the gas-liquid film boundary. The dissolved oxygen at the interface, Ci, can be assumed to be the same as the saturated DO concentration C* since transfer of oxygen in the air bubble to the interface is very rapid. This results in equation 2.23 (Noorman *et al.* 2006)

$$J = K_L(C^* - C_L) \tag{2.23}$$

The C* term in equation 2.23 is given by equation 2.24 (Noorman *et al.* 2006)

$$C^* = \frac{p}{H} \tag{2.24}$$

C* is generally regarded as the saturated value of DO, while C_L denotes the value of DO at in the bulk liquid. The (C^*-C_L) part of equation 2.23 is often thought as the driving force of the process. When C* and C_L are radically different (i.e. when there is almost no oxygen present in the bulk liquid) the transfer proceeds at a rapid pace as oxygen is added to the system. As the difference in values between C* and C_L decrease the process slows until when the two values are identical and the transfer process stops . This can be changed if impeller speed or gas composition is altered. As with oxygen concentration, the sum of the resistance to transfer yields the overall transfer coefficient as expressed in equation 2.25 (Noorman *et al* 2006)

$$\frac{1}{K_L} = \left(\frac{1}{Hk_{gt}}\right) + \frac{1}{k_l} \tag{2.25}$$

Resistance to transfer in the liquid phase boundary layer is greater than that in the gas phase (i.e. therefore $1/(Hk_g) << 1/k_l$) which allows equation 2.25 to be simplified. Due to the problem of measuring interfacial area, transfer of a gas (such as oxygen) is usually expressed per unit of volume of the reactor studied. From this principle, the overall volumetric mass transfer coefficient can therefore be derived as shown in equation 2.26 (Noorman *et al* 2006)

$$Ja = K_L a(C^* - C_L) \quad (2.26)$$

In equation 2.26, Ja is used for generic transfer of gases and for oxygen transfer is usually renamed OTR. OTR can also be expressed as the difference in oxygen concentration over time, yielding equation 2.27

$$\frac{dC_L}{dt} = K_L a(C^* - C_L) \quad (2.27)$$

K_La is a combined co-efficient (i.e. of K_L and a), both entities are combined as measuring them separately is usually quite difficult and inaccurate. The interfacial area of the bubbles can be difficult to measure dependant on the number of bubbles that can be monitored, which usually rely on reactor conditions (such as impeller speed, airflow rate, rheology of the medium, and design of the reactor).

2.2.2 Bubble Size and Oxygen Transfer

As previously noted the impeller system in a STR is responsible for the mixing and decreasing the size of the gas bubbles produced by the sparger. At any one time there are a number of different factors which affect the size of the bubble seen within such a reactor system.

2.2.2.1 Initial Bubble Formation

Initial formation of the bubble occurs at the orifice of the sparger. A number of factors influence the development of the bubble size including viscosity, gas flow rate, gas and liquid density, surface tension, pressure drop, and orifice diameter (Peel 1995). This applies to any reactor where bubbles are formed from a single sparger. In the case of the STR bubbles are initially formed by sparging the dispersed phase (i.e. the gas) through the sparger via the orifices into the continuous phase (i.e. the fluid or fermentation medium). For aerobic fermentation systems the dispersed phase is usually compressed air, or though can also be a mixture of air/oxygen or pure oxygen. Bubbles are formed when the buoyancy force exceeds the surface tension of the fluid and the bubble is then able to break away from the orifice. Buoyancy force and surface tension can be calculated by means of equations 2.28 and 2.29 (Nielson *et al* 1994).

$$BF = \frac{\pi d_{b,i}^3}{6}(\rho_L - \rho_G)g \tag{2.28}$$

$$ST = \pi d_0 \sigma \tag{2.29}$$

The initial bubble diameter depends not only on the force balance mentioned, but also on the diameter of the sparger orifice. Equalising equations 2.28 and 2.29 together produces equation 2.30 which can be used to estimate the initial bubble diameter, which can be rearranged to produce equation 2.31 (Calderbank and Jones 1961)

$$\Pi d_0 \sigma = \frac{\Pi d_{b,i}^3}{6}(\rho_1 - \rho_g)g \tag{2.30}$$

$$d_{b,i} = [\frac{6\sigma d_0}{g(\rho_L - \rho_G)}]^{1/3} \tag{2.31}$$

In equations 2.28 and 2.31, the acceleration due to gravity is considered. This will form a crucial part of the argument as to why high centripetal fields are able to break bubbles down to such a small size. As the gas flow rate increases the average diameter of the bubbles produced also increases, this implies that equation 2.31 can only be used successfully until a certain gas flow rate is reached. After a certain critical gas flow rate is reached, a swarm of bubbles is produced from the sparger and then a continuous jet flow will then be formed. Some resistance to bubble formation can also occur, this mostly being due to liquid viscosity and the fluid surrounding the sparger.

2.2.2.2 Bubble Breakage by Velocity Gradient

After the initial formation of the bubble has occurred, bubble breakup is achieved by use of the impeller system. For impeller designs such as Rushton impellers break up occurs due to the existence of a velocity gradient, defined as the change of fluid velocity across a finite distance. As a result the velocity of the fluid film adjacent to the impeller tends to be higher than the velocity of the bulk fluid. The difference between the two relative velocities produces a shear rate which can be calculated.

Within a shear field, bubbles have a tendency to deform. Where a large velocity field exists the spherical shape of the bubble is not maintained as the surface tension is not strong enough. As a result the bubble (known as the primary bubble) is split to form two daughter bubbles (Nielson *et al* 1994).

2.2.2.3 Bubble Coalescence

In fluids that a have a low viscosity, bubble coalescence can readily occur which lowers the transfer rate in the system. As two bubbles approach each other, the outer contact surfaces become flat so that only a thin film of liquid separates them. As the bubbles become closer, the film becomes thinner until a point is reached where the film is so thin that it bursts. The consequence of the coalescence of two bubbles is that the surface area available for transfer is reduced. The tendency for the liquid film to thin is strongly affected by the properties of the fluid the bubbles are dispersed in. In multicomponent fluids such as fermentation medium, the thickness of the film will be greater due to the interaction of the molecules of different species. Substances such as glycerol, when added to water will form a thicker layer around the bubbles than in just pure water alone. This extra thickness causes repulsion to occur between the various bubbles, and the rate of bubble coalescence is reduced.

2.2.2.4 Bubble Size Measurement

Analysis of bubble size can be quite important when studying the hydrodynamic behaviour of a reactor. This can be quite a challenging task, the most widely used method being that of image analysis conducted by either digital camera or camcorder. In such a method, the camera is placed at a certain distance from the reactor that then can record the bubbles as they rise in the reactor. The camera itself is rigged up usually to a data storage device whereby the results can be looked at later and the oxygen bubble size gained from the measurements of the bubbles seen in the photographs provided. This technique has the advantage that the method is non-invasive (therefore not disturbing the contents of the reactor) and is a fairly easy and straightforward method to execute.

One such system that used an imaging technique to investigate bubble size was a study by Hepworth *et al.*(1994) who although not looking at enhancing the mass transfer of oxygen in the study, was looking to investigate the bubble size and the role bubble size plays during the dispensing of beer. Due to the nature of the fluid (i.e. the beer) most bubble techniques can

not be used, and so an imaging technique (digital camera) was used. This paper showed that an imaging system could be used to great advantage to analyse bubble formation and size, being able to record and store the images on a P.C for later analysis off-line.

Apart from imaging analysis, other techniques exist for bubble determination. Capillary suction probes (CSP) have been used in previous research to capture bubble size (Laakkonen *et al 2*005). Unlike the imaging technique described above, this technique is an invasive one and uses a probe placed within the reactor to examine bubble size. The main advantage that this technique that compared to digital optical techniques used, the CSP method is quite cheap and is easy to use. In the method a probe is placed at an appropriate placed within the reactor, bubbles rising within the reactor pass through the probe and are converted into elongated slugs, which are recorded by the probe as they pass through. There have been some doubts over the reliability of the probe, including the fact that the method is an invasive method and could alter the results of the study being looked at. A research paper by Laakkonen *et al* (2005) used this method when looking at the oxygen bubble size in three different sized reactors that were agitated by a Rushton turbine, the 14dm^3 reactor being agitated by a flat blade turbine in order to compare effects of different impeller systems. In the research three different systems were investigated a simple air-water system, an air-NaCl (aq) system, and a CO_2-n butanol system, which aimed to look at local gas bubble size and distribution. Apart from the different impeller systems used, different stirring speeds and gassing rates were also investigated to determine if they had any effects on the bubble size and distribution. In the study it was found that the smallest bubbles were produced in the CO_2-n butanol system, the bubble size was also noted to decrease further as the fluid proceeded from the impeller into the fluid stream as it progressed towards the liquid surface. The CSP method was also tested for its reliability also and was found to be very accurate in the results it was able to produce. The experimental system is shown below in figure 2.11

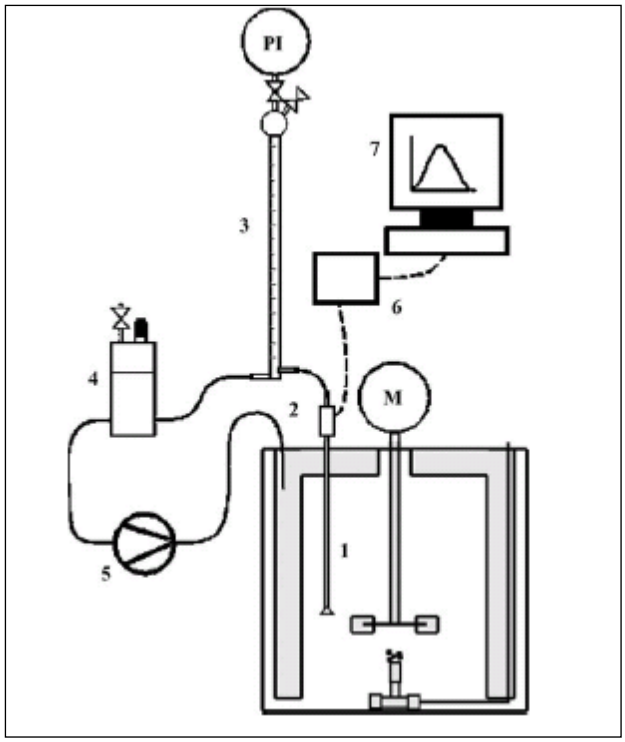

Key:

(1) Capillary;
(2) Capillary suction probe;
(3) Burette for gas separation;
(4) Pressure equalization tank;
(5) Gear pump;
(6) Signal processing unit;
(7) Computer for data acquisition

Figure 2.11: The CSP method setup (adapted from Laakkonen *et al* 2005)

2.2.2.5 Bubble Size and Mass Transfer

The mass transfer of oxygen into a chemical or biochemical reactor can be one of the limiting factors of the process. Oxygen mass transfer limitations will mean that the microbial culture does not receive the adequate amount of oxygen needed for its metabolic processes to occur at a normal rate, and so the rate of the reaction will therefore decrease as a result. One of the factors affecting this mass transfer rate is the size of the oxygen bubble into the reactor; a small oxygen bubble will have a much larger interfacial area available for mass transfer, but also the bubble experiences a larger residence time in the reactor again increasing mass transfer. In some instances, reactor systems have been set up whereby small oxygen bubbles have been produced and it has been expected that the overall mass transfer of the system would be enhanced, however smaller bubbles also have a tendency to show coalescent behaviour. This coalescent behaviour, the behaviour by which small bubbles merge together to form larger ones, therefore means that progress made enhancing mass transfer is reversed as large bubbles once again become present in the reactor.

A bubble and transfer study by Oliveria *et al* (2004) investigated the bubble diameter and gas hold up in a gassed Oscillatory Baffled Column (OBC) using two digital cameras one near

the base of the column and one 650 mm from the base. The reactor itself was placed in a square box filled with water that was used to stop the curvature of the reactor wall effecting results. It was shown in the paper that as the oscillatory velocity increases the bubble diameter observed decreases and increases the bubbles hold up time in the reactor. It has also been shown in the paper that the bubble mean size and gas hold time have an influence on the mass transfer rate noticed within the reactor.

2.2.3 Determination of K_La

There are a number of ways in which the value of K_La can be determined. The choice of which method is used usually depends on the system being studied. The first is the static gassing out method, devised by Wise in 1951 (Stanbury *et al* 2000), the method is the simplest to carry out. The method involves first de-aerating the liquid (either water or fermentation medium) either with gas (such as nitrogen) or with an oxygen consuming substance (such as sodium sulfite). Once oxygen free, oxygen is then put back into the liquid until the saturated concentration point is reached. The process is monitored by the presence of a DO probe. Equation 2.27 (section 2.2.1) can be integrated to give equation 2.32 (Richardson *et al* 2005).

$$\ln\left(\frac{C^*}{C^*-C_L}\right) = K_L a t \qquad (2.32)$$

If looked at graphically, a plot of ln (C^*/C^*-C_L) v t will produce a straight line graph with a slope equal to K_La, shown in figure 2.12

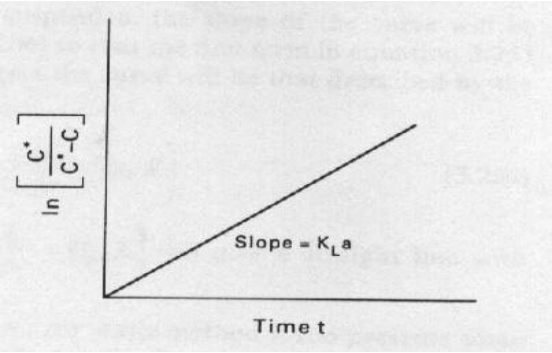

Figure 2.12: Graph for the Static Gassing out Method (Richardson *et al* 2002)

Problems occurring with the method include the use of pure water instead of fermentation medium which leads to inaccurate determination of mass transfer potential. The use of sodium sulfite in an active fermentation medium is expensive and can cause changes to the broth composition. Results can also be affected by the lag time of the DO probe used. If this proves to be the case, a modification can be made to equation 2.27 (section 2.21) which can take account of the probe response time based on a first-order process (Boodhoo *et al* 2008; Lamping *et al* 2003; Bandino *et al* 2000). This will then give a more reliable estimate of the transfer capability of the system (Sajc *et al* 2006).

$$C_p = \frac{1}{t_m - \tau_P}\left[t_m \exp\left(\frac{-t}{t_m}\right) - \tau_P \exp\left(\frac{-t}{\tau_P}\right)\right] \qquad (2.33)$$

The second method established is the dynamic gassing out method. This method primarily is used with an active respiring fermentation culture. Once again a DO probe is used to monitor the DO level in the reactor. Usually the fermentation medium (without the culture) is used to calibrate the probe via the static gassing method. Once the D.O is confirmed as being 100 % of saturation, the culture is added, the probe relaying information of the D.O level. At a predetermined point the oxygen supply to the reactor is switched off for a period of time. The D.O is monitored during this phase; the oxygen supply is switched back on after the period of time is over, or if the D.O level falls below a certain critical limit. Once the oxygen supply is switched back on, the D.O level should increase as a result. This is shown graphically in figure 2.13

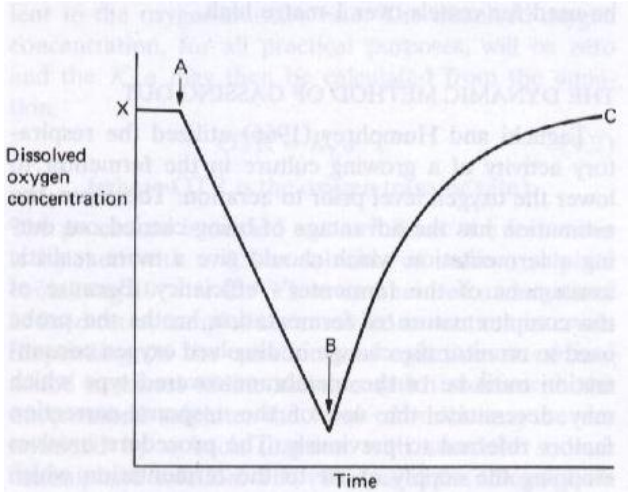

Figure 2.13: The Dynamic Gassing out method (from Shuler *et al* 2002)

It can be assumed that at the beginning of the fermentation, a pseudo semi steady state exists, as the DO will only show a small decrease. This is because there are few microbes in the system, the growth rate giving the impression of a constant biomass concentration. A material balance can therefore be written for the oxygen in the system.

{Accumulation rate of oxygen in fermenter} = {OTR}-{OUR of culture}

This material balance can be re-arranged, which gives rise to equation 2.34

$$\frac{dC_L}{dt} = K_L a(C^* - C_L) - xQ_{O_2} \qquad (2.34)$$

In figure 2.17, the period when the oxygen supply is suspended (line AB) the OUR of the system will determine the curve produced. This allows the respiration rate of the microbe to be evaluated. When the oxygen supply is re-established (line BC), a re-arranged version of equation 2.34 describes the dissolved oxygen in the bulk liquid, C_L (Equation 2.35)

$$C_L = C^* - \frac{1}{K_L a}\left(\frac{dC_L}{dt} + Q_{O_2} x\right) \qquad (2.35)$$

A plot of C_L against $\left(\frac{dC_L}{dt} + Q_{O_2} x\right)$ will yield a straight line graph, with a slope equal to $-1/K_L a$ (shown in figure 2.14)

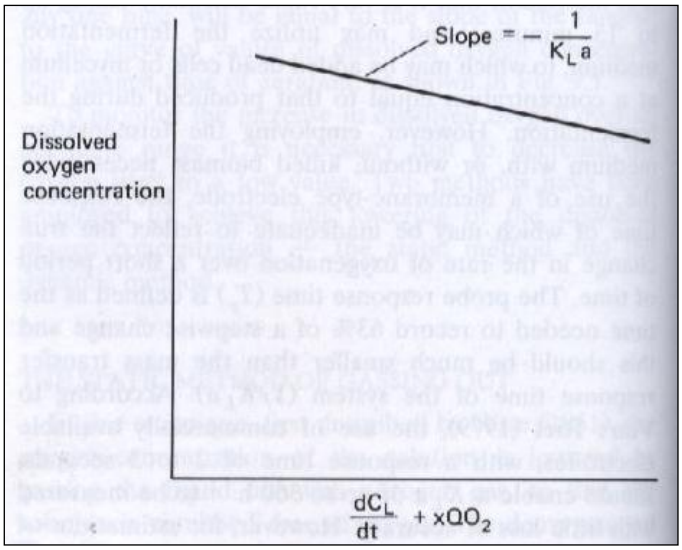

Figure 2.14: Dynamic Gassing out method, for $K_L a$ calculation (from Shuler *et al* 2002**)**

Although there are many advantages of using this method instead of the static method, there are also some disadvantages. For example it is crucial that the DO level does not fall below the C_{crit} level. This will not only affect the transfer, but could also affect the microbes metabolism as it goes into shock as there is not enough DO present. The method therefore can be difficult to apply for high oxygen demanding microbial strains. The DO probe used needs to be a membrane type, to be able to pick up the sometimes swift changes in DO concentration.

The final two methods do not rely on a DO probe for analysis. The first of these methods is sulfite oxidation. Developed in 1944 by Cooper *et al*, $K_L a$ determination occurs by the oxidation of a solution of sodium sulfite. The reaction itself proceeds on the basis of using the reaction rate of a known solution of sodium sulfite (usually around 0.5M) to be converted into sodium sulfate using a cobalt or copper catalyst. The reaction scheme is below:

$Na_2SO_3 + 0.5O_2 \rightarrow Na_2SO_4$

The reaction rate is incredibly fast, once the oxygen has entered the solution, it is immediately used to convert sulfite into sulfate. Given this fast reaction rate, the reaction scheme is therefore the same as the OTR and that it equals the OTR. If DO concentration C_L in the bulk liquid is assumed to be 0, $K_L a$ can be calculated from equation 2.40.

$$OTR = K_L aC^* \qquad (2.40)$$

The sodium sulfite is placed in the reactor along with the catalyst (around 10^{-3} M). Aeration and agitation are set up at fixed rates; samples are then removed at predetermined time intervals (based on the aeration and agitation regime used). This is added to excess iodine (in solution) which as the reaction proceeds, reacts with any present sulfite present. The level of iodine reacted with the sulfite is determined through back titrations using sodium thiosulfate solution. The amount or volume of thiosulfate used in the titration can then be plotted on a graph against sample time; the slope of the line is used to calculate the OTR. Although the technique is simple to use, the time to make a single determination is a limiting factor. In some instances one determination can take around 3 hours to complete. Accuracy of analysis can be affected by surface active molecules (such as amino acids or proteins) present in the medium. Some research suggests that because the reaction occurs in the liquid film (surrounding the bubble), the value of $K_L a$ is over estimated by this method.

A similar type of method is that devised by Deront *et al* (1997) the oxidation of cuprous chloride is used as a means of determining $K_L a$ values within a co-current packed bed type reactor. Deront noticed that physical absorption methods of determining $K_L a$ in an up flow reactor could be underestimated, as the gas and liquid may have reached an equilibrium under where the sampling point. The oxidation reaction of cuprous chloride via hydrochloric acid is shown in the following scheme

$$4CuCl + 4HCl + O_2 \rightarrow 4CuCl_2 + 2H_2O$$

The rate of reaction is such that the concentration of DO during the experiment is 0; therefore the variation of the concentration of $CuCl_2$ with time can be calculated with equation 2.35 below

$$\frac{dC_{CuCl}}{dt} = -4K_L aC^* \qquad (2.35)$$

In equation 2.35 the factor four is used because of the stoichiometry of the overall reaction scheme. Equation 2.35 can be integrated between the initial and final concentration found in the reactor, shown in equation 2.36

$$K_L a = \frac{C_{CuCl,0} - C_{CuCl,f}}{4C^*(t_f - t_0)} \tag{2.36}$$

The final method is a novel method, proposed by Ortiz-Ochoa *et al* (2005) incorporates the use of the bio-oxidation of cathechol via Catechol-2,3-dioxygenase to give 2-hydroxymuconic semialdehyde to give a more efficient method of estimating K_La in a small scale fermenter system. The main aim behind the development was to provide an accurate measuring system in a small scale reactor for K_La, one that would also be fast, controllable, and simple to conduct. The method uses the enzyme Catechol-2,3-dioxygenase to take 1 mole of oxygen to convert 1 mole of cathechol, yielding the bright yellow product of 2-hydroxymuconic semialdehyde. The authors suggest that if the enzyme in the system is in excess, the oxidation rate being of zero order then equation 2.37 suggests:

$$\frac{d(2-HS)}{dt} = OTR \tag{2.37}$$

Results have shown that the method is fast and does not have time limitations, end point complications, and the use of large oxygen probes.

2.2.4 Factors affecting $K_L a$

Two major factors, namely gas flow rate and agitation can have a profound effect on the K_La. This needs to be considered when enhancement of transfer processes is being undertaken (see section 2.3.3). In STRs, the value of K_La is seen to increase with increasing airflow rate. This increase does not occur indefinitely and a point is reached where the airflow rate increases but the value of K_La does not as shown in figure 2.15

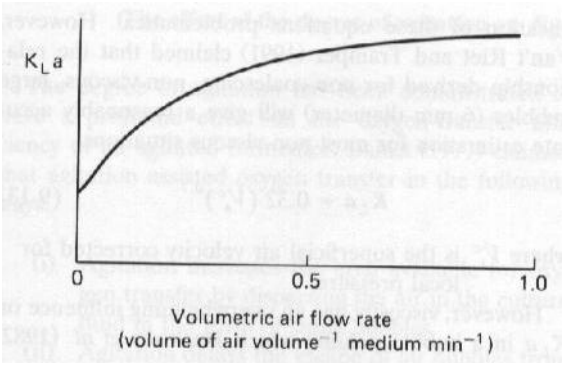

Figure 2.15: The effect of airflow rate on the value of $K_L a$ (Shuler *et al* 2002)

The range of values for the airflow rate is generally between 0.5-1.5 vvm (Stanbury *et al* 2000). Figure 2.15 illustrates that as airflow increases; the increase in $K_L a$ is not linear. This is because of a phenomenon known as flooding. This occurs when the gas flow is too fast; dispersion of all the bubbles may not be completely achieved by the impellers. This leads to stagnant zones which receive little or no gas, reducing the transfer rate. In essence if flooding is occurring with a STR, the agitation and airflow regime is unsuitable, allowing the flow pattern to be dominated by the airflow. Studies conducted have tried to pin point the moment flooding occurs, in order to increase the maximum amount of gas in to the reactor. Figure 2.16 shows the movement away from an unaerated vessel dominated by the action of the impeller to one where the system is flooded and dominated by the airflow rate. In essence figure 2.16 demonstrates that as airflow increases the prominence of the airflow pattern becomes such that a vast majority of the bubbles escape from the liquid medium without being touched by the impellers. The compromise and therefore the balanced working of agitation and airflow are shown in 2.16 (Stanbury *et al* 2000).

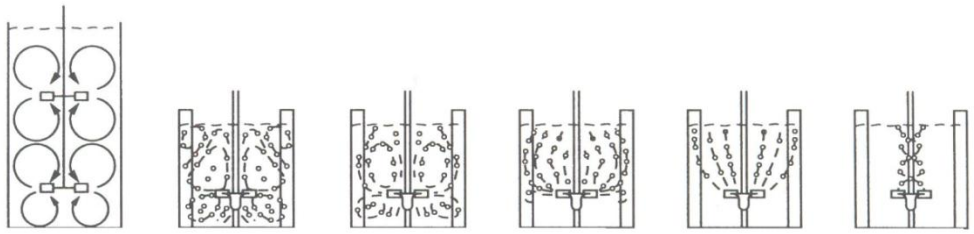

Figure 2.16: Balance between agitation and airflow rate (Stanbury *et al* 2000)

Transfer within STR vessels has been shown to be greatly influenced by the agitation regime utilised. Agitation by impellers causes bubbles to break to form smaller daughter bubbles, it prevents bubble escape, and decreases resistance to transfer by thinning the gas-liquid boundary layer (Stanbury *et al*. 2000). In some instances agitation can prevent coalescence behaviour, although low viscosity systems tend to have a high degree of coalescent behaviour. Studies have modelled the relationship between K_La and power consumed, yielding an expression similar to equation 2.38 (Van't Riet 1979, Nocentini *et al* 1993)

$$K_L a = m(\frac{P_g}{V})^{\alpha} U_s^{\beta} \qquad (2.38)$$

There are a number of different factors which could affect the result obtained. Scale up from lab to industrial level has shown to play a role (Bartholomew 1960). In Bartholomew's study vessels with multiple impellers were studied whereby the lower impellers would have the greatest effect on transfer relative to the amount of power needed. An earlier study by Cooper *et al* (1944) using the sodium sulfite method (section 2.2.3) to calculate K_La found slightly higher exponents than Bartholomew. These two studies are not directly comparable, the Cooper study examined systems with one impeller, and the sodium sulfite method has a high error compared to the gassing out techniques favoured by later studies.

2.3 Process Intensification

Process Intensification (PI) is a philosophy of reactor design intended to reduce the cost of a reactor by downscaling the size of equipment. The best known examples of PI tend to be associated with the intensification of transport processes such as heat and mass transfer. One of the ideas behind PI is that ever molecule within a given reactor will experience the same processing environment, thereby providing a uniformity to the process (Reay *et al* 2008). This is achievable by a number of different methods. This section of the literature review will explore how process intensification is defined, alongside applications for enhancing oxygen transfer, and the need for provision of Bioprocess Intensification.

2.3.1 Defining Process Intensification

One of the early definitions of PI is a "strategy for making dramatic reductions in the size of a chemical plant so as to reach a given production objective" (Ramshaw 1985). The size of a

chemical plant could be reduced by decreasing the equipment or number of operations used. PI is seen therefore as a design philosophy whereby decreased operations and/or equipment leading to similar or enhanced performance for a given system (McCarthy *et al* 2007, Boodhoo *et al* 2006). In order to be viable commercially Ramshaw argued that the decrease in size must be at least an order of magnitude from the current system (Ramshaw 1985). The order of decrease in equipment argued by Ramshaw has since been viewed as too large by most engineers. Modern views of PI believe that reduction by a factor of two is sufficient to achieve the goal of PI (Stankiewicz *et al* 2000).

PI principles were initially used to cut capital costs for a reactor. Once applied other benefits (such as increased safety, more efficient use of reagents, and reduction of unwanted side products) were quickly apparent (Stankiewicz *et al* 2003, Ramshaw 1985). Later views of PI define it as "the development of novel apparatus and techniques that, compared to those commonly use today, are expected to bring about dramatic results and improvements in manufacturing and processing, substantially decreasing equipment size and/or production capacity, ratio, energy consumption, or waste production and ultimately resulting in cheaper suitable technologies" (Stankiewicz *et al* 2000). Stankiewicz applies a broader definition showing that PI can be employed in a number of areas within a plant, but to be viable PI techniques need to be applied across a whole process.

This is still not a complete view of PI. Stankiewicz in his definition left out enhancement of safety as a possible goal. In the modern chemical plant safety of the reactor is critical, a smaller chemical plant will by design have fewer dangerous chemicals on site. A more complete definition of PI can be summed up as "Any chemical engineering development that leads to a substantially smaller, cleaner, safer, and more energy efficient technology is process intensification" (Reay *et al* 2008)

2.3.2 The Benefits of Process Intensification

The main breakthrough in the concept of P.I is in the late 1970's with research led by Prof Colin Ramshaw at ICI Runcorn (Reay *et al* 2008, Stankiewicz *et al* 2000). The Oil and Gas industry is a prime example where lack of space on rigs has lead to usage of PI to enable the effective and efficient use of space (Richardson *et al* 2002). In contrast the Chemical Process Industry has been slow in utilising these techniques, the focus traditionally being on production of products rather than the technology used to produce them. Given the current

economic climate and the drive towards more efficient, greener systems, and increased competition globally, PI techniques are becoming widely used within the chemical industry

One of the first developments from Ramshaw's group was with the use of high centripetal fields leading to the creation of the HiGEE or Rotating Packed Bed Reactor. Other designs of other novel reactor technology designed by Ramshaw's group at ICI Runcorn include the Spinning Disc Reactor, catalytic plate reactor and rotex heat adsorption heat pump. One of the noticeable aspects of PI is the reduction of footspace compared to its traditional counterpart. A clear example is the Spinning Disc Reactor (SDR) which takes up less foot space than the traditional Stirred Tank Reactor (STR) (Vicevic *et al* 2008). In the future it is envisaged that PI could produce a chemical reactor which is mobile, increasing the flexibility of the reactor, and reduce the amount of stored chemicals (Hendershot 2000).

There are other benefits that PI can offer other than cutting cost and footspace. Efficient use of energy has been studied in recent years; with Heat Exchanger (HEX) technology making it possible to reduce the amount of energy needed for certain reactor systems (Mercer 1992). A SDR used for polymerisation of styrene showed a decreased used of energy compared to its STR counterpart (Jachuck *et al* 1997). The application of PI philosophy towards reduction in energy consumption will help meet energy targets agreed within various conservation protocols such as Kyoto. To reduce energy consumption, PI is used to enhance transport processes which will lead to smaller differentials in temperature, and or concentration. A chemical operation that runs with very high heat transfer coefficients will by its very nature generate less entropy. The result being that this is considered the ideal thermodynamic situation (Reay *et al* 2008). Environmental concerns have lead research into reactors that produce less pollution. Visually intensified reactors are much smaller and therefore less obtrusive. The current move within the industry is to establish fluid dynamics within the reactor that lead to total green technology (Reay *et al* 2008). A smaller reactor which uses effluent treatment will not require as much energy as its counterpart traditional reactor.

Enhanced safety can also be achieved by intensification. As noted previously the definition established by Stankiewicz did not include safety as a PI goal even though this is quite a crucial aspect in itself. A reduction in size means that it is less likely that exothermic "runaway" reactions occur, thereby leading to an increase in safety. The reduction of the size of the plant leads to a reduction in the amount of chemicals that have to be stored,

intrinsically leading to a much improved safety level. A quick literature search on the history of the chemical process industry quickly reveals a number of high profile disasters where a number of deaths have been due to poor safety. One of the worst examples is that of the release of 40 tonnes of methyl isocyanate at Bhopal in 1984. It has been speculated that a continuous plant (rather than the batch one at the centre of the release) had been in place a lot fewer deaths would have resulted (Reay *et al* 2008).

2.3.3 Bioprocess Intensification

Previously it has been noted that PI techniques have been exploited to enhance transport processes such as heat and mass transfer. For a number of aerobic fermentation systems, oxygen transfer can be a rate limiting feature. The main reason for this being that oxygen is poorly soluble in liquid medium. For a temperature of around 35 ^{o}C at atmospheric pressure, the saturated oxygen concentration in water is around 7.1 ppm (Mortimer 1956). If an oxygen transfer rate limitation is present during fermentation, then this can present a problem. If the oxygen transfer rate into the reactor is outstripped by the oxygen uptake rate of the microbe, this will stop the microbe from growing at its optimum rate. Eventually the lack of oxygen will lead to the non viability of the culture. For cultures that are obligate aerobes this process will occur much faster than facultative aerobes. Bioprocess intensification can almost be classified as an offshoot of PI

In the context of bioprocess intensification, previous research into oxygen transfer limitation has investigated bubble size. It has been observed that the smaller the bubbles the faster the transfer rate that results. This is because the smaller bubble has an enlarged surface area, leading to an enhancement to the 'a' coefficient in K_La. A large number of fermentations are carried out in the STR where the impeller system is responsible for mixing and the shredding of bubbles down to a small size. Although small bubbles and good mixing can be achieved by the Rushton impeller it is possible that the microbes present can also be damaged. This is because the blades on the impeller provide the high shear environment and effectively nick the edge of the bubbles to cut them down to a smaller size. This could also happen to a microbial cell which came close to the impellers. This phenomenon would increase as biomass concentration increases, so that fed-batch operations may ultimately be limited by this.

To address possible shear damage to microbial cells by impellers, designs of new reactor technology have been implemented, of which one example is the airlift reactor. In this reactor mixing occurs via the movement of gas engaging/disengaging from the liquid media. The reactor was developed primarily for fermentations with shear sensitive cultures, and so is often found in manufacture of biopharmaceutical proteins (obtained from animal cell cultures). The reactor consists of two zones, of which only one is aerated. The broth in this "riser" section flows upwards as the density of the fluid is lighter due to the presence of air. At the top of the reactor the air disengages, and the broth becomes denser, floating down the downcomer section. At the bottom of the reactor the broth once again encounters the air stream, becomes less dense, and rises up the reactor (Chisti 2006; Schuler *et al* 2002; Stanbury *et al* 2000). Due to this movement of gas, high viscosity systems can be used, and bubble coalescence is not an issue. Industrial examples of air-lift fermenters include one constructed by Imperial Chemicals Industries for the production of single cell protein (Billingham U.K.), and one used for the production of Quorn by Marlow Foods (Marlow U.K.). Figure 2.17 shows the reactor used by Marlow Foods (Billingham UK) to produce Quorn.

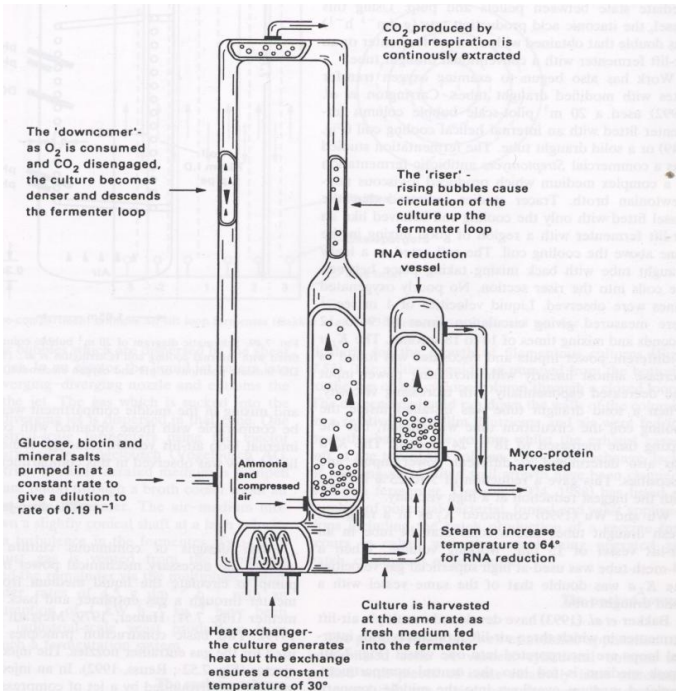

Figure 2.17: Schematic diagram of the airlift fermenter used by Marlow Foods for the production of either myco-protein or SCP in continuous flow culture (Stanbury *et al* 2000).

Variations of this reactor have differences on where the riser (or draft tube) section is placed, either internally or externally. However the external types are not as common on an industrial scale as their internal counterparts. To ensure maximum oxygen transfer, the cross sectional area ratio (of riser to downcomer) should be around 1.8 -4.3 (Chisti *et al* 2006). Compared to the STR the airlift design is much more energy efficient, but production wise is comparable between the two designs. The performance of the design is based on the rate of gas injection and the circulation of liquid around the reactor. Enhancement of liquid circulation is achieved by ensuring all gas disengages at the top of the riser, so that there is no gas present in the downcomer section. This ensures that the gas hold up difference between the two sections is at its greatest. Airlift reactors are built with a large aspect ratio, as the liquid circulation increases with the square root of the reactor height (Chisti *et al* 2006).

Although microbial cultures are not damaged by shear stress, transfer rate within the reactor can be less than a well-mixed STR (Nikakhtari *et al* 2005B). In order to address this balance, research conducted by Nikakhtari *et al* (2005A) placed a block of porous material inside the riser section of an external loop airlift reactor (shown figure 2.18). The idea being that air bubbles in the riser would have to make their way through the packing, which because of the intricately wound fibres would shear the bubbles down to a small size but not the microbial culture. In the first study conducted, nylon mesh (porosity of 96.0 %) was shown to have a increased the value of K_La by a factor of 3.73 (Nikakhtari *et al* 2005A). The experimental results were in good agreement with the mathematical model (Nikakhtari *et al* 2005A) However it was discovered that organic chemicals from the mesh were leaking into the fermentation medium and interfered with cell cultivation (Nikakhtari *et al* 2005B). The nylon was therefore replaced with stainless steel (porosity of 99.0 %), with none of the other conditions altered. It was noted that the K_La values increased by a factor of 2.45, less than the column with nylon mesh. It was believed that the slightly lower value was due to the stainless steel having a higher porosity. The higher porosity of the stainless steel provided lower gas drop potential (Nikakhtari *et al* 2005B). In both experiments an air/water system was used. Other material used as packing has included expanded clay balls or Biolite (Deront *et al* 1998).

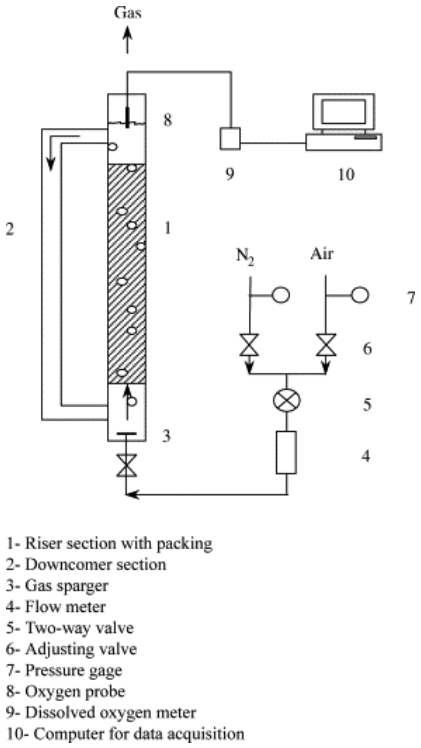

Figure 2.18: Schematic of the external loop airlift bioreactor (packing could be Nylon Mesh or Stainless Steel) (Nikakhtari *et al*. 2005B)

Another method of enhancing oxygen transfer reported in the literature is to decrease the resistance to mass transfer between the gas-liquid boundary layer. Decreasing this resistance is accomplished by thinning the gas-liquid boundary layer, which increases the K_L part of the overall volumetric mass transfer co-efficient K_La (section 2.2.4). In the Chemical Process Industry this is achieved by intensifying the mixing in a STR type design via an impeller system. This cannot be used in fermentation reactions as microbial cultures are extremely sensitive to shear stress (Galaction *et al* 2004). It was discovered that during experiments with single cell protein production that small amounts of insoluble organic compounds (such as hydrocarbon substrates) brought about an increase in the oxygen transfer rate. This was achieved without the need to intensify the mixing already present in the vessel (Galaction *et al* 2004). Oxygen vectors are defined as "compounds that, when added to growth media can enhance the oxygen transfer rate in microorganisms, resulting in a higher oxygen capacity for oxygen solubility as compared with water." (Galaction *et al* 2004). Compounds that have been successfully utilised include hydrocarbons, and perfluorcarbons. Such a system has been used with a *Propionibacterium shermanii* (produces vitamin B12) in which n-dodecane was

used as the oxygen vector. It was found that the K_La value in the systems with the added hydrocarbon could be up to nine times greater than the systems without hydrocarbon present (Galaction *et al* 2005). The experiments were conducted in a non-respiring system (the bacteria's respiratory activity inhibited by chemical methods); the K_La value in a respiring system could be much higher due to the decrease in resistance to oxygen mass transfer. This was achieved by increasing the concentration gradient of oxygen between the aqueous and organic phase. It was also noted the hydrocarbon added could also be used by the bacteria as a source of fuel (carbon) and so the overall level of n-dodecane would decrease as a result. This effect still needs to be investigated (Galaction *et al* 2005). The alcohol ethanol has been used as an oxygen vector (Bi *et al* 2001). The exact method of how oxygen vectors affect oxygen transfer rate is still not understood. One possible explanation is that the hydrocarbon is absorbed to the bubbles surface, whether or not a continuous film has been established (Galaction *et al* 2004). The passage of oxygen to the microbe passes from the air bubble passes through this organic phase first before passing to the aqueous phase. It is believed that this extra step causes the reduction of resistance to mass transfer (Galaction *et al* 2004).

Another method of decreasing resistance at the gas-liquid boundary layer has focused on intensive mixing. Intensive mixing of such a system not only could produce smaller bubbles, but also reduce the resistance to mass transfer. Methods of achieving could be by vibration fields (Grinnis *et al* 2004) or by the use of a modified Oscillatory Flow Reactor known as the Oscillatory Baffled Bioreactor (OBB). The reactor is described as being a novel continuous plug flow reactor, whereby the contents of the reactor are mixed by oscillatory movement imposed on the fluid (Reay *et al* 2008). The contents of the reactor pass through a series of orifice plates which are able to shear bubbles down to a small size, thereby enhancing transfer processes. Research conducted by Ni *et al* (1995) showed that the K_La for a yeast system was enhanced when the system was conducted in an OBB (Ni *et al* 1995). The reason behind the enhancement was due to increased gas hold up, and decreased bubble size noted within the system. Scale up of the OBB has been proved to be more predictable than that of STR's (Ni *et al* 1995). A schematic of the reactor is noted in figure 2.19

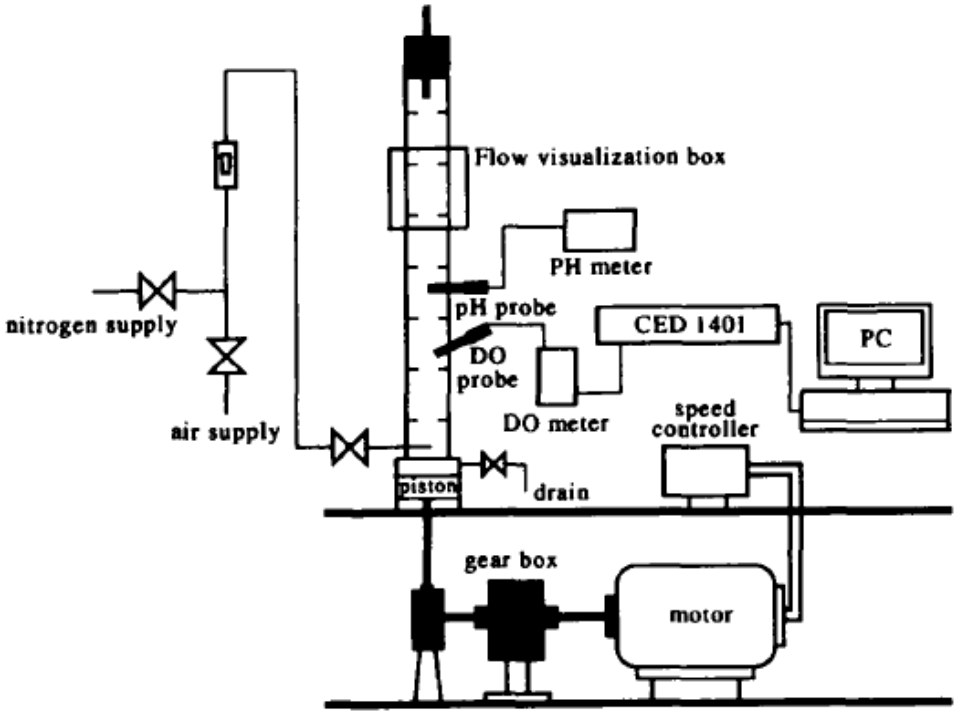

Figure 2.19: Schematic of the OBB Reactor (Ni *et al* 1995)

2.3.4 The HiGEE Bioreactor (HBR) for Bioprocess Intensification

2.3.4.1 General Overview

As noted previously one of the first intensified reactors designed by Ramshaw was the Rotating Packed Bed Reactor (RPB) also known as the HiGEE reactor. The reactor makes use of highly porous packing material, which has high specific surface area compared to similar packing used in conventional packed towers. As a high centripetal field is used inside the reactor, the material used as the packing must be able to withstand the forces generated (Burns and Ramshaw 1996). Generally the packing has a material that is highly uniform, although some examples have been noted where grading of material helps to alter localised flooding conditions (see below). Previous examples of RPBs have materials with specific surface areas of 500-5000 m^2 m^{-3}, and voidages greater than 85 %. (Burns *et al* 2000)

Gas and liquid flow within the reactor is usually counter current. One of the phases will be injected from the periphery of the rotor and percolate through the packing. The second phase then enters from the centre of the rotor and is flung towards the packing by the high centripetal field that is generated by the RPB. Due to the thin film between the gas-liquid

phases, a high transfer rate can be expected (Aoune and Ramshaw, 1999). The liquid then disengages from the rotor by means of a drainage point leading to a collector.

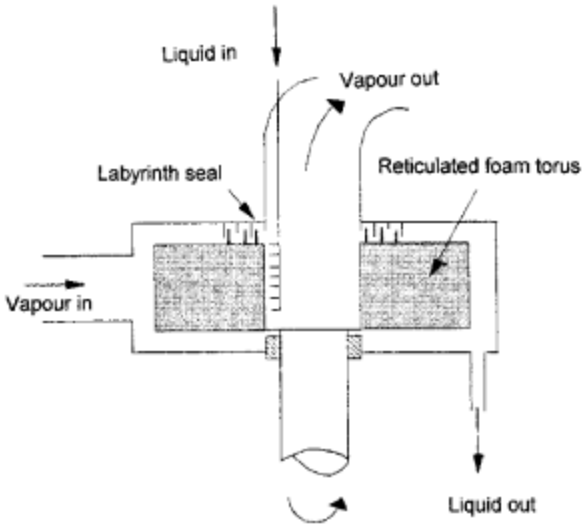

Figure 2.20: A schematic of a current RPB (Peel *et al* 1998)

Due to the high throughput of liquid the drainage point needs to be capable of draining all the fluid to prevent accumulation within the rotor (Reay *et al* 2008). High voidage packing is capable of breaking bubbles into a fine size and therefore enhancing the transfer with such a system. This is a similar idea to the use of bubble breakers within air lift reactors, but with the added benefit of being placed in a high centripetal environment. Early development of the RPB occurred at ICI with a prototype unit for ethanol/propanol distillation. Once improvements to the liquid distribution had been made to ensure uniformity, the RPB was able to contain over 20 theoretical distillation stages in the 25 cm packing (Reay *et al* 2008).

Apart from the high voidage packing, the RPB exploits high centripetal forces for use in intensifying transport processes such as mass and heat transfer. This concept of high centripetal force has been utilised as part of Spinning Disc reactors for short residence reactions such as polymerisation (Boodhoo *et al* 2000). For processes such as oxygen transfer (which can be seen as absorption of oxygen into a fluid) a term known as the buoyancy term can dictate behaviour in the system. For systems where either ρ or g are close to 0, then surface forces can dictate what occurs within the system. The advantage that the RPB has is that the magnitude of the acceleration is much greater than that due to gravity (around 9.81 m

s^{-2}) (Peel 1995). Acceleration within a given centripetal field is given by equation 2.39 (Peel 1995)

$$g^* = \omega^2 r = ng \qquad (2.39)$$

An important concept for reactors such as the packed tower and RPB is that of flooding. Flooding within such reactors is connected to the classic Sherwood flooding correlation which is used to explain fluid behaviour which runs counter current to the gas or vapour. As the flow of fluid increases, the amount of interfacial interaction increases. A point is reached where movement of the fluid outwards from the centre becomes increasingly difficult and eventually stops. When this occurs the liquid accumulates in the column as its path outwards from the centre is impeded. This is the point when flooding is said to be occurring, and the reactors mass transfer efficiency drops and becomes non existent.

The upper flooding limit of an RPB is therefore an important consideration when considering enhancement of transport processes such as mass transfer. For a new RPB a series of experiments at different gas and liquid flow rates will be used to establish the flooding conditions of the reactor. This is then used to provide parameters for any experiments (such as transfer experiments) that subsequently follow. Due to the radial flow of both liquid and gas, mass flux is greater towards the inner rotor zones rather than at the periphery because of the gradually decreasing flow areas towards the inner regions. This combined with the centripetal force applied will mean that flooding will tend to occur faster at the inner radius than at the edge of the reactor. This is in contrast to flooding within a packed tower where a flooding state is reached simultaneously throughout all of the packing (Reay *et al* 2008).

The hydrodynamic behaviour of a RPB was studied by digital photography investigating fluid behaviour, velocity and hold up measurements by Burns *et al* (1996). In the experiments conducted a black polyurethane packing was used in combination with diluted white emulsion paint (3-7 %) to examine how the liquid behaved in the centripetal field. It was shown that the liquid was able to pick up the speed of the rotor within 1 cm of the periphery of the rotor. Furthermore as the speed of the rotor was increased, flying droplets of liquid were noted in the rotor (Burns and Ramshaw 1996).

As noted previously, distillation was one of the early applications that the RPB system had been used for. Other applications such as gas stripping have also been explored with the RPB. Previous research conducted by Peel (1995) used a packed rotary contactor for deoxygenating of water by use of a stripping gas. The aim of the research was to provide a more cost effective and efficient method of stripping oxygen from river or sea water (Peel *et al* 1998). The research focused on a 1.0 m diameter rotor for which a number of hydrodynamic and transfer experiments were conducted. Originally the packing had been Declon H20, and experiments with a much finer packing Declon H30 showed no significant improvement in transfer rate. Overall the rotor showed good transfer capability. More recent examples of stripping operations with RPB reactors have included the removal of ozone from gaseous feeds (Chia Chang *et al* 2007). Other applications that RPB type systems have been used for include absorption of compounds such as Volatile Organic Compounds (VOC) (Zhao *et al* 2010) and mass transfer studies with a variant of the RPB in the form of a rotating solid foam reactor (Tschentscher *et al* 2009). Additional variations on the basic design of the RPB have been noted to include a Rotating Zigzag Bed Reactor which can function without the need for liquid distributors (Wang *et al* 2007).

2.3.4.2 Calculation of Mass Transfer

Once the hydrodynamic study has been conducted, this is used to provide the conditions for further testing the capability of the reactor. In a large number of cases this will include testing the mass transfer capability of the new reactor. As with conventional reactors the transfer capability of the RPB can be determined from either the absorption or desorption of gas from a fluid. Section 2.3.4.1 has already illustrated examples where oxygen is stripped from water (Peel *et al* 1998).

The method on calculating the transfer capability of a RPB reactor can be assessed via the Number of Transfer Units (NTU) and the liquid side volumetric mass transfer coefficient K_La. This method is based on well-established gas-liquid mass transfer theory and is derived from previous work (Kelleher and Fair, 1996; Peel, 1995, Peel *et al*. 1998). The liquid side mass transfer process across the packed bed of a RPB is shown in equation 2.40 (Kelleher and Fair 1996)

$$\pi(R_o^{\ 2} - R_i^{\ 2}) = \frac{L}{\rho_l h K_l a}\int_{x_i}^{x_o} \frac{dx}{x - x_e} \tag{2.40}$$

From equation 2.40, NTU (or the difficulty in separation) can be defined via equation 2.41

$$NTU = \int_{x_i}^{x_o} \frac{dx}{x - x_e} \tag{2.41}$$

Research conducted by Peel (1995) illustrated that the equilibrium constant (x_e) can be calculated by means of equation 2.42. This applies for dilute concentrations of gases in liquid for where Henry's law is applicable

$$x_e = \frac{L_m}{mG_m}(x - x_o) \tag{2.42}$$

The m term in equation 2.42 is the slope of the equilibrium line for D.O in water and is produced from equation 2.43 and is related to the Henry constant for oxygen

$$m = \frac{H}{P_T} \tag{2.43}$$

By means of equations 2.42 and 2.43, the NTU (equation 2.41) has been evaluated by Peel (1995) as equation 2.44

$$NTU = \left(\frac{1}{1 - \frac{L_m}{mG_m}}\right) \ln\left[\left(1 - \frac{L_m}{mG_m}\right)\left(\frac{x_i}{x_o}\right) + \frac{L_m}{mG_m}\right] \tag{2.44}$$

Equation 2.44 can be simplified due to the fact that the Henry constant is quite large (approx. 43,400 atm at 25^{o}C) (Liley *et al* 1984). As a result m achieves a rather large value, and equation 2.44 can be approximated to the form shown in equation 2.45 (Peel *et al* 1998)

$$NTU \approx \ln\left(\frac{x_i}{x_o}\right) = \ln\left(\frac{C_i}{C_o}\right) \tag{2.45}$$

From the basis of the NTU calculations, the $K_L a$ of the RPB can be determined, shown in equation 2.46

$$K_L a = \frac{NTU.L}{\rho_l h \pi (R_o^{\ 2} - R_i^{\ 2})} \tag{2.46}$$

2.4 Summary

The literature review presented in this chapter has focused on the principles of fermentation and how different parameters such as agitation and oxygen transfer can affect growth. It then focuses on the principles of oxygen transfer and how this can be enhanced using the goals of Process Intensification. Finally a review of rotating packed bed technology was undertaken, focusing on the operating principles of the technology, its performance in previous applications to a range of processes and the development of mathematical expressions for its mass transfer characterisation.

As noted previously there is not a great deal of literature that deals with the use of a HBR. with a fermentation system. One such paper that investigated the use of a similar type of reactor was used for a *Xanthomonas* sp. In this case however there was no packing used within the reactor, enhancement of the process was achieved simply by use of centripetal force alone (Yang *et al* 1996). The aim of this project is to build upon the studies started by Toogood (2005) and Ndlovu (2004) within the school and investigate the capabilities of a set of porous mesh impellers for their oxygen transfer capability and to examine whether they can sustain a microbial community with the BioFlo III reactor. Ultimately the packing used for the impellers will be implemented in the HBR whose performance in a fermentation process will then be investigated.

Chapter 3: Aims and Objectives

The purpose of this chapter is to introduce the aims and objectives of the research to be conducted. As noted in Chapter 1 the research to be conducted is based upon previous work carried out within the School of Chemical Engineering and Advanced Materials at Newcastle University. The present study builds and expands upon the earlier work, leading up to the development and performance evaluation of a newly fabricated HiGEE bioreactor (HBR).

3.1 Aims and Objectives of the project

The two main aims for the PhD project are:

(1) A comprehensive characterisation of a range of porous mesh impellers (knitted wire mesh, Declon mesh and fibre mesh) in a conventional STR and critical comparison of their oxygen transfer capability and performance in fermentation processes to a standard double Rushton turbine impeller.

(2) Characterisation and evaluation of a newly fabricated HBR which uses a selected porous packing for fermentation application.

In order for these aims to be achieved a number of objectives need to be accomplished as outlined below:

1. ***Mass transfer and power consumption characterisation of the porous mesh packing used as impellers within a Stirred Tank Reactor (STR)***

   Previous research made use of an 11 cm diameter set of porous mesh impellers which were also used in this work for benchmarking. The 11 cm diameter set was fabricated to allow the simulation of a rotating packed bed of material inside a STR. In addition, for the present study, a new 6 cm set of impellers were constructed to allow a direct comparison with the 6 cm diameter Rushton impeller. The oxygen transfer capability and power consumption of all impellers will be investigated in both air/water and air/50%water-50%glycerol medium under a range of aeration rates and agitation rates. Empirical correlations relating the volumetric mass transfer coefficient K_La to the variable parameters (P/V, Us, m/m_w) will be developed using regression analysis tools and these will be compared to available literature correlations where appropriate.

2. ***Measurement of bubble size and bubble size distributions in STR***

   To validate the transfer results obtained in point 1, mean bubble size and size distribution will be measured using each of the impellers tested under the same range

of conditions. Digital photographs will be taken and the images obtained analysed using ImageJ software.

3. ***Testing of capability of porous mesh packings to accelerate and sustain microbial growth in an aerobic fermentation system in STR***

   An *E.coli* K12 batch fermentation will be used as a simple fermentation system to investigate the effects of enhanced oxygen transfer on the microbial growth. In comparison to the previous work conducted, biomass concentration analysis is to be performed in a more rigorous manner alongside oxygen transfer and power consumption analysis of all impellers.

   A second fermentation with *P.putida* KT2442 will investigate the optimisation of the production of a biopolymer known as polyhydroxyalkanote (PHA) which has not been undertaken previously. For this fermentation a batch and fed-batch fermentation will be conducted, with octanoic acid used as the substrate for both fermentations. The assessment of PHA yield and reactor productivity will be an important measure of performance.

   For both fermentation systems biomass concentration will be determined by Optical Density (OD) and Dry Cell Weight (DCW). Total Viable Count (TVC) will also be assessed.

4. ***Commissioning and performance testing of a newly fabricated HBR for bioprocessing application***

   This will include:

   (a) A flooding study to determine operating limits for the gas and liquid flow rates in the reactor

   (b) A mass transfer characterisation study of the HBR to determine the level of oxygen transfer that can be achieved under given operating conditions of rotational speeds and gas and liquid flow rates with and without packing in the enclosed rotating chamber

   (c) A gas bubble size measurement experiments conducted with and without packing installed in the HBR

   (d) A fermentation study using *P.putida* KT2442 to produce PHA in the HBR operating in batch mode, with continuous external loop recycle. The results gained

from these fermentation experiments (biomass concentration, PHA yields etc.) will be compared to the counterpart experiments conducted in the STR.

3.2 Basis of Research:

As noted in Chapter 2, previous research has been conducted using the proposed mesh impellers in oxygen transfer and *E.coli* fermentation experiments in the STR. The purpose of this section is to highlight the improvements implemented in the current study in order to produce a more comprehensive and reliable data set for the impeller characterisation and *E.coli* fermentation experiments in the STR. These are listed as follows:

1. In the previous study conducted by Toogood (2005) the gas-liquid mass transfer performance of a set of 11 cm impellers were examined in water. Due to time constraints only the 11 cm knitted wire impeller was tested in higher viscosity medium. This research will aim to reproduce some of the experiments conducted, and also examine in detail the performance of 11 cm Declon and fibre mesh impellers in a range of media of varying viscosities.
2. In order to make a direct comparison to the Rushton impeller, a set of 6 cm mesh impellers will be manufactured and examined in terms of their oxygen transfer and power consumption alongside the 11 cm set as outlined in (1) above.
3. Power consumption will be measured in a more accurate manner by use of a torque meter positioned on the impeller shaft.
4. The oxygen transfer of the impellers will be calculated in a more robust manner by considering the impact of probe response on the results, and with the use of a more accurate D.O probe. The results (with probe response taken into account) will then be used to produce a more accurate linear regression analysis.
5. In order to investigate the theory that smaller oxygen bubbles are produced, a comprehensive bubble study will be undertaken with the aid of a digital camera. This has previously not been done.
6. For the fermentation runs, a chemically defined medium will be utilised in order to guarantee that each fermentation is consistent. This will also reduce the amount of antifoam needed. Alongside optical density readings, total viable count and dry cell weight analysis will be conducted (which had not been done previously). Oxygen transfer measurements will be conducted (when practical) at different stages during the fermentation at hours 2, 4, 6 for a total fermentation cycle of 8 hours.

Chapter 4: Experimental Methodology

This chapter provides detail on the experiments conducted. It will first focus on the initial experiments performed to characterise the porous packings in terms of their oxygen transfer capability, bubble size and power consumption, before investigating their cell growth capability in an *E.coli* K12 fermentation system. The chapter will then examine the methodology used for scale up of the *E.coli* K12 system, alongside the creation of a second fermentation system involving *P.putida* KT2442. Finally the hydrodynamic and transfer capability of the HBR reactor will be investigated, alongside its potential as an intensified bioreactor with use of the *P.putida* KT2442 fermentation system.

4.1 BioFlo III Reactor System

The initial mass transfer, bubble study, and *E.coli* K12 fermentation systems were all investigated within a BioFlo III reactor system (New Brunswick, N.J USA) shown in figure 4.1. The reactor is constructed of borosilicate glass and housed in the bioprocessing lab at CEAM within Newcastle University. A number of ports are available located on the top of the reactor for probes to be housed; ones which were not used were sealed and blanked off until required. The diameter (D_T) of the reactor had been measured as 18 cm. To ensure the vessel was well mixed during each run a set of four baffles (diameter of 1.5 cm) were installed around the edge of the reactor. The Dissolved Oxygen (DO) of the reactor could be monitored via use of a 12 mm DO probe (InPro® 6820 Mettler Toledo Switzerland) which was placed through the top of the reactor. The probe response time was noted for the probe and is discussed in Chapter 5 (c.f. section 5.2). Feedback controllers allowed for control of temperature, and agitation. An airflow meter (on the main control panel) allowed regulation of the air supply into the reactor. Four motors below the main control panel are used to control antifoam, acid and base addition, and substrate feeding. Compressed gases are distributed by a 4 hole ring sparger (each hole around 1.0 mm in diameter). The sparger itself was placed 2 cm below the lowest impeller. To characterise power consumption a torque meter (Dantum Electronics UK) was housed on the outside part of the impeller shaft which was able to relay data in regards to the torque and power consumed to a laptop pc. Readings of temperature, agitation rate, and DO were sent via means of a Pico data recorder to a PC for data logging purposes.

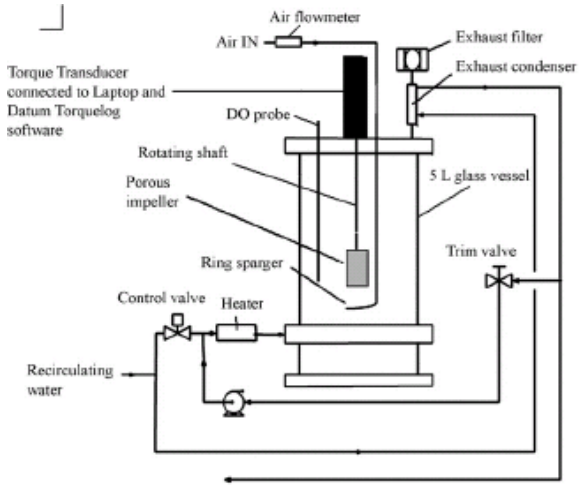

Figure 4.1a: Schematic of the BioFlo III Reactor

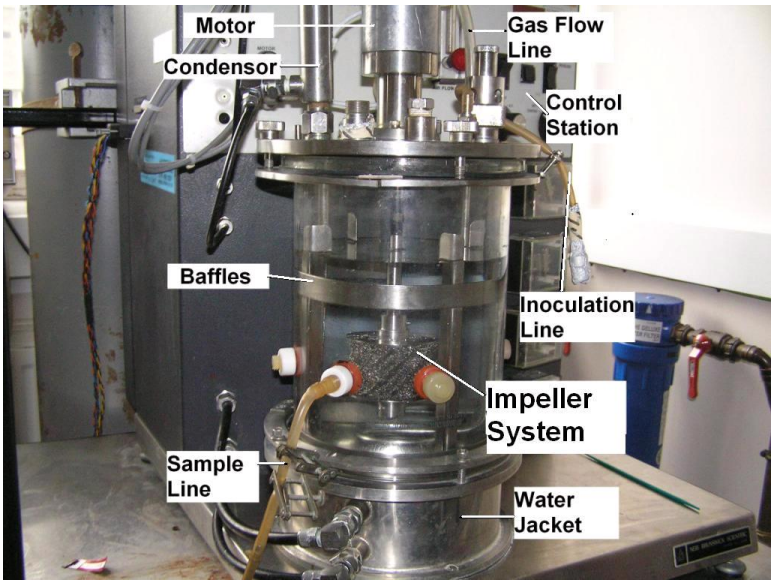

Figure 4.1b: Picture of the BioFlo III Reactor system

4.1.1 Initial Porous Packing Characterisation Studies

The oxygen transfer and power consumption of different types of porous packings were investigated (shown figure 4.2). The Knitted Wire mesh impeller (A) was manufactured from stainless steel, and wound very tightly together to form the basis of the impeller. The Fibre Mesh impeller (B) was manufactured from compacted fibre mesh, and the Declon® mesh impellers (C) were manufactured from PVC rigidised polyurethane foam. Two sets of impellers have been characterised. Firstly a 6 cm impeller was manufactured, this allowed direct comparison between the new porous packings and a standard Rushton impeller. A second set of 11 cm impellers were also manufactured. This was to allow the simulation of a

rotating packed bed of porous packing to occur within a STR and therefore this breached the normal guidelines for the diameter of impellers to the diameter of the reactor.

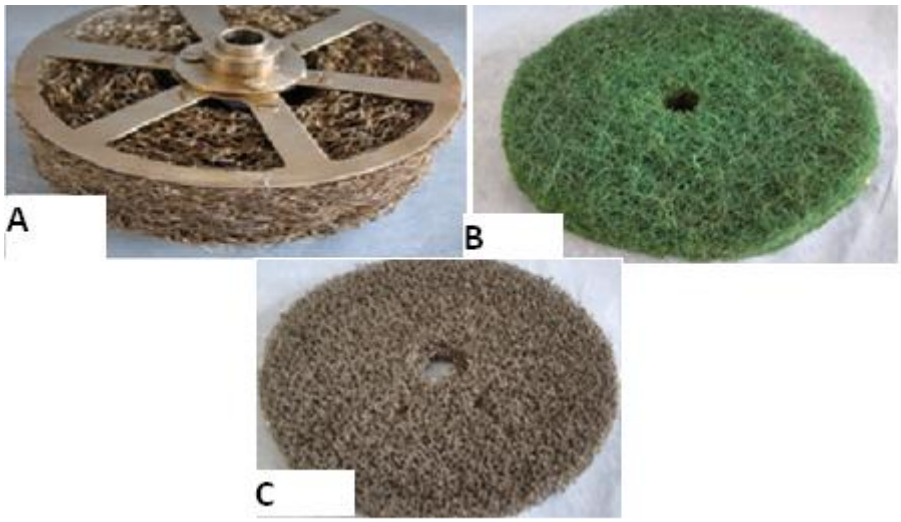

Figure 4.2: Porous mesh impellers used in the present study

The oxygen transfer of the system was characterised by use of the static gassing out method (described in section 2.2.3). Firstly the DO probe was calibrated by use of a two point calibration. This occurred by vigorous sparging of the liquid with nitrogen which scrubbed any dissolved oxygen in the liquid. Once the reading was stable this was then set as the zero point. The second calibration point was then taken by vigorous sparging with compressed air until a stable reading was achieved. This was then set as the 100 % saturated point. The experiments were conducted in a similar manner, the DO was reduced to zero as done previously, before the agitation and airflow was set to the desired parameters. The data logger was then switched on, and the gas supply changed to compressed air. The data logger then recorded the increase in dissolved (via the DO probe) within the liquid (in this case deionised water). As noted previously the Pico data logger recorded temperature, agitation rate (rpm) and DO levels every 10 seconds. The readings were then sent to a Microsoft Excel spreadsheet which were then analysed to produce the final K_La results for each experiment conducted. To facilitate an unbiased study a central composite experimental design was produced in Minitab. Factors studied in the experiments including the impeller (Rushton and the various packings), agitation rate (200, 500, 1000 rpm), airflow rate (0.2, 0.6, and 1.0 vvm, equivalent to 1, 3, and 5 l min^{-1}), and viscosity (pure water at 0.7 mNs m^{-2} and a 50 % water-50 % glycerol mixture by volume having a viscosity of 4.7 mNs m^{-2}).

Power consumption of the Rushton impeller and the porous packings were measured using the torque meter as previously described. As the meter was placed directly onto the impeller shaft it was able to measure the exact amount of power that was being pulled by the impeller system. The data logger provided with the meter was connected to a laptop P.C., which was able to record power consumption (kw), torque (Nm), and agitation speed (rpm). For analytical purposes later on, power consumption was converted to (P/V) W m^{-3} when analysed using Microsoft Excel.

4.1.2 Air Bubble Study

In the initial mass transfer experiments it had been postulated that the reason for the enhanced oxygen transfer was because of decreased bubble sizes being produced by the packing material used. In order to see if this hypothesis was correct, a bubble study was designed in order to properly test this theory. Digital photography was used in order to calculate the mean bubble size of each impeller under various different conditions. The camera used was a Sony™ 8.1 megapixel camera, which allowed individual bubbles in the reactor to be noted. For each run multiple photographs were taken, and the photograph with the clearest image taken for analysis. For each experiment the same area of the reactor was photographed to allow for continuity and repeatability amongst all the photographs taken. The images were then taken from the camera via a USB lead to a laptop PC. Analysis of the photographs was performed with Image J (a piece of freeware software). To analyse an image using ImageJ, a scale first needed to be established. This was achieved by measuring a known distance between two points, and subtracting the number of pixels between the two x points. For the BioFlo III reactor, the baffle (present in all pictures) was used as the marker. Once the number of pixels for this distance was known, this was then set up using the software. The procedure is shown in section A3 of Appendix A.

Once the scale had been set, measurements of area and circularity were chosen to be measured. For each photograph a random selection of 30 bubbles from across the picture were analysed. Where there were less than 30 bubbles in the photograph, all the bubbles were analysed. Once the results had been gathered by the software, they were then transferred to the appropriate spread sheet in Microsoft Excel™. At this point the bubble area (assuming that every bubble was a sphere) was converted to diameter by means of equation 4.1.

$$B_D = \sqrt{\frac{4A_b}{\pi}} \qquad (4.1)$$

The results collected the mean bubble diameter and the mean bubble circularity. A histogram showing the distribution of bubble sizes for each experiment was plotted, alongside graphs showing the change in bubble size alongside agitation rate and airflow rate. This process was repeated for all the experiments conducted. For the bubble study the effect of viscosity was examined by use of the same fluids used for the initial mass transfer experiments. As noted in section 4.1.2 although only a minimal amount of DF 204 antifoam was used, this would still affect the oxygen transfer in the system as surfactants will alter the surface tension of the fluid they are placed into. As a result to investigate DF 204 effect on oxygen transfer, a bubble study was carried out with the SMS media with/and without the antifoam present. At the same time density, viscosity and surface tension readings were taken for all fluids used in the bubble study.

4.1.3 E.coli K12 Fermentation Study

The oxygen transfer capability of the porous packings was further tested with a live fermentation system, in this case the organism chosen was *E.coli* K12. The organism was chosen for its robust and reproducible growth seen in previous research (Ndlovu 2004).

Spitzens Minimal Medium (SMS) was chosen based on recommendations from industry (Dewer S, Personal communication) and academia (Harwood C, Personal communication). The medium's composition was: Ammonium Chloride (2 g l^{-1}), Dipotassium Hydrogen Phosphate (14 g l^{-1}), Potassium Hydrogen Phosphate (6 g l^{-1}), Sodium Citrate (1g l^{-1}), and $MgSO_4.7H_2O$ (0.2 g l^{-1}). The medium was sterilised at 121 ^oC and after cooling the carbon source (1.5 ml l^{-1} 50 % glucose stock), C.A.S. amino acids and a Trace Element Solution (TES) (both 1 ml l^{-1}) were added to the medium to aid growth. The medium was aseptically transferred into multiple sterile shake flasks (250 ml) in 40 ml aliquots. One colony of the K12 culture was utilised to inoculate each 40 ml flask. The flasks were then placed into an orbital shaker at 37 ^oC/120 rpm for 8 hours whilst growth was observed from off-line OD measurements of samples taken every hour.

A shaker flask study was undertaken to choose an appropriate medium and to ensure that reproducible results could be gained from the system. The experiments were carried out in 250 ml shaker flasks. To the media systems studied one colony of *E.coli* was used to inoculate the flask, which was then maintained in an orbital shaker at 37 ^{o}C/120 rpm. OD readings were taken every hour using a UV-Vis spectrophotometer (Jenway 6105 UK). These were grown as 8 hour cultures. A further set of flasks set under the same conditions were left as a 12 hour overnight culture (ONC), with OD readings taken at the beginning and end of the run.

Once the fermentation system had been optimised the system was then scaled up to perform experiments with the BioFlo III reactor system based upon protocols used for a previous study (Ndlovu 2004). In these experiments the oxygen transfer performance and the ability of the porous packings to support microbial growth was tested. The Fibre and Declon mesh packings could not be used in the fermentation experiments as they could not stand up to the high temperature sterilisation required, and therefore the Rushton and knitted wire impellers were used in this study. The torque meter was utilised to report on the power consumed by each impeller during each run.

The study was based on a previous series of experiments which have been published separately (Boodhoo *et al.*, 2008). A central composite experimental design was implemented. Factors studied included agitation rate (200, 300, 400 rpm), airflow rate (1.0, 1.25, and 1.5 vvm) and impeller design. The chosen medium was used at a working volume of 4 L to allow extra headroom for foaming to occur. As with the shaker flask study 1 colony of *E.coli* K12 was used to inoculate a shaker flask with 40 ml of medium. This was then placed in the orbital shaker at 37 ^{o}C/120 rpm and left for 12 hours to grow. The BioFlo III reactor was charged with 4 L of medium, the appropriate impeller placed on the central shaft, and the vessel lid placed on. All the probes were then added, the reactor then sterilised in an autoclave at 121 ^{o}C. In the morning the reactor was taken from the autoclave, and re attached to the control station. Once the temperature of the media had reached 35 ^{o}C, the DO probe was calibrated using the static gassing out method. The reactor was then set at the desired agitation and airflow rate for the run, and the data logger switched on. Once this was complete, the inoculum was then tested for growth via OD sample, and inoculated into the BioFlo III reactor. The reactor was then left for 8 hours to allow the culture to grow. During the run OD, Total Viable Count (TVC), and Dry Cell Weight (DCW) readings were taken

every hour. The OD readings were taken using the same spectrophotometer that had been used for the shaker flask study. The TVC count analysis was undertaken by using 1.0 ml of culture and used a serial dilution (with buffer solution). Selected samples of the dilution were then plated out onto SMS plates, and left to grow for 24 hours in an incubator at 37 ^{o}C. The dry cell weight analysis was conducted by taking 1 ml of sample which was placed in pre-weighed micro-centrifuge tubes and centrifuged at 13000 rpm for 10 minutes. The supernatant produced was then discarded, and the micro-centrifuge tubes placed in an incubator at 65^{o}C until the weight had stabilised (typically 1.5 days). Once the fermentation had reached 8 hours, the reactor was shut down, and placed into the autoclave for waste sterilisation. This was once again carried out at 121 ^{o}C. Once the main cycle was completed then the reactor and impeller were thoroughly washed through with water, and then prepared for its next run with a fresh batch of medium. Analysis of the viable counts and dry cell weight occurred the next day, and placed alongside the OD readings taken in a Microsoft Excel spread sheet for analysis.

4.1.4 P.putida KT2442 Batch Fermentation System

A second fermentation system was investigated within the BioFlo III reactor. In this instance a *P.putida* KT2442 fermentation was chosen to investigate the effect the knitted wire and Rushton impellers would have on the oxygen transfer, biomass concentration and PHA produced. The same Rushton and knitted wire impellers were used in this study as had been used in the *E.coli* K12 fermentation study. The organism used in the study was supplied by Dr Marta Tortajada (Biopolis, Spain), the strain had been optimised for growth on M63 medium. The medium was comprised of 13.6 g of KH_2PO_4 l^{-1}, 0.2 g $(NH_4)_2SO_4$ l^{-1} and 0.5 mg $FeSO_4 \cdot 7H_2O$ l^{-1}. This was supplemented with 14 ml Trace Element Solution.

A shaker flask study was first established to ensure that growth would occur within the flasks. For this the procedure described by Dr Marta Tortajada was followed (Tortajada *et al.* 2008). This involved inoculating 1 colony of *P.putida* KT2442 into 10 ml of LB culture medium. This was placed in a shaker flask and placed in an orbital shaker for 8 hours at 30 ^{o}C/220 rpm. After the 8 hours the 10 ml of inoculum was then placed in 200 ml of LB and left to grow overnight. After 18 hours a sample of this was then placed into the M63 medium for 24 hours. Growth of the various different cultures was monitored by OD readings taken throughout the run of the experiment by a UV-Vis spectrophotometer (Jenway 6105 UK).

Once the shaker flask study had confirmed that growth would occur, the system was scaled up to include experiments within the BioFlo III reactor. For this step the 200 ml M63 flask was replaced with a sample of the 200 ml LB culture going into 4 l of M63 media which had been charged into the BioFlo III reactor and sterilised in the autoclave.

4.1.5 P.putida KT2442 Fed Batch Fermentation System

A second *P.putida* fermentation system was established to investigate the potential to run a longer fed batch type system with the knitted wire impellers. The first 24 hours of growth proceeded as section 4.1.4 but with Octanoic acid used as the carbon source at a level of 3 ml l^{-1}. After 24 hours a second pulse of octanoic acid was fed into the reactor, and fed batch operations commenced. After discussion with Dr Tortajada, the octanoic acid feed was set up to give a μ of around 0.2-0.25 h^{-1} (at 0.8 ml $^{l-1}$ per hour added).

Samples were taken at regular intervals, with phase microscopy images taken at hour 48. The sample of the medium for DSP was taken at hour 48 also (see section 4.1.6). The working volume was maintained at 4 l, with 1M HCl/1M NaOH used to control pH at 7.0.

4.1.6 PHA Analysis

Analysis of the final fermentation medium occured in two distinct ways. Firstly phase contrast microscopy was used to image a small sample of medium taken from the reactor. This confirmed whether PHA had accumlated within the cells. The microscope was used at 100x magnification.

Extraction of PHA occured in conjunction with The Centre for Process Innovation (C.P.I). For this 1 l of fermentation medium was centifiuged DOwn to a pellet which was subsequently freeze dried. The pellet was taken to C.P.I., where homogenisation and extraction with chloroform allowded any PHA present to be extracted from the cell. After a day of drying, the sample was weighed and converted to % yield by use of the dry cell weight value obtained during the fermentation.

4.2 HiGEE Bioreactor (HBR)

A newly fabricated HBR bioreactor system was used to intensify some of the experiments so far carried out in the BioFlo III reactor. The reactor (shown figure 4.3) was manufactured from 316 L stainless steel, the rotor of the HBR having a calculated volume of approximately 9.73 l. Rotational speeds of between 25-1500 rpm are achievable with the reactor. The packing in the reactor was based on the material used for the knitted wire impeller for the BioFlo reactor. Multiple layers of knitted wire mesh (stainless steel) packing (Knitmesh Technologies, UK) (95% voidage with a surface area per unit volume of 1300 m^2/m^3) was rolled tightly together. On rolling, the material had an outer diameter of 244 mm, an inner diameter of 150 mm and an axial depth of 134 mm. A view of the rotor complete with packing is shown in Figure 4.3b. Fluid was pumped into the reactor via a peristaltic pump (Watson Marlow 505S) at flow rates of around 0.4-1.4 l min^{-1}. The fluid was introduced into the reactor through a rotary union on the central shaft. Injection into the reactor occurred via 4 distributors each having 28 holes (diameter of 1mm). The liquid injectors were spaced evenly at a radial distance of 25 mm from the centre of the rotor. After leaving the injectors the liquid was flung outwards by the action of the centripetal force exiting the reactor environment at its periphery through a collector.

Compressed gas (sterile air for fermentation or nitrogen for the mass transfer experiments) was injected through six injectors (30 holes, diameter of 0.2 mm) stationed on the outer edge of the rotor periphery. DO and pH probes (Mettler Toledo. UK) were placed downstream in a sample vessel. A one pass system was used for the oxygen transfer experiments so that the liquid was passed to a drain after one pass through the rotor unit. For the fermentation experiments after passing through the rotor, the liquid was instead allowed to re-circulate through the external recycle loop, This is shown in Figure 4.3a. A Perspex lid was initially present on top of the reactor to allow for visual observation of gas bubbles formed and the onset of flooding conditions. Prior to the fermentation experiments the lid was replaced by a stainless steel version. The slip ring assembly allowed for 4 ‘k’ type thermocouples to be positioned within the packing at different radial positions and axial depths allowing monitoring of the temperature within the reactor.

Initial mass transfer experiments conducted with the reactor found the highest NTU was 0.98 which was deemed to be much lower than expected based on results than had been published

previously (Peel 1995). This was attributed to contamination of the oxygen-stripped liquid product exiting the rotor by air entrained through the gap between the shaft and the edge of the collector. As the reactor had been efficient in stripping a large amount of oxygen from the water, oxygen in the air leak into the collector was instantly absorbed by the water, resulting in misleading DO concentrations being recorded downstream (see Chapter 5, section 5.5). Provision was therefore made to include a nitrogen blanket around the gap near the edge of the collector. The nitrogen blanket flow rate was kept constant at 4 l min^{-1} during operation.

(I)

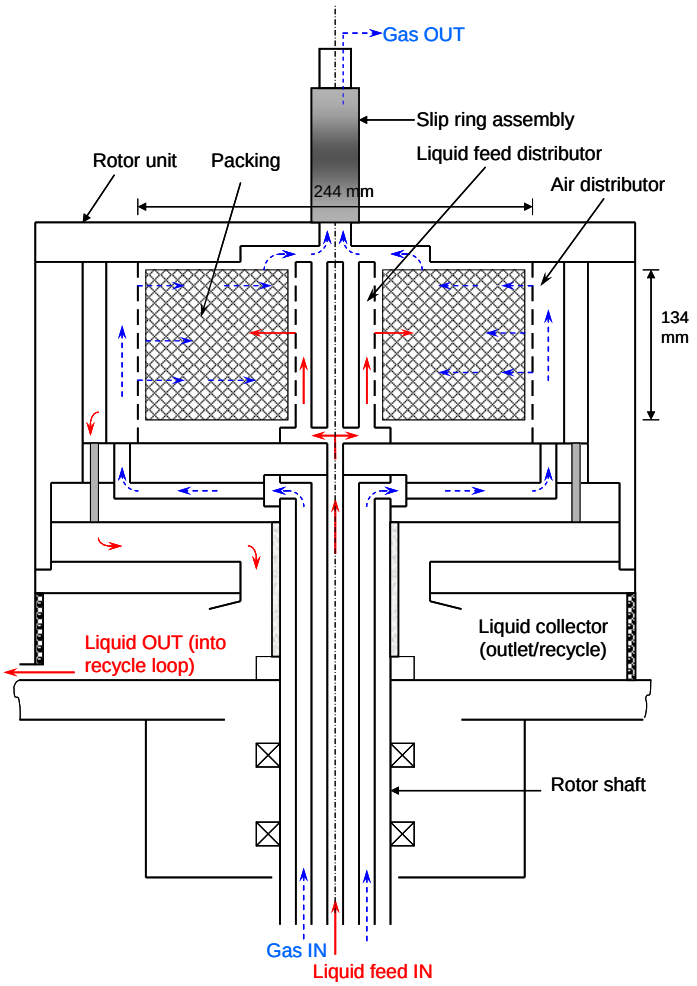

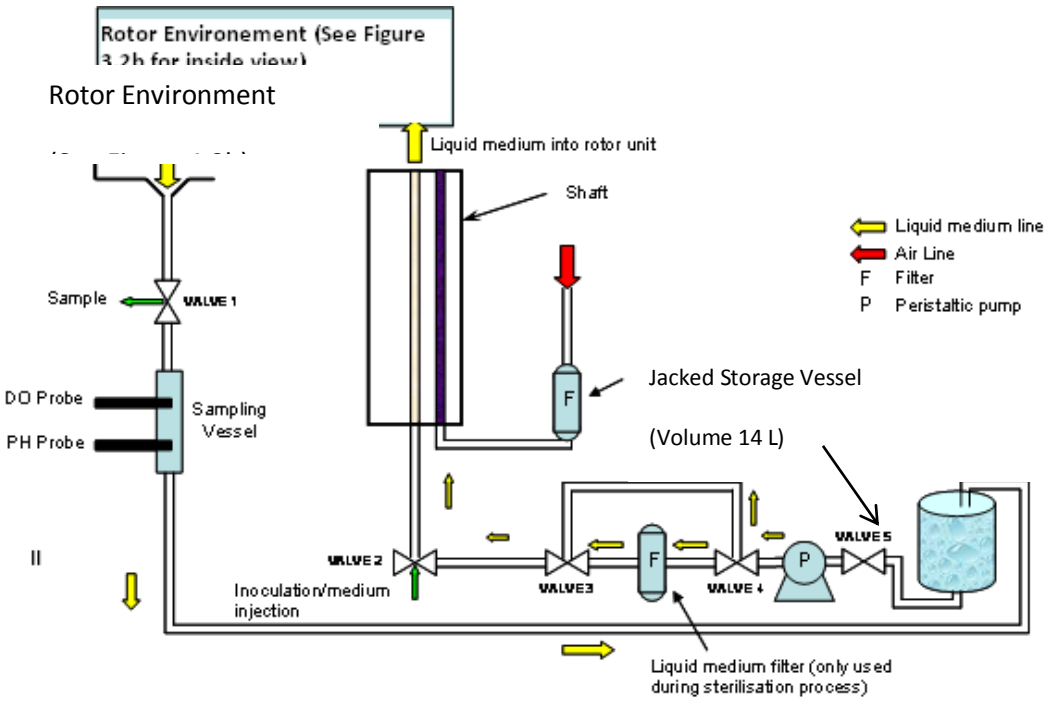

(II)

Figure 4.3a**:** Schematics of the newly fabricated HBR Bioreactor with (I) showing an overall schematic and (II) showing the liquid recirculation loop (Residence time for storage jacket based on flow rate of 1.4 l min^{-1})

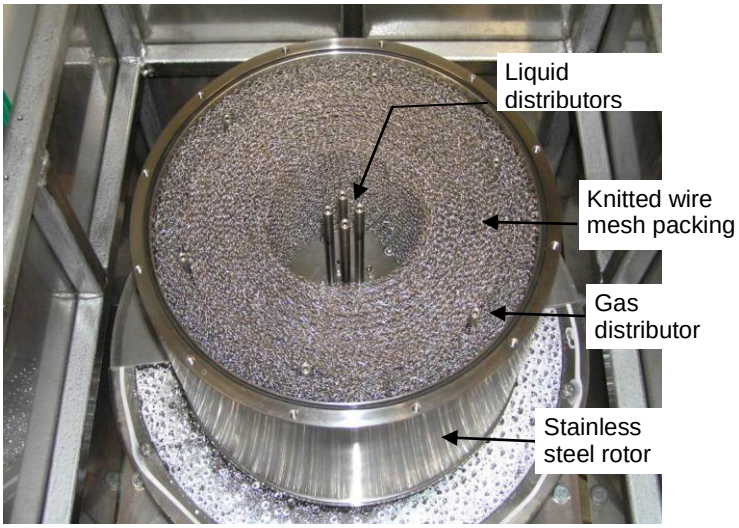

Figure 4.3b: View of the packing material inside the rotor chamber

4.2.1. Flooding Study

A comprehensive series of experiments focused on investigating the flooding and hydrodynamic characteristics of the reactor. The flooding experiments were based upon those conducted by M Jassim (2002). Firstly the flooding characteristics of the reactor were studied, as this set future conditions to be performed for transfer and fermentation experiments. Liquid flow rate and rotational speed were kept constant whilst the gas flow was increased from an initial value of 5 l min^{-1} and incremented in set intervals of 2 l min^{-1}. When excess splash of the liquid was observed within the eye of the rotor this was noted as the flooding point for the conditions set. Following this a new liquid flow rate was chosen with the same rotational speed. Flooding experiments were conducted for a wide range of rotational speeds and liquid flow rates in order to build up a robust overall picture of flooding conditions within the HBR system. Analysis of the experiments was then conducted in Microsoft Excel.

4.2.2. Nitrogen Bubble Study

A bubble study was conducted with the HBR reactor to investigate what bubble size could be produced by the system both with and without packing. For these experiments the reactor was operated with deionised water and nitrogen gas on a recycling loop. 14 l of fresh deionised water was measured into the holding tank so an exact amount of water being circulated around the system was known. One area of the reactor was used to take digital photographs so that the same area was taken for every experiment. A Phantom Miro 4 high speed digital camera (EPSRC Instrument Pool) was used for the study, several pictures were taken and the best one chosen to be analysed. Several conditions of rotation speed, airflow rate were chosen in advance to be studied, which were then placed into a central composite design in Minitab™. As with the bubble study for the BioFlo reactor, Image J and Microsoft Excel were used to analyse the bubbles data size and circularity. Experiments were conducted with the reactor both with and without the packing material.

Analysis of the experiments focused on mean bubble diameter and circularity. As with the bubble study in the BioFlo system, a histogram was plotted for each bubble experiment. The mean figures for each experiment were plotted on appropriate graphs against rotational speed, airflow rate, and liquid flow rate. A second set of graphs were then plotted which compared the bubble size produced in the new HBR system (with and without packing) compared to the BioFlo results.

4.2.3. Transfer Experiments

A series of experiments was performed with the HBR reactor to characterise the transfer potential of the reactor with packing installed. To facilitate this, deionised water was de aerated with nitrogen in a one pass system. The reactor was allowed to fill and the conditions set for the run as needed. Two DO probes were used to monitor oxygen levels in the water, one placed in the holding vessel supplying the reactor (InPro 6800 connected to a M700 monitor on loan from Mettler Toledo UK) and one in the sampling vessel downstream from the collector (InPro 6820 connected to a M300 monitor). This allowed real time monitoring of the oxygen content as the water passed through the reactor. Both DO probes were calibrated in air, and this reading noted when stabilised. Both probes were then placed in the holding vessel to note the DO value. This was to ensure that both probes were giving similar values which were then recorded. Once this had been established the 6280 DO probe was placed in the sampling vessel whilst the 6800 DO probe was left in the holding tank.

Two canisters of nitrogen gas were used during the experiments (as opposed to one during the previous flooding and bubble study). As per the previous experiments one canister was used to de-aerate the water via the gas injectors in the rotor. The second canister was used to supply a nitrogen blanket around the collector to prevent oxygen from the atmosphere being sucked into the collector during an experiment, thereby affecting DO readings. A fixed flow rate of 4 l min^{-1} was set for the blanket. Parameters set for the transfer experiments were based on the ones found in the flooding experiments that were below the flooding line plotted.

4.2.4. *P.putida* KT2442 Batch Fermentation Experiments

As with the BioFlo III system, a *P.putida* KT2442 fermentation was set up within the HBR reactor to produce PHA. In this instance the experiments had two aims, firstly to establish that the HBR could be used as a bioreactor, and secondly that the fermentation system could be intensified in the HBR system.

As with the BioFlo III system, M63 medium was used in the main reactor whilst LB media was used for the upstream processing elements. Preceding each run the reactor was chemically sterilised with 1 % Sodium Hypochlorite to ensure that no growth from unwanted organisms would occur during the experiment. After sterilisation with Sodium Hypochlorite the system was rinsed out with freshly sterilised deionised water to avoid contamination of

the system with the Sodium Hypochlorite. Once complete, freshly sterilised M63 medium was placed into the holding vessel, which was then allowed to re-circulate around the reactor. With no organisms in place, the media was required to pass through filters to ensure that no organisms were present. As the media re-circulates through the reactor, air is pushed through the injectors in order to saturate the media ready for the experiment. This process took around an hour to complete. The temperature of the media was kept constant at 30 ^{o}C by use of a circulating water bath which heated the media contents whilst it was in the holding vessel. Digital thermocouples (both in the rotor and the holding vessel) were used to note the temperature of the system throughout the run. A DO probe (InPro 6820, Mettler Toledo Switzerland) connected to the M300 meter was used to note DO values during the fermentation, which was sent to a USB data logger. In the same sample vessel alongside the DO probe a pH probe was used to monitor the pH of the system. As the pH needed to be kept at 7.0, a small flask of acid (1 M HCl) and base (1 M NaOH) was connected to the reactor. The meter connected to the pH probe monitored the pH throughout the run, with the values recorded to a USB data logger.

Once the media was saturated with oxygen from the air supply, the filters were then by-passed and the inoculum added from the shaker flask. The reactor was then run for 24 hours with OD and dry cell weight analysis being conducted throughout the experiment. Once the experiment was complete the spent media was then sterilised and the reactor cleaned and sterilised with chemical media ready for the next experimental run. The sterilisation also includes the tips for the pH and DO probes.

At the end of each fermentation cycle, 1 litre of medium was used for DSP analysis and phase contrast microscopy (see section 4.1.6)

Chapter 5: Experimental Results and Analysis-Mass Transfer Characterisation

This chapter outlines the experiments conducted initially for both the BioFlo III and HiGEE Bioreactor (HBR) systems. The chapter reports on the experiments conducted in the BioFlo III, concentrating on the principal transfer and bubble study results produced with a range of porous packing materials used as impellers (Knitted Wire mesh, Declon and Fibre mesh packings), benchmarked against the standard double Rushton impeller in a range of liquid media. The focus of the chapter then shifts to the hydrodynamic experiments performed with the newly fabricated HBR where the results produced from the flooding, bubble, and oxygen stripping experiments are presented. For all the experiments performed, the results are discussed in light of data that has been published in previous work. For the experiments conducted with the porous mesh impellers, the results are discussed with reference to previous work conducted within the school (Toogood 2005)

5.1 Dissolved Oxygen (DO) Probe Response

The DO probe response time can be an important parameter to consider when measuring K_La. If the probe has a much faster response time than the mass transfer time constant t_m (where $t_m = 1/K_La$), then the effect of the probe response can be neglected and the simplified equation (expressed in equation 5.1a below) for the static gassing out method as described in Chapter 2, section 2.2.3 can be used (Boodhoo *et al* 2008).

In the present study, the response time of the probe (τ_p) was noted as 35 s (at 35^oC), which produces a probe sensitivity (κ_p) of 0.0029 s^{-1} (where $\kappa_p = 1/ \tau_p$). Based on the previous research conducted (Toogood 2005), the value of K_La is expected to be of the same order of magnitude as the probe sensitivity, which will likely mean there is a significant delay in DO measurement due to the slow response of the DO probe. To ensure that the transfer results obtained are as accurate a reflection as possible, the response time of the DO probe has been accounted for in this study by modifying the equation (5.1 a) with a first order probe response used in previous studies (Badino *et al* 2000, Lamping *et al* 2003). The resulting modified expression is shown in equation (5.1 b). On integration of equation (5.1b), appropriate substitution of integral limits and rearrangement, equation (5.1 c) is obtained which allows evaluation of $_{tm}$ and therefore K_La (Boodhoo *et al* 2008).

$$\frac{dC_L}{dt} = K_L a(C^* - C_L) \tag{5.1a}$$

$$\frac{dC_P}{dt} = \frac{1}{\tau_P}(C_L - C_P) \tag{5.1b}$$

$$C_P = \frac{1}{t_m - \tau_P}[t_m \exp(\frac{-t}{t_m}) - \tau_P \exp(\frac{-t}{\tau_P})] \tag{5.1c}$$

5.2 Oxygen Transfer Capability of the Porous Packings

The transfer capability of the porous packings was examined as described previously (c.f. section 4.1.1 of Chapter 4). The results outlined are for the initial air/water and air/water-glycerol systems studied.

5.2.1 Air/Water Results

5.2.1.1 Results and Discussion

The transfer capability of the 6 and 11 cm porous mesh impellers are contrasted against that of the Rushton impellers. As noted previously, the two Rushton impellers were placed 6 cm apart along the impeller shaft, whilst the packing for the porous mesh impellers occupied this same length to ensure consistency in the experiments. Figures 5.1 (a and b) illustrate the effect of agitation for all impellers studied.

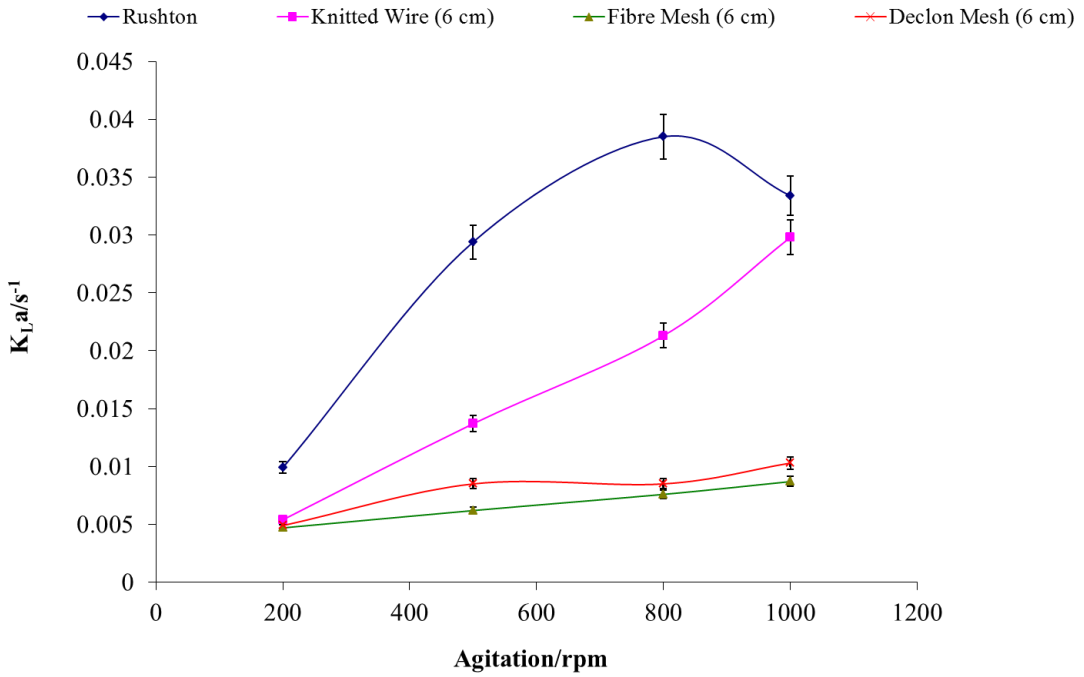

Figure 5.1a: The effect of agitation rate on K_La results in the Air/Water System at a constant air flow rate of 1.0 vvm (≡ 5 l min^{-1}) for the 6 cm diameter impellers

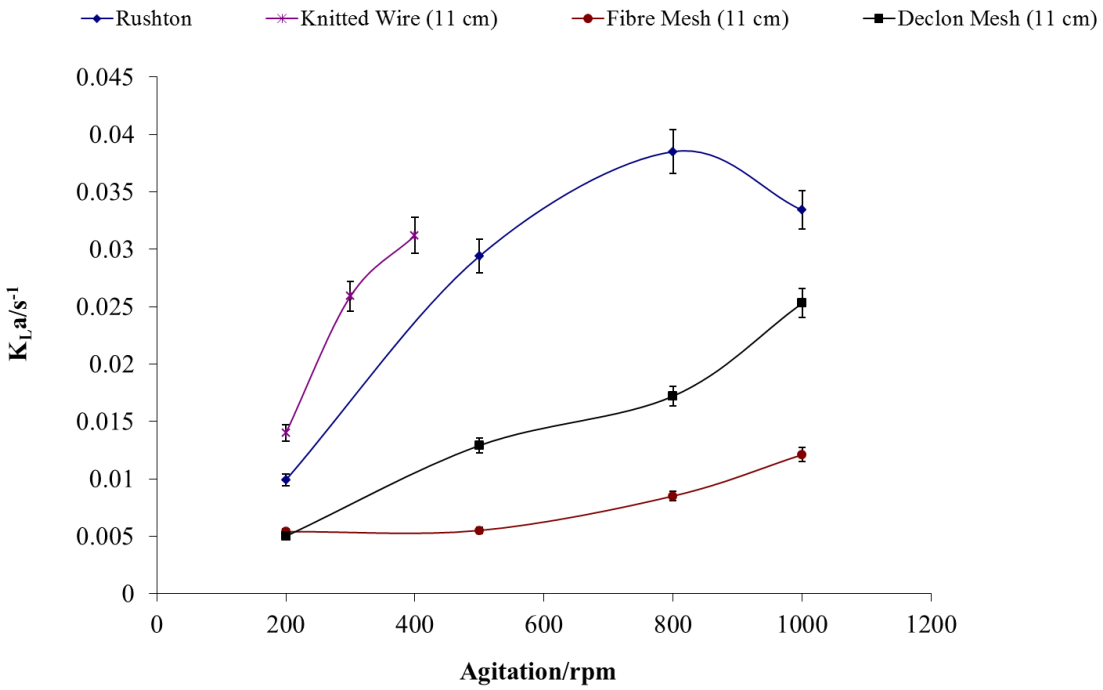

Figure 5.1b: The effect of agitation rate on K_La results in the Air/Water System at a constant air flow rate of 1.0 vvm (≡ 5 l min^{-1}) for the 11 cm diameter porous mesh and 6 cm diameter Rushton impellers

The 6 cm Rushton impeller produced the highest K_La at 0.0385 s^{-1} (800 rpm), whilst for the porous mesh impellers a K_La value of 0.0312 s^{-1} was recorded for the 11 cm Knitted Wire Impeller (400 rpm). The increase in agitation is noted to have caused an increase the value of K_La for all impellers studied. Increased agitation results in increased turbulence, and therefore better mixing and faster mass transfer across the gas and liquid phase boundary (Buwa *et al* 2006). The cause for the increase in K_La is due to a decrease in the average bubble diameter within the system. The decrease in bubble diameter is brought about by the increasing shearing action which is experienced by the air bubbles in the reactor. For impellers incorporating blades (such as the Rushton design) air bubbles are shredded by the tips of these blades, whereas for the mesh impellers the bubbles are shredded by passing through the packing structure itself. Regardless of the method of shearing, smaller bubbles have an enhanced surface area available for transfer to occur. Enhancement of K_La by increasing agitation rate has been documented in previous research. For instance, Chen *et al* (1999) performed a series of experiments with single and dual impellers during which it was noted that increased agitation (or increasing power as noted by the authors) led to an increase in the value of K_La observed.

The diameter of the impellers has been noted to make a difference to the value of K_La observed. Figure 5.2 notes the values obtained for the Fibre Mesh impellers for a constant airflow rate of 1.0 vvm

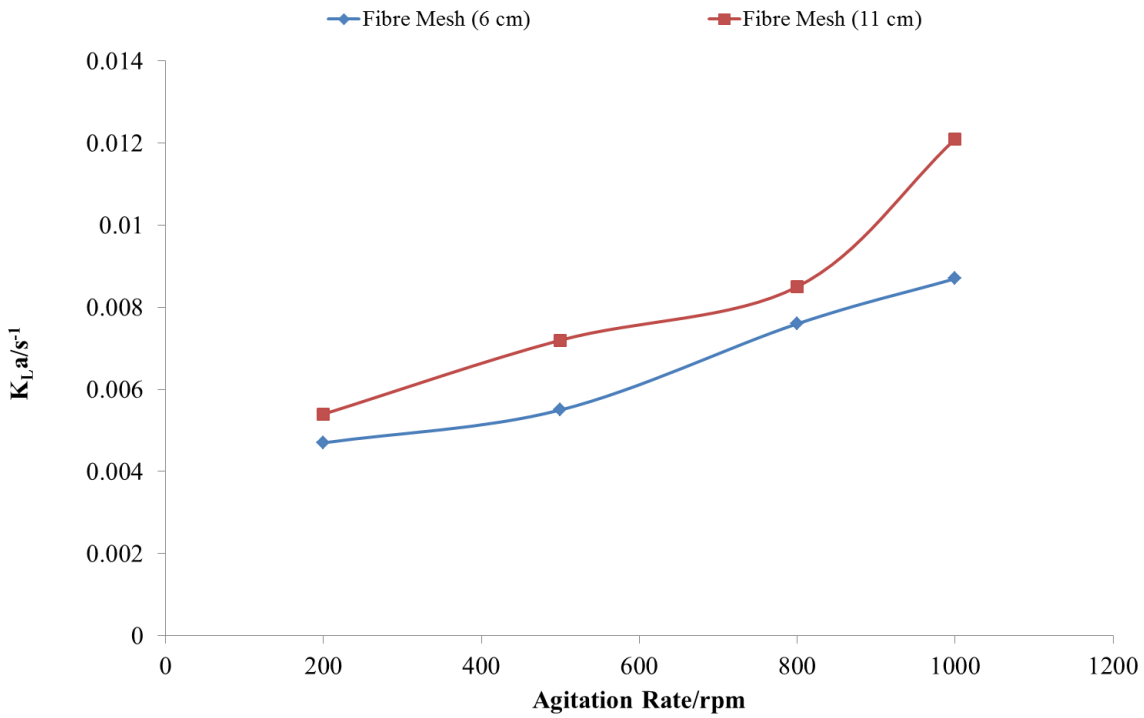

Figure 5.2: The effect of impeller diameter on the value of $K_L a$ observed. The figure illustrates the values obtained for the Fibre Mesh impellers (6 and 11 cm) in the Air/Water system for a constant airflow rate of 1.0 vvm

Figure 5.2 notes that the 11 cm Fibre Mesh impeller produces the higher $K_L a$ values compared to the 6 cm impeller. This is believed to be due to the interaction between the air stream and the impeller. For the porous mesh impellers the air stream rises straight from the sparger and through the tightly packed material of the impeller. For the 6 cm impellers a small percentage of the air bubbles may be missed by the impeller and therefore not sheared down to a smaller size. The 11 cm impellers occupy a much larger space within the reactor and therefore catch all the air bubbles coming from the sparger. This results in a larger $K_L a$ value being observed. This observation has been noted for all the porous mesh impellers studied. Nikakhtari *et al* (2005A) noted that when packing was installed in the riser section of an airflow fermenter (the packing filling the full width of the riser section) the values of $K_L a$ were noted to increase as a result (Nikakhtari *et al* 2005A, Nikakhtari *et al* 2005B)

Power draw is an important consideration (Ascanio *et al* 1994), illustrating how efficient each impeller's transfer capability is. The vast majority of research papers investigating mass transfer illustrate the effect of power consumption on the value of $K_L a$ as opposed to agitation rate. The use of a torque meter has been reviewed in other published literature (Ascanio *et al*

1994, Tschentscher *et al* 2009). As a result figures 5.1a and 5.1b have been replotted to illustrate the effect of power consumption on the value of K_La which are noted in figures 5.3a and 5.3b

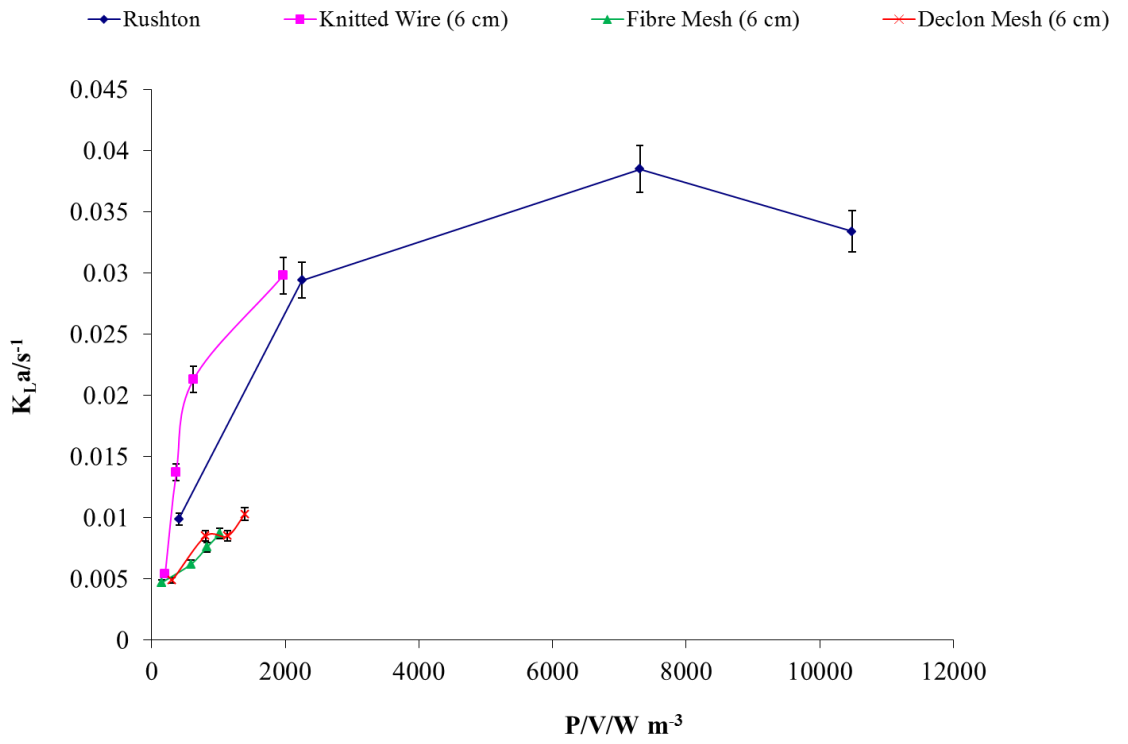

Figure 5.3a: The effect of power consumption (P/V) on K_La results in the Air/Water System at a constant air flow rate of 1.0 vvm (≡ 5 l min^{-1}) for the 6 cm diameter impellers

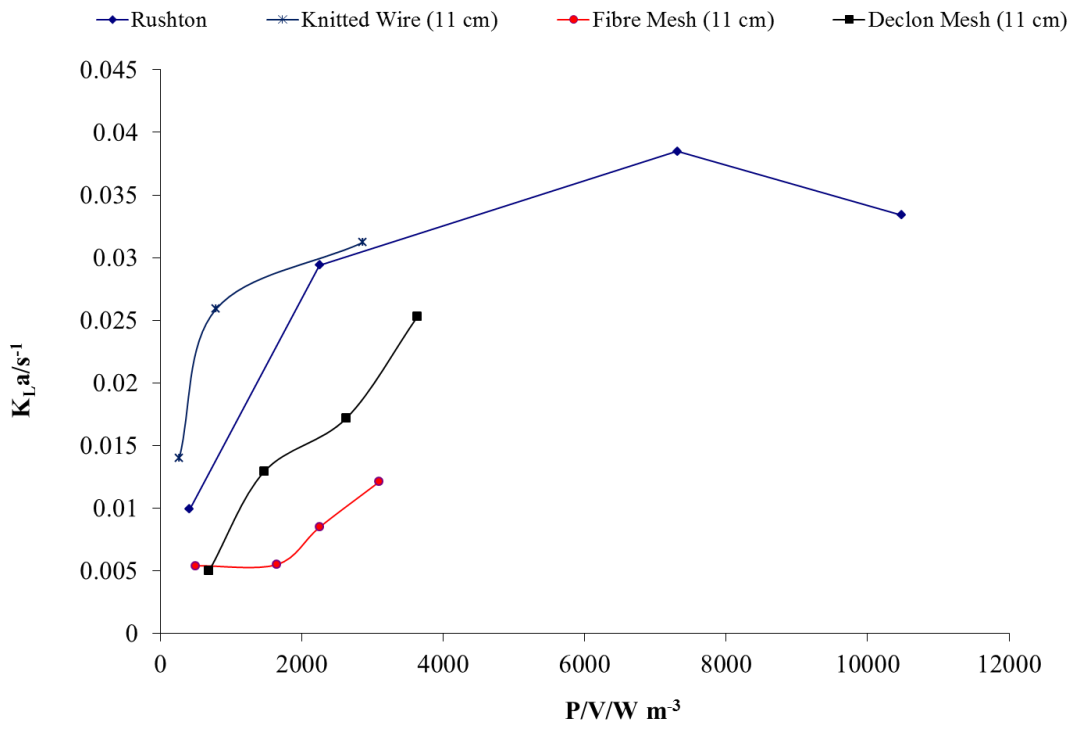

Figure 5.3b: The effect of power consumption (P/V) on K_La results in the Air/Water System at a constant air flow rate of 1.0 vvm (≡ 5 l min^{-1}) for the 11 cm porous mesh and 6 cm Rushton impellers

The definition of power draw is given by Ascanio *et al* (1994) as the amount of energy needed over a period of time to produce movement within a reactor (Ascanio *et al* 1994). Power consumed by the impeller system is often a significant cost in reactors, increasing with the size of the reactor. It is therefore a goal to induce efficient mixing with a reactor with the minimum amount of energy expended (Bader 1987). The present study alongside other research has highlighted one of the main limitations of the Rushton design being the large amount of power draw required to achieve its oxygen transfer values (Moucha *et al* 2009). For a power consumption of around 1000 W m^{-3} the two knitted wire impellers give the highest transfer values. The highest transfer results achievable for the knitted wire impellers is around 0.03 s^{-1} at a power consumption of around 2800 W m^{-3}. For the Rushton impeller, a 30 % increase in K_La to 0.04 s^{-1} can be achieved, but this is accompanied by a fourfold increase in power consumption to around 8000 W m^{-3}. This would appear to suggest that the 11 cm knitted wire impeller especially can utilise the power it draws much more effectively.

Figures 5.1 and 5.3 show that for the Rushton impeller the value of K_La increases with either increasing agitation rate or power but after 800 rpm (≡ 8000 W m^{-3}) the value of K_La

decreases as the power/agitation increases further. A large amount of power in the larger agitation range for the Rushton impeller appears to be wasted by being dissipated in vortex formation, which had a negative impact on the oxygen transfer value observed. Despite the presence of baffles to redirect the flow of the fluid, vortex formation was observed to occur during repeat runs of the experiments with the Rushton impeller at 1000 rpm.

Airflow rate and its effect on the value of K_La have been examined by the present study. Previous research conducted (both experimental and simulation) has highlighted the importance of air flow rate. Figures 5.4 a and b illustrate the effect of airflow rate on the value of K_La in the present study for all impellers studied.

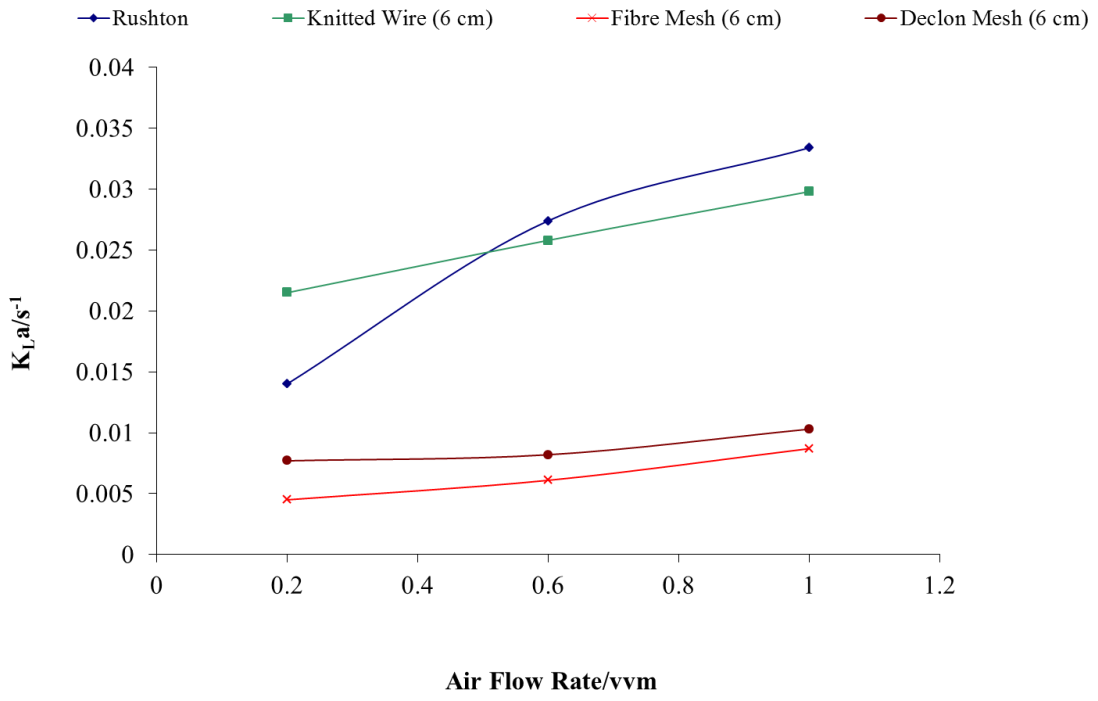

Figure 5.4a: The effect of air flow rate on K_La results in the Air/Water System at a constant agitation rate of 1000 rpm for the 6 cm diameter impellers

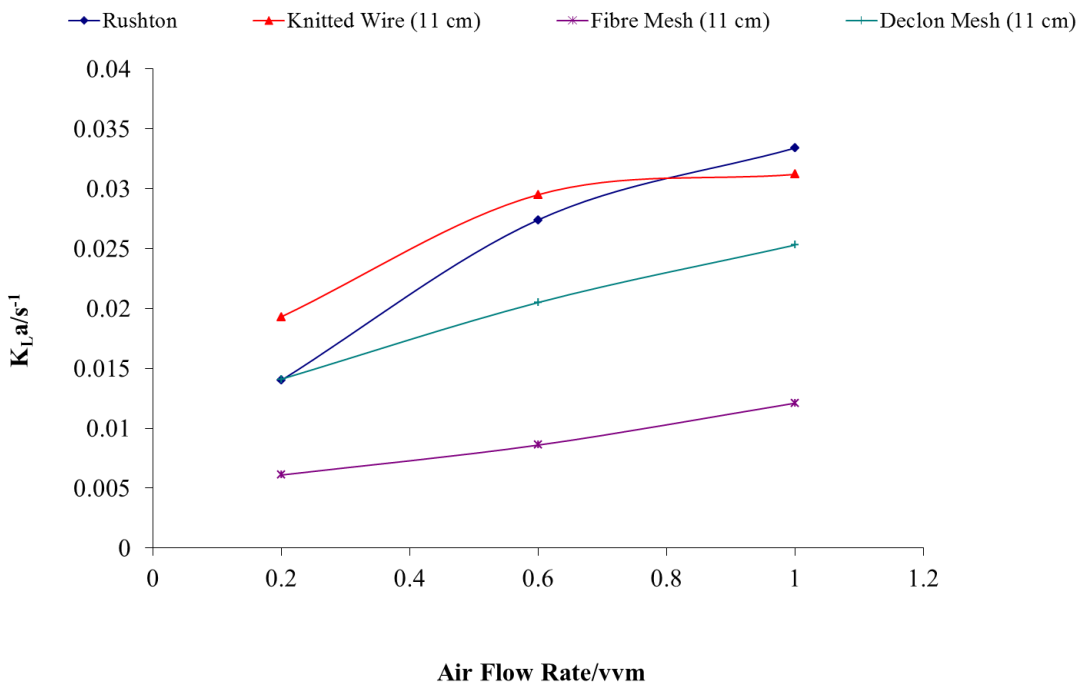

Figure 5.4b: The effect of air flow rate on K_La results in the Air/Water System at a constant agitation rate of 1000 rpm (400 rpm for the 11 cm Knitted Wire Impeller) for the 11 cm diameter porous mesh and 6 cm diameter Rushton impellers

The results noted in the figures above illustrate that the value of K_La increases with an increase of air flow rate, although the increase for some of the impellers is not a linear one. As airflow in the reactor increases, the gas hold up increases leading to a higher surface area being created. This effect results in an increase in K_La values being observed, this has also been noted by Puthli *et al*. (2008). For some of the impellers a larger increase in K_La values occurs between 0.2-0.6 vvm than between 0.6-1.0 vvm. It is possible that at some of the lower agitation rates the higher air flow rates led to the flooding of the impeller which would result in a depression of the K_La value observed. This has been noted by several different papers previously (Bombac *et al* 2006, Gezorket *al* 2000, Paglianti *et al* 2000, Stanbury *et al* 2000, Taghavi *et al* 2010). It has also been observed that as air flow rate increased the amount of power consumed by the impellers decreased. As an illustration of this effect, Figure 5.5 displays the airflow rates employed for the 6 cm Rushton impeller against the average power consumption.

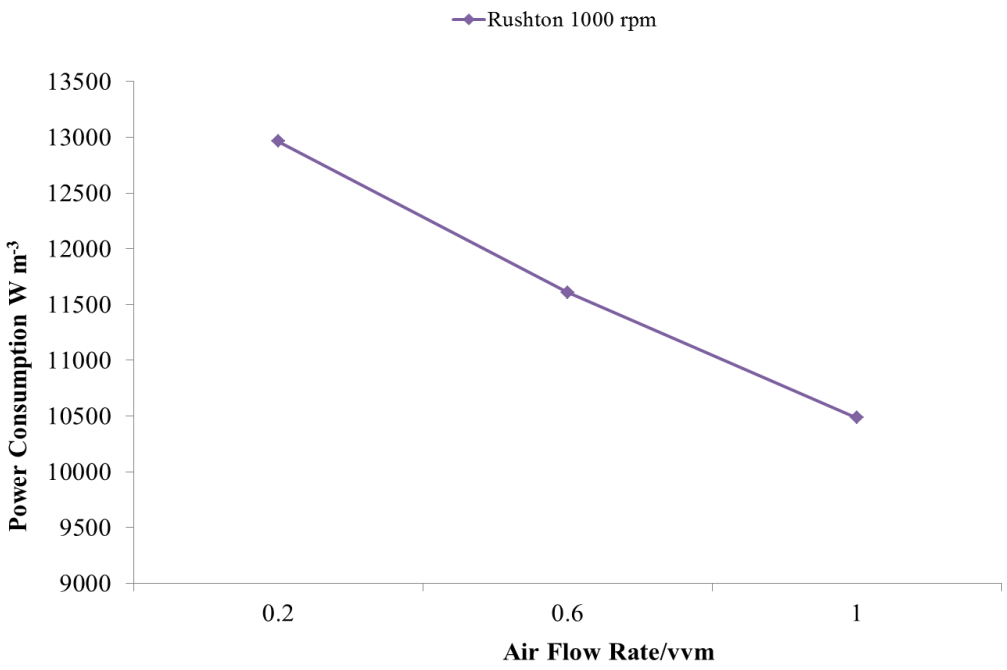

Figure 5.5: The effect of air flow rate on power consumption for the Rushton impeller at 1000 rpm in the air/water system studied.

The increasing air flow rate within the reactor causes additional turbulence within the reactor. Furthermore the additional air causes the density of the fluid to become less dense resulting in decreasing power consumption in order to enable mixing of the reactor (Toogood 2005). This trend has been noted for all the impellers within the current study. This trend had also been noted by the previous study conducted within the school. The power consumption data obtained in the current study is useful for use in future studies to obtain a high K_La value for the minimum power required to achieve this.

5.2.1.2 Analysis

In order to ascertain whether the results in the current study are accurate, they have been compared against values noted in previous work. This was achieved by performing a simple linear regression, the resulting generalised expression is shown in equation 5.2. Equation 5.3 is the correlation developed by Van't Riet (1979) for a single Rushton impeller, equation 5.4 is the expression from Nocentini *et al* (1993) developed for a dual Rushton system.

$$K_L a = m(\frac{P}{V})^{\alpha} U_s^{\beta} \tag{5.2}$$

$$K_L a = 0.026(\frac{P}{V})^{0.4} U_s^{0.5} \tag{5.3}$$

$$K_L a = 0.015(\frac{P}{V})^{0.59} U_s^{0.55} \tag{5.4}$$

In the studies by Van't Riet and Nocentini *et al* the correlations were developed for pure water systems. The mass transfer results for the Rushton turbine obtained in the present study were also subjected to a linear regression analysis, for which equation 5.5 has been obtained. The correlation for the current study has then been compared to the previous two correlations graphically which are noted in Figures 5.6 a and b

$$K_L a = 0.017(\frac{P}{V})^{0.35} U_s^{0.42} \tag{5.5}$$

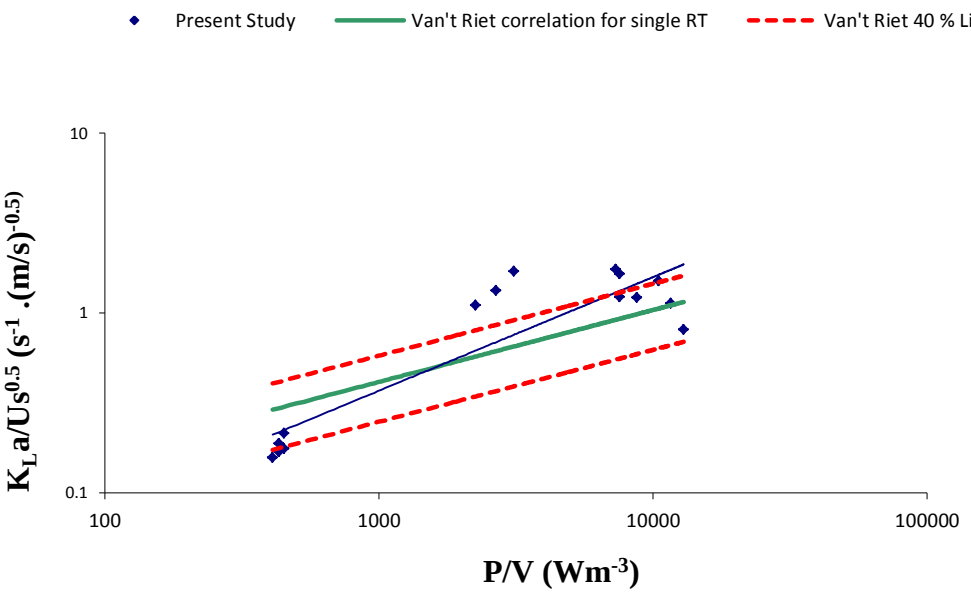

Figure 5.6a: Comparison of Rushton impeller correlation with Van't Riet Correlation (Van't Riet 1979)

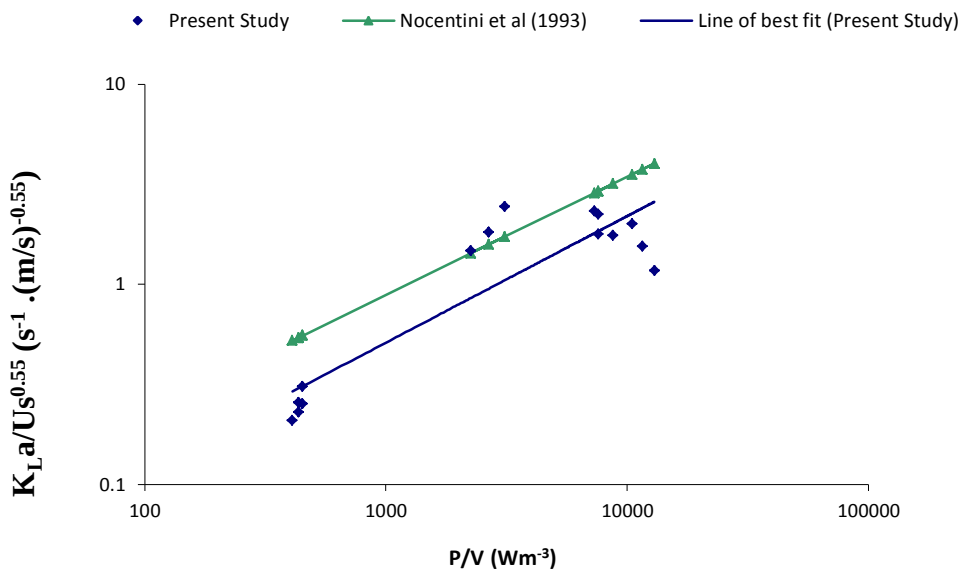

Figure 5.6b: Comparison of Rushton impeller correlation with Nocentini Correlation (Nocentini *et al* 1993)

Figure 5.6a also notes 40 % limits which had been established by Van't Riet as an upper/lower limit to where it was believed most transfer results would be established for similar systems studied. In the case of the present study, some of the results do go above the upper 40 % limit indicating the K_La/Us value was higher than expected for the P/V value observed. In figure 5.6b a large amount of the data in the current study is below the correlation developed by Nocentini *et al* (1993) suggesting that the K_La/Us values are not as high as those obtained by Nocentini *et al* (1993) for a similar P/V value. Both figures note a higher degree of scatter in the current study compared to the correlations developed by Van't Riet (1979) and Nocentini *et al* (1993). In addition the figures and correlations also show reasonable agreement with each other. In particular the power index for P/V of 0.35 in the present study (equation 5.5) is close to the one noted by Van't Riet (1979) of 0.40 (equation 5.3). For all 3 correlations, the coefficients are positive which indicate that they have a positive effect on the value of K_La.

The mesh impellers have also been subjected to a linear regression analysis in order to compare their results with those developed by Van't Riet (1979) and Nocentini *et al* (1993). Firstly the correlations obtained are noted in Equations 5.6-5.11

$$K_L a = 0.00687\left(\frac{P}{V}\right)^{0.39} U_s^{0.30} \quad \text{(6 cm Knitted)} \tag{5.6}$$

$$K_L a = 0.034(\frac{P}{V})^{0.36} U_s^{0.50} \quad \text{(11 cm Knitted)} \tag{5.7}$$

$$K_L a = 0.022(\frac{P}{V})^{0.38} U_s^{0.63} \quad \text{(6 cm Fibre)} \tag{5.8}$$

$$K_L a = 0.00334(\frac{P}{V})^{0.39} U_s^{0.37} \quad \text{(11 cm Fibre)} \tag{5.9}$$

$$K_L a = 0.00109(\frac{P}{V})^{0.59} U_s^{0.36} \quad \text{(6 cm Declon)} \tag{5.10}$$

$$K_L a = 7.79 * 10^{-5}(\frac{P}{V})^{1.01} U_s^{0.43} \quad \text{(11 cm Declon)} \tag{5.11}$$

As with the Rushton impellers, the correlations developed above for the mesh impellers have been compared to those developed by Van't Riet (1979) and Nocentini *et al* (1993) and are noted in figures 5.7a-5.7d

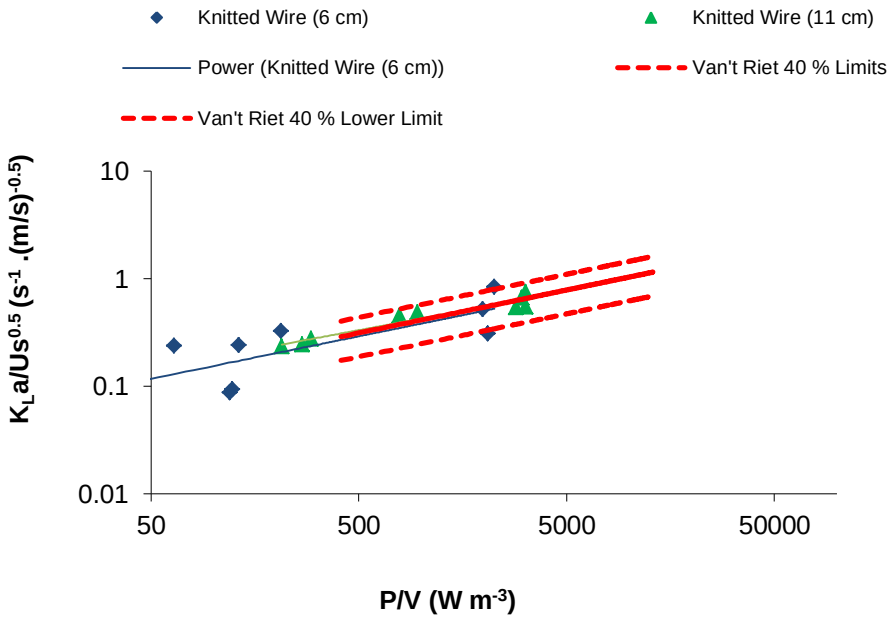

Figure 5.7a: Comparison of the Knitted Wire Impellers with the Van't Riet correlation (Van't Riet 1979)

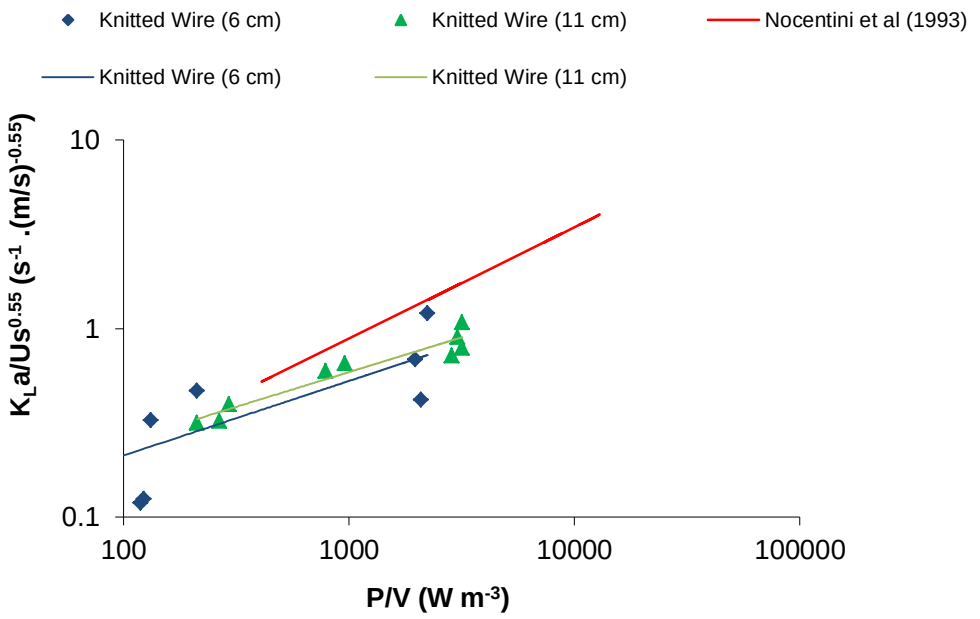

Figure 5.7b: Comparison of the Knitted Wire mesh impellers to the Nocentini *et al* correlation (1993)

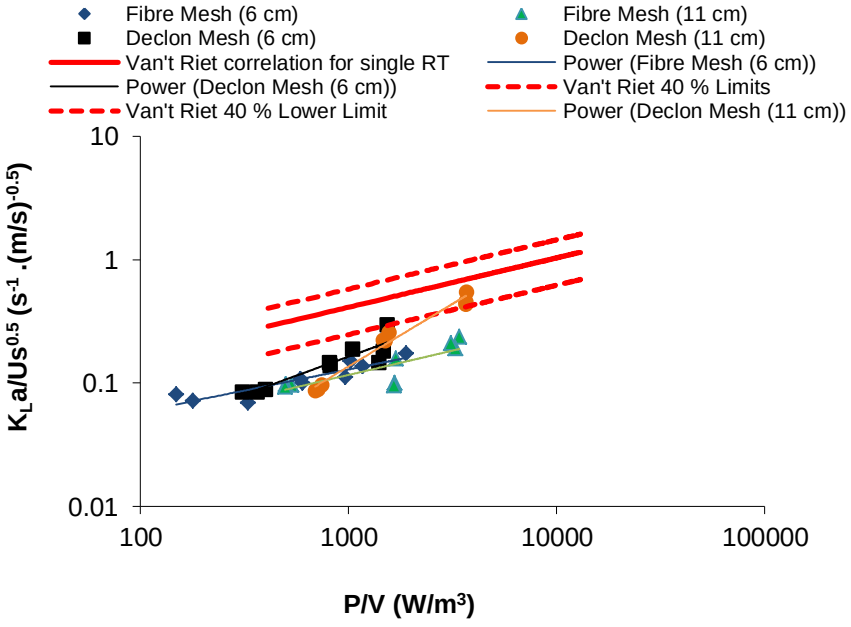

Figure 5.7c: Comparison of the Fibre and Declon Mesh Impellers with the Van't Riet correlation (Van't Riet 1979)

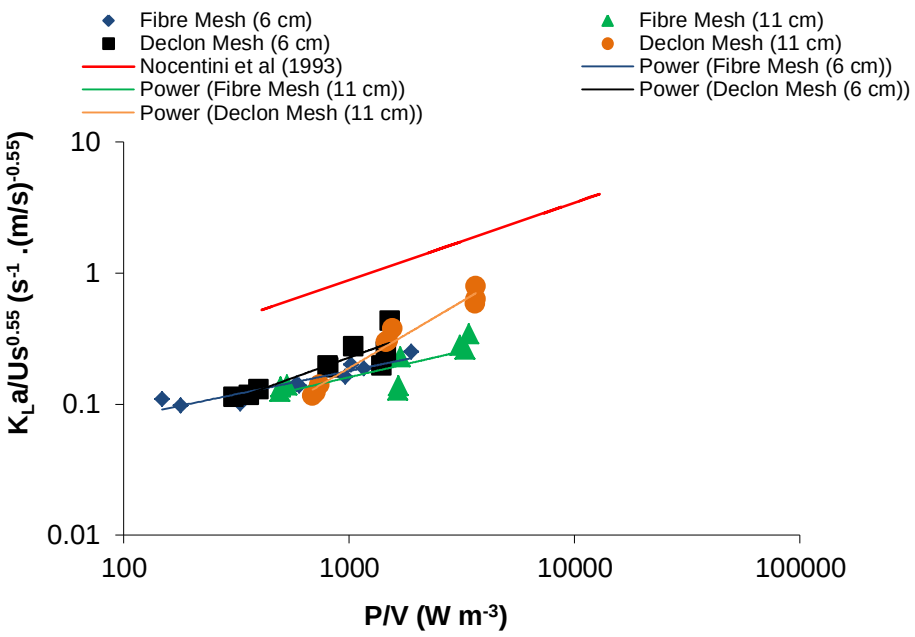

Figure 5.7d: Comparison of the Fibre and Declon Mesh impellers to the Nocentini *et al* correlation (1993)

There is a reasonable agreement between the correlations developed for the Knitted Wire Mesh Impellers in the current study and those developed by Van't Riet (1979) and Nocentini *et al* (1993). In figure 5.7a, it is clear that the gradients of the best line fits through the individual data sets for the knitted wire mesh are similar to that of the correlation, indicating that the index for the parameter (P/V) for the data in the present study and the literature correlation are in close agreement. This is also evident from the equations presented (equations 5.3, 5.6 and 5.7). In contrast, the comparison of the knitted wire mesh data with the Nocentini *et al* (1993) correlation in figure 5.7b indicates that the (P/V) index represented by the gradient of the best line fits through the present data is somewhat lower from that given by the correlation (an index of 0.59 from equation 5.4). Therefore, from figures 5.6a and 5.7a, it can be confirmed that the variation of K_La with power density (P/V) parameter for the knitted wire mesh data gathered in this study is more closely represented by the Van't Riet correlation than that by the Nocentini et al. This is also clearly apparent in the regression equations developed in this study (equations 5.6 and 5.7) and the literature correlations as expressed in equations 5.3 and 5.4.

The correlations developed for the fibre and Declon mesh impellers can be similarly compared with the literature correlations, as illustrated in figures 5.7c and 5.7d. It is noted

that in both instances the data for the fibre and Declon mesh fall well below the established literature correlations. This, in fact, applies to almost all the data when compared to the Van't Riet (1979) correlation, whereby the data from the current study consistently fall below the lower 40 % limit line. The slope of the best line fits through the data sets varies to some degree when compared to that of the individual correlations. It appears from figure 5.7c that the trendlines for both fibre mesh impellers are almost parallel to the Van't Riet correlation, indicating that the (P/V) index for each is quite close to 0.4. This is independently verified by the regression equations 5.8 and 5.9 where P/V indices of 0.38 and 0.39 respectively are obtained. In contrast, the slope of the Declon Mesh trendlines seems to follow the Nocentini *et al* correlation in figure 5.7d more closely.

The experimental results for the Air/Water study conducted illustrate that agitation and airflow rate have a positive impact, albeit to various degrees, on the value of K_La for all impellers studied. In order to study the effect of these parameters on the value of K_La in more detail, a main effects plot was produced in Minitab for each of the impellers studied. These are shown in figures 5.8a-5.8g

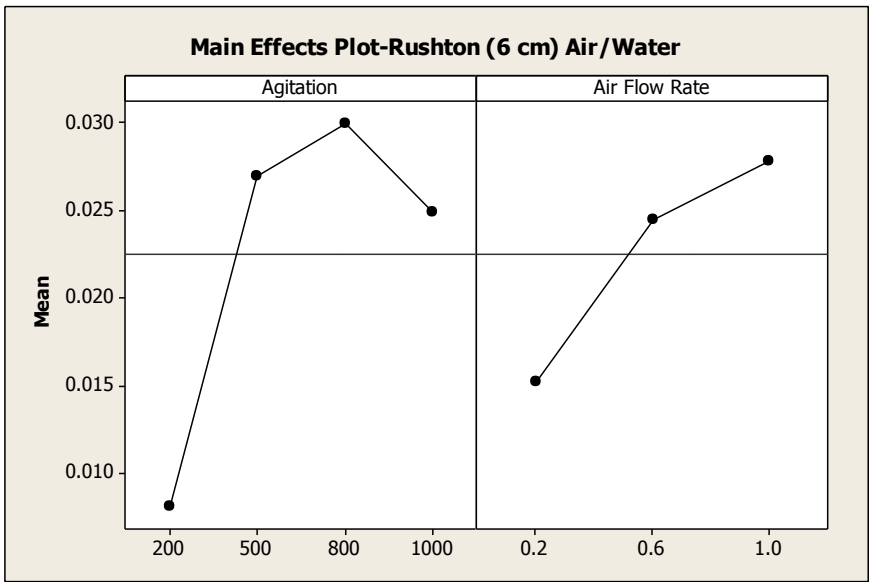

Figure 5.8a: Main Effects Plot for the Rushton impeller

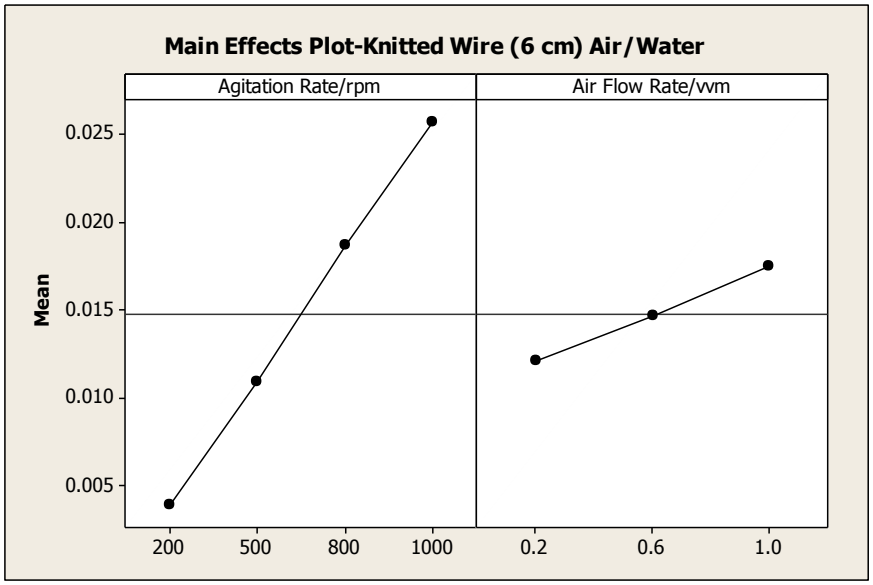

Figure 5.8b: Main Effects Plot for the 6 cm Knitted Wire Impeller

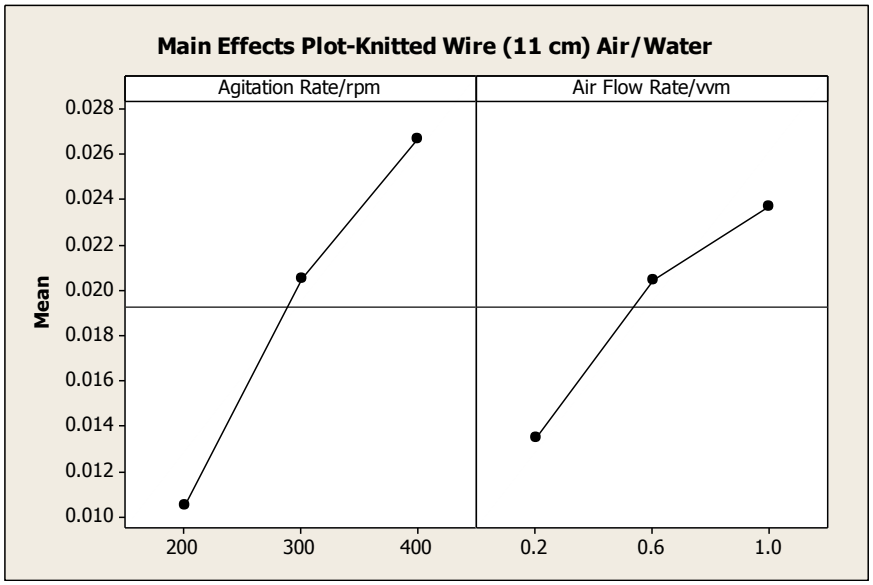

Figure 5.8c: Main Effects Plot for the 11 cm Knitted Wire Impeller

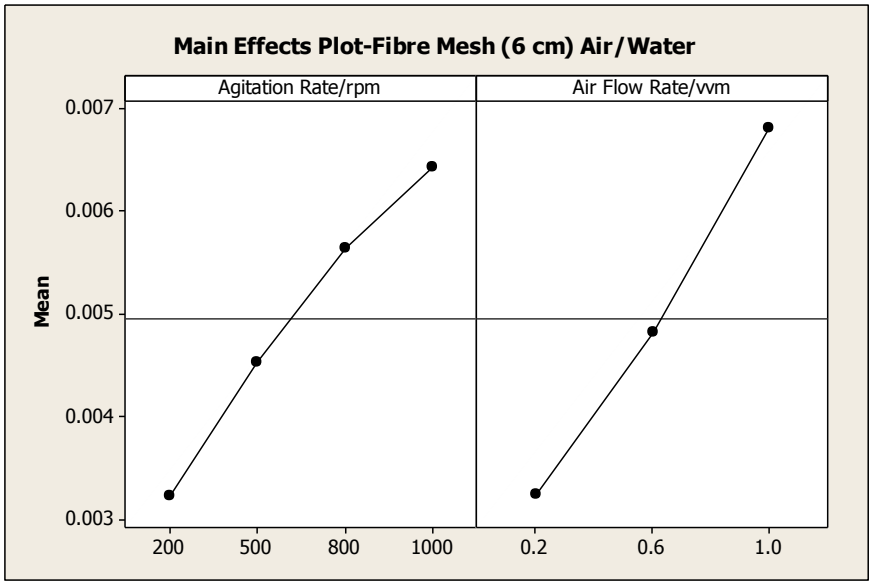

Figure 5.8d: Main Effects Plot for the 6 cm Fibre Mesh impeller

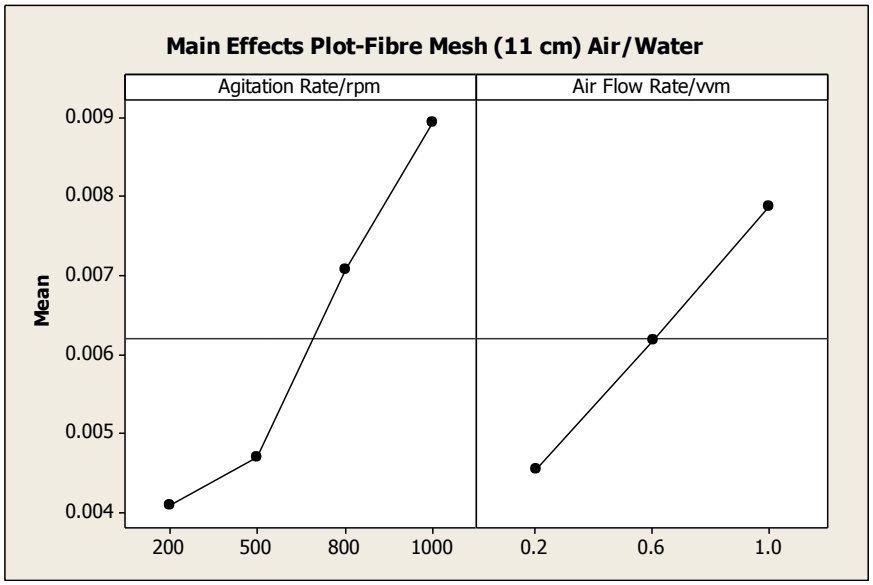

Figure 5.8e: Main Effects Plot for the 11 cm Fibre Mesh impeller

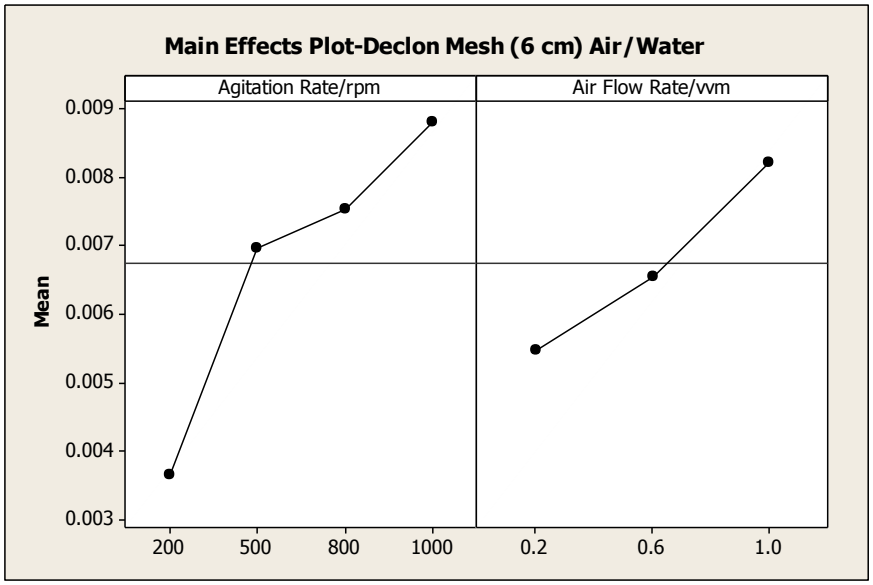

Figure 5.8f: Main Effects Plot for the 6 cm Declon Mesh impeller

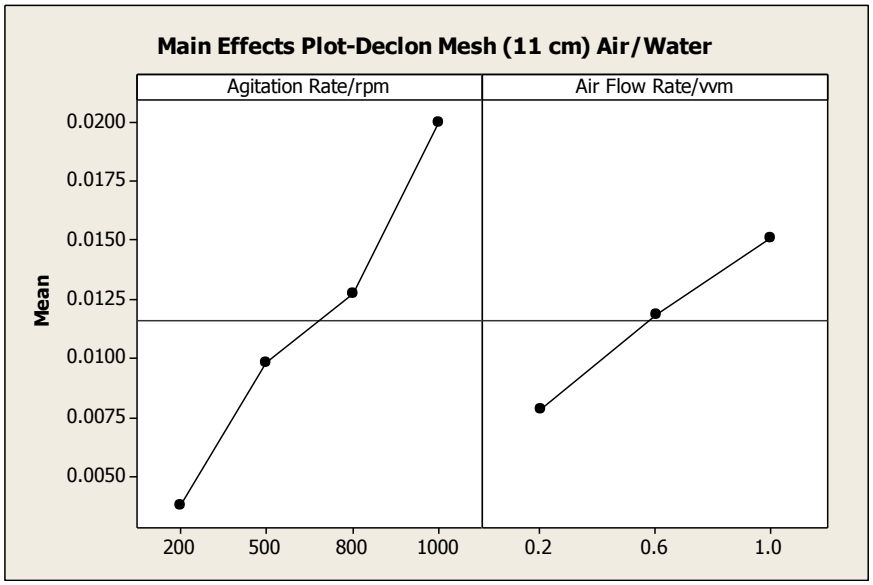

Figure 5.8g: Main Effects Plot for the 11 cm Declon Mesh impeller

The main effects plots in the figures illustrate that for most of the impellers tested the agitation rate had the greater effect on the value of K_La. This result also validates the findings in the linear regression analysis which also found that the coefficient of the P/V (which is representative of the agitation rate) was the larger of the two in most cases. Both parameters however had a positive impact on the K_La values observed for all impellers studied. The main effects plot also illustrate that the highest mean K_La is usually produced for an agitation rate of 1000 rpm and airflow rate of 1.0 vvm for the porous packings, whereas for the Rushton impeller the highest K_La value is produced at 800 rpm.

5.2.2 Air/Water-Glycerol (50 % each by volume) Results

5.2.2.1 Results and Discussion

To investigate the effect of viscosity on the transfer rate, a series of experiments were performed with a 50 % (by volume) mixture of water and glycerol. With the working volume of the system being 5 l, 2.5 l of each component was used. The viscosity of the mixture used at 35^{o}C is 4.7 mNs m^{-2} (compared to 0.7 mNs m^{-2} for the pure water system) (Boodhoo *et al* 2008). Due to the increase in viscosity the maximum rpm achieved was 800 rpm correlating to the maximum power that could be drawn from the motor. For the 11 cm knitted wire impeller a maximum rpm of 400 rpm was achieved. The probe response (noted in section 5.1) was also applied to these results to ensure consistency throughout the study.

The transfer capability of the porous mesh impellers were compared to that of the Rushton impeller and are noted in 5.9 a and b

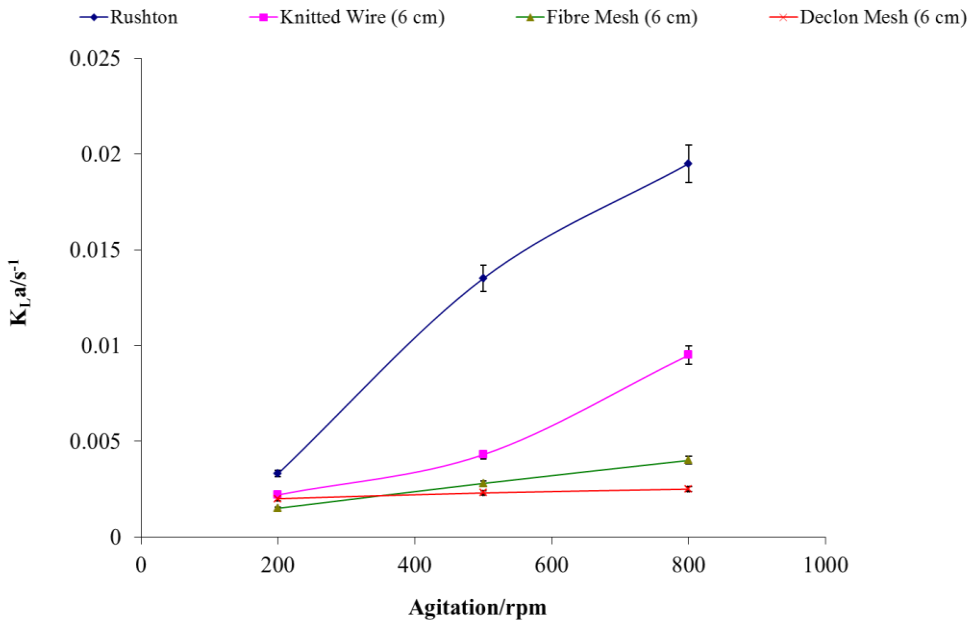

Figure 5.9a: The effect of agitation rate on K_La results in the Air/Water-Glycerol System at a constant air flow rate of 1.0 vvm (≡ 5 l min^{-1}) for the 6 cm diameter impellers

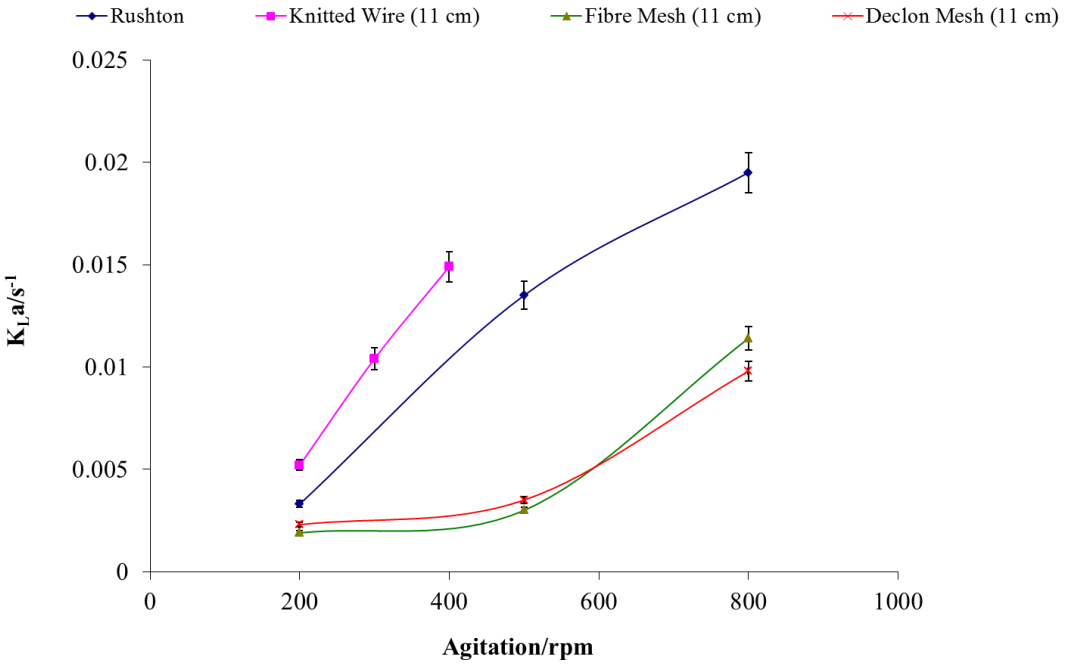

Figure 5.9b: The effect of agitation rate on K_La results in the Air/Water-Glycerol System at a constant air flow rate of 1.0 vvm (≡ 5 l min^{-1}) for the Rushton and 11 cm diameter impellers

Figure 5.9a illustrates that the Rushton impeller produces the largest transfer values compared to the other 6 cm impellers, whereas figure 5.9b notes that the 11 cm knitted wire impeller outperforms the Rushton impeller (in terms of K_La values) in the lower agitation range. Both the 6 and 11 cm version of the fibre and Declon mesh impellers produce a much lower K_La value compared to the Rushton and the 6 and 11 cm knitted wire impellers, although the values between the fibre and Declon mesh impellers themselves are quite similar. As noted earlier for the air/water results, enhancement of the agitation rate results in increased turbulence within the system. This also results in faster mixing of the reactor contents and faster mass transfer across the gas-liquid boundary layer (Buwa *et al* 2006). Both figures indicate an overall increase in K_La values with agitation rate for all impellers studied within this system.

As with the air/water study conducted previously, the power draw of each of the impellers studied was considered. Figures 5.10 a and 5.10b illustrate the effect of power consumption on the measured K_La for all impellers studied.

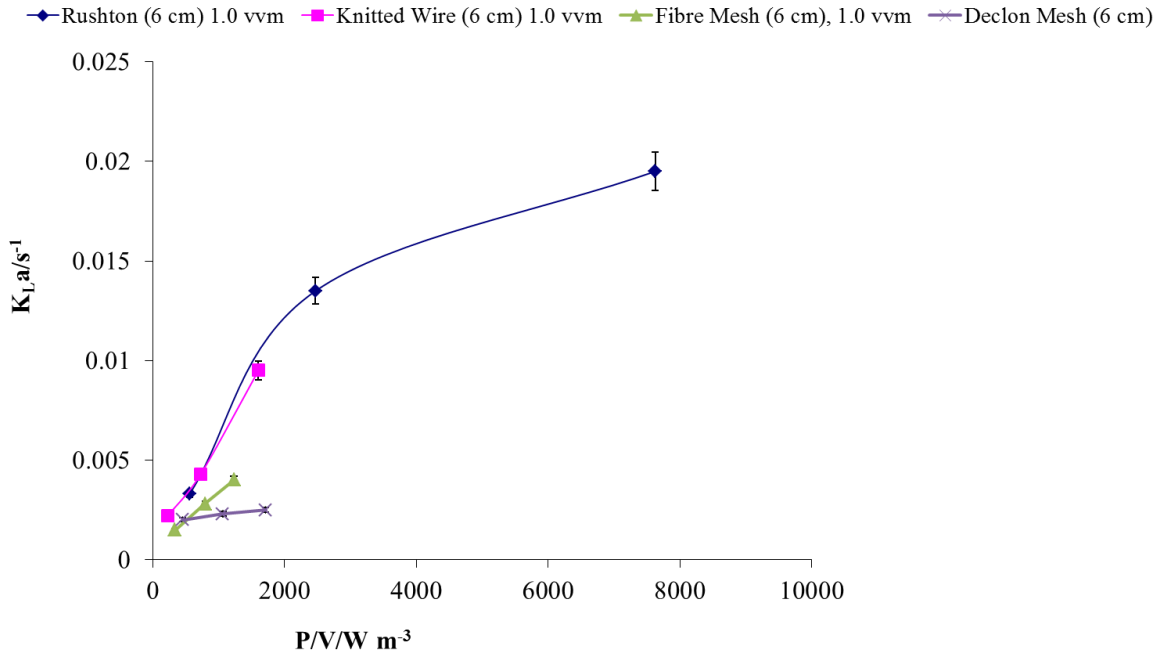

Figure 5.10a: The effect of power consumption (P/V) on K_La results in the Air/Water-Glycerol System at a constant air flow rate of 1.0 vvm (≡ 5 l min^{-1}) for the 6 cm diameter impellers

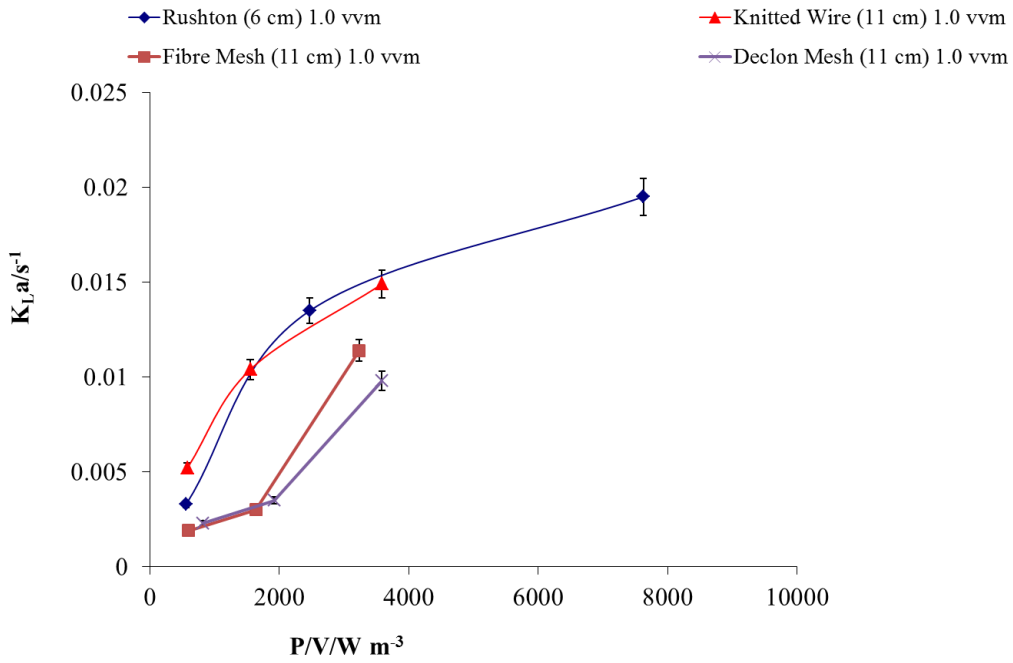

Figure 5.10b: The effect of power consumption (P/V) on K_La results in the Air/Water-Glycerol System at a constant air flow rate of 1.0 vvm (≡ 5 l min^{-1}) for the 6 cm Rushton and 11 cm diameter Mesh Impellers

As with the air/water study, Figures 5.10 a and b illustrate that the Rushton impeller although producing the highest K_La value (0.0195 s^{-1}), it is the impeller with the largest range of power data, with the highest P/V value recorded at approximately 7627 W m^{-3} (producing the K_La value of 0.0195 s^{-1}). In contrast the 11 cm Knitted wire impeller produces a K_La value of 0.0149 s^{-1} for a P/V value of approximately 3587 W m^{-3}. This however is not a straight forward comparison as the P/V value for the 11 cm Knitted wire impeller was produced for an agitation rate of 400 rpm whereas the P/V value for the Rushton impeller was obtained at a P/V of 800 rpm. On figure 5.10b, assuming that the trend for the 11 cm Knitted wire impeller can be extrapolated; it would be likely that this impeller would produce a higher K_La value than the Rushton impeller, alongside a lower P/V value. This would mean that the 11 cm Knitted wire impeller is more efficient at utilising power to produce a higher K_La value.

Airflow rate was the second parameter studied with the Air/Water-Glycerol system and its impact on the value of K_La. Figures 5.11 a and b illustrate this effect.

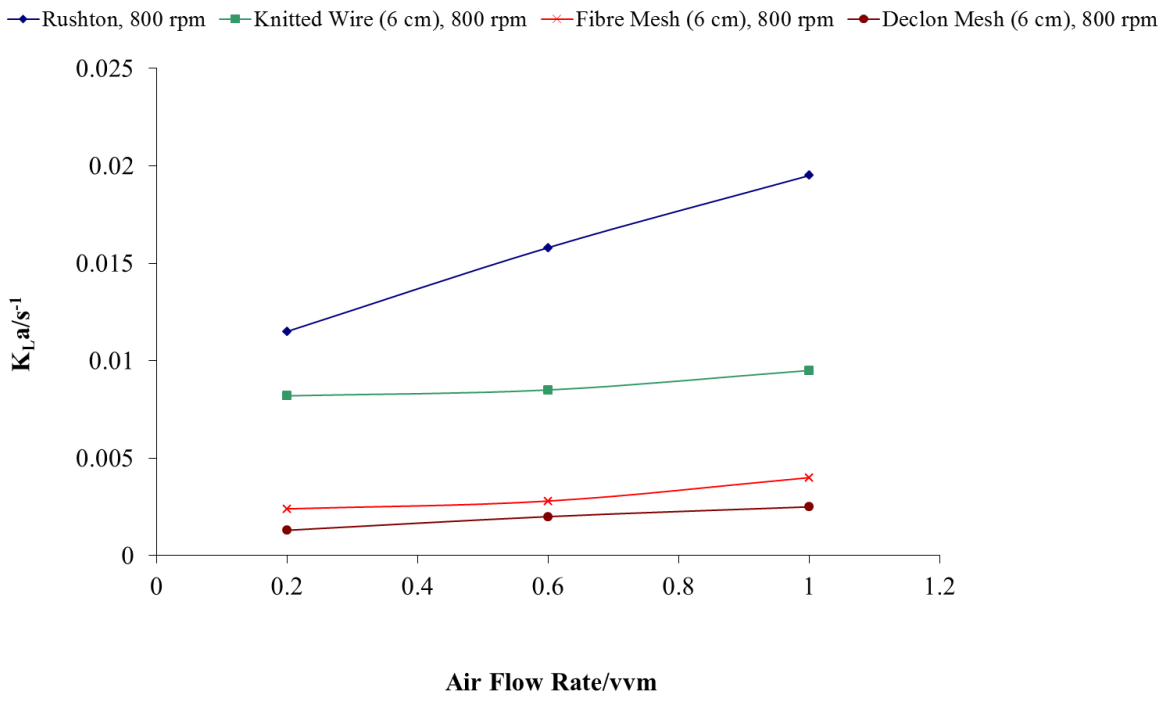

Figure 5.11a: The effect of air flow rate on K_La results in the Air/Water-Glycerol System at a constant agitation rate of 800 rpm for the 6 cm impellers

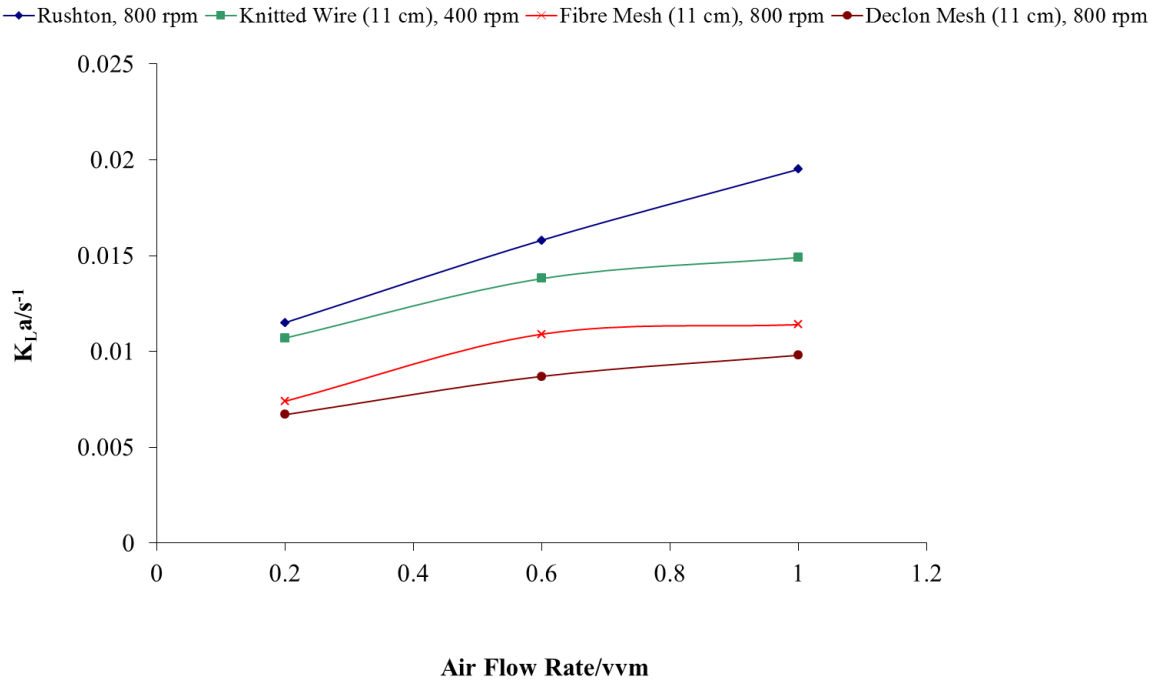

Figure 5.11b: The effect of air flow rate on K_La results in the Air/Water-Glycerol System at a constant agitation rate of 800 rpm (400 rpm for the 11 cm Knitted wire impeller) for the 6 cm Rushton and 11 cm Mesh Impellers

The Rushton impeller produces the highest K_La result noted at 0.0195 s^{-1} for an airflow rate of 1.0 vvm (≡ 5 l min^{-1}). As with the results for agitation, the Fibre and Declon mesh impellers produce the lowest K_La results (0.0114 s^{-1} and 0.0098 s^{-1} respectively). The general trend for the study has shown that as air flow rate increased, the value of K_La was seen to increase; this had been previously noted by the previous study conducted within the school (Toogood 2005). As noted earlier, Puthli *et al* (2008) had noted that the increase in air flow rate leads to an increase in gas hold up, contributing to a larger surface area being made available. The increase in air flow promotes additional turbulence and lowering of the density of the fluid. Although there is an increase in the value of K_La, the effect of air flow rate does not seem to have as much of an impact as increasing of agitation rate had. The power consumption of the impellers was again seen to decrease with increasing air flow rate (as in the case of the Air/Water system studied). As an example the power consumption for the Rushton impeller at 800 rpm is plotted against air flow rate (Figure 5.12)

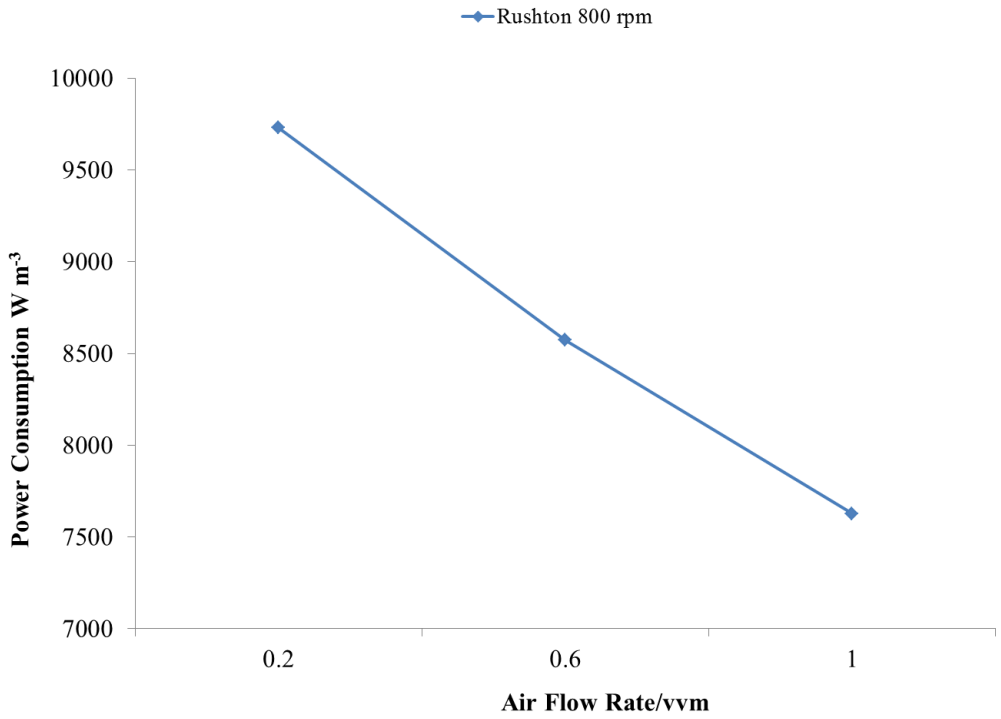

Figure 5.12: The effect of air flow rate on power consumption for the Rushton impeller at 800 rpm in the Air/Water-Glycerol studied.

The effect of viscosity has been noted to have an impact on the K_La value observed for each impeller. Figures 5.13 a and 5.13 b note the K_La values obtained for both systems studied for the Rushton impeller (Figure 5.13a) and the Knitted Wire impellers (Figure 5.13b)

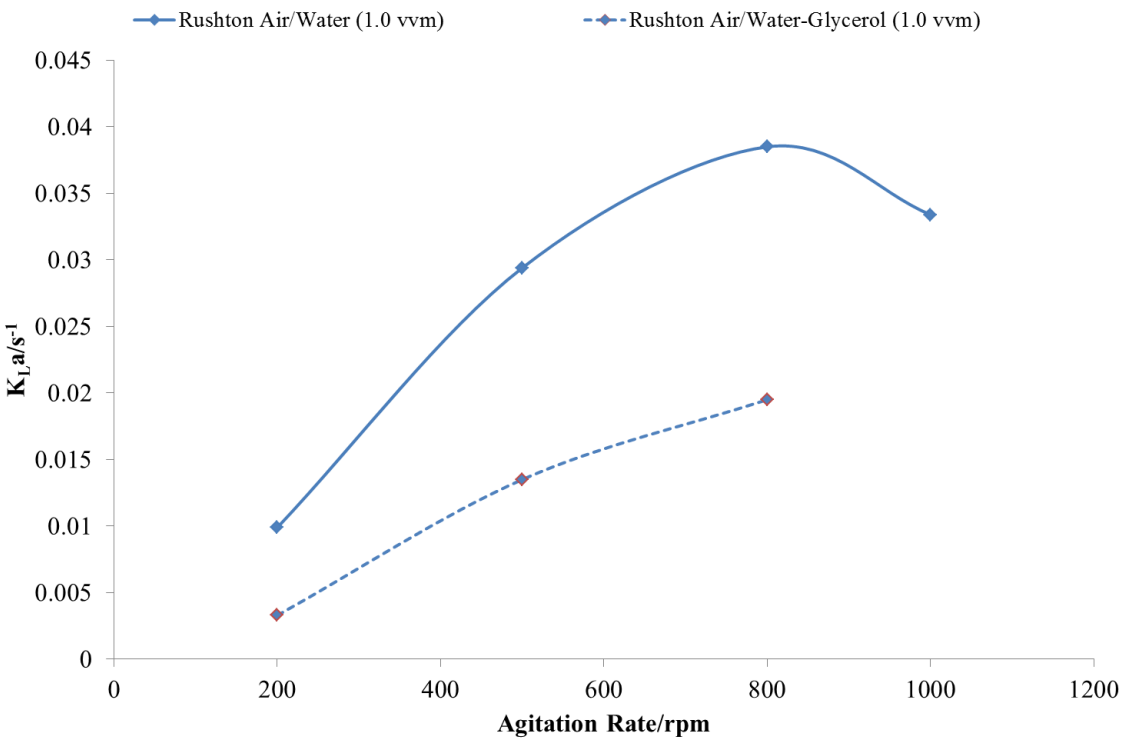

Figure 5.13a: The effect of viscosity on K_La values for the Rushton impeller

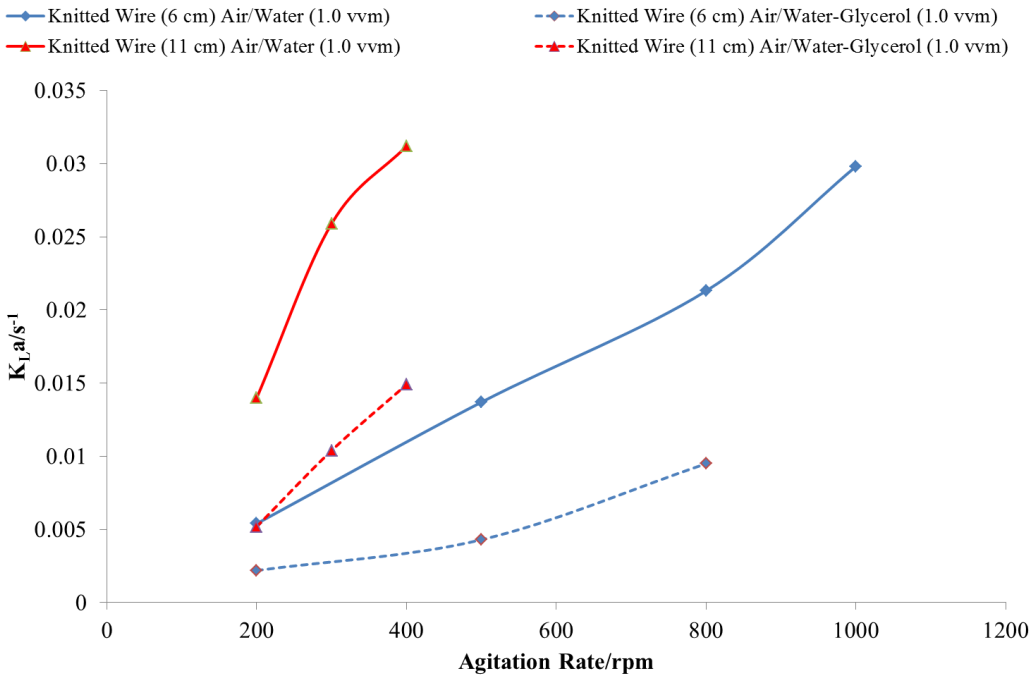

Figure 5.13b: The effect of viscosity on K_La values for the Knitted Wire (6 and 11 cm) impellers

Figure 5.13 notes that with increasing viscosity the value of K_La was observed to decrease. This was noted with all impeller studied. Higher viscosity has been shown to have a negative

effect on K_La, and is denoted in the regression analysis by a negative coefficient. The effect of increased viscosity is quite a complex one. In terms of K_La, its value tends to decrease with increasing viscosity. This is due in part to the fact that oxygen solubility decreases with increasing viscosity. Resistance to gas-liquid transfer increases with increasing viscosity. In this scenario any turbulent eddies formed need to have a sufficiently high energy in order to overcome the thicker viscous layers (Puthli *et al*. 2008). In some instances the level of viscosity may play a role in how it will ultimately affect K_La values.

Noted in a later section of this chapter is the effect viscosity has on bubble size. This plays a crucial role in oxygen transfer and the mean bubble size was noted to decrease with increasing viscosity. For a full discussion of this see section 5.3.2

5.2.2.2 Analysis

As with the previous data discussed, the results for the Rushton impeller in the present air/water-glycerol system were compared to literature correlations. In this case the effect of viscosity is considered; therefore a slightly different correlation is applied, noted in equation 5.12

$$K_L a = m(\frac{P}{V})^{\alpha} U_s^{\beta} (\frac{m}{m_w})^{\gamma} \tag{5.12}$$

From previous literature two correlations were chosen to compare the current study to. The first one was developed by Nocentini *et al* (1993) and the second one formulated by Puthli *et al* (2008). These two correlations are noted in Equations 5.13 and 5.14 respectively with the correlation developed for the Rushton impeller in the current study noted in Equation 5.15

$$K_L a = m(\frac{P}{V})^{0.62} U_s^{0.4} (\frac{m}{m_w})^{-0.75} \tag{5.13}$$

$$K_L a = 0.0013(\frac{P}{V})^{0.57} U_s^{0.54} (\frac{m}{m_w})^{-0.84} \tag{5.14}$$

$$K_L a = 0.0047(\frac{P}{V})^{0.69} U_s^{0.55} (\frac{m}{m_w})^{-0.71} \tag{5.15}$$

Originally the value of the coefficient (γ) for the Viscosity term (m/m_w) in equation (5.13) was -1.17 (Nocentini *et al* 1993). This value was based on a system whose viscosity was 62 mNs m^{-2} (compared to 4.7 mNs m^{-2} in the present study). The authors suggest that for a lower viscosity system the γ coefficient could be as low as 0.75 (Nocentini *et al* 1993) which is reflected in equation (5.13) used for the comparison. The correlation developed for the Rushton impeller in the current study has been plotted against the correlations found in Nocentini *et al* (1993) and Puthli *et al* (2008) (Figures 5.14 a and b respectively)

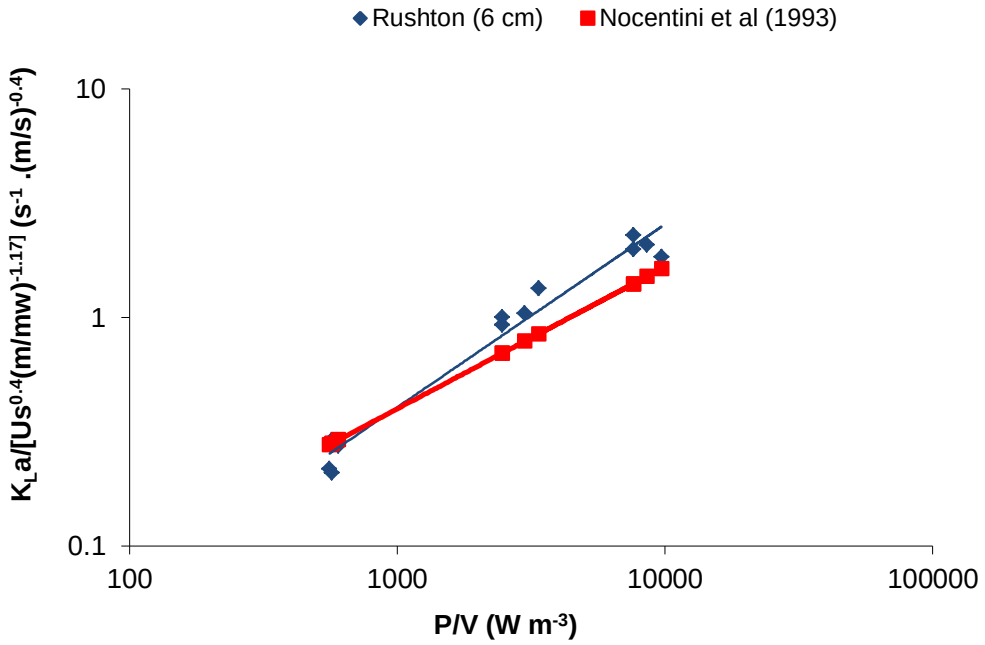

Figure 5.14a: Comparison of Rushton impeller data to the Nocentini *et al* (1993) correlation

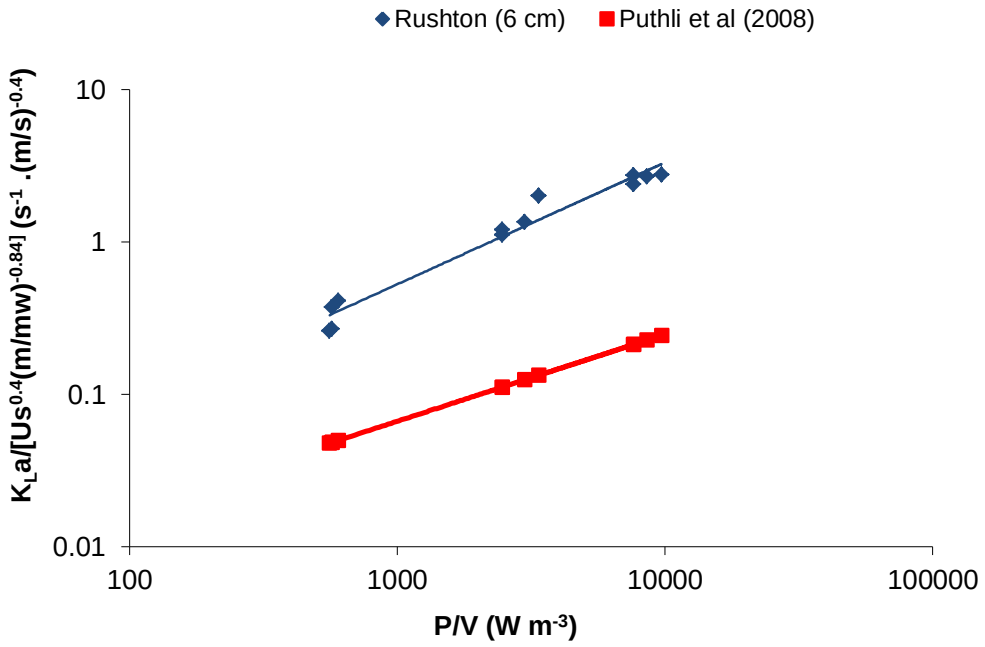

Figure 5.14b: Comparison of Rushton impeller data to the Puthli *et al* (2008) correlation.

The correlation obtained for the Rushton impeller for the present study shows good agreement with the correlation obtained by Nocentini *et al* (1993) as shown in Figure 5.14a. The majority of the data for the current study lies slightly above the trend line for the Nocentini *et al* correlation suggesting that slightly higher $K_L a$ values were obtained for this study for a similar power consumption value. When comparing the results to Puthli *et al* (2008) in Figure 5.14b, the slope of the trendline fit for the present data is quite similar to that of the correlation although the $K_L a$ data generated by the current study are shown to be higher than the Puthli *et al* (2008) study at the same power density. This was to be expected as the γ coefficient for the Puthli *et al* (2008) and the Nocentini *et al* (2003) study are lower and therefore the value of $K_L a$ from these correlations will also be lower.

The mesh impellers were also subjected to a linear regression analysis (as with the Air-Water results) and correlations developed conforming to the generalised equation noted in Equation 5.13. The correlations obtained are noted in Equations 5.16-5.21

$$K_L a = 0.00352\left(\frac{P}{V}\right)^{0.52} U_s^{0.30} \left(\frac{m}{m_w}\right)^{-0.74} \qquad \text{6 cm Knitted Wire} \qquad (5.16)$$

$$K_L a = 0.013(\frac{P}{V})^{0.41} U_s^{0.39} (\frac{m}{m_w})^{-0.44}$$ 11 cm Knitted Wire (5.17)

$$K_L a = 0.00681(\frac{P}{V})^{0.50} U_s^{0.57} (\frac{m}{m_w})^{-0.53}$$ 6 cm Fibre Mesh (5.18)

$$K_L a = 0.000298(\frac{P}{V})^{0.74} U_s^{0..39} (\frac{m}{m_w})^{-0.33}$$ 11 cm Fibre Mesh (5.19)

$$K_L a = 0.00417(\frac{P}{V})^{0.47} U_s^{0.44} (\frac{m}{m_w})^{-0.79}$$ 6 cm Declon Mesh (5.20)

$$K_L a = 6.91*10^{-5} (\frac{P}{V})^{1.06} U_s^{0.46} (\frac{m}{m_w})^{-0.64}$$ 11 cm Declon Mesh (5.21)

The correlations developed in the equations above show that in general the P/V coefficient had the largest positive impact on $K_L a$ whilst the (m/m_w) coefficient had the most negative impact on the value of $K_L a$. The above correlations have also been plotted against the Nocentini *et al* (1993) and Puthli *et al* (2008) correlations and are presented in Figures 5.15a-c

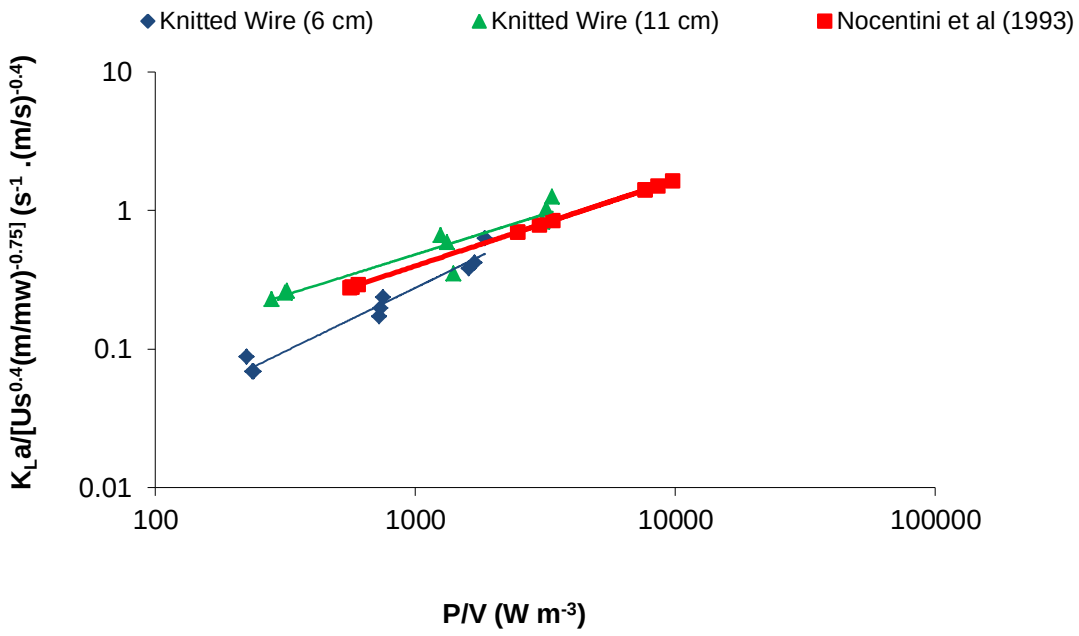

Figure 5.15a: Comparison of the Knitted Wire impellers to the Nocentini correlation (Nocentini *et al* (1993)

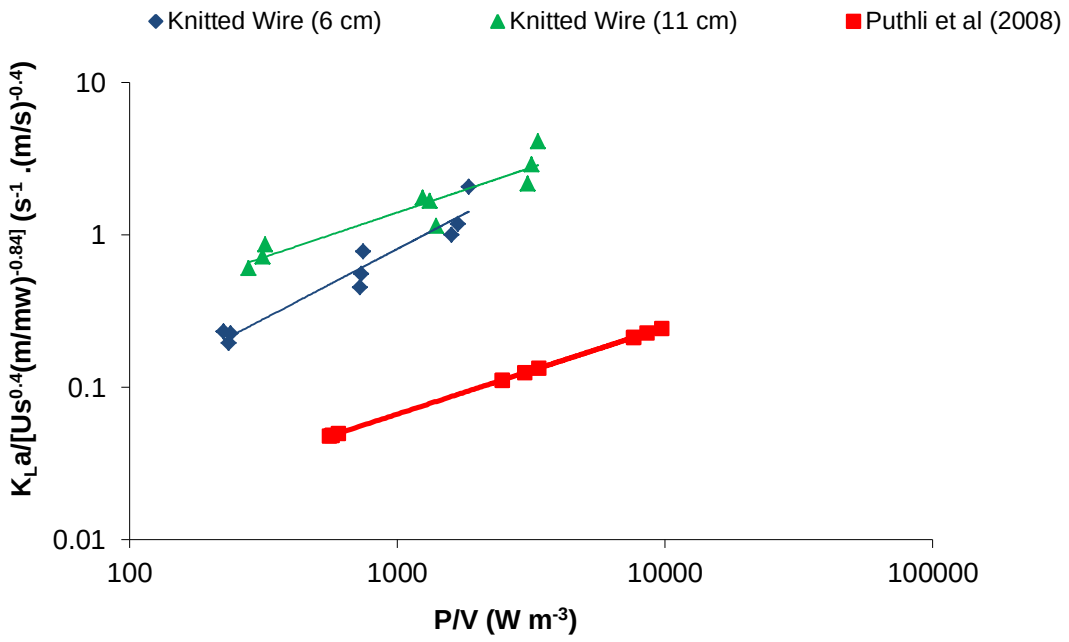

Figure 5.15b: Comparison of Knitted Wire impellers to the Puthli correlation (Puthli *et al* 2008)

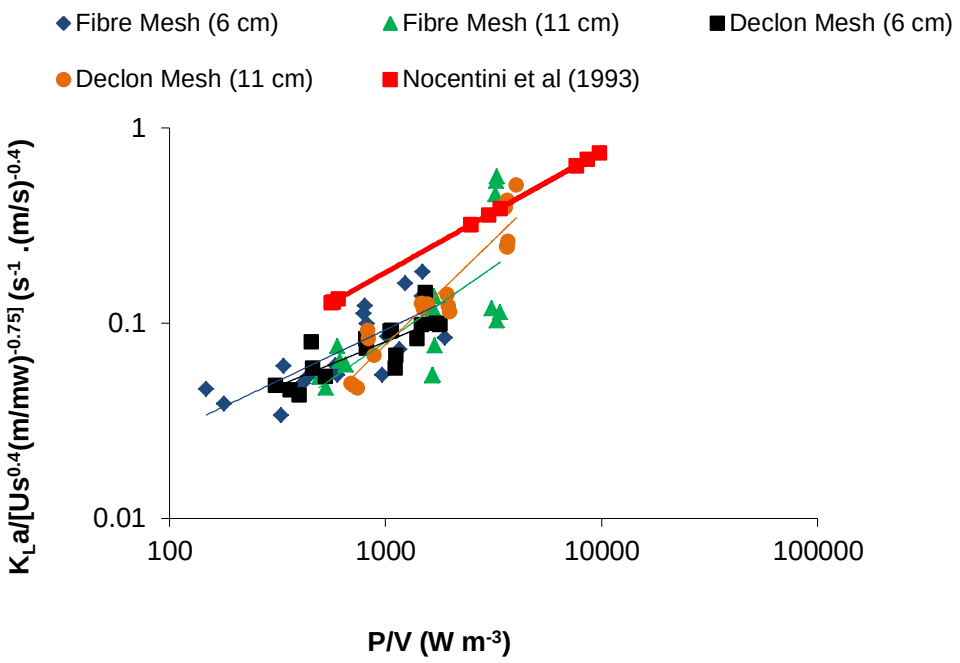

Figure 5.15c: Comparison of the Fibre and Declon Mesh impellers to the Nocentini correlation (Nocentini *et al* 1993)

On comparison of the mesh impellers to the Nocentini *et al* (1993) correlation in figure 5.13a, the correlations for the knitted wire impellers are close to the literature correlation with some of the data falling on the left hand side of the literature correlation. This illustrates that a similar transfer value was obtained for the knitted wire impellers compared to the Nocentini *et al* (1993) study. On comparison to the Puthli *et al* (2008) correlation, the two knitted wire impellers each produce a correlation which is significantly higher than the literature data. This demonstrates that the K_La values in the current study are much higher for a similar power draw compared to the results by Puthli *et al*. The other mesh impellers (fibre and Declon) produce correlations which are consistently below the Nocentini *et al* (1993) correlation suggesting that the K_La values obtained were not as a high for a similar power consumption value. Overall, the correlation developed by Nocentini *et al* (1993) for Rushton turbines in high viscosity media appears to reflect the trends of the porous mesh packing data (especially those for the knitted wire mesh packing) more closely. As seen in the regression equations presented above, there are notable variations in the relative viscosity indices obtained from the correlations developed for porous packings in this study compared to the literature correlations for Rushton turbines but this is to be expected as the mixing patterns and therefore mass transfer in high viscosity media are likely to depend on the type of impeller used.

5.2.3 Summary

The aim of the current study was to investigate the transfer capability of a series of mesh impellers compared to a standard Rushton impeller design. The following trends have been observed:

1. The value of K_La was seen to increase with increasing agitation rate and increasing air flow rate for all impellers studied. This was noted to be due to the increased turbulence with the reactor (leading to a faster transfer rate) and smaller bubbles within the reactor (smaller bubbles have a higher surface area available for transfer to occur).
2. The value of K_La was observed to decrease with increasing viscosity. Higher viscosity has been shown to have a negative effect on K_La, and is denoted in the regression analysis by a negative coefficient. The effect of increased viscosity is quite a complex one. In terms of K_La, its value tends to decrease with increasing viscosity. This is due in part to the fact that oxygen solubility decreases with increasing viscosity. Resistance to gas-liquid transfer increases with increasing viscosity. In this scenario any turbulent eddies formed need to have a sufficiently high energy in order to overcome the thicker viscous layers (Puthli *et al*. 2008). In some instances the level of viscosity may play a role in how it will ultimately affect K_La values
3. Out of all the porous mesh impellers, the knitted wire mesh performed best, giving highest K_La at any given agitation rate and aeration rate. This may be because the openness of the knitted wire structure compared to the more compact structure of the fibre and Declon mesh impellers allows a greater degree of interaction between the gas bubbles and the liquid medium for enhanced mass transfer. Another reason for this could be smaller bubbles being produced due to the ease of larger bubbles being sliced off by the thin filaments of the knitted wire. This is investigated in Section 5.3 of this chapter.
4. Although the highest K_La values were obtained by the Rushton impeller under the conditions studied, this was at the expense, however, of the largest power draw at any agitation rate and aeration rate from this conventional impeller. In contrast, the 11 cm knitted wire impeller produced a slightly smaller K_La value than the Rushton turbine but for a greatly reduced power draw. In terms of Process Intensification (PI) this is an important characteristic to consider for a cost efficient reactor system.

5.3 Air Bubble Study

Identification of the mean bubble size produced by each impeller was investigated by use of a digital camera system. Measurement of bubble size was considered important as it is known that the mean diameter of bubbles produced by the impellers is related to the transfer capability examined in section 5.2

Conditions studied for each impeller was the same as those for the previous transfer study allowing direct correlation between the two sets of data. Typical photographs examined by Image J software are shown with the 6 cm Declon Mesh impeller in Figure 5.16a and the 6 cm knitted wire impeller in Figure 5.16 b. Both photographs are for a fixed air flow rate of 1.0 vvm, with an agitation rate of 200 rpm.

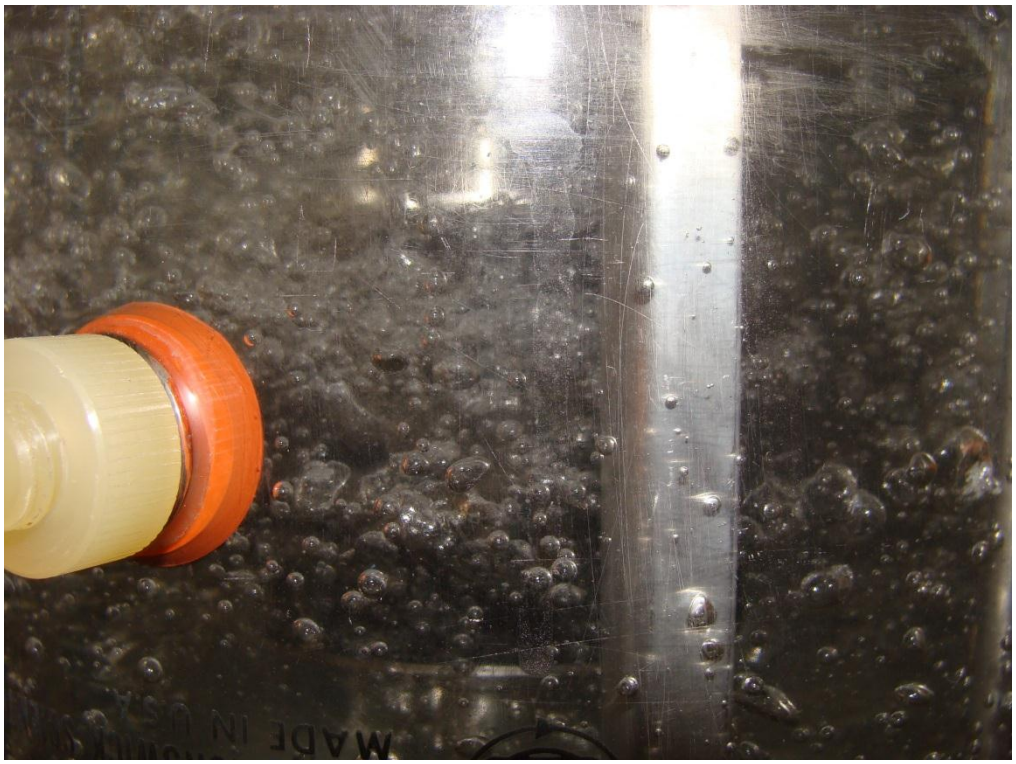

Figure 5.16a: Picture of air bubbles taken with the 6 cm Declon Mesh impeller at 200 rpm/1.0 vvm

Figure 5.16b: Picture of air bubbles taken with the 6 cm Knitted Wire impeller at 200 rpm/1.0vvm

5.3.1 Air/Water Results

The results obtained for the mesh impellers have been contrasted to those obtained for the Rushton impeller. Figures 5.17 a and b show the effect of agitation rate on mean bubble size for all impellers studied.

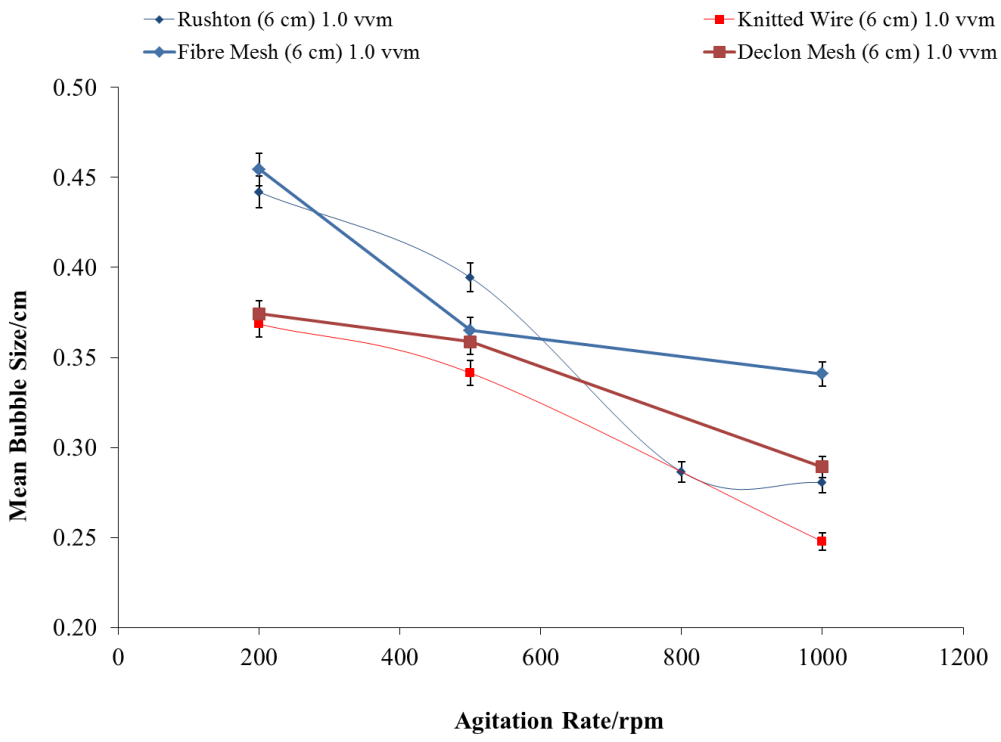

Figure 5.17a: The effect of agitation rate on Mean Bubble Diameter in the Air/Water system for the 6 cm impellers

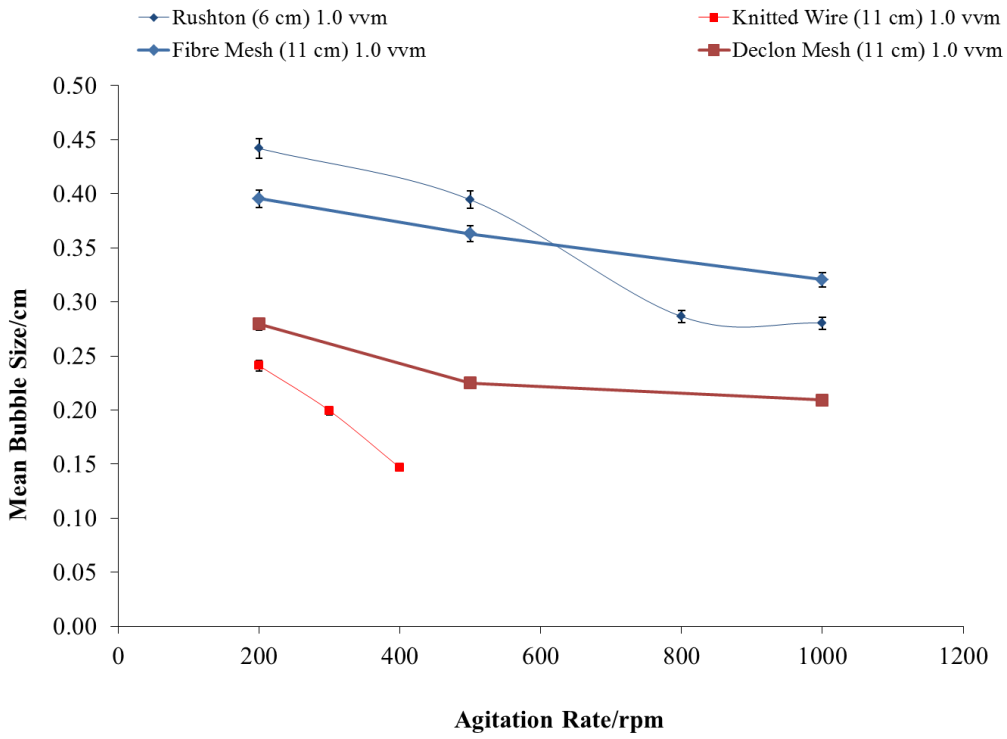

Figure 5.17b: The effect of agitation rate on Mean Bubble Diameter in the Air/Water system for the 6 cm Rushton and 11 cm Mesh impellers

Both graphs indicate that there is a decrease in the mean bubble size alongside an increase of the agitation rate. As the agitation rate increases there is a greater amount of power available to the impellers to be able to shear down the bubble. In the case for the Rushton impeller, increasing the agitation rate increases the chance that a bubble will strike one of the blades and be sheared to a smaller size. For the Rushton impeller this trend has been established in prior research and in other literature (Martin *et al* 2008). Research by Martin *et al* (2008) showed that for an impeller of a design like the Rushton impeller, bubbles are drawn to the impellers by their motion and then shredded by the blades. The faster the agitation rate the faster the bubbles are drawn towards the impeller and are then shredded down to a smaller size (Martin *et al* 2008).

The impeller diameter is an important parameter in determining size of bubbles formed. As shown in Figure 5.18, the 11 cm knitted wire impeller produced the smallest bubble diameter, followed by the 6 cm knitted wire impeller. A similar observation can be made with the Declon mesh impeller.

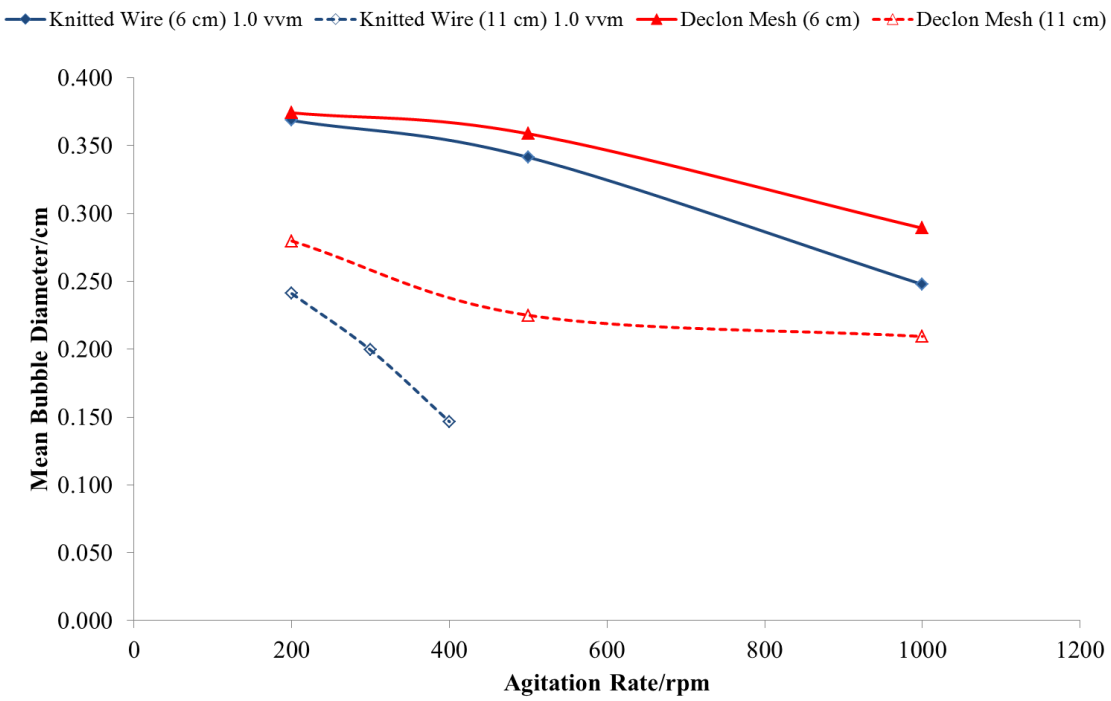

Figure 5.18: Comparison of mean bubble diameter for the Knitted Wire (6 and 11 cm) and Declon Mesh (6 and 11 cm) impellers

The reduction in bubble size is believed to be caused by the tightly bound material that comprises the impeller. As air bubbles rise from the sparger they encounter the highly porous

material, which are intricately wound together and are able to break bubbles into a much smaller size. This applies to both the 6 and 11 cm impellers. Similar research conducted by Tschentscher *et al* (2009) indicates that highly porous material fashioned as impellers could effectively reduce the bubble size observed. In the case of the 11 cm impellers, a further decrease in bubble size occurs due to the relative large volume the material occupies within the reactor. Not only does this catch a greater number of "stray" bubbles (that may be missed with the 6 cm knitted impeller) but also minimises the probability of coalescence occurring after the bubbles have left the sparger. Previous research investigating using highly porous material as bubble splitters within airlift columns also noticed an increase in transfer due to a decreased bubble size because of coalescence being minimised (Nikakhtari *et al* 2005B).

In the present study there appears to be no decrease in bubble size for the Rushton impeller between 800-1000 rpm. This is in fact not the case as there is a negligible decrease from 0.286 cm to 0.280 cm. The decrease may be due to experimental error rather than due to the conditions in the reactor causing such a minute decrease. Regardless of whether the bubble size stayed the same or decreased very slightly, this is quite an unusual result. It is likely that the vortex generated by the Rushton impellers at such high agitation rates causes more energy to be dissipated in the vortex than to be used in shearing the bubbles.

Airflow rate was the second parameter used to study the mean bubble size in the reactor system with the various impellers. Figure 5.19a and b illustrate the effect of airflow rate on the impellers examined in the current study.

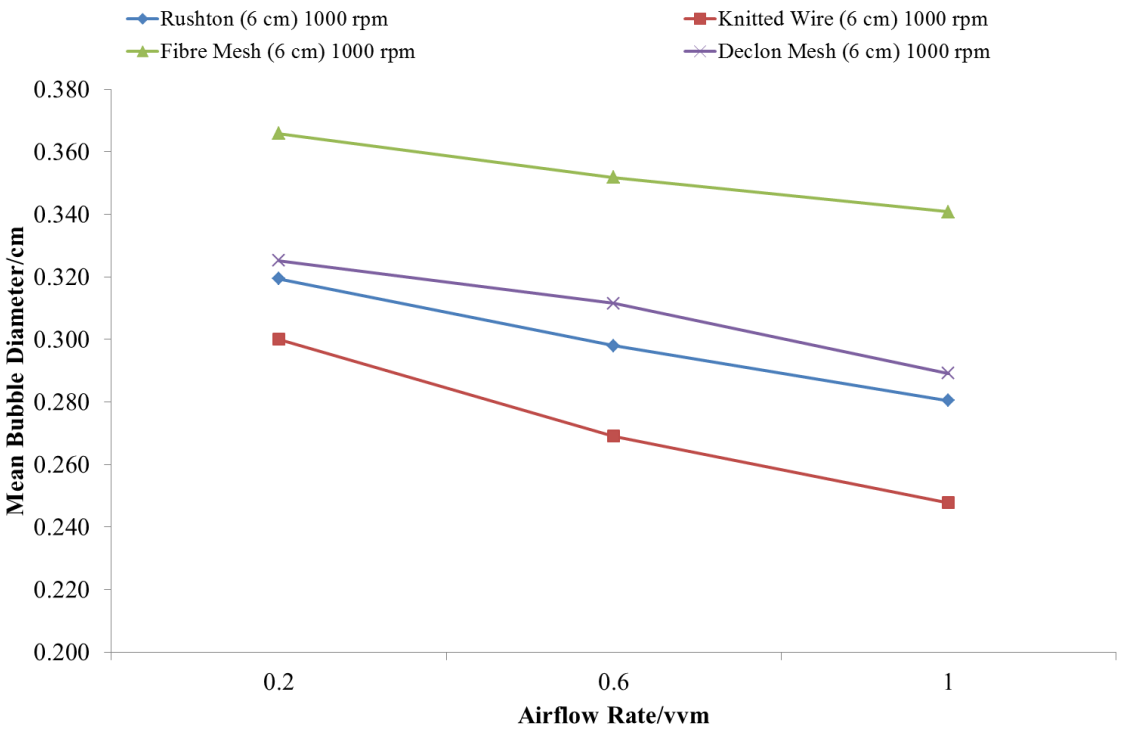

Figure 5.19a: The effect of Airflow rate on the Mean Bubble Diameter in the Air/Water system for the 6 cm impellers

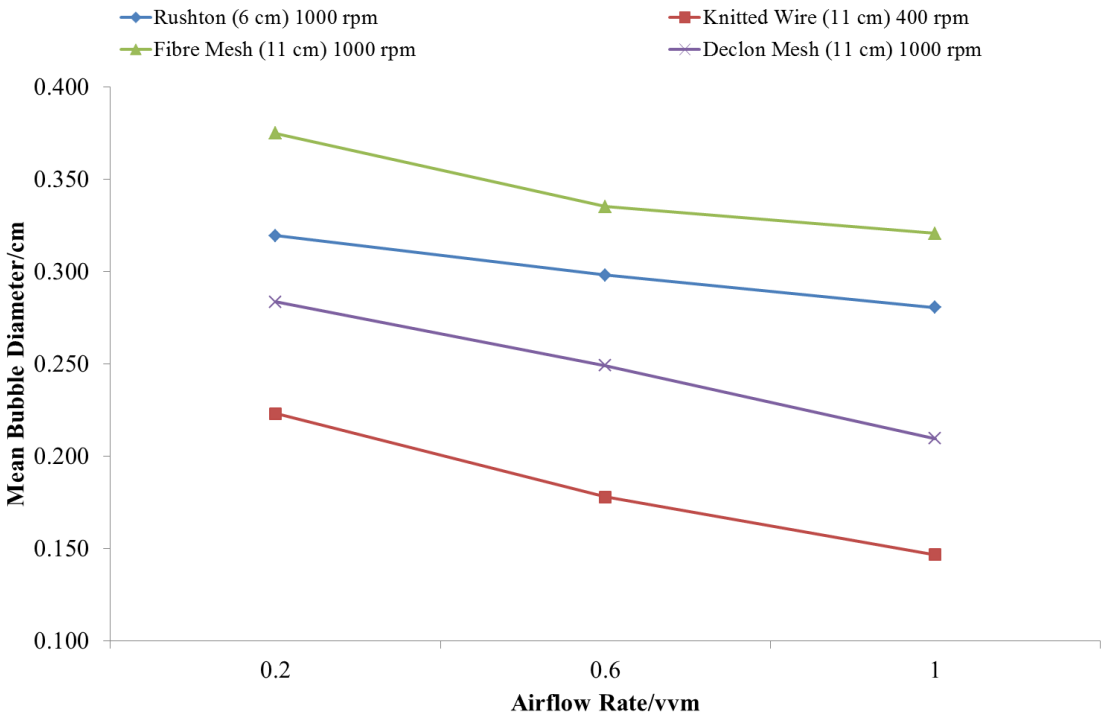

Figure 5.19b: The effect of Airflow rate on the Mean Bubble Diameter in the Air/Water system for the 6 cm Rushton and 11 cm mesh impellers

The increase in airflow rate is consistently observed to cause a decrease in the mean bubble size for all the impellers studied. This may be explained by the increasing flow of air producing a greater number of smaller bubbles as they form faster at the sparger before overcoming the forces pinning them down and break away. Puthli *et al* (2005) noted in their research that increased air flow rate lead to a higher oxygen transfer rate due to an enhanced gas hold up value. This in turn lead to an enhanced surface area being available for transfer, which could imply that smaller bubbles are produced (Puthli *et al* 2005). These results should be analysed in the context of the established theories of bubble formation, of which there are many of contradictory nature, especially at high gas flowrates, as elaborated on by Peel (1995) and more recently by Yang *et al* (2007). In particular, Calderbank and Jones (1961) have developed a theory of bubble formation from orifices which suggests that as the gas flowrate increases, larger bubbles are expected to form as the frequency of bubbles formed becomes relatively constant. This applies to the jet regime of bubble formation where the Reynolds number at the orifice, $Re_o \left(= \frac{\rho_l u_{or} D_{or}}{\mu_l} \right)$ is greater than 2100. The Reynolds number applicable to the gas flows used in this present study with the specified orifice dimensions of 0.5 mm (6 off) is well above 2100, indicating that this theory should be relevant to this study. However, the fact that gas flowrates are observed to have an opposite effect on the size of the bubbles in this present study shows that this theory may not be applicable here. In contrast, Leibson *et al* (1956) found that when gas flow through the orifice is fully turbulent (i.e above Re_o= 10,000), a swirling jet stream of bubbles is formed which eventually breaks up into a large number of much smaller bubbles, which is in better agreement with the experimental observations reported in this study. The stark differences between the observations in the studies by Calderbank and Jones (1961) and that by Leibson *et al* (1956) appear to be related to the position of the bubble size measurements with respect to the gas distributor, with Leibson and co-workers focusing on regions well away from the distributor.

5.3.2 Air/Water-Glycerol (50% v/v) Results

The effect of viscosity on mean bubble diameter was also investigated in the current study. The effects of agitation and airflow rate were also studied with the high viscosity system. Figures 5.20 a, b and Figures 5.21 a, b compared all impellers for the air/water-glycerol system and the effect of agitation rate and airflow rate respectively, whilst Figures 5.20 c and

5.21c compare the difference in viscosity between selected results for the two systems studied.

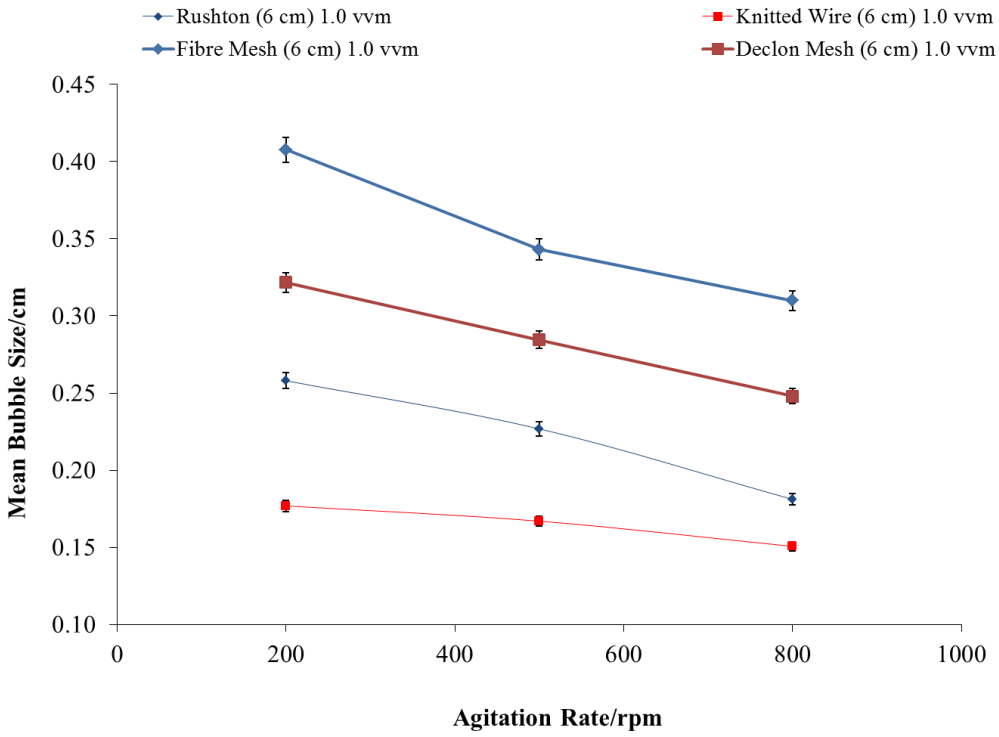

Figure 5.20a: The effect of Agitation rate on Mean Bubble Diameter in the Air/Water-Glycerol system for the 6 cm impellers

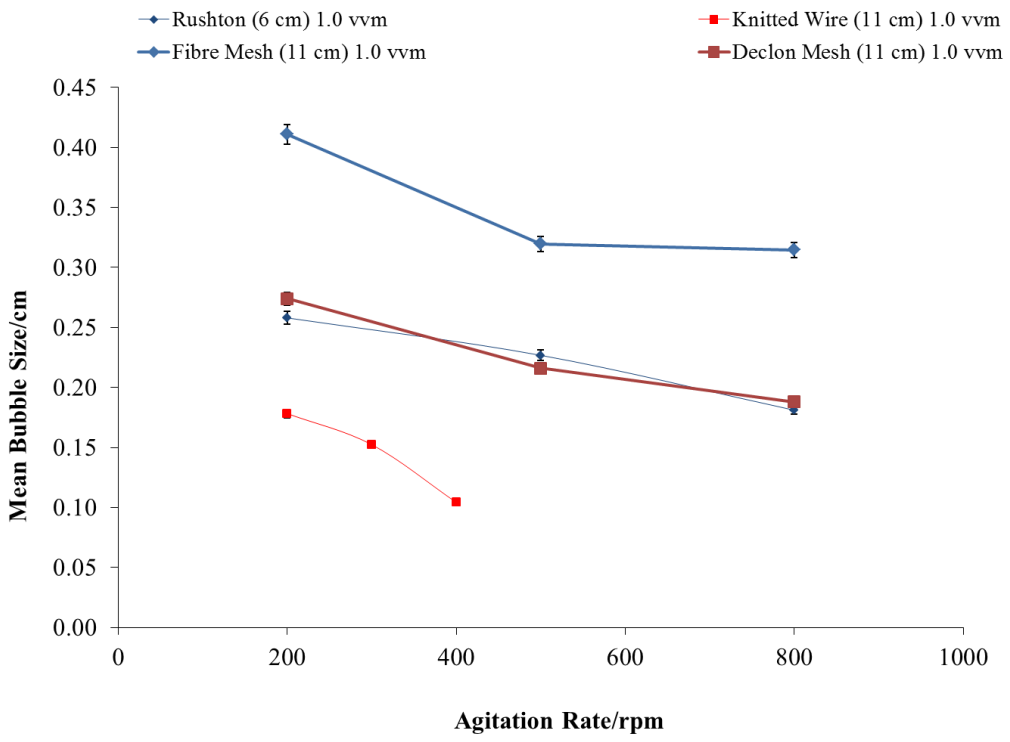

Figure 5.20b: The effect of Agitation rate on Mean Bubble Diameter in the Air/Water-Glycerol system for the 6 cm Rushton and 11 cm Mesh impellers

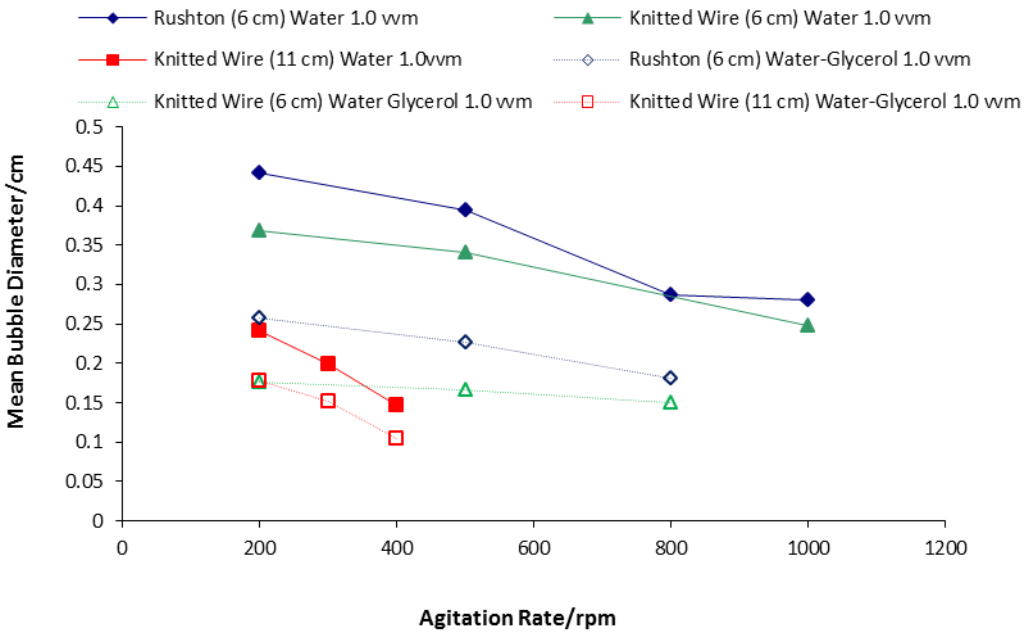

Figure 5.20c: The effect of Agitation rate on Mean Bubble Diameter for the Air/Water and Air/Water-Glycerol systems for the Rushton and 6/11 cm Knitted Wire impellers

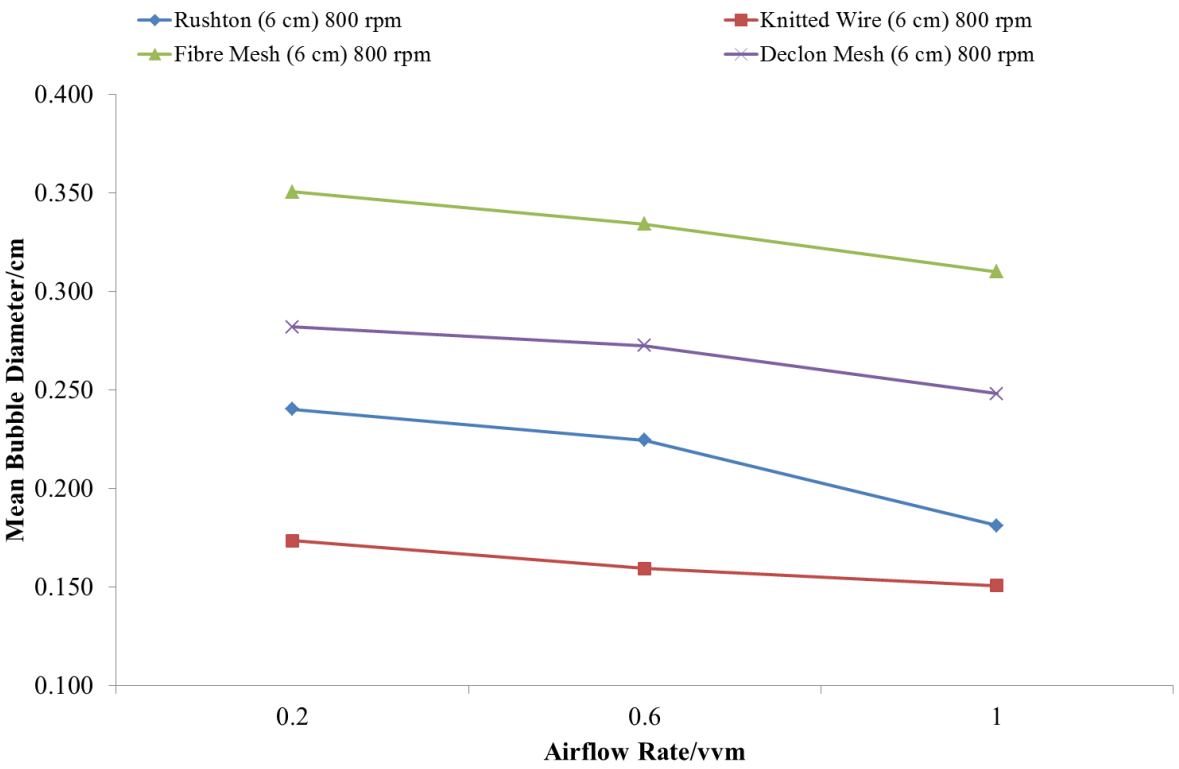

Figure 5.21a: The effect of Airflow rate on Mean Bubble Diameter in the Air/Water-Glycerol system for the 6 cm impellers

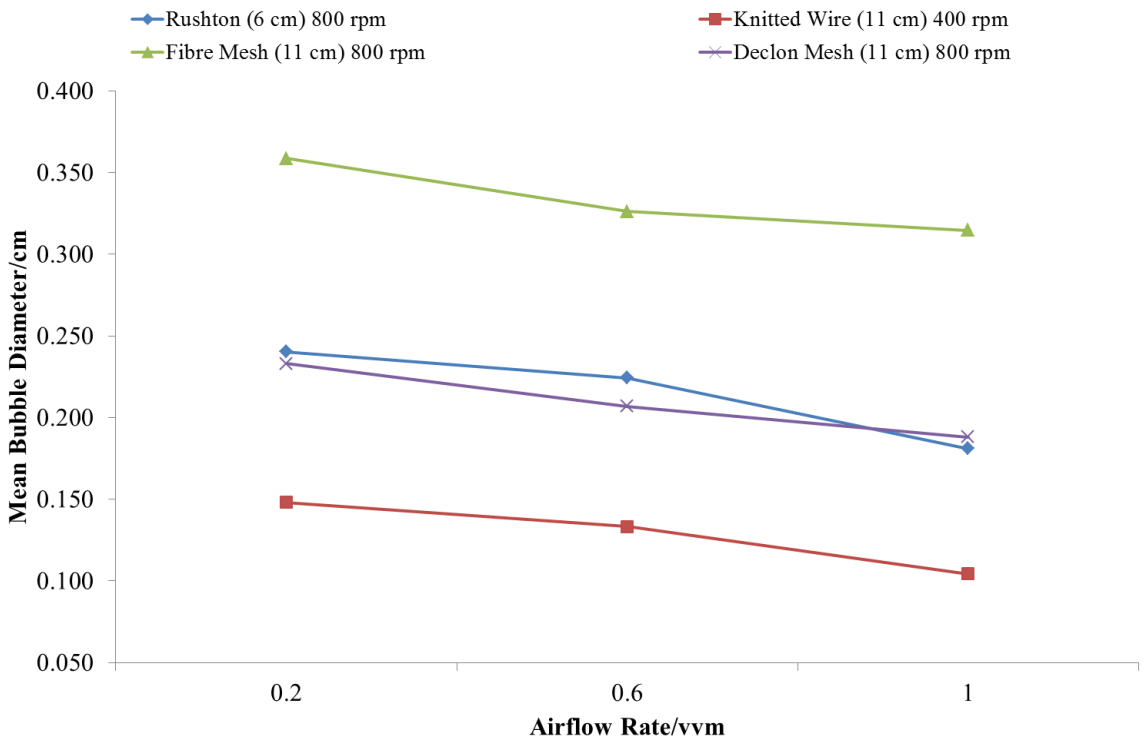

Figure 5.21b: The effect of Airflow rate on Mean Bubble Diameter in the Air/Water-Glycerol system for the 6 cm Rushton and 11 cm Mesh impellers

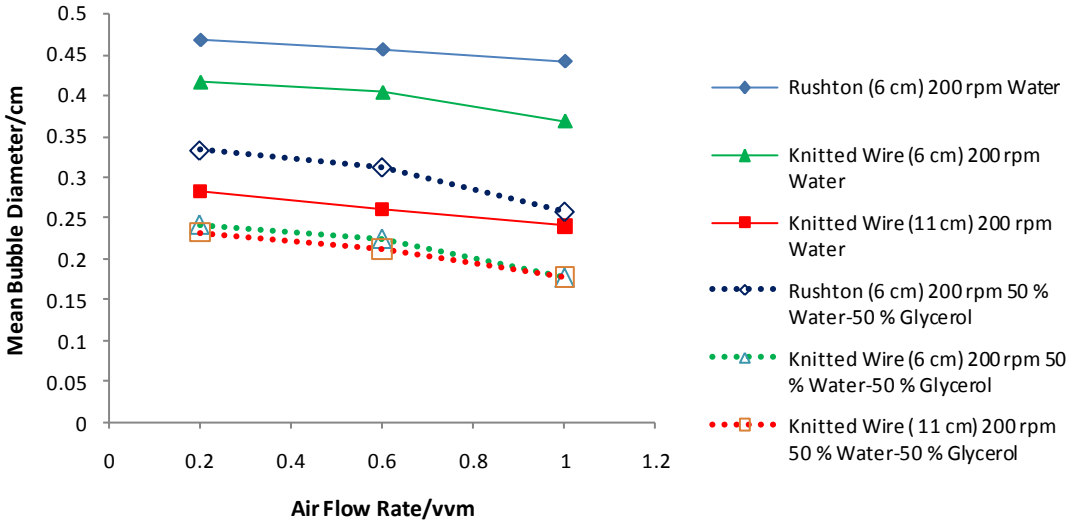

Figure 5.21c: The effect of Airflow rate on Mean Bubble Diameter for the Air/Water and Air/Water-Glycerol systems for the Rushton and 6/11 cm Knitted Wire impellers

The increase in agitation rate and airflow rate leads to a decrease in the mean bubble diameter to be observed. The reason for this has already been discussed in section 5.3.1 earlier. Interestingly, an increase in viscosity causes a decrease in bubble size as seen in (figures

5.20c and 5.21c) for all the impellers tested. This observation is in marked contrast to what had been expected, from the observed drop in oxygen transfer rate in the water-glycerol system. This effect of viscosity on bubble size may be explained by two factors: (1) the reduced surface tension of the water-glycerol mixture (2) reduced coalescence properties of the water-glycerol system. In the first instance, since gas bubble formation at the orifice is directly dependent on surface tension of the surrounding liquid (see section 2.2.2.3) in the literature review) , it is expected that initial bubble formed at the orifice of the sparger is smaller in the water-glycerol system due to its reduced surface tension. As a result when the bubble is broken up, even smaller daughter bubbles are formed. The fact that coalescence of gas bubbles is reduced when glycerol is added into the system is likely to contribute to the formation and continued existence of smaller bubbles in the water/glycerol mixture. The reduced coalescence effect arises as a result of a fine layer of glycerol/water surrounding the outer bubble surface which acts to repel other bubbles in the immediate vicinity. As a result coalescence is suppressed and the smaller bubbles initially formed therefore remain. Smaller bubbles also rise more slowly, thereby increasing their residence time in the liquid and giving more opportunity for a further enhancement for oxygen transfer. It could be expected therefore that the transfer in the water-glycerol system would be higher due to these smaller bubbles. However, the increase in viscosity also lowers oxygen solubility in the fluid, therefore lowering the K_La value. There is some debate as to whether the non coalescent behaviour of the fluid affects mass transfer values. Nocentini *et al* (1993) believe that with water /glycerol concentrations up to 50% (with respect to weight) the dominant effect is the non coalescent behaviour of the fluid. In this case with bubble sizes stable at a smaller size the interfacial area available for mass transfer is higher and therefore K_La values will be higher than that of water. After this 50% (with respect to weight) mark the dominant factor becomes the viscosity effect (lower solubility of oxygen) and the K_La decreases below that of the water system. In the present study, the higher viscosity system is 50 % water and 50 % glycerol by volume. This roughly equates to 55 % glycerol by weight. The results for the present study are therefore in line with the observations found in Nocentini *et al* (1993) which show a lower K_La value for the water-glycerol system, but with a decreased bubble size.

5.3.3 SMS Fermentation Medium

A bubble study was investigated with use of the medium to be used for the *Escherichia coli* K12 fermentation. The impellers investigated were the Rushton and Knitted Wire impellers,

with the conditions selected those to be investigated for the *E.coli* study. In this instance an airflow rate of 1.0 vvm is equivalent to 4 l min^{-1} due to the fluid volume being reduced to 4 l to reflect the fermentation study to be conducted. The effect of agitation and airflow rate were studied with figures 5.22 a and 5.23 a showing the effect of agitation and airflow rate respectively. Figures 5.22b and 5.23b also illustrate the differences between the 11 cm Knitted Wire impellers for the Air/Water, Air/Water-Glycerol and SMS Fermentation medium for agitation rate and airflow rate respectively.

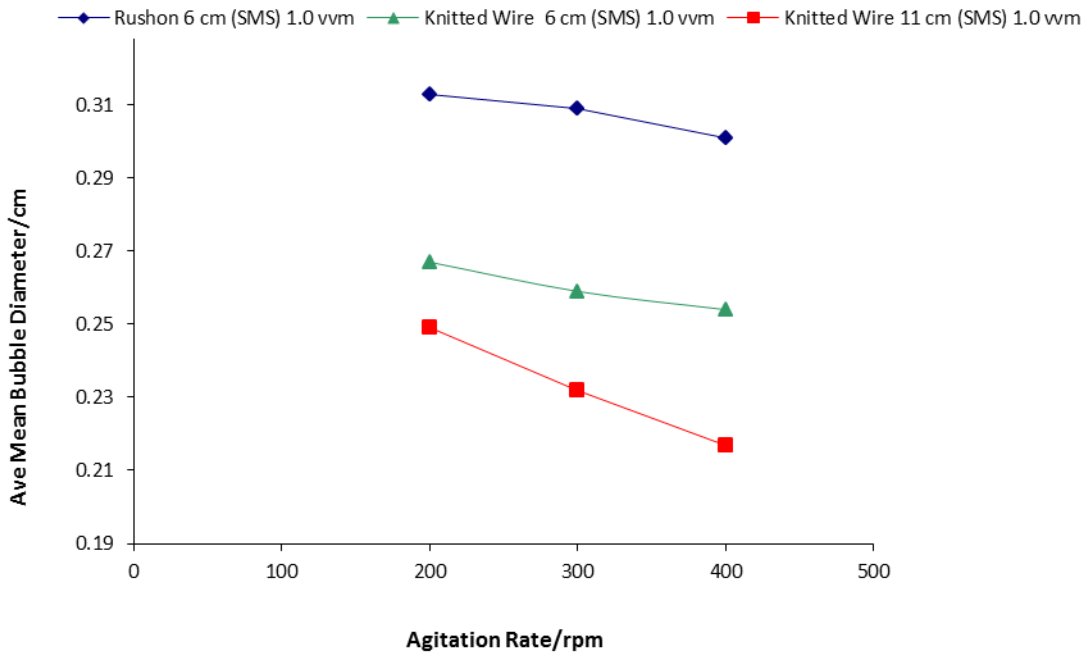

Figure 5.22a: The effect of Agitation rate on the Mean Bubble Size for the Rushton (6 cm) and Knitted Wire (6 and 11 cm) impellers in SMS Medium

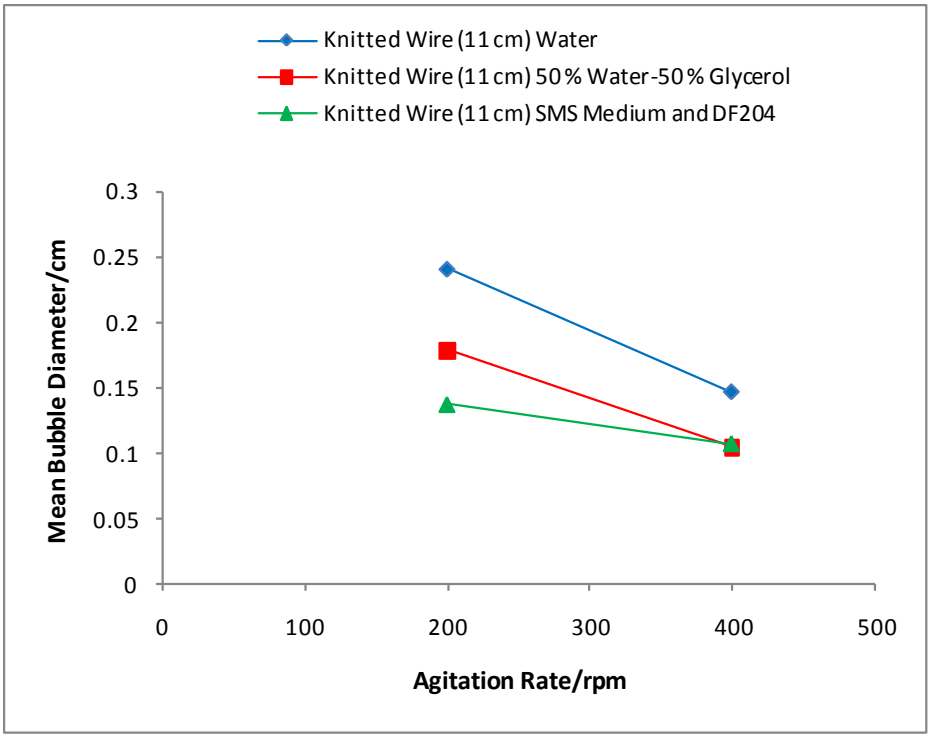

Figure 5.22b: The effect of Agitation rate on the Mean Bubble Size for the 11 cm Knitted Wire impeller (Airflow rate at 1.0 vvm) for the Air/Water, Air/Water-Glycerol, and SMS Medium systems.

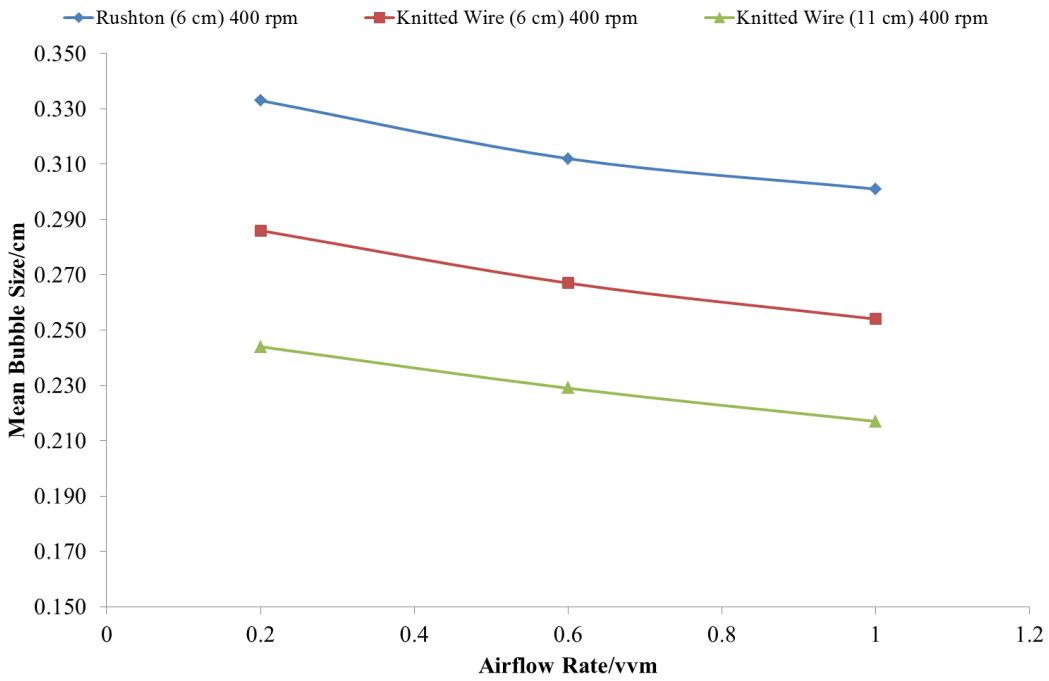

Figure 5.23a: The effect of Airflow rate on the Mean Bubble Size for the Rushton (6 cm) and Knitted Wire (6 and 11 cm) impellers in SMS Medium

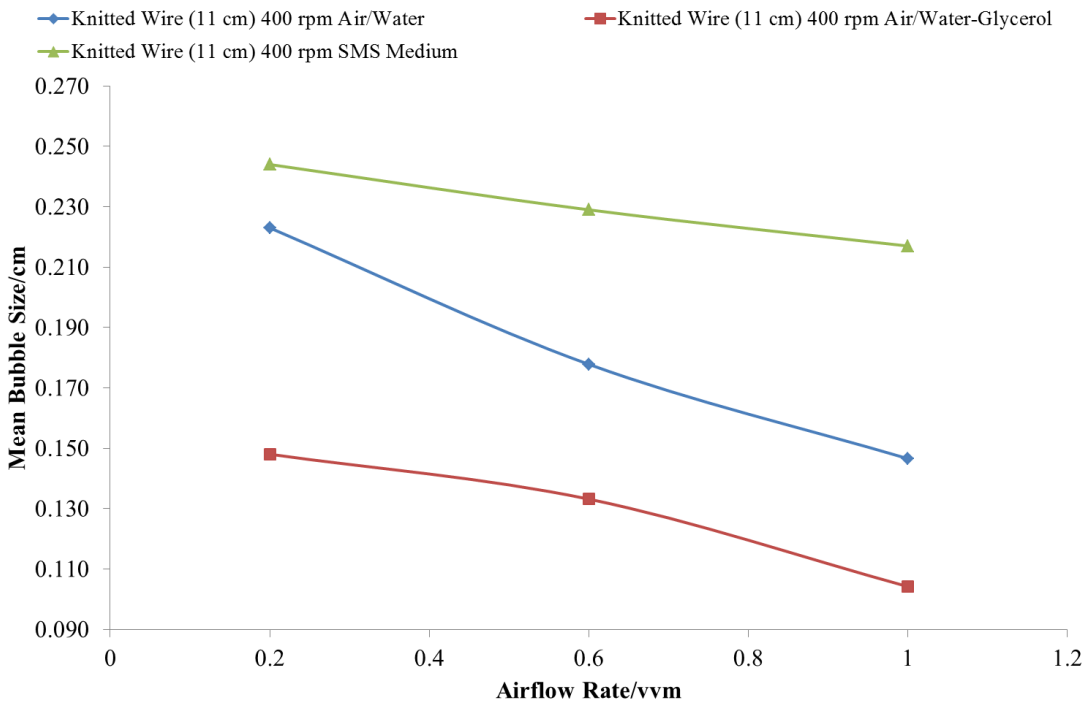

Figure 5.23b: The effect of Airflow rate on the Mean Bubble Size for the 11 cm Knitted Wire impeller (Agitation rate at 400 rpm) for the Air/Water, Air/Water-Glycerol, and SMS Medium systems.

The same trends for agitation rate and airflow are prevalent again-a decrease in mean bubble size is observed with increasing agitation rate or airflow rate. When all three impellers are observed in the SMS medium, the 11 cm knitted wire impeller produces the smallest mean bubble diameter. In figure5.18b the emphasis is on one impeller across the three different systems studied so far. In this instance the smallest mean bubble diameter produced is in the 50 % water-50 % glycerol system, although the air flow rate for the fermentation system is slightly lower (4 l min^{-1} compared to 5 l min^{-1}).

To combat foam during the fermentation experiments, 20 µl/4 l SMS was added. The 11 cm knitted wire impeller was most prone to foaming occurring. It is known that antifoams have an effect on the transfer rate in the system (Gogate *et al* 2005, Koch *et al* 1995). A second study with SMS medium therefore took place, with the additional antifoamer added to observe any changes with bubble size. Figure 5.24a illustrates the effect of each impeller system, whilst figure 5.24b shows the effect for the 11 cm knitted wire impeller compared to the study without DF204 added.

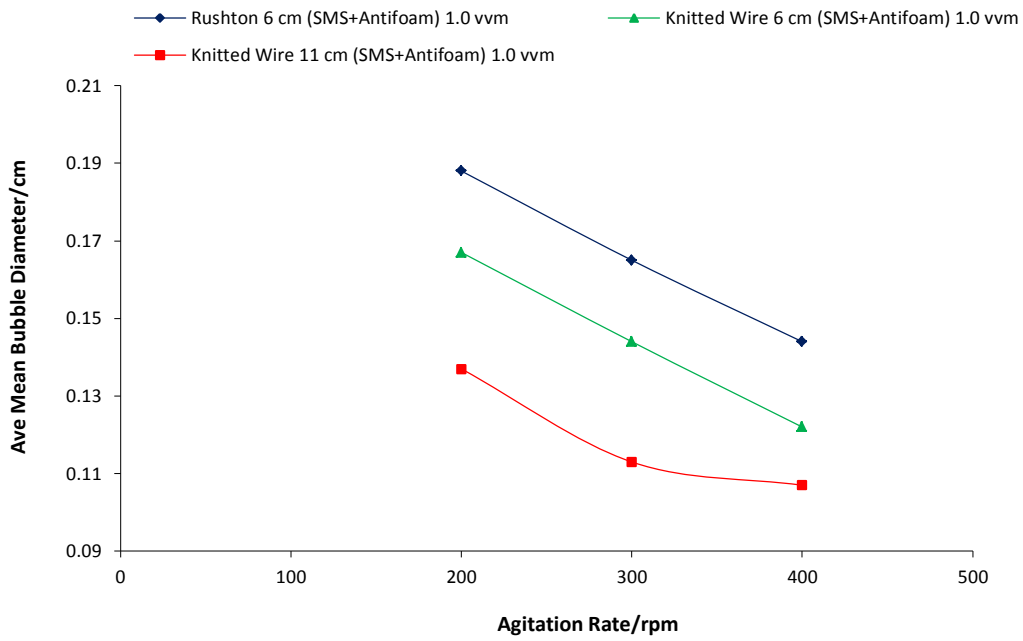

Figure 5.24a: The effect of the addition of DF204 on the Mean Bubble Size for the Rushton (6 cm) and Knitted Wire (6 and 11 cm) impellers

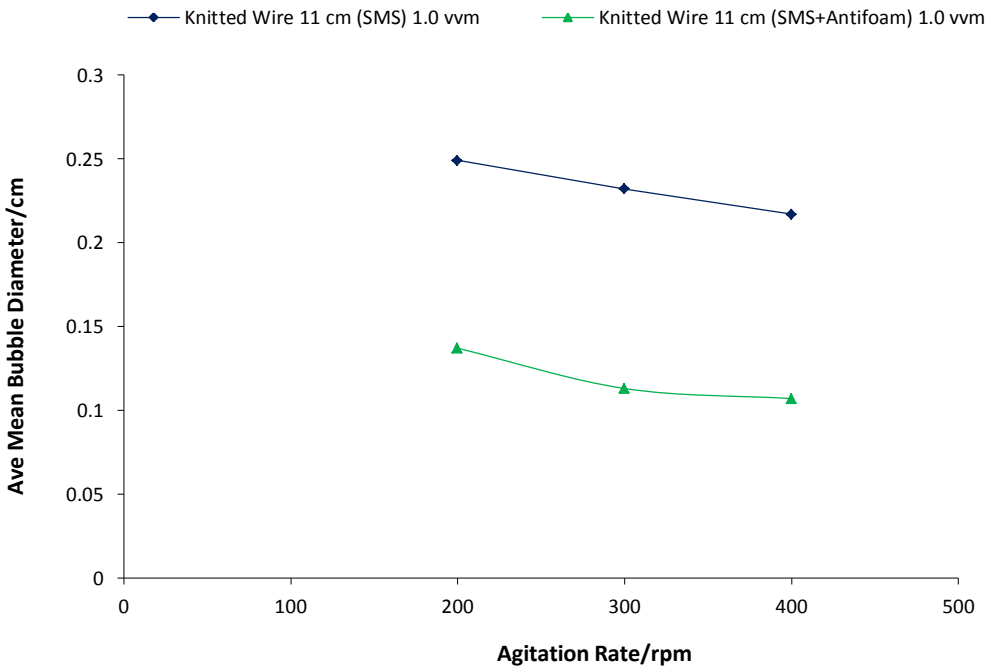

Figure 5.24b: The effect of antifoamer addition on the SMS medium system for the 11 cm knitted wire impeller.

Figure 5.24a notes that the 11 cm Knitted Wire impeller produced the lowest mean bubble size in this SMS combined with antifoam system. Figure 5.19b illustrates that the addition of DF204 to the SMS medium had the effect of lowering mean bubble size further.

The effect of antifoam on bubble size (or on oxygen transfer) is not well understood. Antifoam agents such as DF 204 tend to alter the surface tension of the fluid, which alters coalescence within the system. Gogate *et al* (2000) noted that this alteration of the gas phase leads to alterations of the gas hold up, ultimately leading to a change in mass transfer. In terms of bubble production the fact that in the present study the surface tension of the fluid was reduced in the presence of antifoam will have a marked effect on the force balance at the orifices of the sparger. With a reduced surface tension, it will be easier for bubbles to break away from the sparger as they do not experience as much force pinning them down. Once they have broken away, the antifoam coats the surface of the bubble and prevents coalescence, as discussed earlier. Koch *et al* (1995) described the effect that antifoams may have on the K_La value. Firstly, due to the lowered surface tension of the fluid, the Sauter mean bubble diameter is lowered in the impeller regions (enhancing K_La) but because of coalescent promotion away from the impeller regions increases the Sauter mean bubble diameter (lowering K_La). From results from bubble columns it has been shown that the two opposing effects forces roughly cancel each other out where bubble size is concerned. Further, Koch and co-workers stipulate that the presence of antifoam affects the film coefficient (K_L). This had not been proven in an STR, until Koch *et al* (1995) conducted experiments with different concentrations of antifoam in a STR and studied is effect on K_La. The addition of low concentrations of PPG has shown that the Sauter mean bubble diameter is hardly affected by the addition of PPG, but gas hold up is greatly decreased. This would seem to suggest that the K_La of the reactor is lowered because of the antifoams effect on K_L alone.

One of the main problems with PPG type antifoams is that if they are added in full at the beginning their effect at first is minimal as they tend to sit as a puddle on top of the fluid until they are mixed into the fermentation media. To combat this behaviour other organic chemicals have been introduced to enhance the dispersion of the antifoam. At present there has been no real study investigating how bubble size is altered by the presence of antifoam. In terms of oxygen transfer a number of studies have investigated how antifoam may impact it. One theory proposed by Arjunwadkar *et al* (1998) is that as antifoam is added a large drop

in transfer results until a critical concentration point is reached (at around 0.035 %) from when there is only a small drop in transfer. This drop has been related to the gas hold up, which had been estimated to have dropped by around 20-25 % which was not related to a drop in power consumption. Furthermore accumulation of antifoam agent at the gas-liquid interface may provide further resistance to transfer, resulting in the value of K_La to further decrease (Arjunwadkar *et al* 1998)

5.3.4 Summary

The present study investigated the mean bubble diameter in a number of different Newtonian systems. The effects of agitation and airflow rate were studied and the following observations have been noted:

1. Increasing the agitation or airflow rate decreases the mean bubble diameter. In the case of increasing agitation rate this is due to greater amount of power available to the impellers to be able to shear down the bubble. For increasing airflow rate the decrease is brought about because of increasing flow of air produces a greater number of bubbles as they form faster at the sparger before overcoming the forces pinning them down and break away
2. In the majority of cases the mesh impellers produce a smaller mean bubble diameter compared to the Rushton design. This is believed to be caused by the tightly bound material that comprises the impeller. As air bubbles rise from the sparger they encounter the highly porous material, which are intricately wound together and are able to break bubbles into a much smaller size. A further decrease is noted for the 11 cm mesh impellers due to due to the relative large volume the material occupies within the reactor. Not only does this catch a greater number of “stray” bubbles (that may be missed with the 6 cm knitted impeller) but also minimises the probability of coalescence occurring after the bubbles have detached from the sparger
3. The addition of solutes in the SMS system produces a smaller bubble diameter at 200 rpm (compared to both the Air/Water and Air/Water-Glycerol system). For 400 rpm the bubble size is again lower for the SMS medium than the Air/Water system but roughly the same size as the Air/Water-Glycerol system. The addition of DF204 brings about a further reduction in bubble size as observed in this study which represents a complex phenomenon yet to be fully understood.

5.4 HiGEE Bioreactor (HBR)-Hydrodynamic Study

The focus of this section is the initial experiments conducted with the HBR. The results reported include the flooding and nitrogen bubble study investigated as part of the hydrodynamic study of the reactor. In the present study the term hydrodynamic capability is taken to be the characteristics of the gas and liquid in the reactor (Peel 1995). The bubble study will be compared to the previous results obtained with the STR. The transfer capability will also be examined later in the chapter by investigation of oxygen stripping from water with the use of Nitrogen gas. For both bubble studies a Phantom Miro 4 high speed digital camera was loaned from the EPSRC instrument pool.

5.4.1 Flooding

Flooding in packed bed reactors such as the HBR is an important operational consideration. To characterise the conditions under which flooding would occur, a series of experiments utilising various different rotational speeds, nitrogen and liquid flow rates were performed. The experiments were also performed with and without the highly porous packing material. The flooding data from the present study were plotted against the results of Jassim (2002) which is representative of the classic Sherwood plot (Sherwood *et al* 1938) (Figure 5.25). The results gained from the flooding study present the upper operational limit for the HBR These results are then used in order to establish parameters for the later studies. With packing inserted (inner diameter of 150 mm) a higher throughput of both gas and liquid can be employed within the HBR Without packing inserted the flooding curve is seen to lower as a result, indicating that a lower throughput of gas and liquid can be utilised in the HBR.

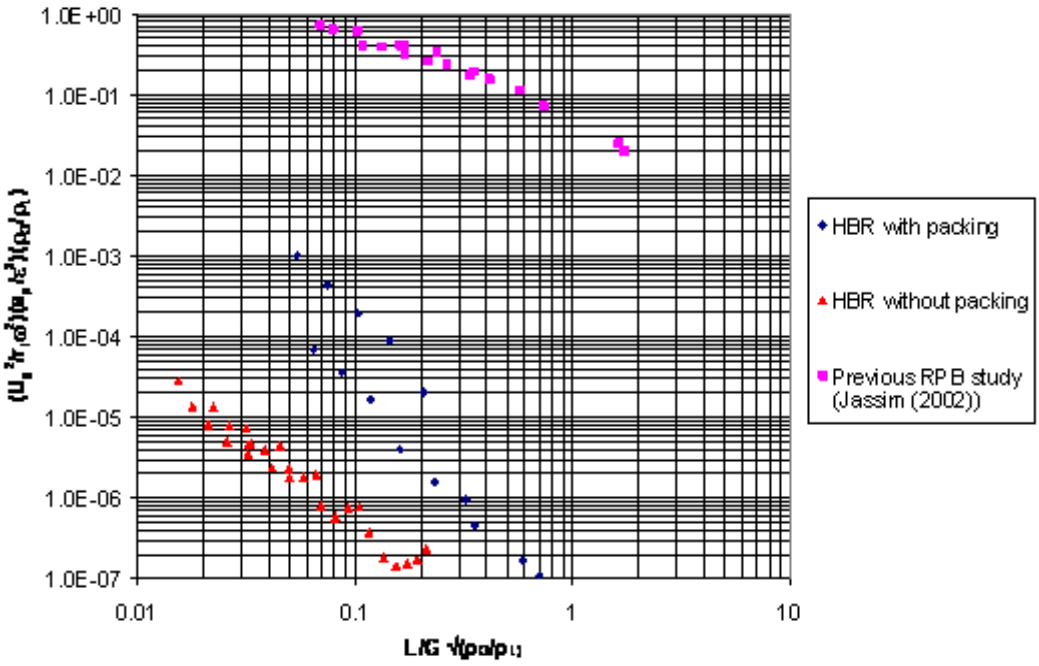

Figure 5.25: Comparison of flooding data for the present study against Jassim (2002)

The plot in figure 5.25 serves as an illustration of how two systems compare to each other when plotted on the same graph. There is a significant difference in the flooding results noted between the present study and the previous study by Jassim (2002). The latter study operated with the gas phase as the continuous phase and the liquid phase flowing over the packing as a thin film (Jassim 2002). In contrast, in the reactor presented in the current study, the liquid phase is the continuous phase with the gas phase employed as a dispersed phase. Such a difference in operation would have a profound impact on the visual observation of the onset of flooding. In the HBR, for instance, the dimensions of the eye of the rotor (i.e. the edge of the continuous liquid boundary) is continuously moving inwards under conditions of higher gas rates, higher liquid rates and/or low rotor speeds. This could cause more splashing to occur at lower flow rates, leading to an assumption that flooding limit has been reached.

A second possible cause of the lower flooding limit in the current HBR may be attributed to the packing used in the system. As shown in figure 5.25 the insertion of packing leads to much higher throughput of gas and liquid in the HBR This is because the presence of packing in the reactor allows more efficient coupling of the liquid phase with the body of the reactor when it is being rotated. The packing used in the present study was in the shape of a doughnut with an outer diameter of 244 mm and an inner diameter of 150 mm. There is scope to insert more packing material within the HBR by significantly reducing the inner diameter

to about 50 mm. This is likely to increase the allowable throughput of liquid and gas, thereby increasing the flooding limit within the reactor.

5.4.2 Bubble Study

A visual study of gas bubble size was completed to examine how the operating parameters of the HBR affected the bubble size noted. Figure 5.26 shows an example picture of bubbles formed within the HBR.

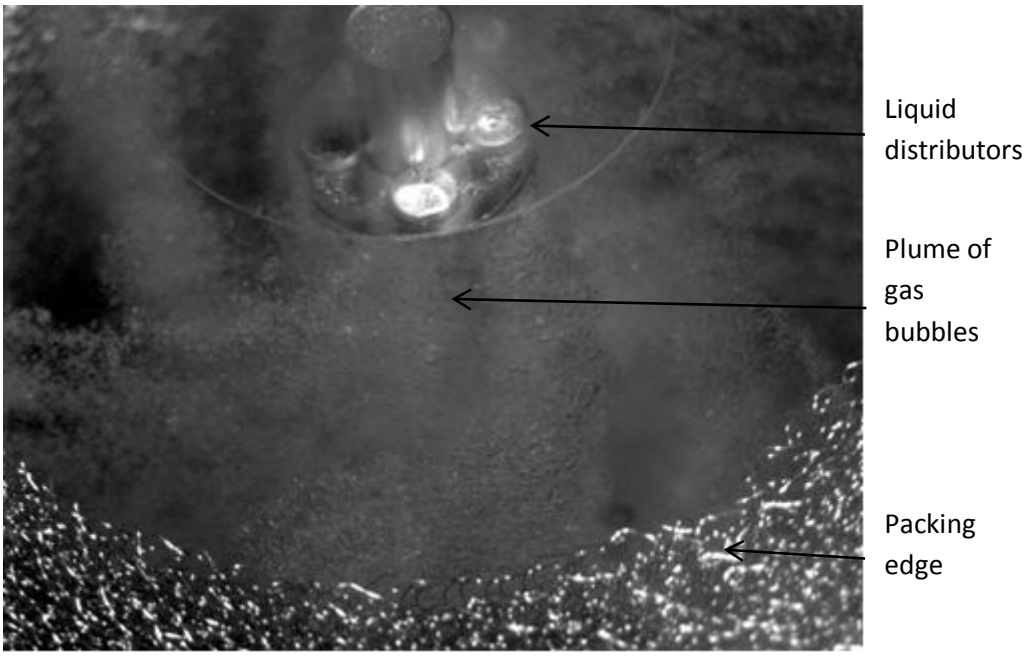

Figure 5.26: Digital image taken with the Phantom Miro 4 High Speed Digital Camera (picture taken at 1200 rpm, 0.6 l/min liquid flow rate and 16 l/min gas flow rate)

The mean bubble diameter and size distribution of the bubbles was noted as the bubbles travelled inwards from the edge of the packing section through the liquid phase and onwards to the eye of the rotor, as shown in figure 5.26. Figures 5.27a and b illustrate the effect of liquid flow rate, airflow rate, and centripetal force on the mean bubble diameter noted.

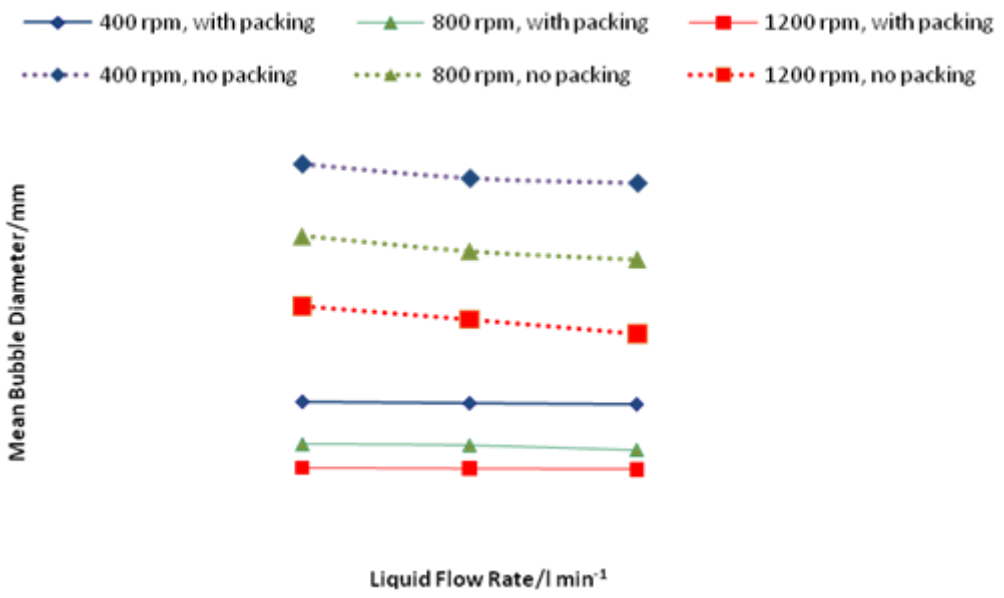

Figure 5.27a: Effect of Rotational Speed and Liquid Flow Rate on Mean Bubble size in HBR (constant gas flow rate of 8.6 l min^{-1})

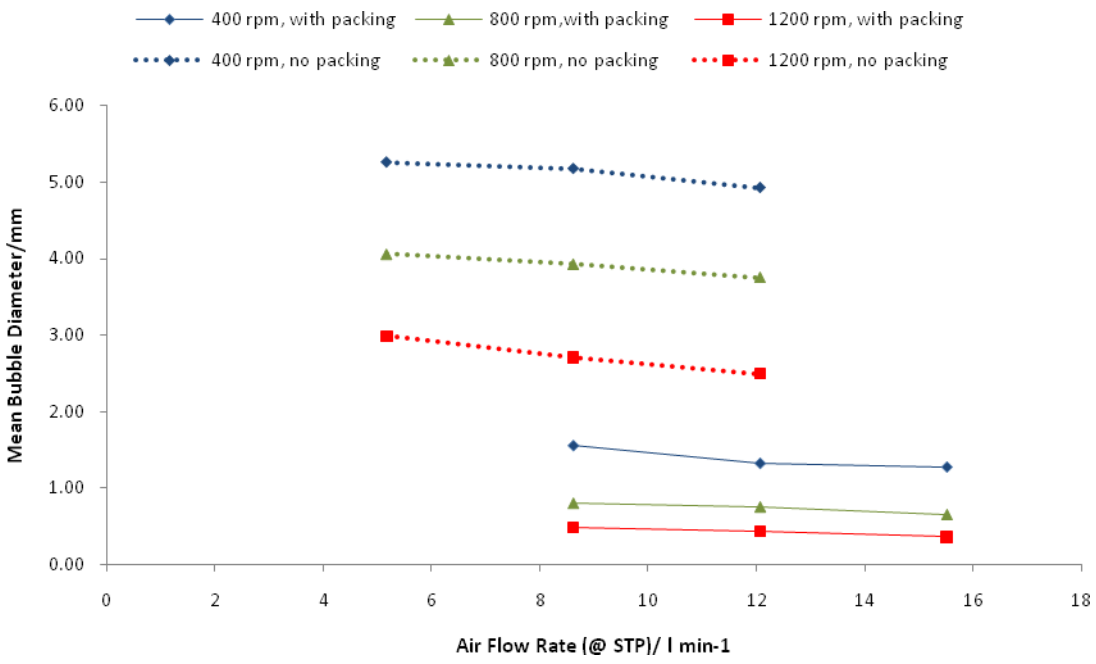

Figure 5.27b: Effect of Rotational Speed and Air Flow Rate on Mean Bubble size in HBR (constant liquid flow rate of 0.6 l min^{-1})

Mean bubble diameter was seen to decrease with both increasing rotational speed and increasing airflow rate. The decrease in bubble size produces a larger interfacial area which should produce larger gas-liquid transfer rate as a result. As the rotational speed increases, the

bubbles experience a larger centripetal force which causes them to be shredded down to a smaller size. Increasing the speed of the rotor from 400-1200 rpm decreased the mean bubble diameter from 1.3 to 0.4 mm (with packing) and from 5.6 mm to 3.8 mm (without packing). As the airflow rate increases, the bubbles are able to break off from the injectors much faster and therefore form smaller bubbles. For traditional reactor systems operating a normal gravity (such as the STR), predicted bubble size at the orifice of the injector is roughly proportional to $g^{-1/3}$ (Calderbank *et al* 1961) or $g^{-1/5}$ (Davidson *et al* 1960). These values are noted to be dependent upon the gas flow rate employed (Davidson *et al* 1960, Calderbank *et al* 1961). It is reasonable to assume that the same principle applies to the current study, but due to the high centripetal environment it is believed that mean bubble diameter will be smaller when formed on the injector. The initial size of the bubble also plays a role in the mean bubble diameter as well as the packing material employed, and this can be seen in the present study whereby the bubble diameter decreases with increasing rotational speed.

The mean bubble diameter of the HBR was noted by digital photography, for which the position of observation may play a role in the values recorded. Due to the photographs being taken at the centre of the HBR, the effect of the centripetal force is less than the outer periphery of the HBR As the effect of centripetal force is less, the bubble diameter will be larger here than at the periphery. As the acceleration experienced by the gas bubbles increases proportionally as distance from the centre increases, the mean bubble diameter will be at their smallest at the outer edge of the system. If the size of the rotor was to be increased then theoretically the mean bubble diameter may also be seen to decrease. This theory has been noted experimentally by Peel (1995).

Liquid and gas flow rates appear to have a negligible effect on the size of the gas bubbles produced at a given rotor speed in the range of flow rates studied. A similar observation about the effect of gas flow rate was made by Peel (1995) who modelled gas bubble sizes at different gas flow rates in a centrifugal field de-oxygenator. The theory of bubble formation from orifices suggests that as the gas flow rate increases, larger bubbles are expected to form as the frequency of bubbles formed becomes relatively constant (Calderbank and Jones, 1961). This applies to the jet regime or bubble formation where Re_o>2100. The Reynolds number applicable to the gas flows used in this HBR with the specified orifice dimensions is well above 2100, indicating that this theory should be relevant to this study. However, the fact that gas flow rates are observed to have little impact on the size of the bubbles clearly shows that the packing has a more dominant effect in determining bubble size. Indeed, it is

observed that insertion of packing material into the HBR has an effect on bubble size. Both figures 5.27a and 5.27b note a decrease in bubble size with the system that includes packing. The reason for this decrease is that as the bubbles travel from the sparger to the centre of the reactor they encounter the densely packed stainless steel which then shreds the bubbles down to a smaller size. Furthermore due to the nature of the packing, coalescence of the bubbles in the current study is minimised compared to the study without packing. Both these factors play a role in the reduction of the mean bubble diameter.

5.4.3 Summary

A series of initial experiments have been conducted with the HBR to examine the capabilities of this reactor related to the throughputs and gas bubble size. The following conclusions can be drawn from the present study:

1. The flooding study was used to characterise the upper operational limits of the reactor. With packing inserted in the rig a larger throughput of gas and liquid can be pushed into the reactor before flooding occurs. Due to certain limitations in the reactor (packing diameter and operation of the reactor) the throughput of liquid and gas was not as high as expected. It is suggested that throughput may be increased by decreasing the inner diameter of packing so that it occupies a larger proportion of the cross-sectional area of the rotor.
2. The bubble study performed in the HBR has noted that very small bubbles can be produced. The bubble size decreases as rotational speed increased, with gas flow rate and liquid flow seemingly having no large influence. On the other hand, the packing within the reactor was noted to have a profound effect on reducing the mean bubble diameter.

5.5 HiGEE Bioreactor-Transfer Experiments

The transfer capability of the HBR was studied which both included and excluded the packing material. The calculation of Number of Transfer Units (NTU) and K_La is as presented in Chapter 2 (see 2.4.3). Assessment of the HBR. transfer capability was performed by stripping of oxygen from saturated water with the use of nitrogen gas.

5.5.1 Results and Discussion

5.5.1.1 NTU Calculation

A set of initial experiments found the highest NTU to be around 0.98, which compared to other results for similar reactor designs seemed low. The cause behind such a low result was

due to the deoxygenated water carrying a high proportion of oxygen when sampled downstream of the collector. It was theorised that this was because a small amount of oxygen was leaking into the collector from the outside environment. As the reactor had been efficient in stripping a large amount of oxygen from the water, any oxygen present in the collector was instantly absorbed by the water leading to the higher DO concentration noted by the DO probe. As a result a modification was made to the collector to include a nitrogen blanket. This blanket would stop any oxygen leaking into the collector and absorbing into the deoxygenated water. The nitrogen for the blanket was provided from the same source as that used by the injectors, a t-valve separating the two nitrogen flows. The nitrogen blanket flow rate was kept constant at 4 l min^{-1}. Due to the volume of the collector, it was estimated that it would take around 6 minutes for the full blanket to be established. Therefore as a result, the nitrogen flow was established 10 minutes prior to reactor start up to ensuring the blanket was fully established.

The operating conditions for the transfer study were the same as those employed for the bubble study conducted. The effect of liquid and gas flow rates are noted in figures 5.28 a and b

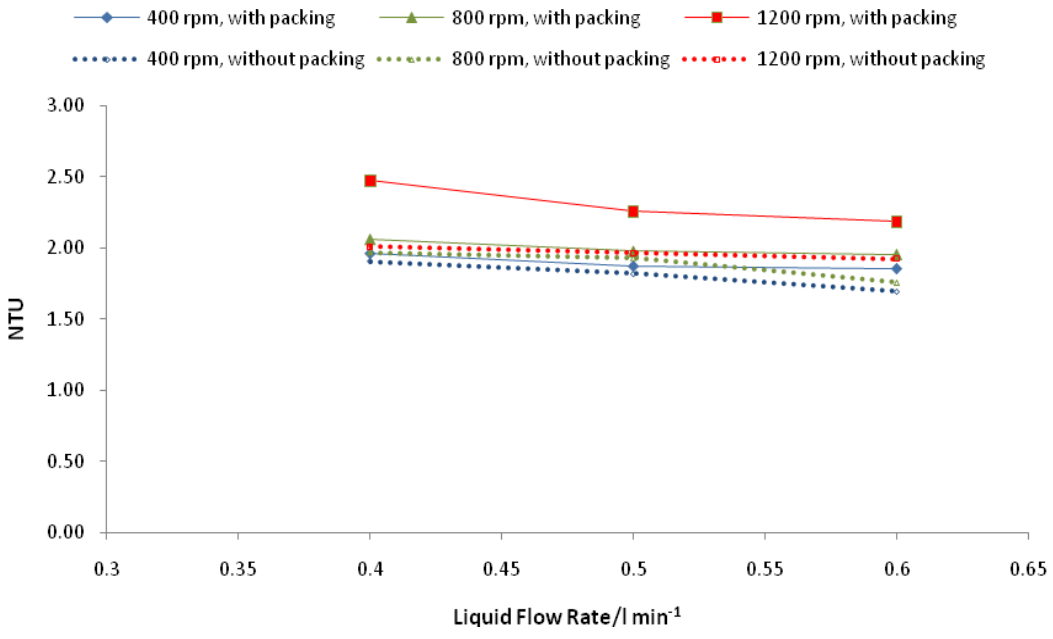

Figure 5.28a: Effect of Rotational Speed and Liquid Flow Rates on NTU Values for the HBR

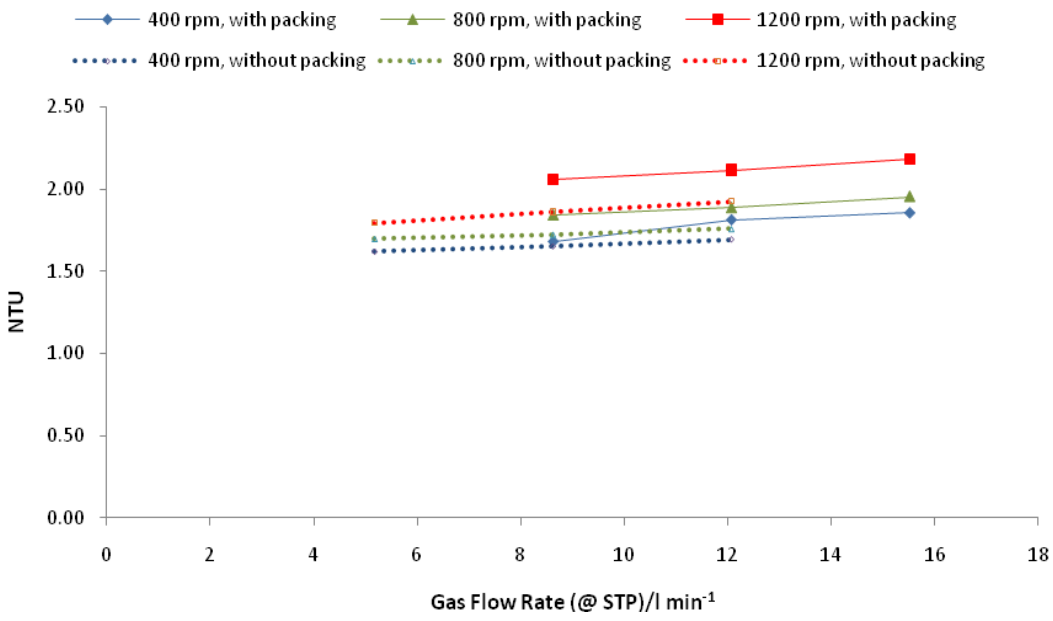

Figure 5.28b: Effect of Rotational Speed and Gas Flow Rates on NTU Values for the HBR.

As both rotational speed and gas flow rate increase, an increase was observed in the value of the NTU for the system. It has been shown previously in Figures 5.27 a and 5.27b that an increase in rotational speed contributes to a decreased bubble size. As a result the interfacial area is greater leading to the enhanced gas-liquid transfer. Increasing gas flow rate increases the gas hold up with the HBR leading to a greater contact time between the liquid and gas phases and bringing about higher transfer rates. Conversely increasing liquid flow rate brought about a decrease in NTU.

5.5.1.2 K_La Calculation

As noted in chapter 4, the method of calculating the liquid side overall volumetric mass transfer coefficient (K_La) is based on established gas-liquid mass transfer theory (Kelleher *et al* 1996, Peel 1995, Peel *et al* 1998). Figures 5.29 (a and b) illustrate the effect of rotational speed, liquid flow and gas flow rate on the K_La value observed.

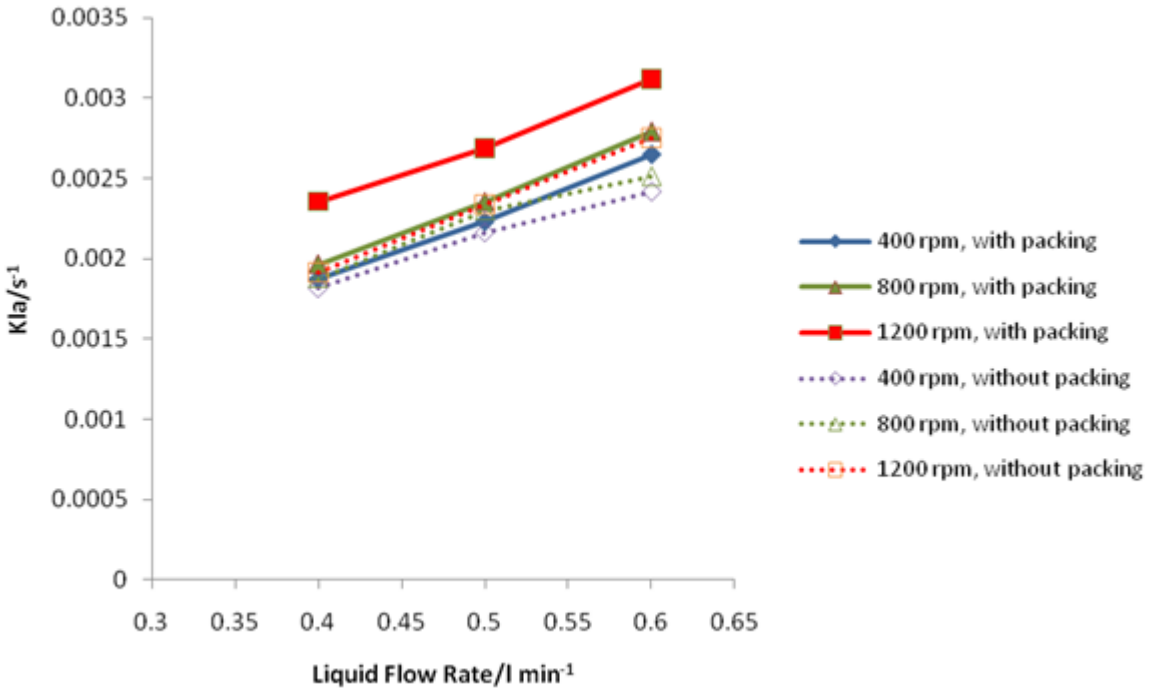

Figure 5.29a: The effect of rotational speed and liquid flow rate on K_La for the HBR

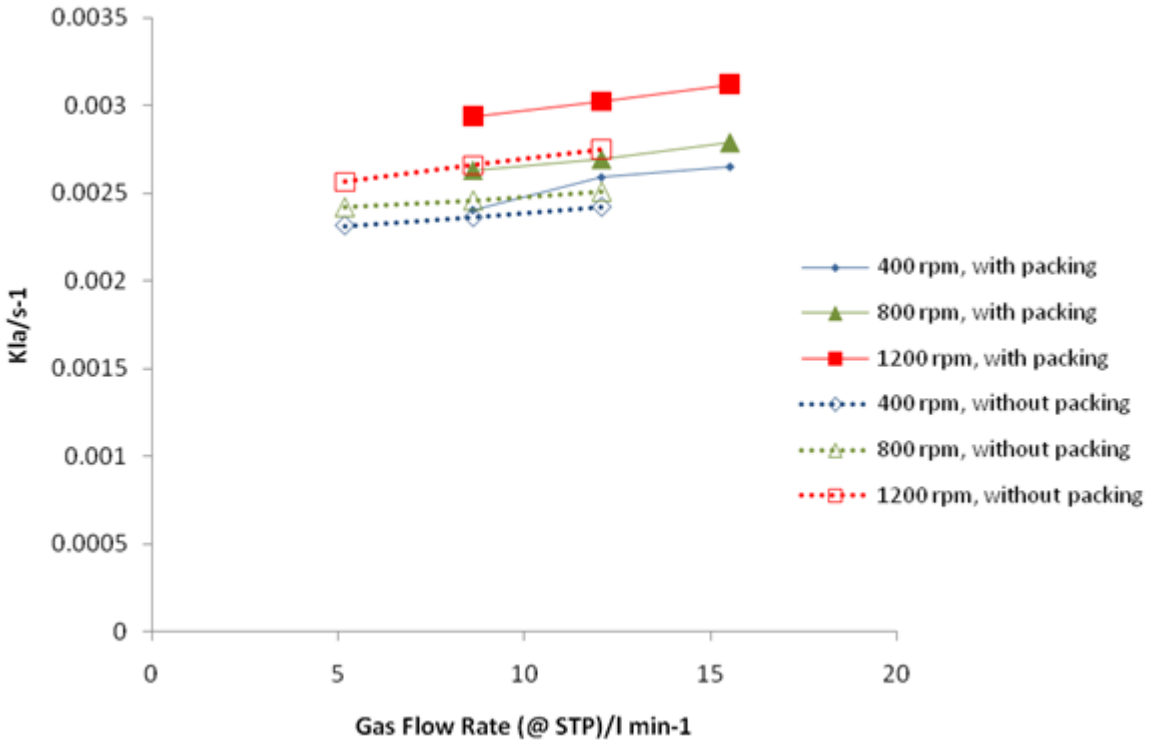

Figure 5.29b: The effect of rotational speed and gas flow rate on K_La for the HBR

The plots both note that as rotational speed, liquid flow rate, or gas flow rate increase then the value of K_La increases too. Increasing the rotational speed produces smaller bubbles which enhances the interfacial area available for faster gas-liquid transfer to occur. Smaller bubble production had already been previously established (section 5.4.2). In terms of the NTU the highest value obtained was 2.47 (with packing) and 1.91 (without packing).

The method used to calculate K_La in this study are not as good as expected. On inspection the values presented are lower than the results for the STR. Comparison based on this method is not without flaws, one of the major differences is that the method for the HBR is based on a continuous system, whereas the method for the STR is based on a batch system. Therefore a comparison between the two systems is not very accurate. In comparison to results gained from other high centripetal field environments, the results are very low. Research from Kumar *et al* (1990) has shown that K_La values of around 0.1 s^{-1} are achievable. In this study the reactor was a Rotating Packed Bed gas-liquid contactor with an axial depth of 2.5 cm and radii of 3 and 15.5 cm respectively. Although the radii between the Kumar study and the present HBR are similar, the larger axial depth of the Kumar system can account for the much larger K_La values gained with that system.

The low throughput of gas and liquid is also a factor in the low K_La values recorded. As shown in figure 5.25 the amount of gas and liquid employed was limited by the upper flooding conditions, which as compared to the Jassim study were quite low (Jassim 2002). As noted in section 5.4.1 under certain conditions splashing occurred from the eye of the rotor which leads to those parameters being designated as “flooding” conditions. In the majority of cases this was for a gas flow rates in excess of 18 l min^{-1} and liquid flow rates in excess of 1.0 l min^{-1}. It was also noted that under these conditions flooding conditions were noted to have been established almost immediately after having been set. There is scope for improving the throughput of gas and liquid in the HBR which would then lead to an enhanced transfer value. This could be achieved by reducing the current liquid hold up by allowing more rapid draining from the discharge chamber, or increasing the radial packing depth by adding more knitted wire packing to the central part of the HBR.

5.5.1.3 Analysis

To investigate the effect that each factor had on the K_La observed, a main effects plot was produced in Minitab in figure 5.30a and for NTU values in figure 5.30b

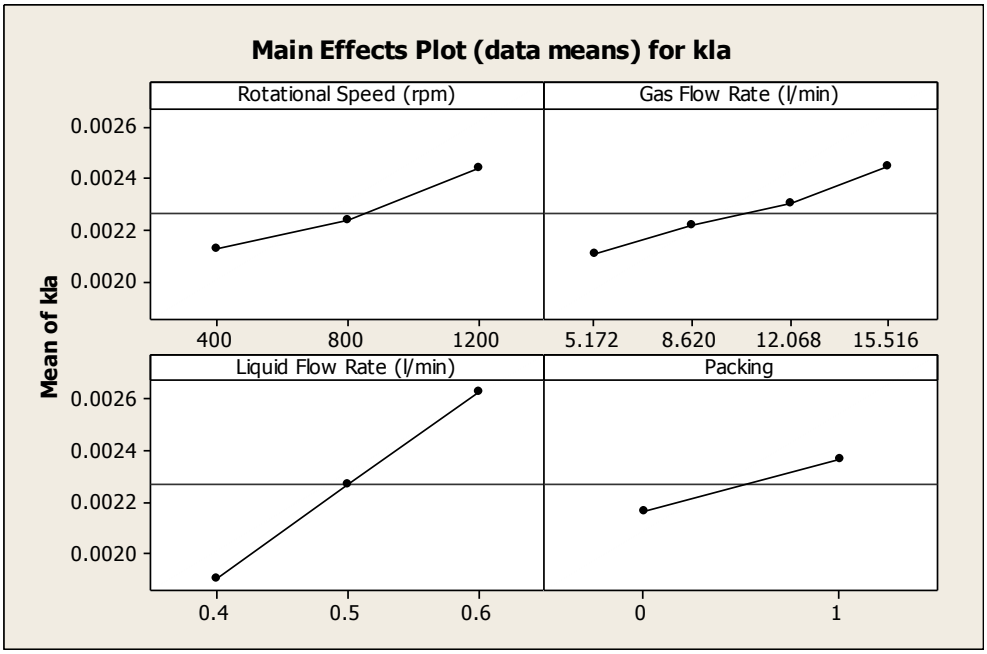

Figure 5.30a: Main effects plot for K_La measurement for the HBR (Key-1 denotes packing present, 0 denotes no packing present)

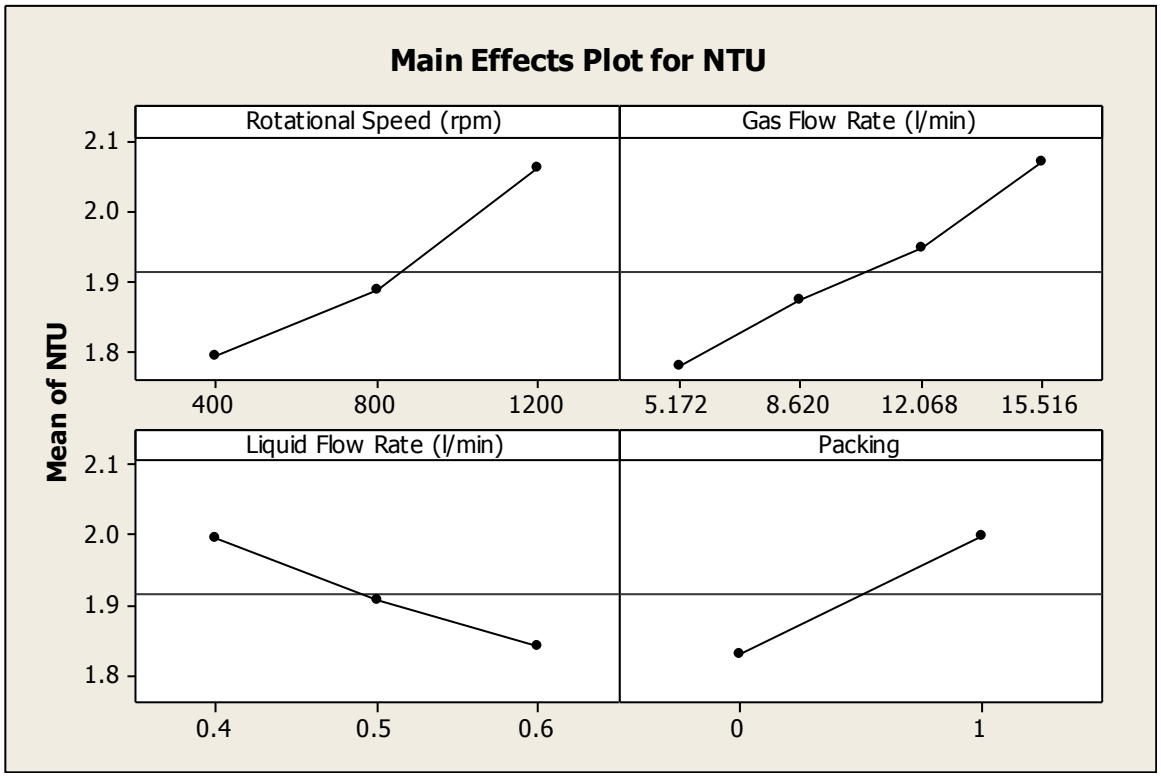

Figure 5.30b: Main effects plot for NTU measurement for the HBR (Key-1 denotes packing present, 0 denotes no packing present)

Figure 5.30a illustrates that liquid flow rate has the greatest impact on the value of K_La, with packing noticed to have the smallest impact. Figure 5.30b illustrates that rotational speed, gas flow rate, and packing have a similar positive effect on the value of NTU. In this plot however, liquid flow rate has a negative effect on the value of NTU observed. The reason for this being that as more liquid is passed through the rotor, the amount of work needed to be done to remove oxygen from the system increases which reduces the efficiency of transfer as a result.

One of the original problems encountered with the HBR was oxygen leaking into the collector and absorbing rapidly into the deoxygenated water stream. Although the nitrogen blanket has been added, it may not be eliminating all the oxygen present. A further adaptation of the blanket, either by increasing the flow rate of nitrogen, or by altering how the gas is injected round the collector may be more successful. The same problem has been encountered with HBR design previously (Peel 1995), and successfully solved with a re-design of the injector system shown through the enhanced transfer values noted.

5.6 Summary

The present study has focused on investigating the transfer capability of a set of porous mesh impellers and of a newly fabricated HBR. The following results have been noted from the experiments conducted:

1. The porous mesh impellers consume less power compared to the Rushton design. In particular the Knitted Wire design can produce similar K_La values to the Rushton design, but a with a much decreased power draw. For all impellers studied the value of K_La was seen to increase with increasing agitation rate and airflow rate, but decreased with increasing viscosity. The K_La values for the Fibre and Declon mesh were found to be consistently lower than the knitted wire mesh design. This observation, in conjunction with potential sterilisation problems of these packings, has led to the decision to take only the Knitted Wire impeller through to the fermentation experiments and for that material to be used as packing within the new HBR.
2. The bubble study conducted noted that all the mesh impellers could produce smaller mean bubble diameters compared to the Rushton design. In this study it was discovered that agitation rate, airflow rate and viscosity caused a smaller mean bubble diameter to be produced when these parameters were increased. At lower agitation rates the bubble diameter in the SMS medium was lower than the Air/Water and

Air/Water-Glycerol system. For the higher agitation rate (400 rpm) the mean bubble diameter was noted to be lower than the Air/Water system but roughly similar to the Air/Water-Glycerol system. Bubble diameter was noted to further decrease when by the addition of DF204 antifoam into the SMS medium.

3. The commissioning of the new HBR commenced with a series of experiments to establish the reactors upper operational limits and transfer capability. The flooding study established that the upper operational limit was lower than expected; this was then used to establish parameters for the experiments that would follow. Packing including within the reactor was seen to have a profound effect on both bubble size and K_La values recorded. Increasing rotational speed contributed to a small mean bubble diameter and higher K_La value. The gas and liquid flow rate was noted to have a negligible effect on the mean bubble diameter. Suggestions have been made to enhance the upper operational limit of the new HBR for future work conducted.

Chapter 6: *Escherichia coli* K12 and *P.putida* KT2442 Fermentation Studies

The chapter focuses on the results for the investigation conducted with *E.coli* K12 and *P.putida* KT2442. The focus of the chapter is a lab scale study on the intensification effects of the knitted wire impellers. For the *E.coli* fermentation, the results from a study conducted in the BioFlo reactor operating in batch mode will be considered, with the results discussed with reference to a previous study conducted within the school by Ndlovu (2004). For *P.putida* fermentations, results for batch and fed-batch experiments in the conventional stirred tank reactor (STR) using a range of impellers will be presented and discussed. Finally, data from *P.putida* fermentations undertaken in the newly fabricated HiGEE Bioreactor (HBR) will be presented and evaluated to establish its capability to support growth of a microbial community.

6.1 Basis of Current Study:

The present study being conducted is based upon previous work conducted by Ndlovu (2004). The current study builds upon the earlier research in the following ways:

1. In the Ndlovu (2004) study, the Rushton and 11 cm Knitted Wire impellers were investigated. The present study additionally includes the 6 cm Knitted Wire impeller.
2. The medium utilised by the Ndlovu study was based on a recipe provide by Avecia. The medium incorporated yeast extract therefore the consistency of each batch could not be guaranteed. In contrast, the present study employed a minimal, well-defined medium where the consistency of each batch could be guaranteed.
3. The number of experiments was increased in the present study and a central composite experiment design was established using Minitab. In addition to the Optical Density (OD) readings, viable count analysis was performed each hour to investigate the viability of the bacteria during fermentation.
4. The Ndlovu (2004) study employed PGE as an antifoaming agent. It was discovered that at the higher agitation/airflow rates employed that this agent was unable to

prevent a large amount of foaming. For the present study trials were conducted with DF204 which proved successful in preventing foaming. As a consequence a small amount of DF204 was added to each fermentation batch conducted in the present study.

6.2 *E.coli* K12 Medium Optimisation:

The procedure and apparatus for the medium optimisation have previously been described in Chapter 3. The first experiments revealed no growth occurring in the flasks, initially thought to be due to too little substrate (1.5 ml l^{-1} of a 50% glucose stock solution). As a result the substrate level was increased to 3 ml l^{-1}. The CAS amino acid solution was added as no growth was evident with the increased level of substrate. After the addition of the CAS solution (1 ml l^{-1}), the problem was found to be with the strain of CH117 used which had been a recombinant type for use on LB medium. A wild type version of CH117 was then employed with the glucose reduced to 1.5 ml l^{-1}. A set of four shaker flasks were grown and the growth curve obtained (based on average OD values) is shown in figure 6.1

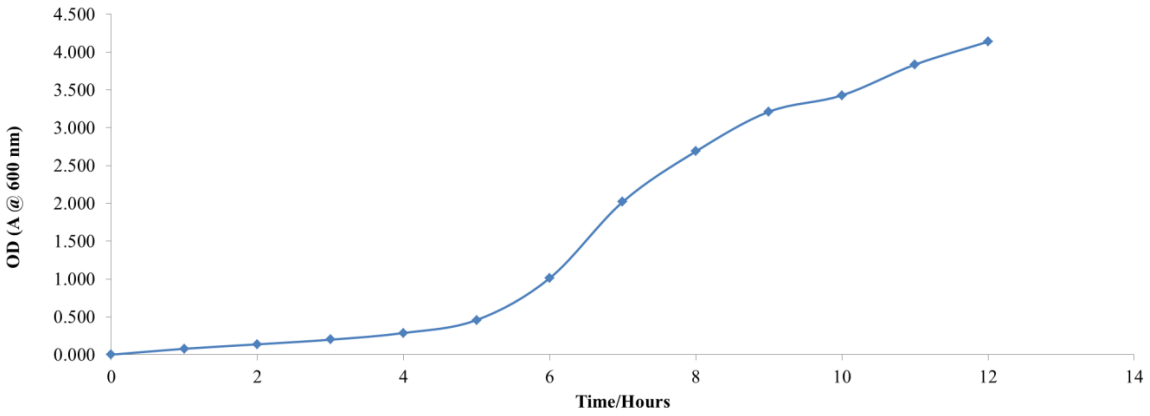

Figure 6.1: Growth curves for Shake Flask cultivation of *E.coli* K12 in SMS medium

The plot in figure 6.1 shows the average OD produced from 4 shaker flask experiments, the figures for which are displayed in table 6.1.

Table 6.1: OD readings obtained for the Shaker Flask Experiment

Time/Hours	OD-Flask 1	OD-Flask 1	OD-Flask 1	OD-Flask 1	Average OD
0	0	0	0	0	0
1	0.079	0.081	0.082	0.071	0.078
2	0.140	0.139	0.138	0.131	0.137
3	0.199	0.187	0.195	0.212	0.198
4	0.270	0.292	0.289	0.294	0.286
5	0.454	0.482	0.455	0.439	0.458
6	1.004	1.024	1.010	1.006	1.011
7	2.028	2.004	2.016	2.032	2.020
8	2.664	2.628	2.706	2.748	2.687
9	3.185	3.248	3.157	3.255	3.211
10	3.464	3.400	3.416	3.432	3.428
11	3.789	3.830	3.850	3.870	3.835
12	4.120	4.150	4.130	4.150	4.138

Table 6.1 illustrates that reproducible growth can be obtained from the shaker flasks studied. The 40 ml aliquots used for the study will also be used as the inoculum for the BioFlo III experiments (section 6.3). As growth in minimal medium is slightly slower than in a rich medium (such as the medium used in the Ndlovu study (2004)) the shake flasks are left as 12 hour Overnight Cultures (ONC).

6.3 *E.coli* K12 Batch Fermentation Experiments

6.3.1 Sterile Process Validation

Both Knitted Wire impellers (6 and 11 cm) were subjected to a sterile hold test to ensure that the sterilisation process was effective, and to guarantee that the sterile barrier would hold during a full fermentation run. For a sterile hold experiment the reactor is operated as normal (i.e. set at given agitation and aeration rates) but the inoculation of bacteria does not take place. OD measurements taken over an 8 hour period revealed that no bacterial growth occurred. This would appear to validate the sterilisation process performed, and there was no breach in the reactors sterile barrier.

6.3.2 Biomass Concentration Analysis

For the *E.coli* fermentations OD, Total Viable Count (T.V.C) and Dry Cell Weight (DCW) analysis were performed. In the present study a wavelength of 600 nm was utilised for the OD whereas for the Ndlovu study (2004) a wavelength of 570 nm was used. Figures 6.2a-6.2c illustrate the OD, TVC and D.C.W analysis for fermentations conducted at an agitation rate of 400 rpm and airflow rate of 1.5 vvm (≡ 6 l min^{-1}).

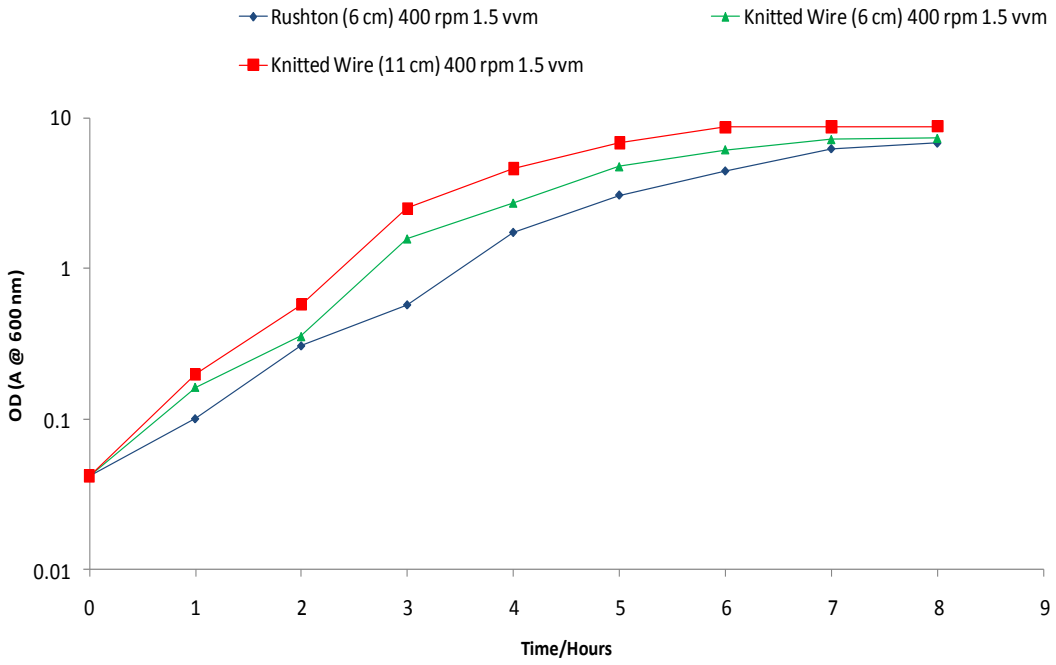

Figure 6.2a: OD values for the *E.coli* K12 Fermentation run at 400 rpm/1.5 vvm for all impellers studied in the BioFlo reactor.

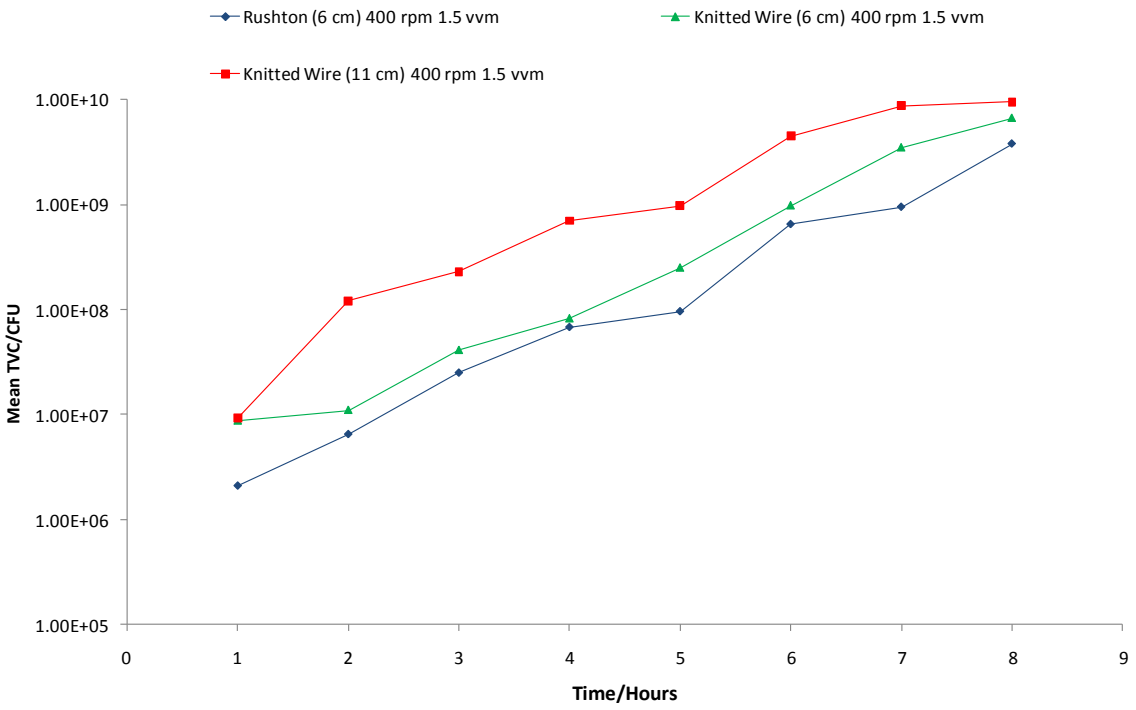

Figure 6.2b: TVC values for the *E.coli* K12 Fermentation run at 400 rpm/1.5 vvm for all impellers studied in the BioFlo reactor.

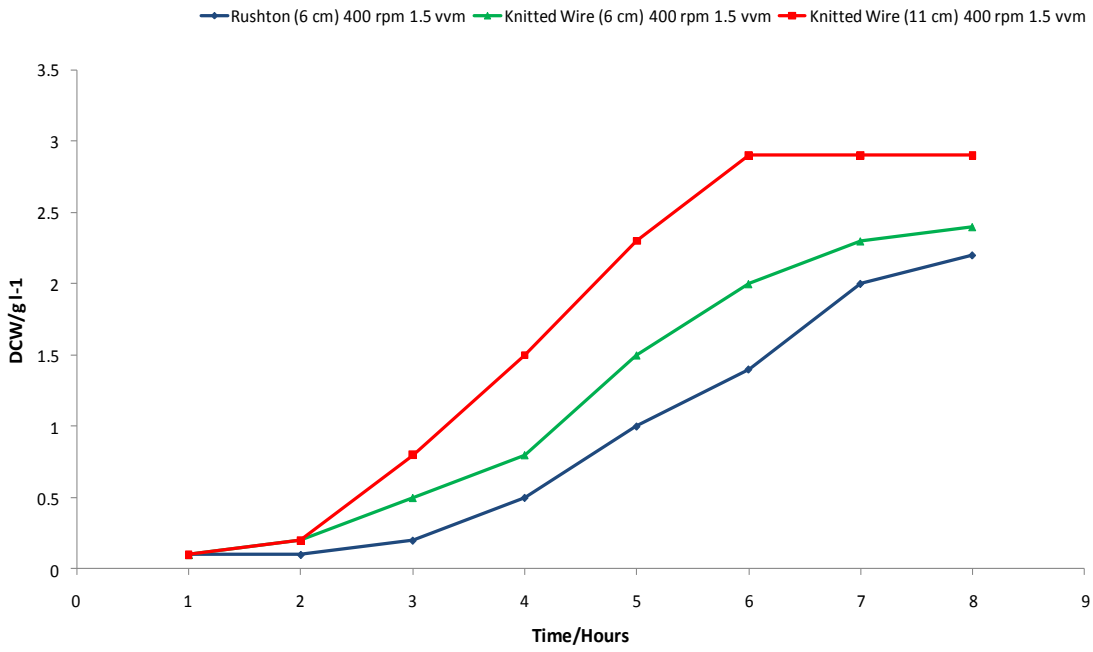

Figure 6.2c: DCW values for the *E.coli* K12 Fermentation run at 400 rpm/1.5 vvm for all impellers studied in the BioFlo reactor.

The figures above show that the two Knitted Wire impellers outperform the Rushton impeller, with the 11 cm Knitted Wire impeller producing the highest values. The growth curves obtained are typical of batch fermentation (Madigan *et al* 2009, Matsui *et al* 2007). As indicated previously, the intricate tightly wound material is able to shred large air bubbles down to a very fine size, enhancing the oxygen transfer rate (OTR). Previous uses of similar material used as bubble splitters in airlift columns also produced a similar enhancement in transfer (Nikakhtari *et al* 2005). The larger 11 cm knitted wire impeller occupies a larger volume much in the same way as the bubble splitters do in an airlift fermenter. The large proportion of space the impellers occupy leads to a minimising of bubble coalescence, further promoting an enhancement of transfer. This again has been noted by researchers investigating bubble splitter type designs (Nikakhtari *et al* 2005).

Transfer enhancement promotes a larger biomass concentration; therefore the method. by which the bubbles are broken is equally important. In the case of the Rushton impeller, the bubbles are broken apart by shearing action at the tip of the impeller blades (Martin *et al* 2008). It is possible under certain circumstances for the blades to break microbial cells as well. A larger biomass concentration will increase the tendency for a greater degree of cell damage occurring, especially at high agitation rates. Cell damage by shear may be further exacerbated when bacteria such as *E.coli* undergo binary fission as the cell wall is not as robust during this process (Nicklin 2003). For the Knitted Wire impellers, breakage of bubbles occurs by splitting through fine filaments rather than by shearing action within the tightly wound mesh structure, which may explain, in part, why higher biomass concentration and higher TVC are achieved with these impellers in comparison to the Rushton turbine.

An interesting observation noted with the Rushton impeller was that runs performed with the higher agitation rates (400 rpm) from hour 6 onwards produced an excessive amount of foaming. This did not occur with the Knitted Wire mesh impellers. An SDS-Page analysis revealed extra protein present in the medium, believed to be coming from lysed cells. One theory is that some of the cells were being broken apart by the impellers, the protein present being intra cellular proteins normally present inside the cell. These results would suggest that even at an agitation rate of 400 rpm, the shearing force at the tip of the Rushton turbine is large enough to destroy the cells. This finding is in agreement with the low TVC values obtained for the Rushton turbine in comparison to all the other impellers, as seen in Figure 6.2b

For all impellers studied the OD reached a plateau around the 6 hour mark, as seen in figure 6.2a. This could be due to the result of two different factors. The first is that oxygen was limited into the system. If this was the case then the cells would not be able to respire properly and therefore would not grow as fast. As shown later in section 6.3.4 this does not appear to be the case as the OTR is shown to be higher than the Oxygen Uptake Rate (OUR) and therefore no oxygen limitation should be observed. The second, more plausible reason is that the amount of glucose after 6 hours of fermentation was quite low; therefore if there was not enough substrate the growth of the bacteria would slow and eventually halt.

The effect of agitation rate and airflow rate on the biomass concentration was investigated. Figures 6.3a and 6.3 illustrate the effect these parameters had on the OD (which is a measure of the biomass concentration) of the 11 cm Knitted Wire impeller

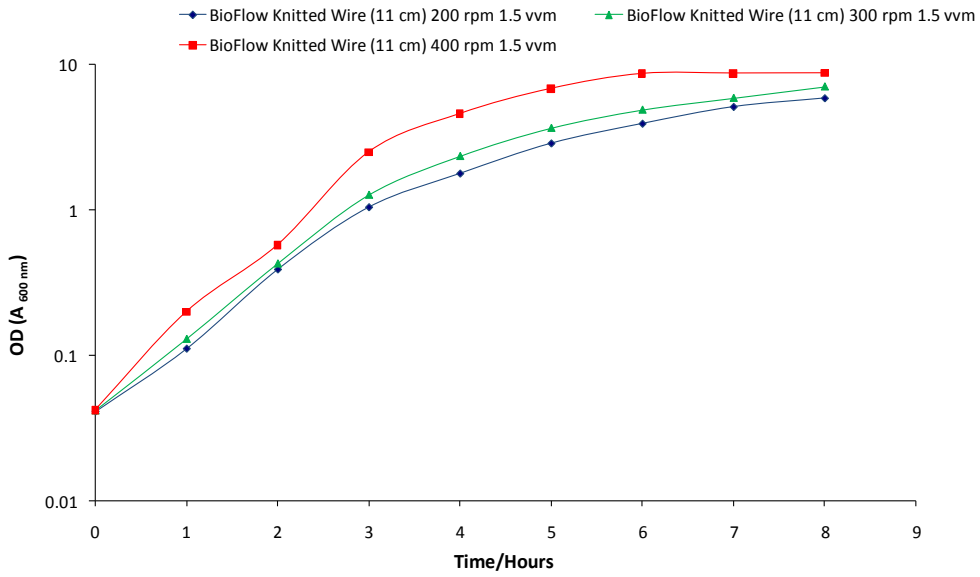

Figure 6.3a: The effect of Agitation rate (Airflow rate at 1.5 vvm) for *E.coli* K12 fermentations conducted with the 11 cm Knitted Wire mesh impeller

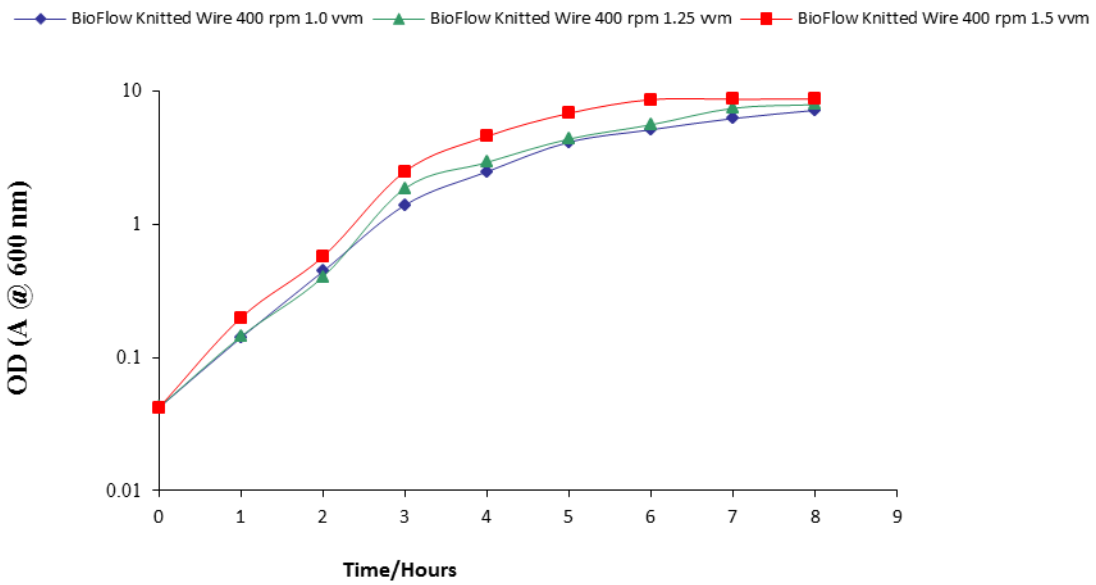

Figure 6.3b: The effect of Airflow rate (Agitation rate at 400 rpm) for *E.coli* K12 fermentations conducted with the 11 cm Knitted Wire mesh impeller

Figures 6.3a and 6.3 b show that OD values increase with increasing agitation and airflow rate, a result that is consistent with theoretical and experimental observations from previous studies using a range of impeller types (Ndlovu 2004 Stanbury *et al* 2002, Schuler *et al* 2000, Yépez Silva-Santisteban *et al.* 2006, Gill *et al* 2008, Patel *et al* 2009, and Mantzouridou *et al* 2002). For all the impellers studied in this work, the overall biomass increased with increasing agitation and airflow rate. The increase in agitation causes higher turbulence and therefore better overall mixing of the reactors contents. Furthermore, the air bubble size also decreases with increasing agitation, as presented in Chapter 4. The decrease in bubble size will lead to an increase in interfacial area for oxygen transfer and hence an increase in K_La and OTR (Tschentscher *et al* 2009). Similarly, increasing the air flow rate promotes a higher rate of bubble production and therefore higher oxygen transfer rates. The previous study conducted by Ndlovu (2004) found that OD values increased with both increasing agitation and airflow rate. The earlier study noted that control of foaming was quite difficult at the higher agitation and airflow rates, the present study made use of a more powerful antifoaming agent (DF 204) to combat this problem effectively.

Comparison of the present study to the study conducted by Ndlovu (2004) yields some interesting results. Although both studies show that increasing agitation rate and airflow rate

enhance the OD observed, the OD noted in the present study is higher than that of the Ndlovu (2004) study. There are two possible reasons for this difference. Firstly, with less foaming in the present study, there is a greatly reduced risk of micro-organisms and substrate being lost from the process by entrainment in the foam. Secondly, although a richer medium was used by Ndlovu (2004) which was expected to yield a higher OD value as a result, it is believed some of the substrate had in fact caramelised during the sterilisation process, as reported by Ndlovu (2004). This meant that an effectively reduced concentration of substrate usable by the bacteria was available to the bacteria during the fermentation.

6.3.3 Oxygen Uptake Rate (OUR)

The OUR of the culture has been experimentally determined for all impellers studied. The well-established dynamic gassing out procedure for determining OUR and K_La in a respiring cell culture was employed in this study as outlined in Section 4.1.3 in Chapter 4. Figure 6.4 notes the O.U.R for the Rushton and Knitted Wire impellers at an agitation rate of 400 rpm and an airflow rate of 1.5 vvm (≡ 6 l min^{-1}).

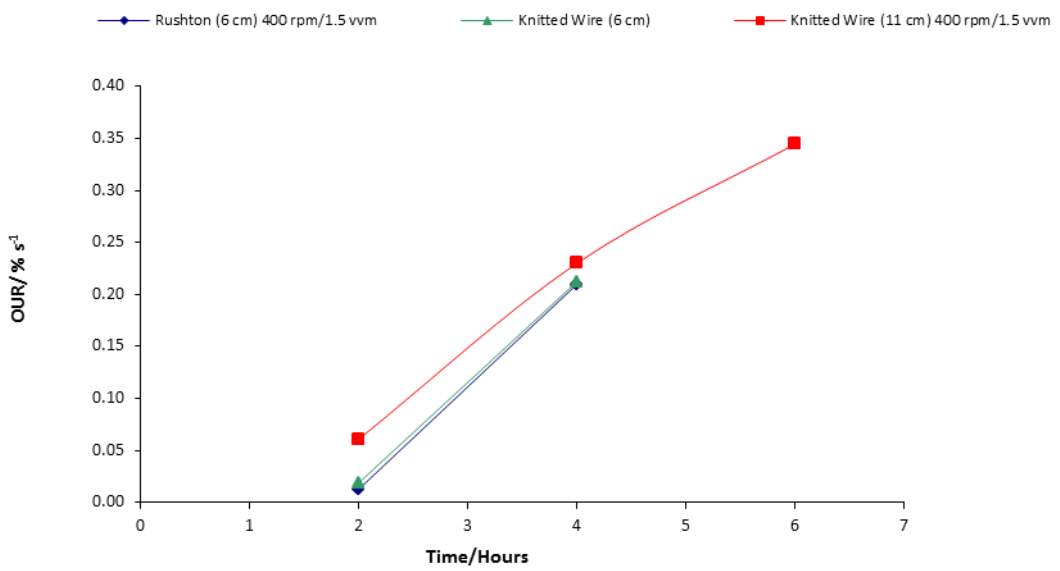

Figure 6.4: OUR values at 400 rpm/1.5 vvm for the Rushton and Knitted Wire (6 and 11 cm) impellers for the BioFlo III system.

Figure 6.4 illustrates that the OUR values for the 6 cm Knitted Mesh and Rushton impellers are similar to each other. The highest OUR values are obtained by the 11 cm Knitted Wire impeller. As noted previously the 11 cm Knitted Wire mesh impeller is able to provide a high K_La value for low power consumption (c.f. Chapter 5, section 5.2.1.1). The OUR is an

indication of how much oxygen is being taken up by the microbes present. Figure 6.4 notes that the system with the 11 cm Knitted Wire impeller has the largest OUR values, therefore the OTR of the impeller needs to meet or exceed this demand, and otherwise the microbial culture will experience a lack of oxygen. This ultimately led to the death of the cells. This can be investigated by looking at the OTR and OUR values for the impeller studied. Table 6.2 illustrates these values obtained for the impellers studied for the fermentation runs at 400 rpm/1.5 vvm

Table 6.2: OUR and OTR values for the Rushton and Knitted Wire (6 and 11 cm) impellers at 400 rpm/1.5 vvm

Impeller	**OUR/ % s^{-1}**	**OTR/ % s^{-1}**
BioFlo Rushton (6 cm)	0.0126	0.0714
BioFlo Knitted Wire (6 cm)	0.0190	0.0199
BioFlo Knitted Wire (11 cm)	0.0608	0.5285

Table 6.2 illustrates that for the conditions studied for the Rushton and 11 cm Knitted Wire impeller the OTR exceeds the OUR and therefore no oxygen limitation should occur in the system. Under these conditions the D.O concentration does not fall below 30 %, as illustrated in a typical plot of the DO profile for the knitted wire mesh shown in figure 6.5a. In the case of the 6 cm knitted wire impeller the OTR and OUR are almost equal to one another. As a result the DO concentration falls below 30 % and the system becomes limited by oxygen transfer. This again is illustrated by a plot of the DO concentration in figure 6.5b

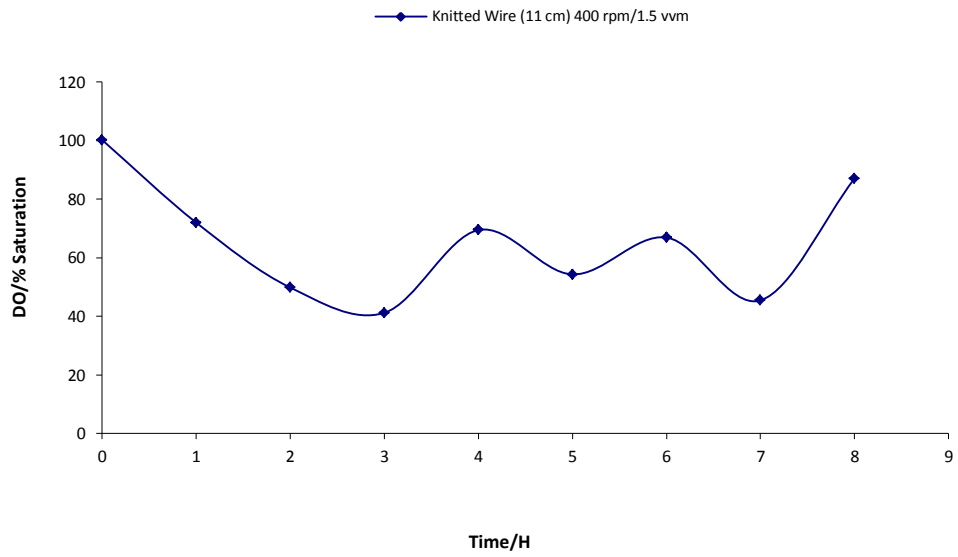

Figure 6.5a: DO Concentration profile for the 11 cm Knitted Wire impeller for the fermentation run at 400 rpm/1.5 vvm

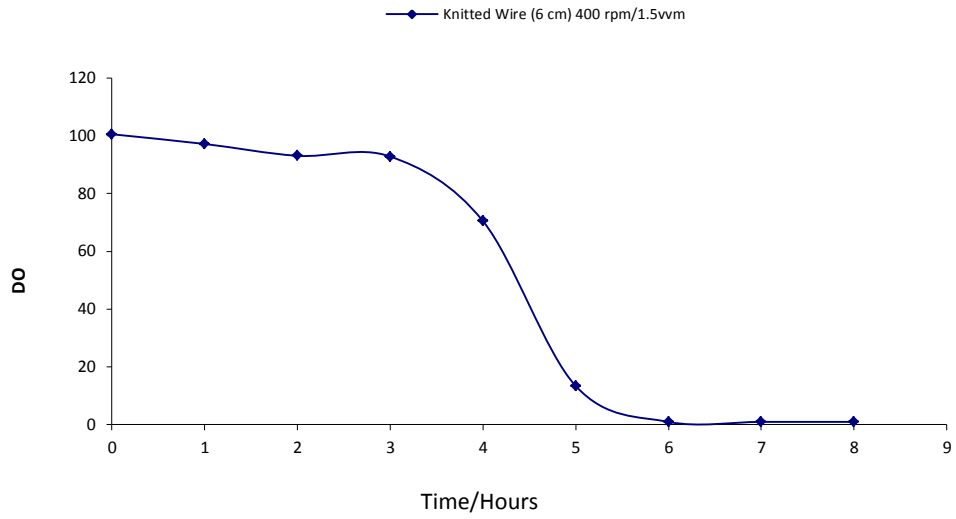

Figure 6.5b: DO Concentration profile for the 11 cm Knitted Wire impeller for the fermentation run at 400 rpm/1.5 vvm

As shown in figure 6.5b with the OTR of the 6 cm knitted wire impeller being close to the OUR of the microbial culture the DO concentration in the system falls to 0 % of saturation by hour 6. This is a repeated trend for the other impellers as well, mainly confined to lower agitation and airflow rates.

6.3.4 Oxygen Transfer Analysis

The biomass concentration results reported in 6.3.2, and OUR data (presented section 6.3.3) directly relate to the oxygen transfer, represented by the volumetric mass transfer coefficient, K_La, that can be achieved by the impellers examined. Figures 6.6a and b illustrate the effect of agitation and airflow rate have upon the K_La value (at hour 2) for the various impellers in the BioFlo system. For the effect of agitation rate, a fixed airflow rate of 1.5 vvm is chosen, whereas for the effect of airflow rate a fixed agitation rate of 400 rpm is used. Comparison of the 400 rpm/1.5 vvm experiments in the BioFlo are noted in table 6.3

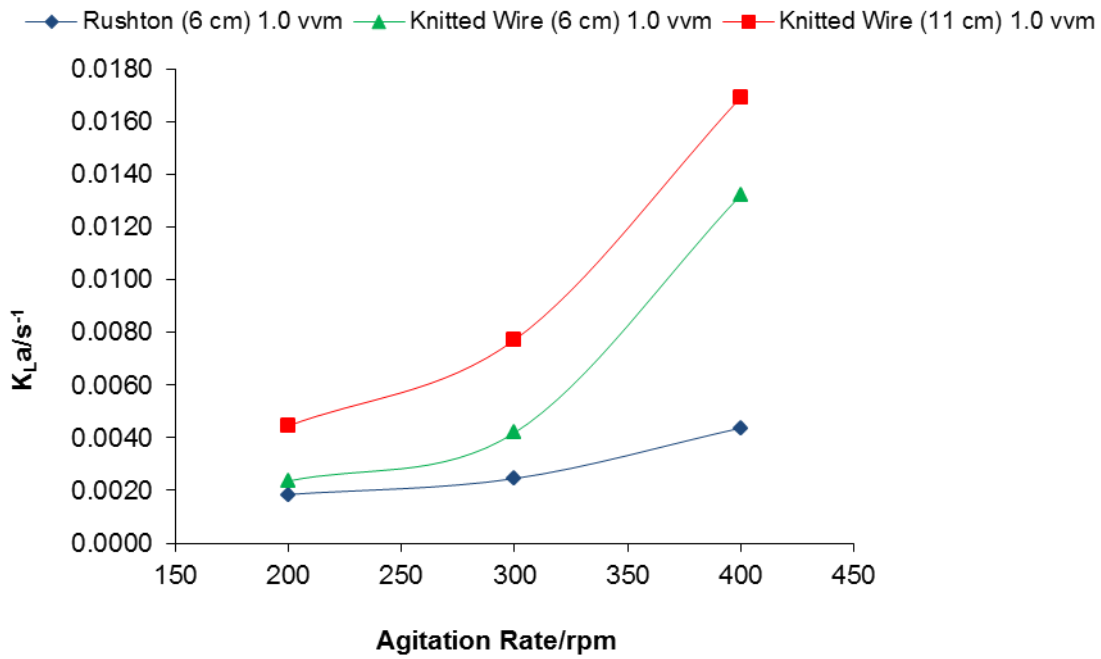

Figure 6.6a: The effect of Agitation rate on the K_La values for the Rushton and Knitted Wire (6 and 11 cm) impellers at 1.0 vvm in the BioFlo III system 2 hours into the Fermentation cycle.

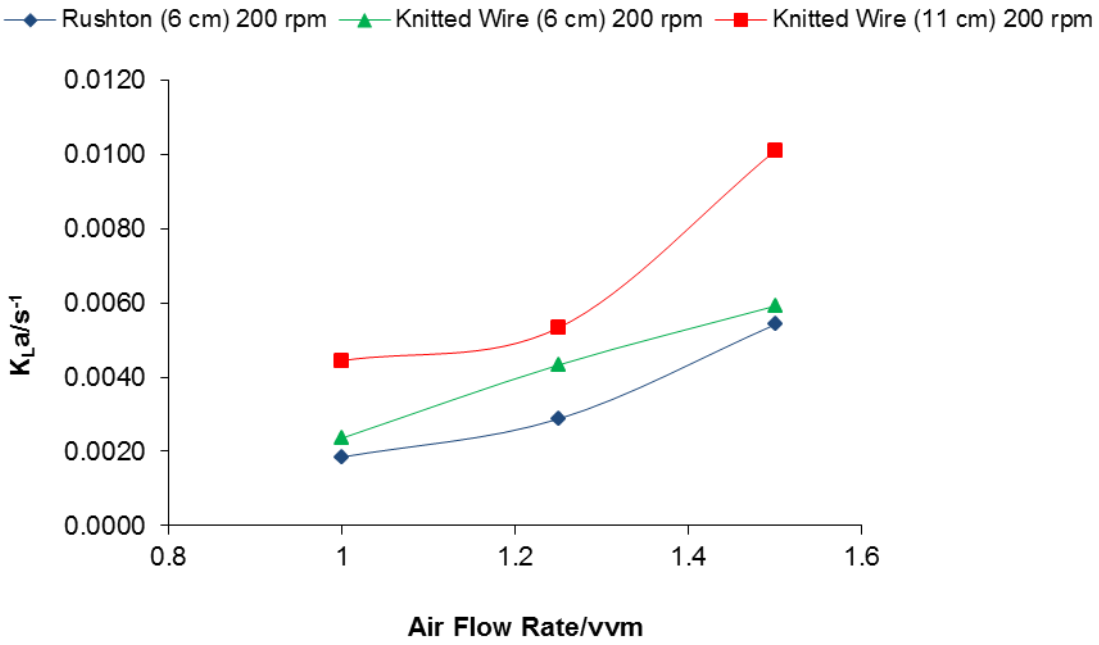

Figure 6.6b: The effect of Airflow rate on the K_La values for the Rushton and Knitted Wire (6 and 11 cm) impellers at 200 rpm in the BioFlo III system 2 hours into the Fermentation cycle.

Table 6.3: K_La values for the *E.coli* K12 fermentation system for the Rushton and Knitted Wire (6 and 11 cm) impellers at 400 rpm/1.5 vvm

Impeller	**K_La/s^{-1}**
BioFlo Rushton (6 cm)	0.0219
BioFlo Knitted Wire (6 cm)	0.0288
BioFlo Knitted Wire (11 cm)	0.0583

Figure 6.6 notes that increasing either agitation or airflow rate has a positive impact on the value of K_La observed. The increase in agitation leads to an increase in turbulence within the reactor which causes faster transfer to occur at the gas-liquid interface. It has already been shown in Chapter 5 that increasing agitation rate will lead to a smaller bubble size with the system for which a larger surface area will then be available for transfer to occur (c.f. Section 5.2.2.1, Chapter 5). Similarly, increasing the air flow rate promotes a higher rate of bubble production and therefore higher oxygen transfer rates (Shukla *et al.* 2004). The increase of K_La values brought about by enhancing agitation and/or airflow rate is a widely established

trend in the literature to date (Patel and Thibault 2009, Boodhoo *et al.* 2008, Shukla *et al.* 2004).

Both Figure 6.6 and table 6.3 note that the higher K_La values are produced by the 11 cm Knitted Wire impeller. As with the K_La results noted in the Air/Water and Air/Water-Glycerol systems this is brought about because of the design of the Knitted Wire impellers. The tightly wound material of the impeller is able to shred the air bubble stream efficiently as it passes through the material of the impeller. This result has been noted in previous research investigating similar packing material fashioned as impellers (Tschentscher *et al* 2009). The research conducted by Ndlovu (2004) also indicated that agitation and airflow rate had a positive effect on the value of K_La observed, with the 11 cm Knitted Wire impeller again giving the highest K_La values.

Figure 6.6 notes the K_La obtained at 2 hours into the fermentation cycle. In some instances it was possible to take measurements of the K_La value during hours 4 and 6 in the fermentation cycle. One such instance is noted in figure 6.7 for the 11 cm Knitted Wire impeller at 400 rpm/1.25 vvm in the BioFlo III system

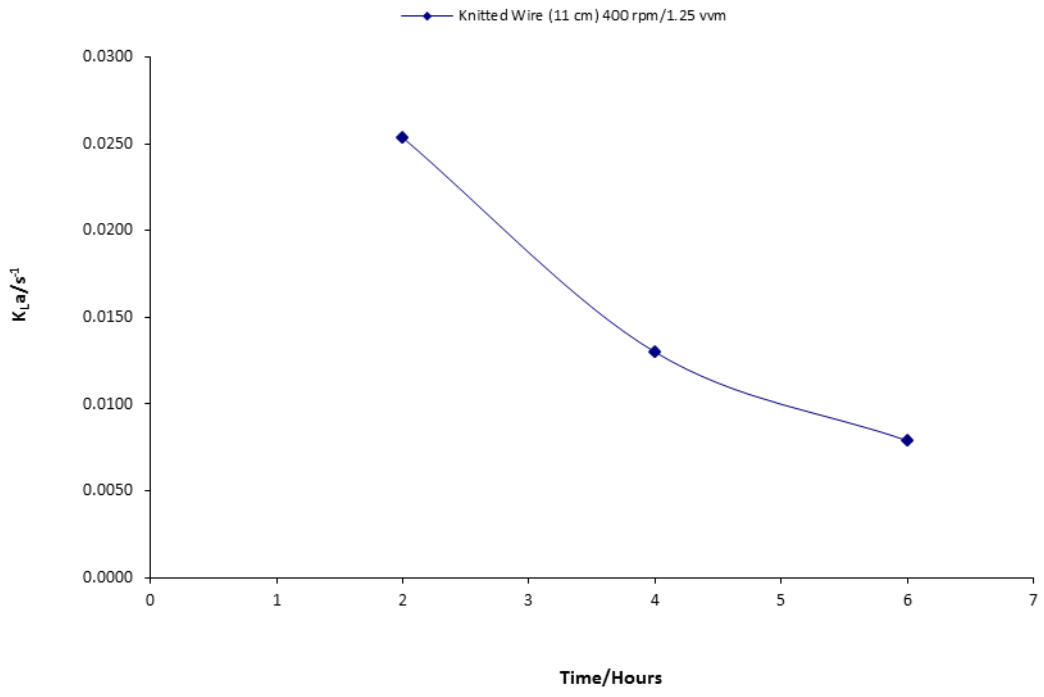

Figure 6.7: The value of K_La for the 11 cm Knitted Wire impeller for a full Fermentation cycle at 400 rpm/1.25 vvm

As the fermentation cycle increases with age, the K_La value measured is noted to decrease. The trend for a lower K_La value to be noted with higher biomass concentration is also noted in the literature (Patel *et al* 2009). The fall in K_La can be attributed to the increase in viscosity in the system. As the fermentation cycle increases in age and the biomass concentration increases the viscosity of the system rises. As noted in Chapter 5 during the initial experiments to examine the transfer capability of the impellers (section 5.2.2) the value of K_La was noted to decrease with increasing viscosity. The same principle applies for the fermentation, the increasing of viscosity with a decreasing K_La being observed has been noted previously (Stanbury *et al* 2000). The problem is further exacerbated in Non-Newtonian fermentation systems (Kilonzo *et al* 2004)

6.3.5 Summary

The current study presents a series of *E.coli* K12 fermentations during which the transfer capabilities and the ability of a set of Knitted Wire mesh impellers (6 and 11 cm) to sustain a microbial community were evaluated. These results were compared to the standard Rushton design and were built on a previous study conducted by Ndlovu (2004). The following points were noted during the experiments:

1. The 11 cm Knitted Wire impeller was noted to produce the highest Biomass Concentration and K_La values. This is similar to the results published in the Ndlovu (2004) study. The design and construction of the impeller are believed to be the reason for this enhancement in performance. The very fine, intricately wound filaments produce consistently smaller bubbles for higher oxygen transfer and cause less shear damage to the growing cells than a Rushton turbine design. The 6 cm Knitted Wire impeller has been investigated for the first time in the current study in a fermentation system and was shown not be as effective an impeller as the 11 cm diameter version of this impeller design. This is attributed to the smaller diameter impeller occupying a smaller volume in the reactor and is therefore not able to minimise the size of the air bubbles produced throughout the reactor volume.
2. Increasing agitation and airflow rate have been noted to have a positive effect on both biomass concentration and the value of K_La observed, in agreement with a large body of previous research conducted using a range of impellers.

6.4 *P.putida* KT2442-Batch Fermentation Experiments (BioFlo III)

The capability of the impellers studied was further tested by investigating the production of PHA. The study was designed to investigate if the Knitted Mesh impellers were capable of producing a higher yield of PHA compared to the Rushton impeller.

6.4.1 Biomass Concentration Analysis

In order to study the impact of each impeller system upon cell concentration, OD, TVC and DCW analysis were performed each hour for the entire run. The final results from each analysis are shown in Figures 6.8a-c.

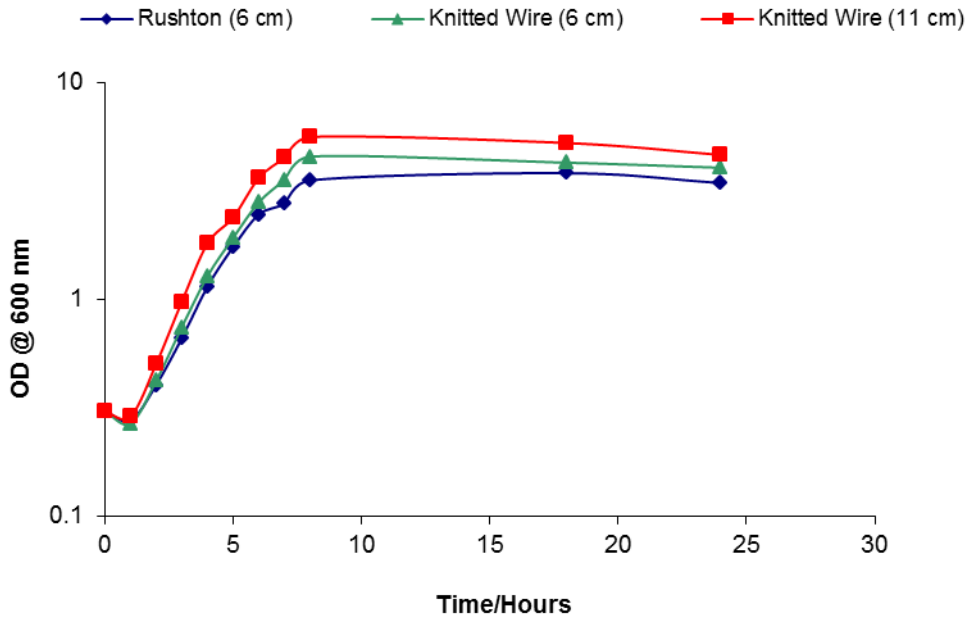

Figure 6.8a: OD readings for the *P.putida* KT2442 Fermentation in the BioFlo III Reactor

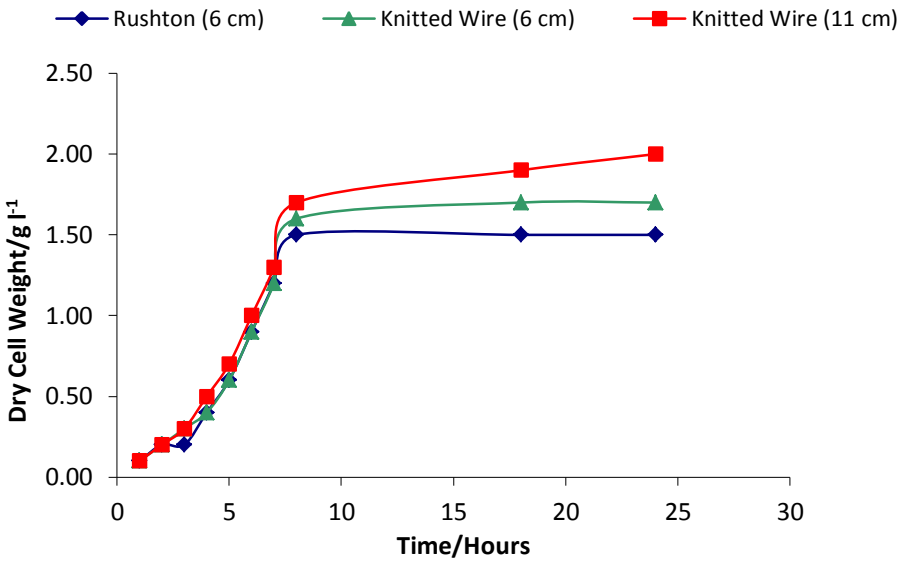

Figure 6.8b: DCW readings for the *P.putida* KT2442 Fermentation in the BioFlo III Reactor

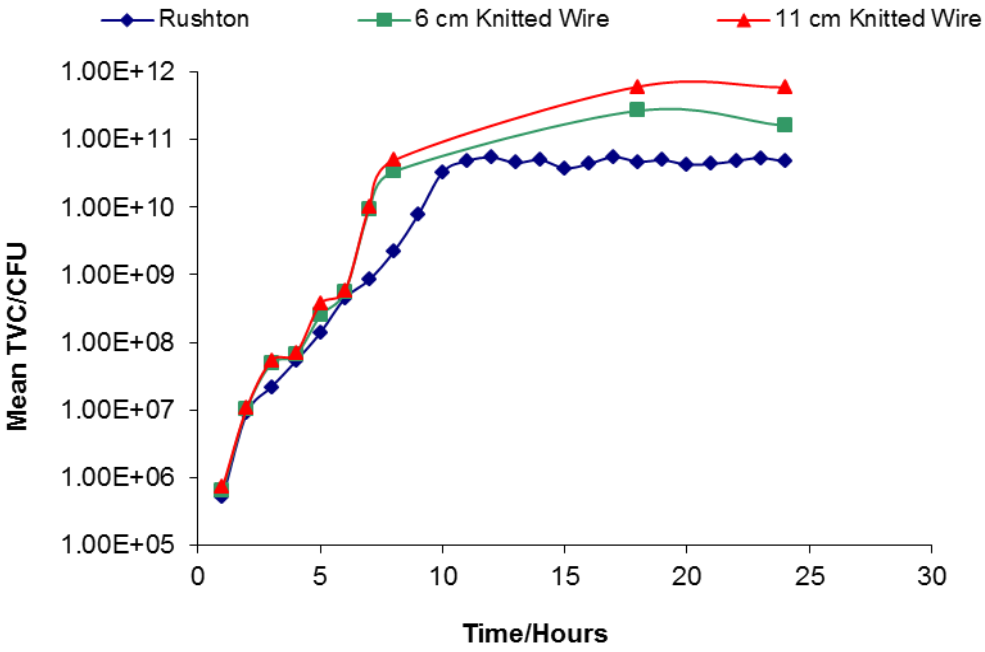

Figure 6.8c: TVC readings for the *P.putida* KT2442 Fermentation in the BioFlo III Reactor

The experiments conducted for this portion of the research illustrate once more that the 11 cm knitted wire impeller is the best performer. This is reflected in the highest OD /TVC /DCW for this impeller. The reason behind the higher biomass concentration for both knitted wire impellers is related to finer bubbles promoting a higher oxygen transfer as has already been discussed in detail earlier (see section 5.2.5).

The growth curve for *P.putida* illustrates that the bacterium grows more slowly than *E.coli*. This results in a shift in the peak OD readings along the right hand side of the x-axis. This is most likely due both to the slower growth rate of *P.putida* (compared to *E.coli*), and the substrate used. In the *E.coli* fermentations, glucose, a relatively simple compound was used as substrate. The carbon in glucose is therefore quite readily available to be assimilated by the bacterium, which is reflected in the growth curve. The sodium octanoate compound used as the substrate for *P.putida* is by contrast a more complex compound. The carbon is more tightly locked away, and not as readily available for the bacteria. As a result it takes a longer time for *P.putida* to assimilate the substrate resulting in a slower growth profile.

Comparing results from the *P.putida* fermentation to the *E.coli* fermentation reveal a lower DCW and higher TVC at the end of the *P.putida* fermentation. This would appear to indicate that although overall there was not as much biomass, a higher proportion of it was viable. This may be in part due to the oxygen demand of the system and is further investigated in section 6.4.3

6.4.2 The effect of pH on the Microbial Growth Curve

The effect of pH on the microbial growth curve was evaluated by conducting experiments with the Rushton impeller at pH 6 and 7. Figure 6.9 illustrates the difference in the resulting growth curve when the pH was altered from 6 to 7. The figure shows the OD results taken for identical operating conditions in experiments conducted with the Rushton impeller.

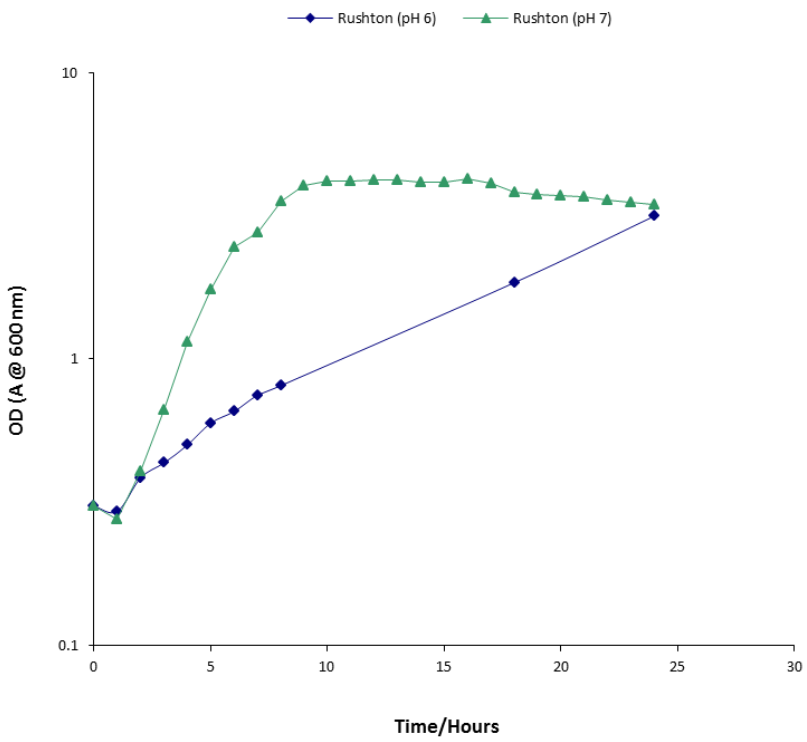

Figure 6.9: The effect of pH on the microbial growth for two fermentation cycles conducted with the Rushton impeller.

The increase of pH has a profound effect on the growth curve obtained. Although the final OD after 24 hours of fermentation time is virtually identical, growth is much slower at pH 6 than at pH 7. The growth rate between hours 0-10 at pH 7 is particularly fast, before the OD declines between hours 11-24. Most *P.putida* strains produce PHA in the stationary phase. *P.putida* KT2440 has been used successfully by Sun *et al* (2007) where the PHA was accumulated in the microbial cells after rapid initial cell growth on nutrient limited medium. Having the fast exponential phase for pH 7 is therefore beneficial, with the stationary phase reached within a shorter space of time. The growth curve for pH 7 is also more consistent with previous research noted in literature (Anderson and Wynn 2001). As noted in chapter 2, due to pH being equal to the log of H_30^+, even small a change in pH will be due to a large change in the H_30^+ ions in the system.

Figure 6.10 shows the pH profile during the 24 hour *P.putida* fermentations for all three impellers studied for a starting pH of 7. The pH generally rises from 7.2 to around 7.45 over the 24 hour fermentation cycle for all impellers. The pH level at 7.0 was controlled during the fermentation run by addition of small amounts of 1M NaOH or 1M HCl. The values presented in figure 6.10 are the values taken before the addition of any chemical was added.

The pH of the system was re-examined after addition of the chemical to ensure that the pH was 7.0.

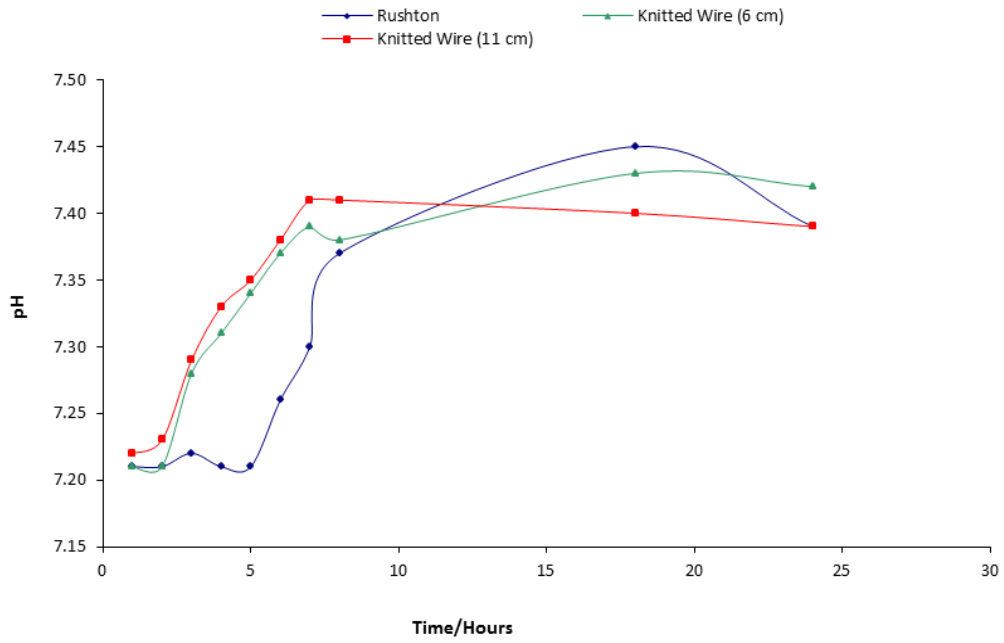

Figure 6.10: The pH profile for the *P.putida* Fermentation for all impellers studied

There is not a significant amount of change to the pH during the fermentation cycle. The Rushton impeller produces the largest pH value noted during the experiment. The reason for the slight increase in pH could be caused by the accumulation of PHA within the microbe (Tortajada *et al* 2008) or could be caused by leakage of ammonium from lysed cells into the fermentation medium

6.4.3 Phase Contrast Microscopy

Digital images were taken at the end of each fermentation cycle to determine the amount of PHA that had been produced. In order to achieve this, a phase contrast microscope was used at 100x magnification, and the resultant images captured with the aid of a digital camera. Figure 6.11 illustrates the difference in the bacteria at the beginning of the fermentation (with no PHA), compared to 24 hours later (when PHA has accumulated within the bacterial cells) for the 11 cm Knitted Wire impeller

[A] 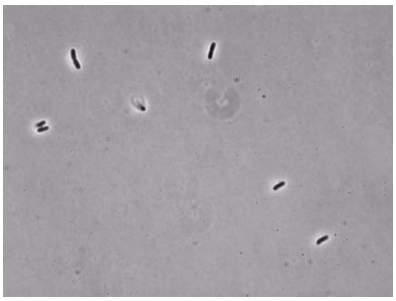 [B] 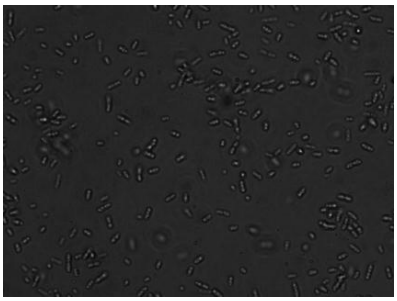

Figure 6.11: Phase Contrast Images of [A] after 2 hours and [B] 24 hours of fermentation for the 11 cm Knitted Wire impeller (Reactor conditions set at 1.0 vvm, agitation rate varied to maintain 40 % DO concentration)

The white granules present in Figure 6.10 [B] are PHA. From the same figure it is evident there are a number of the bacterium containing the biopolymer. It has also been noted that the amount of PHA in the bacterial cells is greater for the porous impellers than the Rushton, reflecting the OD /TVC /DCW results noted earlier in Figures 6.8a-c. Figure 6.12 illustrates the difference between the amounts of PHA produced with the Rushton impeller compared to that produce by the 11 cm Knitted Wire impeller under identical conditions.

[A] 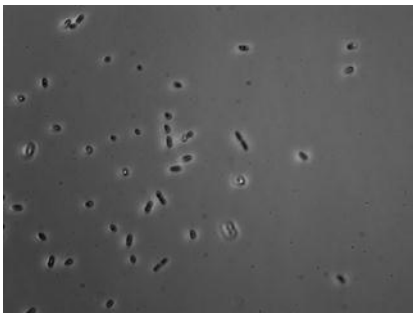 [B] 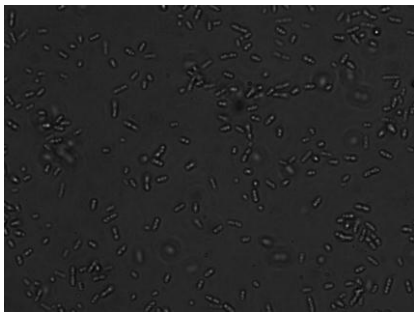

Figure 6.12: Phase Contrast Images of [A] Rushton impeller and [B] 11 cm Knitted Wire impeller at the end of the 24 hour Fermentation cycle

The pictures gained from the phase microscopy images appear to show an enhanced production of PHA for the 11 cm Knitted Wire impeller. Photographs taken for the 6 cm Knitted Wire impeller also note a greater amount of PHA produced compared to the Rushton impeller. This is indicated by a larger number of the cells containing white granular bodies. This trend is consistent with previous research showing that as biomass concentration increases, the amount of PHA increases (Tortajada *et al.* 2008).

6.4.4 Extraction of PHA by NaClO Method.

To quantify the amount of PHA that had been produced with each fermentation cycle, the PHA was extracted by use of the above method. (See Chapter 4, section 4.1.6). The analysis was performed at the end of each fermentation cycle. The % yield of PHA for each experiment (calculated against the DCW values noted in figure 6.8b) are noted in Figure 6.13

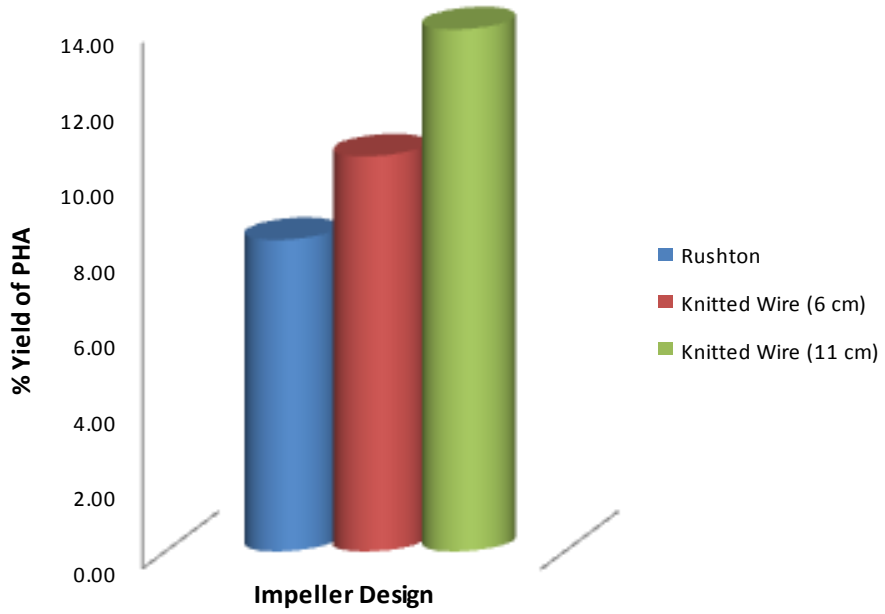

Figure 6.13: PHA yield for the Rushton and Knitted Wire (6 and 11 cm) impellers for the batch *P.putida* KT2442 Fermentation

Figure 6.13 notes that the 11 cm Knitted Wire impeller produces the highest % yield of PHA. This result confirms the digital images that have been taken. This suggests that the 11 cm Knitted Wire impeller is capable of sustaining a higher biomass concentration and produce a larger amount of product too.

Although the 11 cm Knitted Wire impeller produces the highest % yield, the yield overall is quite low when compared to similar systems in literature (A study by Cooper *et al* (2008) produced yields of around 60-80 %) (Tortajada *et al* 2008, Cooper *et al* 2008). It is possible that the low yield is the result of the medium that was used. In the majority of PHA fermentation cycles, the PHA is produced when the bacteria are under stress such as from

lack of a key element or substrate (Tortajada *et al.* 2008). The medium in this case was used to establish if PHA could be produced and therefore did not stress the microbe too much. A modification was made to the medium for use as a fed-batch cycle (see section 6.5).

6.4.5 DO Profile

The main aim of the study was the production of PHA; therefore as a result no transfer experiments were conducted. The DO level in the reactor was programmed to be maintained above 40 % of saturation at all times. This was accomplished by the reactor continuously adjusting the agitation rate of the impeller to maintain the 40 % level. Figure 6.14 shows the DO profile for the 11 cm Knitted Wire impeller

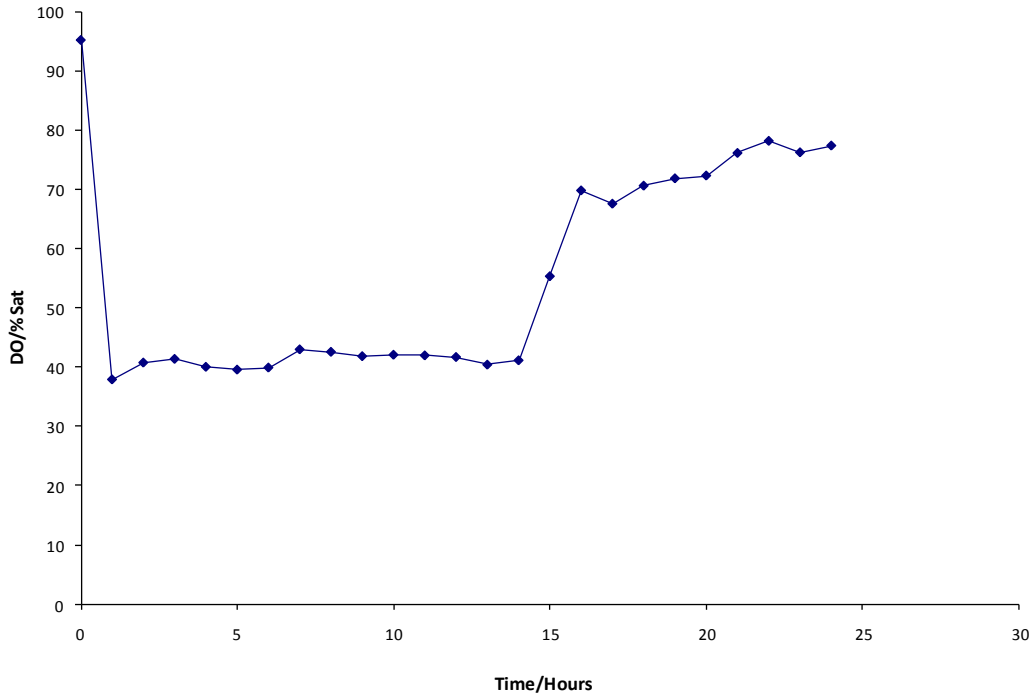

Figure 6.14: The DO profile during the PHA Fermentation Cycle for the 11 cm Knitted Wire impeller

Figure 6.14 shows that there is a rapid drop of DO in the first few hours from just under 100% to 40%. The reactor responds to maintaining the 40 % level by adjusting the impeller speed as necessary. After 15 hours into the fermentation cycle, the DO rises again and in the final few hours stabilises around the 80 % of saturation. The DO profile noted in figure 6.15 is typical for this fermentation, and broadly fits with the OD profile noted in figure 6.8a. As the OD rises, the DO concentration dips as the microbial culture uses the available oxygen to

grow. For the 6 cm knitted wire impeller, this initial dip in D.O. occurred within a shorter time span than for the Rushton and 11 cm knitted wire impellers. This is probably because as with the *E.coli* fermentations the OTR for the 6 cm knitted wire system was nearly the same as the OUR of the culture. In all systems studied, the 40 % was maintained by each of the impellers studied by increasing agitation rate. The 6 cm knitted wire impeller applied the largest agitation rate in order to keep the DO concentration at or greater than 40 %. This could imply that oxygen transfer was not as efficient for this system compared to the larger knitted wire and Rushton impeller

6.4.6 Summary

Batch fermentation with *P.putida* KT2442 was conducted with the Rushton and Knitted Wire impellers in the BioFlo III reactor system. The following points were noted in the experiment series:

1. The 11 cm Knitted Wire impeller produced the highest biomass concentration and % yield of PHA. As with the *E.coli* K12 fermentation this is believed to be due to the design of the Knitted Wire impellers.
2. The pH of the medium was noted to have a large effect on the earlier stages of the growth profile within the system. At a pH of 7 the growth was much faster than with a pH of 6. Subsequently all experiments were conducted at pH 7.
3. The medium used for the batch experiments was used to establish if PHA could be produced within the system. As a result the % yield of PHA was not as high compared to comparable studies within literature. For the fed batch fermentation a different medium was used in an attempt to maximise the yield of PHA (see section 6.5).

6.5 *P.putida* KT2442-Fed-Batch Fermentation Experiments (BioFlo III)

A series of fed batch fermentations were performed with *P.putida* to investigate the impact of the porous mesh impellers on high cell density fermentation. The substrate utilised for the fed batch fermentation was pure octanoic acid. Octanoic acid at a concentration of 3 ml l^{-1} was selected on the basis of a previous study conducted by Tortajada *et al.* 2008.

The first 24 hours of the experiment proceeded as a batch fermentation cycle. Once the 24 hour mark had been reached, a second pulse of octanoic acid was injected at a rate of 3 ml l^{-1} to shock the system and to kick start growth of the microbe once more. A feeding strategy

was established to keep the cultures growing at a rate of approximately 0.2-0.25 h^{-1} (corresponding to 0.8 ml l^{-1} which was added every subsequent hour for the remainder of the fermentation). Alongside the additional substrate, both NaOH (to regulate pH) and antifoamer DF 204 were added during the fed-batch process. The fed-batch procedure lasted for 24 hours, bringing the total fermentation cycle to 48 hours.

6.5.1 The Effect of Substrate

For the initial batch fermentation experiments described (see 6.4) the substrate sodium octanoate had been employed. For the fed-batch system the pure form of the substrate, octanoic acid was used (Tortajada *et al*. 2008). The first 24 hours of the fed-batch growth curve has been plotted against the batch run for the 11 cm knitted wire impeller, noting the difference in OD readings taken (Figure 6.15).

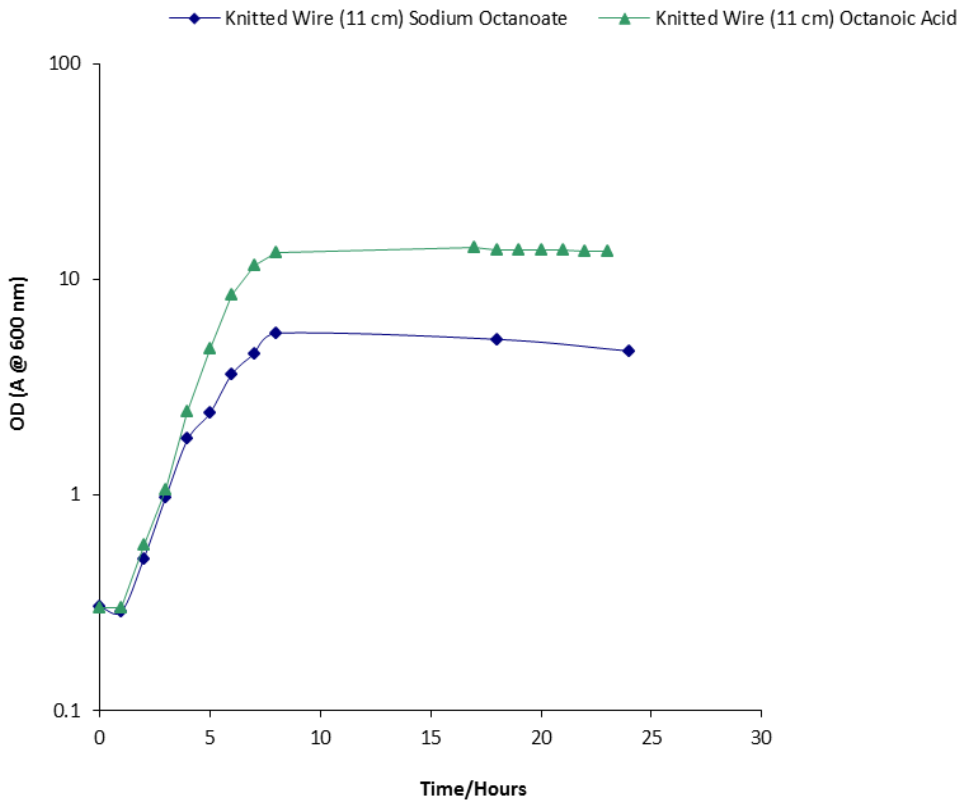

Figure 6.15: The effect of substrate on OD values for the 11 cm Knitted Wire mesh impeller

For the first 5 hours of the fermentation cycle the OD values of both experiments are very similar, only diverging after hour 5. The final OD when sodium octanoate was used is 4.65 and when pure octanoic acid is used is 13.42. This result is repeated for the other impellers studied. This observation highlights the importance of choosing the best substrate for

optimum biomass concentration and metabolite yield in a bioprocess. As noted for the batch experiments this may be due to the complexity of the compound used. In the fed-batch fermentations, pure octanoic acid is used, which is more soluble compared to sodium octanoate. As a result the carbon is therefore more readily available to be used by the microbe. The use of different substrates other than octanoic acid (such as nonanoic acid) has been noted by various different authors (Sun *et al* 2009, Tortajada *et al.* 2008). Most recently research has focused on the use of waste products as substrates such as waste organic matter (Castilho *et al.* 2009) The conclusion of their research is that different substrates can produce different levels of biomass concentration within the same culture, and by extension different levels of product as a result.

6.5.2 Biomass Concentration Analysis

The growth of the culture, as with previous experiments, was analysed with OD /TVC /DCW Figures 6.16a-6.16c plot the results gathered from the runs conducted.

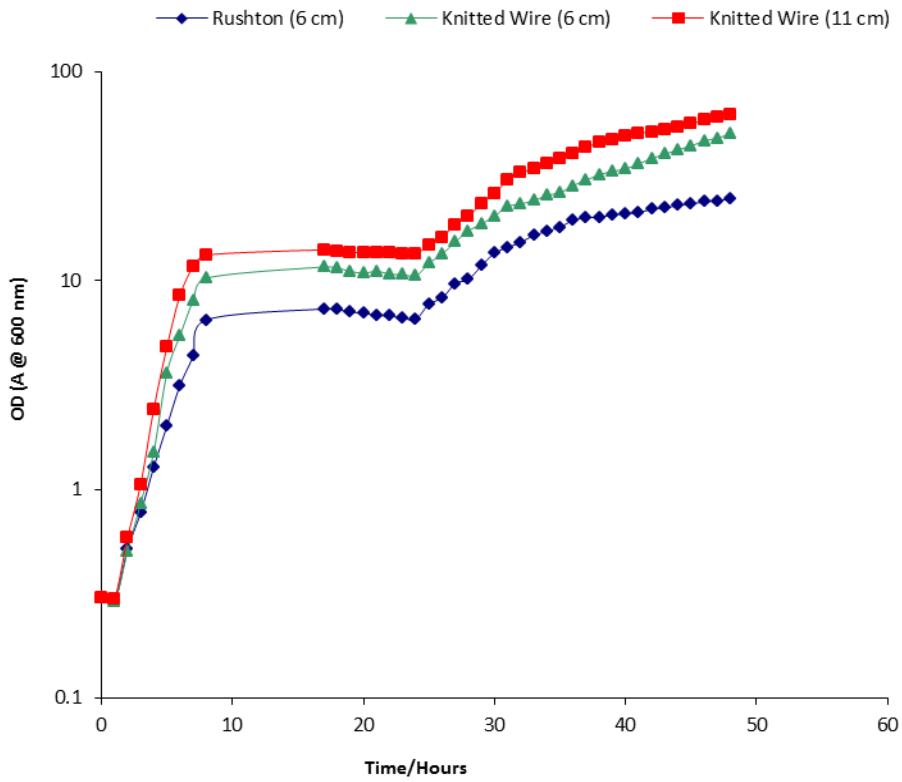

Figure 6.16a: OD values for the *P.putida* fed batch fermentation cycle for the Rushton and Knitted Wire (6 and 11 cm) impellers.

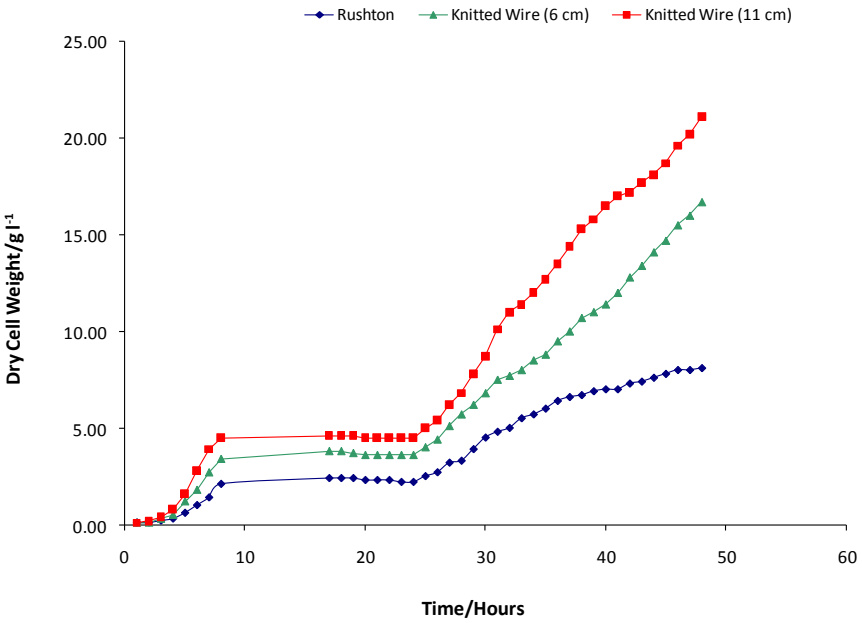

Figure 6.16b: DCW values for the *P.putida* fed batch fermentation cycle for the Rushton and Knitted Wire (6 and 11 cm) impellers.

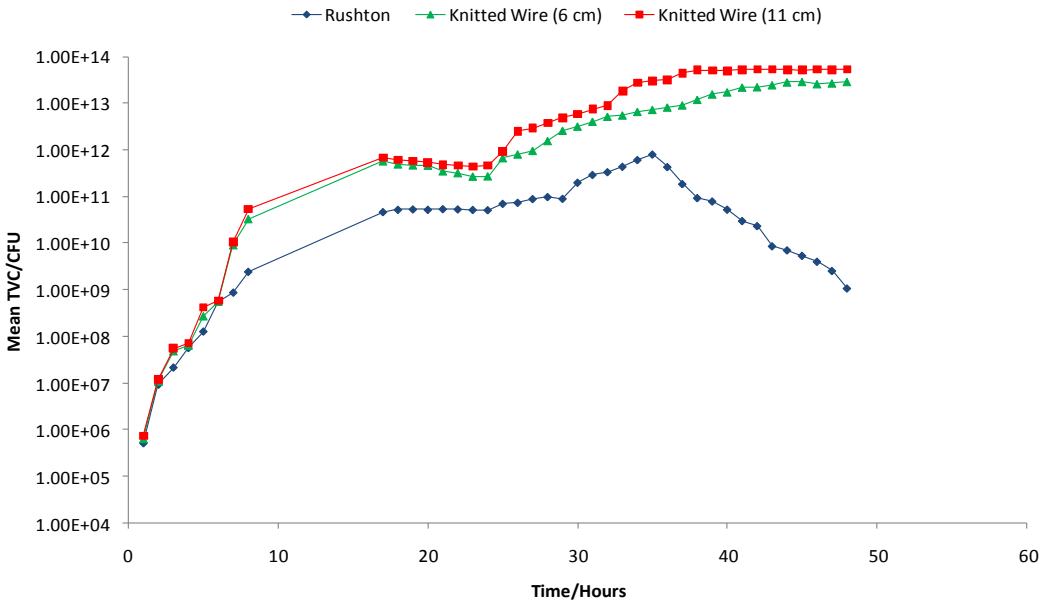

Figure 6.16c: TVC values for the *P.putida* fed batch fermentation cycle for the Rushton and Knitted Wire (6 and 11 cm) impellers.

Although all impellers show significant growth during the fed-batch phase, the increase in the Rushton impeller result is not as large as the knitted wire impellers. This result had been predicted based upon the results reported from the previous studies. In this case the difference between the Rushton and knitted wire impellers is much larger at the end of the fed-batch

process. As noted in prior experiments the Knitted Wire impellers are able to sustain a larger biomass concentration compared to the Rushton impeller. As noted in section 6.4.1 similar packing material has been successfully used to increase biomass concentration in an airlift column. This was brought about due to a much decreased bubble size (Nikakhtari *et al* 2005).

The Rushton impeller design has been noted several times as having sheared bubbles by use of its blades (Martin *et al* 2008). This could also lead to the shearing of microbial cells if they come close to the blades whilst the contents of the vessel are being mixed. In a fed-batch system due to the much higher biomass concentration present the probability of a microbial cell being sheared is therefore much higher. Figure 6.16 notes that the difference in biomass concentration between the Rushton and Knitted Wire impellers becomes larger as the age of the fermentation cycle increases. Furthermore a drop in pH and a large increase in foaming occurred for the Rushton impeller from hour 36-48, the cause of which was not immediately apparent. Around the same time a drop in the value of TVC was noted. Phase microscopy images were taken from the Rushton system at hour 48 (i.e. the end of the fermentation cycle) and shown in Figure 6.17

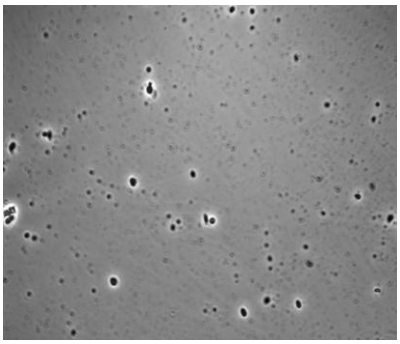

Figure 6.17: Phase contrast microscopy image for the *P.putida* fed batch fermentation conducted with the Rushton impeller. Image was taken at hour 48 in the Fermentation Cycle.

In the fed batch process agitated by the Rushton turbine impeller, there is PHA present despite the cells lysing open. This is probably because the cells had produced some PHA before lysis occurred. This result is not repeated for the two knitted wire impellers. It is reasonable to assume therefore that shear stress generated in the medium by the Rushton impeller may have caused the cells to lyse open.

The photograph for the Rushton system shows that many of the cells have been lysed open. This then accounts for the low pH levels, drop in TVC results and high amounts of foaming in the reactor that occurred from hour 36. This also explains why the growth curve shows a slowing of growth occurring (figure 6.16a) for this system. As shown in figure 6.16a, the second pulse and subsequent feeding regime of octanoic acid leads to a second exponential phase of growth occurring. This of course leads to a higher dry cell weight as a result. For all impellers this second exponential growth curve is not as steep as the first one, indicating that growth was not as fast.

6.5.3 DO Profile

A complete DO profile was recorded via DO probe for the fed-batch fermentation system. The profiles for the 11 cm knitted wire and Rushton impellers are noted in Figure 6.18a and Figure 6.18b.

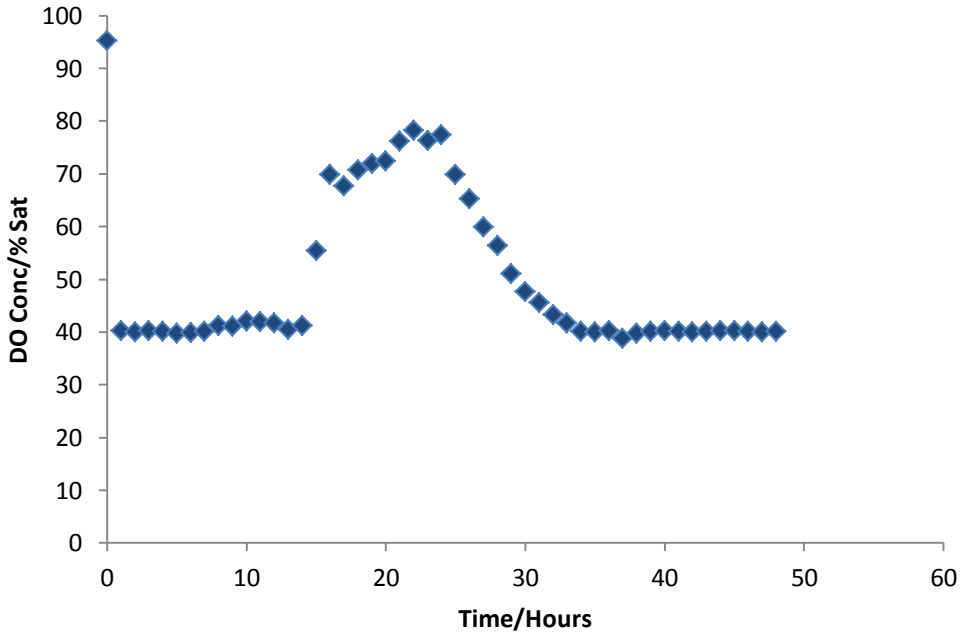

Figure 6.18a: DO profile for the 11 cm Knitted Wire impeller in the *P.putida* KT2442 Fed Batch Fermentation system conducted in the BioFlo III Reactor

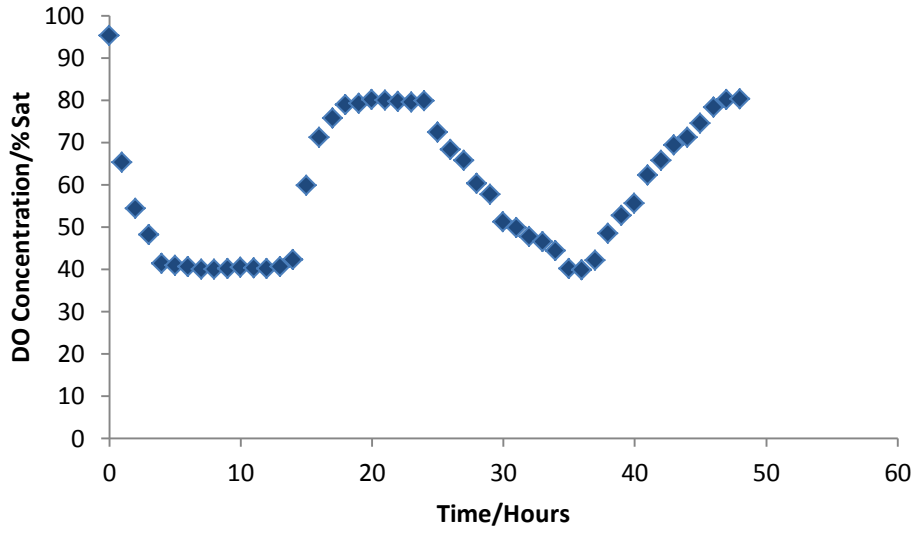

Figure 6.18b: DO profile for the 6 cm Rushton impeller in the *P.putida* KT2442 Fed Batch Fermentation system conducted in the BioFlo III Reactor

The DO profiles match the biomass concentration analysis presented in section 6.5.2 i.e. a drop in DO to 40% saturation is accompanied, as expected, by a rise in the biomass concentration during the exponential phase in first 10 hours of fermentation. The DO initially remains steady at 40% saturation level for some time during the stationary phase when biomass concentration remains constant. The TVC begins to drop slightly due to substrate limitation from hour 18 or so, the DO concentration increases again. After fed-batch operation begins at hour 24, the DO concentration once gain starts to drop reflecting the increasing biomass concentration. From figure 6.18b, it is interesting to note that, after hour 36, the DO level for the Rushton impeller starts to rise again in contrast to the DO profile for the knitted wire mesh (figure 6.18a). This is clearly reflected in the TVC results for the Rushton impeller (figure 6.16c) which recorded a drop at this point. This has been established to be due to the cells having lysed as a result of shearing action by the blades of the Rushton impeller. The cell lysis accounts for the additional foaming and drop in pH noted as the contents of the cells are spilled into the fermentation medium.

6.5.4 Phase Contrast Microscopy

Phase contrast microscopy was once again used to note PHA production at the end of each fermentation cycle. Figure 6.19 illustrates the PHA content for the 6 cm Knitted Wire and 11

cm Knitted Wire impellers. Figure 6.17 (shown earlier) displays the microscopy image obtained using the Rushton turbine impeller.

[A] 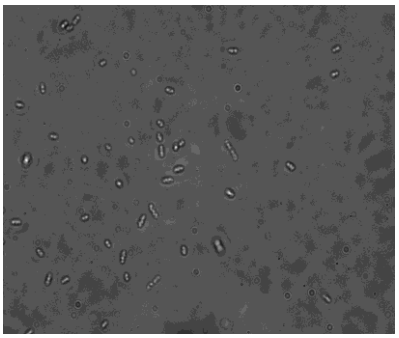 [B] 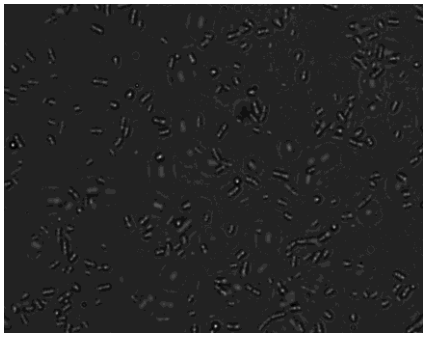

Figure 6.19: Phase contrast images for the Fed Batch *P.putida* fermentations showing [A] 6 cm knitted wire impeller and [B] the 11 cm Knitted Wire impeller. Images were taken at 48 hours into the Fermentation cycle.

The images for the 6 and 11 cm Knitted Wire impeller show a number of cells containing PHA. This illustrates that the impellers can sustain a high level of biomass concentration without any damage occurring to the cells. A higher level of PHA is noted by the phase microscopy images; it is not as much of an increase compared to the increase in biomass concentration. For the Rushton impeller fed batch (Figure 6.17) there is PHA present despite the cells lysing open, as discussed earlier. This is probably because the cells had produced some PHA before lysis occurred. Cell lysis did not appear to occur with the two knitted wire impellers since no excessive foaming was observed. It is reasonable to assume therefore that shear stress generated in the medium by the Rushton impeller may have caused the cells to lyse open.

6.5.5 Extraction of PHA by NaClO Method.

PHA was extracted from the bacteria by utilising the same method. as for the batch fermentation experiments. The procedure was performed on all experiments conducted. Figure 6.20 shows the % yield of PHA (based on DCW) gained for each of the fed batch experiments conducted.

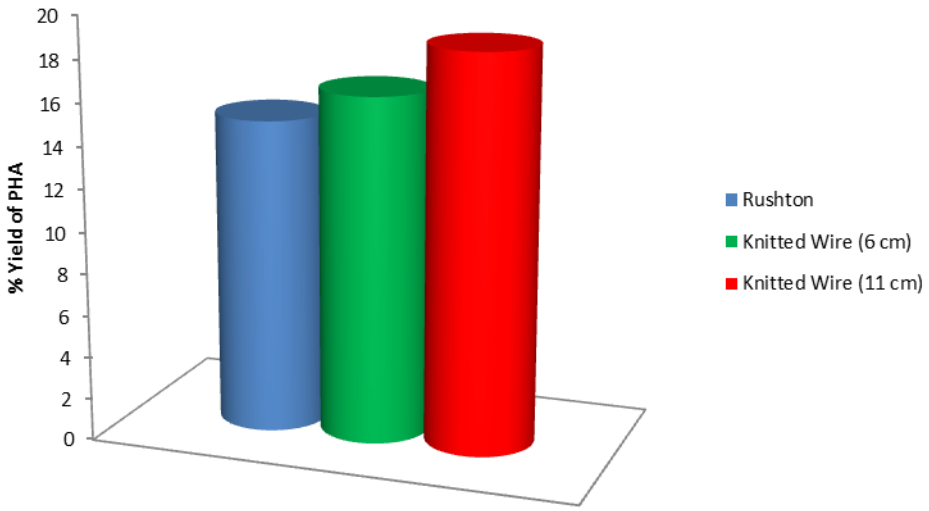

Figure 6.20: PHA yield for the Rushton and Knitted Wire (6 and 11 cm) impellers for the fed-batch *P.putida* KT2442 Fermentation

As with the previous batch experiment, the highest % PHA yield of 19.5% is achieved by the 11 cm Knitted Wire mesh impeller, followed closely by the 6 cm Knitted Wire impeller (16.5%) and then the Rushton impeller (15.5%). The surprising result was for the Rushton impeller which produces a similar PHA yield to the 6 cm knitted wire impeller, despite the phase contrast microscopy images showing lysed cells at hour 48. Indications of cell lysis caused by shear are increased levels of foaming, and a tendency for the pH level to become unstable. Both of these trends were noticed during the Rushton fed batch fermentation. The declining TVC results from hour 36 are also an indication that the number of cells dying exceeded the number of new cells being created. Despite this declining cell number, the PHA extraction revealed a similar PHA yield to that produced by the 6 cm knitted wire impeller. It is possible that this PHA was produced before the cells were lysed.

6.5.6 Summary

A fed batch fermentation study was conducted with all impellers with *P.putida* KT2442. The substrate was changed from sodium octanoate to octanoic acid as noted in the protocols utilised. The following points were noted from the experiments:

1. The highest biomass concentration in excess of 20 g l^{-1} and % PHA yield close to 20% was achieved by the 11 cm Knitted Wire impeller.

2. The substrate used within the medium was noted to have an effect on the growth rate observed. The growth profile for both substrates was similar for the first few hours but subsequently the octanoic acid fermentation produced the larger OD values. Therefore the octanoic acid was used as substrate which was in line with the protocols used.
3. The biomass concentration for the Rushton impeller is not as high as expected. This is due to cells being lysed by the shearing action at the tip of the impeller blades resulting in reduced TVC of the microbe and a lower % yield of PHA observed. No cell lysis was apparent with the knitted wire mesh impellers under the conditions studied suggesting mechanical shear damage to microbial cells can be effectively controlled without compromising on oxygen transfer rate and/or biomass concentration.

6.6 *P.putida* KT2442-Fed-Batch Fermentation Experiments (HBR)

A set of batch fermentation experiments were performed with HBR to enable a direct comparison with the batch STR experiments (section 6.5). The aim was to reproduce the previous experiments to establish if the HBR could successfully establish a healthy fermentation system. The main difference for the HBR is that although the system is operated as batch, the liquid flow is continuously re-circulated around the reactor via an external recirculation loop.

6.6.1 Sterile Process Validation

A sterile hold test was performed with the newly fabricated HBR in order to ensure that the chemical sterilisation was effective and that the sterile barrier could be maintained during a fermentation cycle. The chemical sterilisation process for the reactor was validated by sterile hold test. As with the STR fermentation was conducted without an inoculum added. OD and TVC analysis taken every hour revealed no growth, validating the process.

6.6.2 Biomass Concentration Analysis

The analysis of the Biomass concentration in the HBR was conducted in the same manner as for the BioFlo III experiments. Figures 6.21a-c illustrates the OD /TVC /DCW profiles for the highest and lowest operation conditions respectively. These results are plotted alongside the Rushton results obtained in section 6.4.1 for comparison.

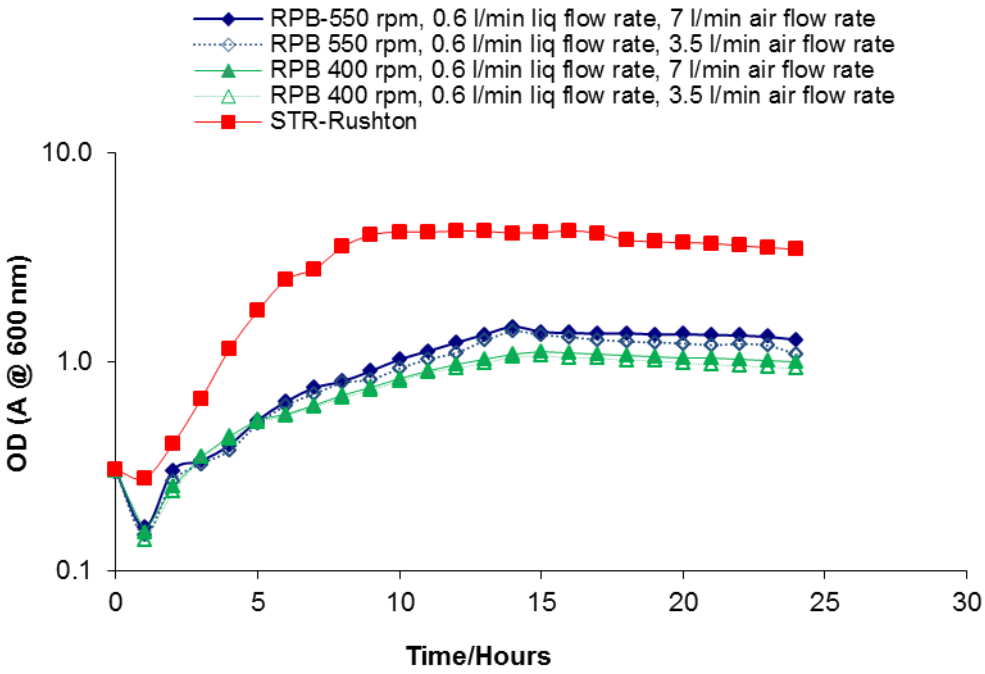

Figure 6.21a: OD values for selected Fermentation experiments conducted with the HBR compared against the Rushton impeller

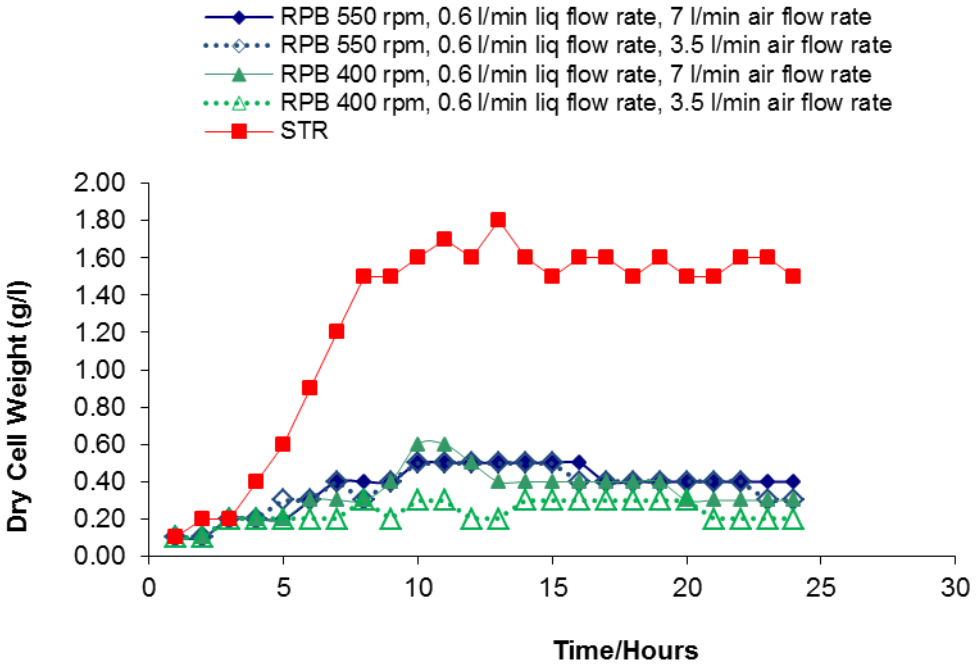

Figure 6.21b: DCW values for selected Fermentation experiments conducted with the HBR compared against the Rushton impeller

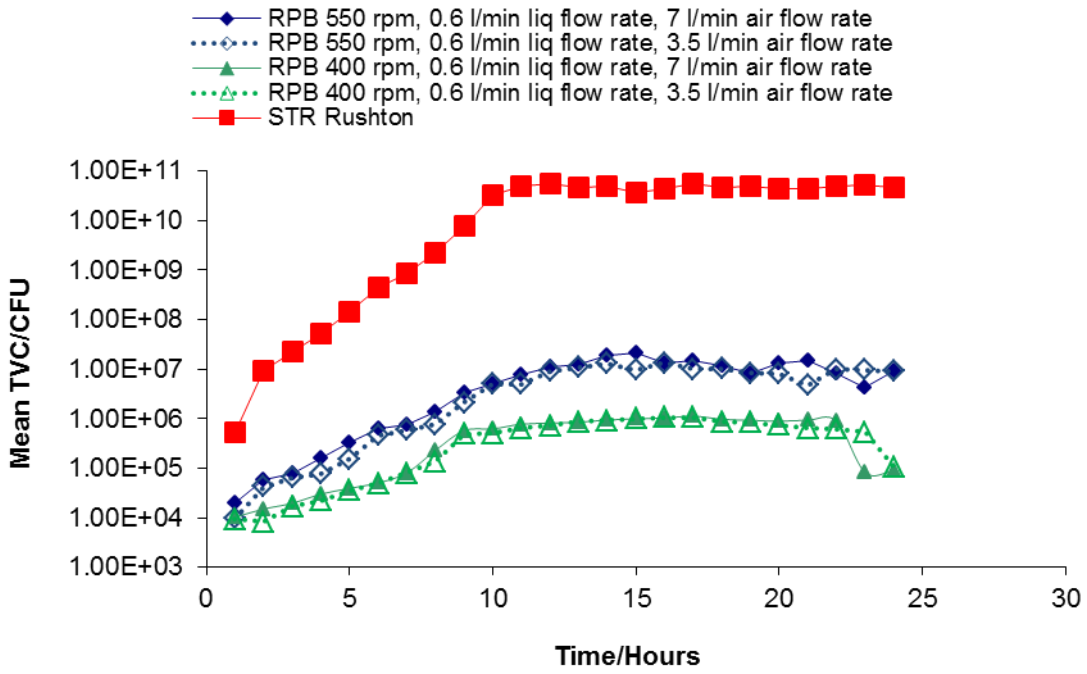

Figure 6.21c: Mean TVC values for selected Fermentation experiments conducted with the H.B.R compared against the Rushton impeller

The plots note that the biomass concentration for the HBR is lower than the ones obtained for the Rushton design. The growth profile for the fermentation in the HBR is slightly different with the peak result shifted to the right, occurring around hour 14 (whereas for the STR system it occurred around hour 10). The largest amount of biomass produced in the HBR occurs for the highest rotational speed and highest air flow rate. The TVC count reveals a lower result for the HBR, especially towards the end of the fermentation cycle. The slight change in the growth curve could be due to the reactor, although there has been no mention of a change in growth pattern with other novel reactors used for fermentation application. Not presented here, an very small increase in biomass concentration was noted to occur within increasing liquid flow rate from 0.4-0.6 l min^{-1}. However the increase is not deemed to be significant in the narrow range of flow rate used (0.4-0.6 l min^{-1}). The TVC analysis records a higher viable cell count at the higher rotor speeds of 550 rpm. The result shows that even at the higher speed of 550 rpm, shear damage does not occur within the rotor environment.

6.6.3 Temperature Profile

A series of thermocouples was positioned around the reactor in order to monitor the temperature throughout the system, as detailed in Chapter 4. The temperature profiles for the highest and lowest operating conditions are displayed in Figures 6.22a (mean temperature in

the reactor), 6.22b (holding tank), and 6.22c (sample vessel), with table 6.4 noting the final temperature values for the system for the two operating conditions alongside the noted temperature differential.

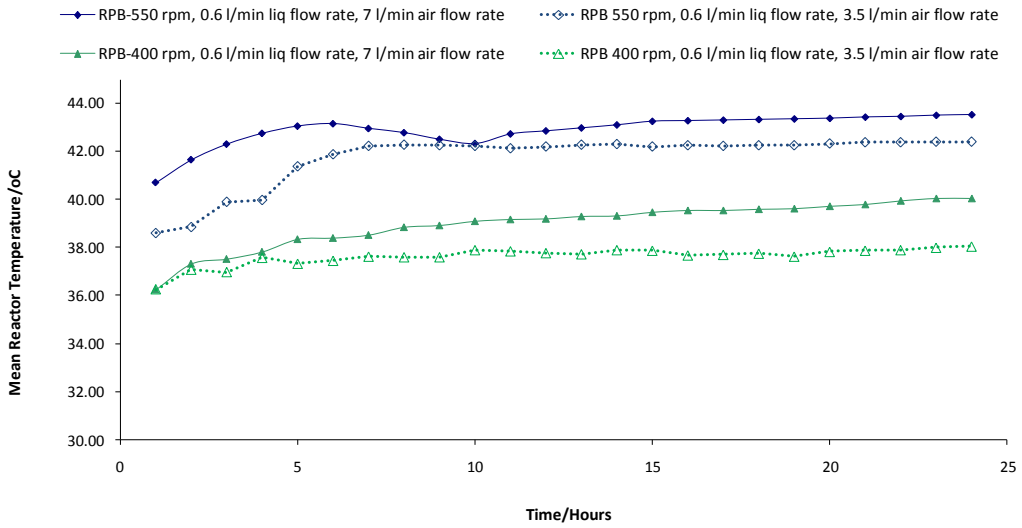

Figure 6.22a: Mean Reactor Temperature during the HBR Fermentation Cycle

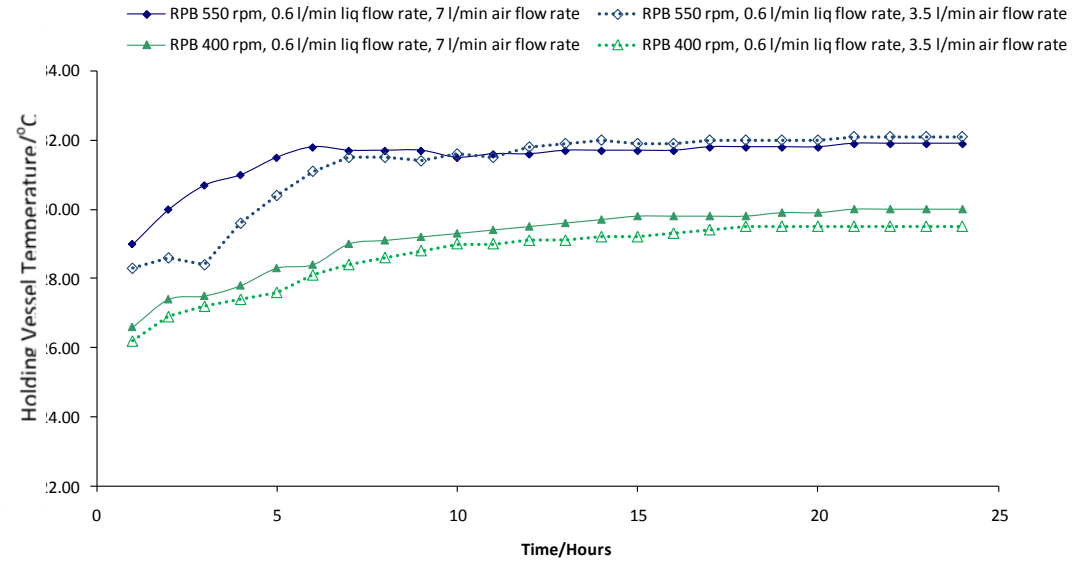

Figure 6.22b: Holding Tank Temperature during the HBR Fermentation Cycle

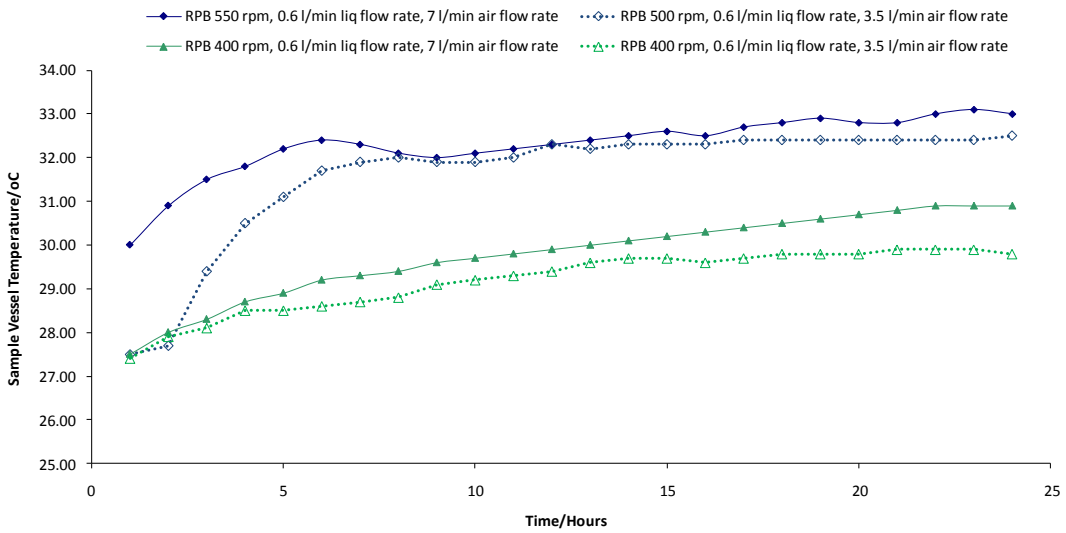

Figure 6.22c: Sample Tank Temperature during the HBR Fermentation Cycle

Table 6.4: Final Temperatures recorded for the highest/lowest operating parameters in the HBR

Operating Conditions	Mean Reactor Temperature/ ^{o}C	Sample Vessel Temperature/ ^{o}C	Holding Tank Temperature/ ^{o}C	Temperature Differential / ^{o}C
550 rpm 0.6 l min^{-1} liq flow rate 7 l min^{-1} air flow rate	43.5	33.0	31.9	10.5
400 rpm 0.4 l min^{-1} liq flow rate 3.5 l min^{-1} air flow rate	38.5	30.5	29.8	8.7

The temperature is seen to vary significantly around different points in the reactor. Although not shown here the temperature difference recorded in the rotor (from thermocouples 1-4) has been noted as the mean temperature ± 1^{o}C. The protocol used for the fermentation has established the optimal temperature for growth as 30^{o}C (Tortajada *et al.* 2008). As a result of the higher temperature in the rotor, microbial growth would have been adversely affected.

There are also differences between the main rotor temperature and the temperature in the re-circulation loop which includes the sample and holding vessel. Due to this temperature differential, microbial growth again will be affected. Though the rotational speed was restricted, the simple heat transfer system which consisted of a water bath regulating the temperature of the holding vessel could not accurately control the reactor temperature. The fermentation medium picked up heat from the rotary union so that temperatures in the packed bed quickly reached in excess of 40^{o}C. The temperature within the recycle loop was seen to be much lower due to the sprayed droplets from the HBR losing heat as it exits from the reactor. As a result, a large temperature differential existed between the rotor and downstream side of the HBR (noted in table 6.4). For further studies with the HBR a more robust temperature control system would need to be implemented.

6.6.4 Phase Contrast Microscopy

Phase contrast microscopy was used to qualitatively determine PHA yield at the end of each fermentation cycle in the HBR The results from hour 24 for one HBR fermentation is displayed in figure 6.23

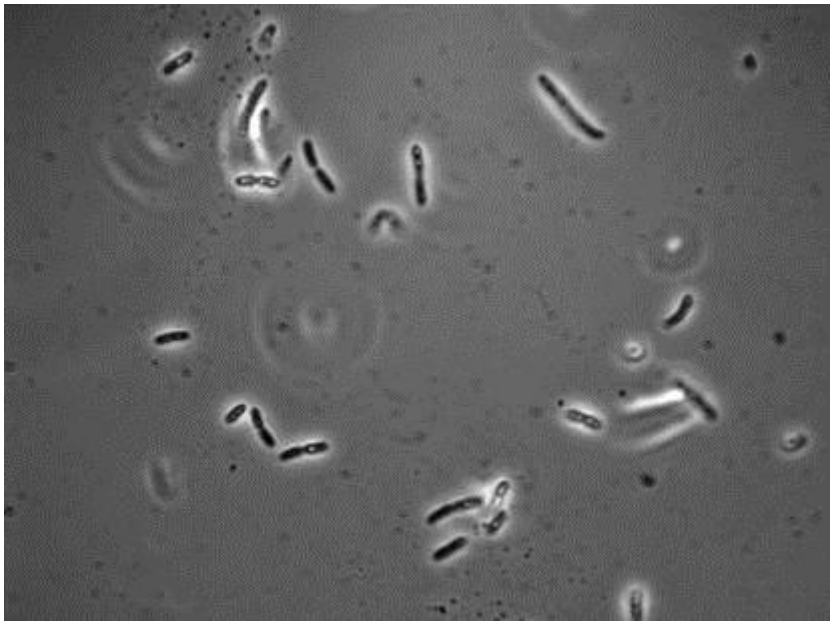

Figure 6.23: Phase contrast image for a HBR Fermentation (HBR operating at 1200 rpm, 0.6 l min^{-1} liquid flow rate, and 7 l min^{-1} air flow rate)

The images in figure 6.23 confirm that the HBR can sustain a microbial community, and produce PHA as shown by the glowing species. However in comparison to the STR (Figure 6.19) the amount of PHA formed is much less. This had been expected given the lower biomass concentration results reported earlier. It is also interesting to note that there is a

change in the morphology of the bacterium compared to the STR fermentations. The bacteria in the HBR are much longer and thinner than the STR counterparts. This may be a response by the bacteria to the HBR environment. Precedence for alteration of morphology appears in the literature of higher more complex organisms such as fungal cultures as a result of adaptation to their environment (Papagianni, 2004). Changes in morphology are brought around as a result of low oxygen or nutrient conditions (Madigan *et al.* 2009). The reason behind the changes in bacteria exposed to the HBR environment requires further study.

6.6.5 DO Profile

The DO profile for the HBR system was noted for all experiments conducted. As previously noted the values were logged on a M700 single channel meter and recorded by aid of a USB logger. The DO profiles for the lowest and highest operating conditions are noted in Figure 6.24

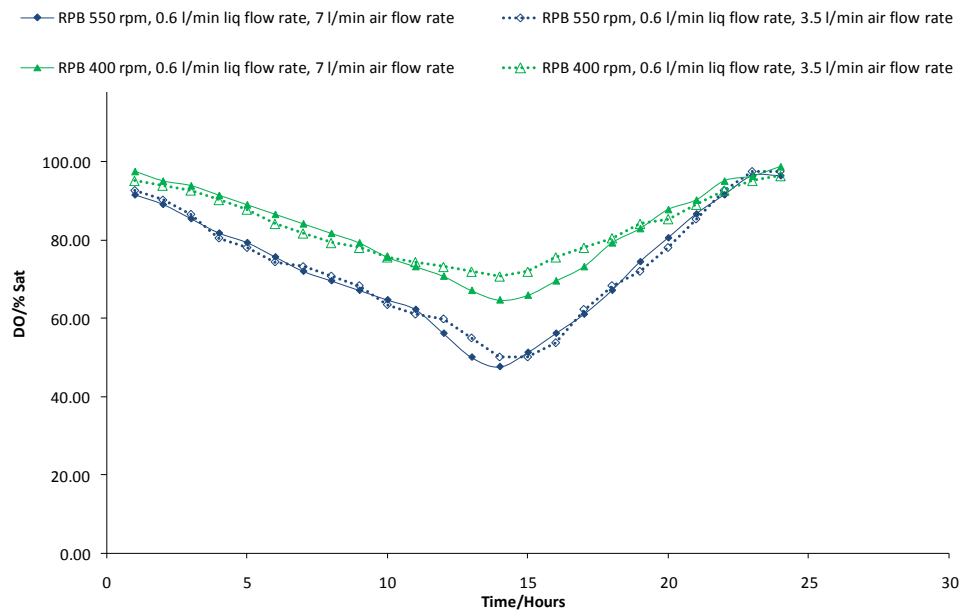

Figure 6.24: DO profiles for the lowest and highest conditions for the *P.putida* KT2442 fermentation in the HBR

Both profiles start and finish at similar DO levels, with the higher condition run dipping lower towards hour 14 than the lower conditions. For the HBR fermentations, DO was not controlled at 40 % (as in the BioFlo batch fermentations). As noted in figure 6.24 the lowest DO value reached was 40 % and therefore the algorithm would not have been activated. The DO profiles displayed here roughly correspond to the biomass concentration profiles shown in Figures 6.21a-6.21c so that as the biomass concentration increases DO decreases. The

lower DO curves for 550 rpm also correspond to the higher biomass concentrations achieved at 550 rpm, as depicted in figure 6.21a. Oxygen mass transfer for these rotational speeds and air flow rates (representing the upper limit for the parameters used in the study) are higher than other operating conditions. This has already been shown in the NTU and K_La results noted in chapter 5 (section 5.5.1).

6.6.6 Extraction of PHA by the NaClO Method.

The yield of PHA produced by each fermentation cycle was once again investigated at the end of the each fermentation cycle. The results for the HBR are presented in Figure 6.25. As expected, under conditions of higher rotational speed (550 rpm) and higher air flow rate (7 l/min), the highest PHA yield of 6.2% is obtained from the HBR

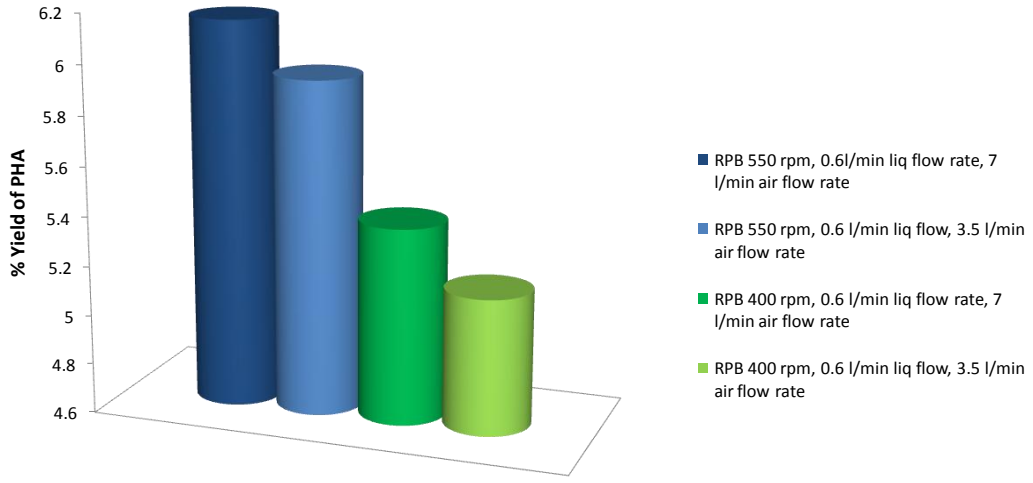

Figure 6.25: % Yield of PHA produced for selected HBR *P.putida* batch fermentations

The DCW, phase contrast microscopy, and % yield analysis all shown a lower result than that produced by conventional reactor technology (Cartwright and Boodhoo, 2008 and Tortajada *et al*., 2007). Two possible reasons have been identified, the first of which is due to the restricted rotational speeds imposed on the reactor (to aid temperature control). As a result of the restricted speeds the K_La value of the system was not as high as expected. Secondly even though the rotational speed was restricted, heat transfer in the system was not accurate and as a result the temperature increased. The fermentation medium picked up heat from the rotary union; temperatures in the packing quickly reached in excess of 40^oC. Due to the known

optimal temperature of growth for *P.putida* known to be 30^{o}C (Tortajada *et al* 2007) this high temperature will have a negative effect on growth.

6.6.7 Summary

The current study investigated the capability of a newly fabricated HBR to function as a fermenter. The *P.putida* KT2442 fermentation system was used to investigate whether the HBR could support and sustain a microbial community. The following points have been noted from the experiments conducted.

1. The HBR was noted to be able to sustain a microbial community, although on comparison to the experiments with the STR the biomass concentration was much less. This was believed to be due to a problem with the temperature control.
2. Poor temperature control was noted in the HBR rig, with temperatures inside the HBR reaching 40^{o}C and a temperature differential of 10^{o}C across the reactor as a whole. This is because the liquid stream picks up heat from the rotary union and then loses this once it is sprayed out from the main rotor. A more robust temperature control is needed if the reactor is to sustain a microbial community.
3. Phase contrast microscopy images have shown that PHA was produced within the HBR As with the biomass concentration analysis, the amount of PHA produced within the HBR was not as much as for the STR. study. With a more robust temperature control system in place there is a potential for a much larger yield of PHA to be obtained.

6.7 Summary:

The current study investigated two fermentation systems and tested the ability of a set of porous mesh impellers and a newly fabricated HBR to support a microbial community. The *E.coli* K12 study was based on a previous study conducted within the school (Ndlovu 2004) and the *P.putida* KT2442 study was conducted in conjunction with an E.U. project on Bio production (Cartwright and Boodhoo, 2008). The following points have been noted from the experiments:

1. For the *E.coli* K12 batch fermentation the Knitted Wire impellers produced the largest biomass concentration noted, with the 11 cm Knitted Wire impeller producing the most biomass concentration. This is in agreement with the Ndlovu (2004) study and is

believed to be caused by the design of the impeller which is able to shred the air bubbles down to a small size but not shear the microbial cells themselves.

2. For all impellers the OTR always exceeded the OUR in the *E.coli* fermentation systems though in some cases for the 6 cm Knitted Wire impeller the two figures were quite close. This implied that the fermentations conducted did not become limited by oxygen transfer, except for some runs with of the 6 cm Knitted Wire impellers where this could have been the case. The results produced by the Rushton and 11 cm Knitted Wire impeller are broadly in line with the study conducted by Ndlovu (2004).
3. A batch fermentation conducted with *P.putida* KT2442 in the BioFlo III reactor noted that the 11 cm Knitted Wire impeller produced the highest biomass concentration and % yield of PHA of all the impellers studied. Despite this the % yield and biomass concentration was lower than comparable studies found in literature. This is believed to be due to the medium for the system not being fully optimised and being used to establish that PHA can be produced with this microbial culture chosen.
4. A *P.putida* KT2442 fed batch fermentation noted again that the 11 cm Knitted Wire impeller produced the highest biomass concentration and % yield of all the impellers studied. The increase in biomass concentration and PHA yield was not very large for the Rushton impeller as it is believed that the impeller blades caused lysis of cells. This was confirmed from the phase microscopy images.
5. A study with the newly fabricated HBR has shown that the reactor is capable of supporting a microbial community. However due to a temperature control issue the biomass concentration and % yield of PHA was much less compared to the STR study. A more robust temperature control system is needed if the HBR is to fulfil its potential as a fermenter.

Chapter 7: Conclusions and Recommendations for Future Work

The ultimate aim of the research for the PhD study was the design, fabrication, and commissioning of a new Rotating Packed Bed (HBR) with application for aerobic fermentations. The work conducted can be neatly divided into three main areas, the initial transfer, power consumption, and bubble experiments with the porous packing impellers, the fermentation experiments with the porous packing impellers, and the flooding, hydrodynamic, transfer and fermentation experiments with the new HBR reactor. With this in mind the following conclusions can be drawn from the research:

7.1 Oxygen Transfer Characterisation and Bubble Study Experiments with Porous Packing Impellers (Chapter 5)

1. The two Knitted Wire impellers can produce a similar transfer value (K_La) to that of the Rushton impeller in both air/water and air/water-glycerol systems studied. For the 1000 rpm/1.0 vvm experiment in the air/water system the Rushton impeller produced a K_La of 0.033 s^{-1}, compared to 0.030 s^{-1} (11 cm knitted impeller) and 0.028 s^{-1} for the (6 cm knitted impeller). The K_La values for the Knitted Wire impellers were produced at a much reduced power consumption level. The K_La values produced for the Fibre and Declon mesh impellers were a lot lower than the Rushton, again for reduced power consumption. For all impeller systems, the value of K_La was seen to increase with increasing agitation and air flow rate
2. The enhanced transfer value of the Knitted Wire impellers can be attributed to smaller air bubbles. The bubble study has shown that both Knitted Wire impellers are capable of producing much finer bubbles than the Rushton. For the 1000 rpm/1.0 vvm experiment when the Rushton impeller produced bubble diameters of 0.28 cm, the 6 and 11 cm Knitted Wire impellers produced bubble diameters of 0.25 cm and 0.15 cm respectively.
3. The effect of viscosity on the transfer rate was noted by investigation of a 50 % mixture (by volume) of water and glycerol. For all impellers studied the K_La value was lower in the water/glycerol system which was brought about due to decreasing oxygen solubility. Bubble sizes for the water/glycerol were smaller than the pure water system, which could have led to an enhanced transfer rate. Due to the decreased

oxygen solubility in higher viscosity systems having a more dominant affect, the transfer results for the air-water-glycerol system are lower despite the smaller bubble diameter.

4. For the 1000 rpm/1.0 vvm K_La results (air/water system), the power consumption readings were 10485 W m^{-3} (Rushton impeller), 2858 W m^{-3} (11 cm Knitted Wire impeller), and 1970 W m^{-3} (6 cm Knitted Wire impeller), 1020 W m^{-3} (6 cm Fibre impeller), 3094 W m^{-3} (11 cm Fibre impeller), 1393 W m^{-3} (6 cm Declon impeller), and 3635 W m^{-3} (11 cm Declon impeller). Although as noted previously the Fibre and Declon mesh impellers did not produce a high transfer level, there was reduced power consumption for the K_La values noted

7.2 *E.coli* K12 and *P.putida* KT2442 Fermentation Study with BioFlo III Reactor (Chapter 5)

1. For transfer optimisation with *E.coli* K12, the two Knitted Wire mesh impellers were able to support a larger microbial community than the Rushton impeller. In terms of OD and DCW, for the 400 rpm/1.5 vvm experiment the Rushton impeller produced an OD of 6.765 and a DCW of 2.2 g l^{-1}. This is contrasted to the 6 cm Knitted Wire impeller which produced figures of 7.308 (OD) and 2.4 g l^{-1} (DCW), and for the 11 cm Knitted Wire impeller of 8.750 (OD) and 2.9 g l^{-1} (DCW). During the 200 rpm/1.5 vvm experiment with the Rushton impeller, foaming in the reactor became more prevalent after hour 6 despite the presence of antifoam. It had been theorised that the foaming was caused by cell lysis, resulting in the presence of protein in the medium. This was then confirmed by S.D.S. Page analysis which showed a large increase in the amount of protein present in the medium after hour 6.
2. For the polyhydroxyalkonate (PHA) optimisation study, the Knitted Wire impellers produced higher O.D .and DCW results when compared to the Rushton impeller. For the experimental run conducted at pH 7 with D.O controlled at 40 % and Rushton impeller, the OD and DCW values were 3.450 and 1.5 g l^{-1} respectively. For the same experimental conditions the 6 cm Knitted Wire impeller produced results of 4.056 (OD) and 1.7 g l^{-1} (DCW), and for the 11 cm Knitted Wire 4.653 (OD) and 2.0 g l^{-1} (DCW). All the readings noted were taken after 24 hours of fermentation time. A change in pH from 6 to 7 also results in a difference to the growth noticed within the system, although the final OD and DCW are relatively similar. This has been

observed for all impeller systems studied. Extraction of PHA from the batch fermentation system noted a higher yield for the 11 cm Knitted Wire impeller

3. For the second *P.putida* KT2442 fed-batch fermentation, the Knitted Wire impellers produced a greater amount of biomass compared to the Rushton both during the batch and fed batch phase. Despite the a great number of the Rushton cells lysing open after hour 36 (during fed batch operation) the % yield results between the Rushton and 6 cm Knitted Wire impeller were very similar. As with the batch fermentation, the 11 cm Knitted Wire impeller produced the highest level of biomass and % yield. The effect of substrate was investigated by use of sodium octanoate and Octanoic acid.

7.3 HBR Reactor Experiments (Initial Work Chapter 5, Fermentation Work Chapter 6)

1. Flooding experiments conducted with the HBR have shown that the packing has a profound influence on the values observed. Flooding occurred at much higher throughputs of gas and liquid when packing was used. Increasing rotational speeds allows higher flooding limits to be reached. The flooding data was then used in the design of experiments for the transfer and bubble study.
2. Using data points below the flooding curve, mass transfer experiments showed that the HBR to be efficient at stripping oxygen from water with the use of nitrogen gas. The highest NTU recorded was 2.47 for the experiment conducted at 1200 rpm with packing, with liquid flow rate of 0.4 l min^{-1} and airflow rate of 9 l min^{-1}. The NTU result for the similar experiment (airflow rate at 7 l min^{-1}) without packing was 2.01. Compared to an earlier HBR system at Newcastle, the NTU values are lower than the ones reported. This is to be expected since the current HBR is smaller; therefore the centripetal force has a greater effect on the larger reactor. Packing was also shown to have an effect on the system, with the larger NTU and K_La values being generated. This is believed to be due to much smaller bubbles being produced.
3. Bubble study conducted confirms the theory behind the transfer experiments. The packing is able to generate much finer bubbles than when packing is not present. Bubble size for the 1200 rpm/ liquid flow rate 0.4 l min^{-1}/airflow rate 9 l min^{-1} (with packing) was 0.42 mm and for the 1200 rpm/liquid flow rate 0.4 l min^{-1}/airflow rate 7 l min^{-1} was 2.97 mm, showing that the packing material has a great effect on the bubble size produced. Compared to the BioFlow system the packing can produce much smaller bubbles. The diameter of the bubble was seen to decrease with

increasing rotational speed and air flow rate and increase slightly with increased liquid flow rate. Bubble size is also smaller for the HBR with packing, and in some instances without packing compared to the BioFlow. Size distribution becomes narrower as rotational speed and air flow increase, and widens as liquid flow rate increases. The distribution of bubble size is smaller compared to the BioFlow experiments.

4. A fermentation study with the organism *P.putida* has shown that a microbial community can be grown and sustained within the HBR without contamination from the outside environment. The study reported increasing biomass concentration with increasing rotational speed, air flow rate, and liquid flow rate. Compared to the BioFlo system, the biomass concentration and % yield of PHA was much lower than expected. This is believed to be caused by the lower than expected transfer results reported alongside problems encountered with temperature control.

7.4 Recommendations for Future Work

Although sufficient time was allocated for the research, there will be always be scope for further experiments to be undertaken in the future. The following areas below are suggested as areas worthy of investigation:

1. Investigation and modelling of the flow patterns and mixing behaviour of the porous impellers. This could occur by use of C.F.D. and experimental analysis. This would then illustrate how uniform the mixing environment could be within the system, leading to a reduction in substrate limitation effects.
2. The testing of the impellers in a higher viscosity system. In the current study the highest viscosity used was with the 50 %water/50 %glycerol mixture at 4.7 mNs m^{-2}. Further bubble and transfer studies would see the effect of a much higher viscosity on the mean bubble and transfer capability of the porous packings
3. A highly viscous fermentation system could be run to further test the porous packings oxygen transfer and cell growth capabilities. An example system would be the production of Xantham Gum from the bacterium *Xanthomonas campestris*. This fermentation system becomes highly viscous and Non-Newtonian as the product is produced. Alongside the new system described in point 2, this would an excellent way to test the capabilities of the packings under Non-Newtonian conditions.
4. Due to the low flooding limits achieved with the current reactor setup, further work is needed to enhance this limit. This could be achieved by the use of more packing in the

centre of the rig, and possible redesign of the outlet part of the collector so that it can cope with a higher throughput of liquid.

5. Design and implementation of a new temperature control system for the HBR. A more robust temperature control would then allow for greater biomass concentration to be produced, and therefore a greater yield of PHA would hopefully be the outcome. Once the HBR has been established in batch mode, fed-batch and continuous fermentation could be carried out with this design, further intensifying the fermentation.

Appendix A: Sample Calculations

A1 K_La Measurement by the Static Gassing Out Method

The oxygen transfer capability of the porous and Rushton impellers was examined via the static gassing out method (see Chapter 5, section 5.1.1 and 5.1.2).

As noted in Chapter 2 (see section 2.2.3) the method (devised by Wise in 1951) involves de aerating the liquid with nitrogen gas for a period of time followed by a re aeration of the liquid with either air or oxygen until the saturation point is reached. The full DO concentration profile for this method is noted in figure A1

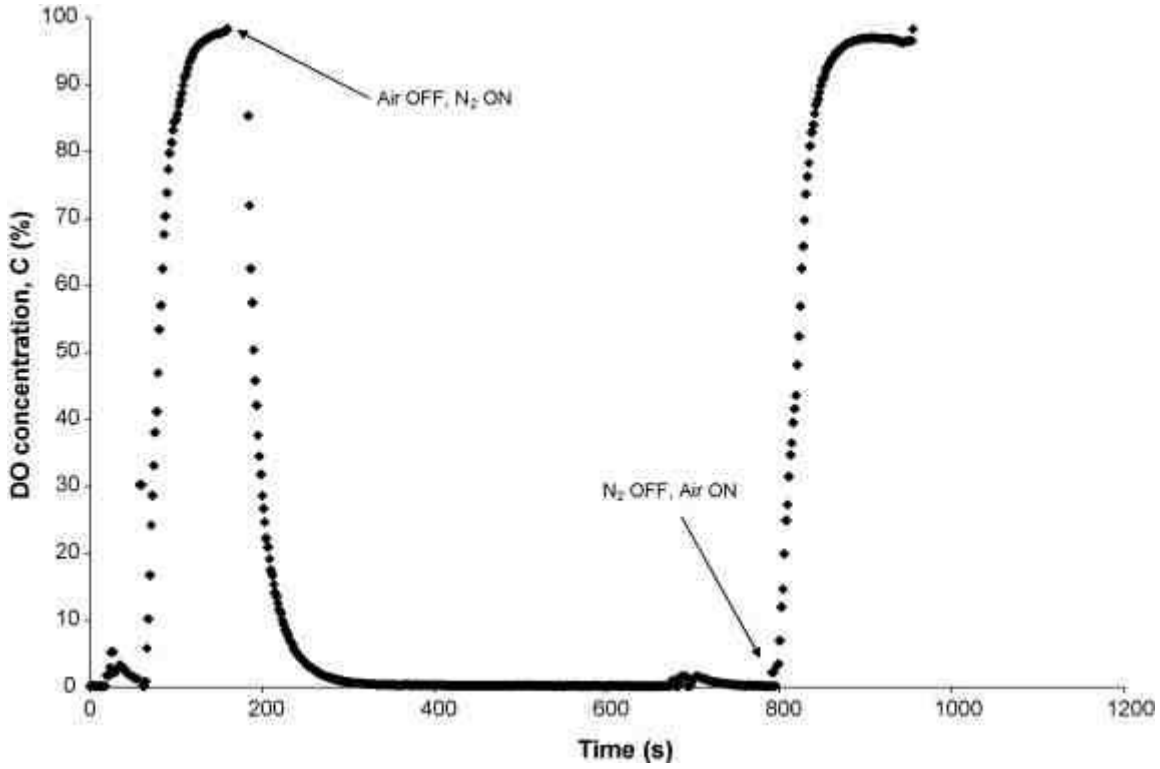

Figure A1: D.O profile for the static gassing out method for calculating K_La (Boodhoo *et al.* 2008)

The values recorded from the D.O probe are logged by computer and placed into Microsoft Excel for analysis. To calculate the value of K_La only the absorption figures are considered (i.e. the period after which the air was switched back on). Figure A2 shows a screen shot of a typical spreadsheet

Table A1: Screenshot of a typical Excel Analysis

	A	B	C	D	E	F
6	Time/Seconds	Temperature/ °C	DO Reading	Agitation Rate	ln (C*/C*-C_L)	
7	0	35.31	0.65	201.98	0.006479612	
8	10	35.32	0.66	202.03	0.006579627	
9	20	35.34	0.87	202.25	0.008682256	
10	30	35.34	2.52	202.32	0.025358574	
11	40	35.34	7.9	202.27	0.081749914	
12	50	35.31	12.48	202.14	0.132396448	
13	60	35.3	16.79	202.18	0.182520305	
14	70	35.29	21.92	201.84	0.24565254	
15	80	35.27	27.4	201.71	0.317808073	
16	90	35.28	32.66	201.79	0.392336249	
17	100	35.27	38.13	201.8	0.476223249	
18	110	35.28	43.4	201.83	0.564296838	
19	120	35.28	48.05	201.91	0.649023805	
20	130	35.28	52.48	201.79	0.737020992	
21	140	35.27	56.93	201.73	0.833972884	
22	150	35.28	60.9	201.6	0.929191556	
23	160	35.27	64.2	201.54	1.015882721	
24	170	35.27	67.27	201.69	1.1038925	
25	180	35.27	70.28	201.76	1.19842384	
26	190	35.3	73.04	201.99	1.29373402	
27	200	35.29	75.8	201.87	1.399094536	
28	210	35.3	78.23	201.87	1.502042505	
29	220	35.27	80.22	201.71	1.59503498	
30	230	35.28	82.15	201.79	1.694319748	
31	240	35.26	83.89	201.55	1.793151535	
32	250	35.26	85.45	201.5	1.890912476	
33	260	35.26	86.83	201.47	1.986156826	
34	270	35.26	88.12	201.62	2.084222427	
35	280	35.26	89.24	201.5	2.177936438	
36	290	35.26	90.29	201.56	2.274563273	
37	300	35.28	91.28	201.77	2.375104502	

Total | Ag1Af1V1I1 | Ag1Af1V1I1REPEAT | **Ag1Af2V1I1** | Ag1Af2V1I1REPEAT

Ready

The applicable mass transfer equation (see section 2.2.1 in Chapter 2) is given by:

$$\ln\left[\frac{C^*}{C^*-C_L}\right] = K_L a t \qquad \text{(A1)}$$

Note that in table A1, the CL values are denoted by DO reading and the C* readings come from the saturated value recorded at the top of the spreadsheet. A graph of $\ln\left[\frac{C^*}{C^*-C_L}\right]$ (on y-axis) vs. t (on x-axis) can be plotted to give a straight line with gradient $K_L a$, as shown in Figure A2.

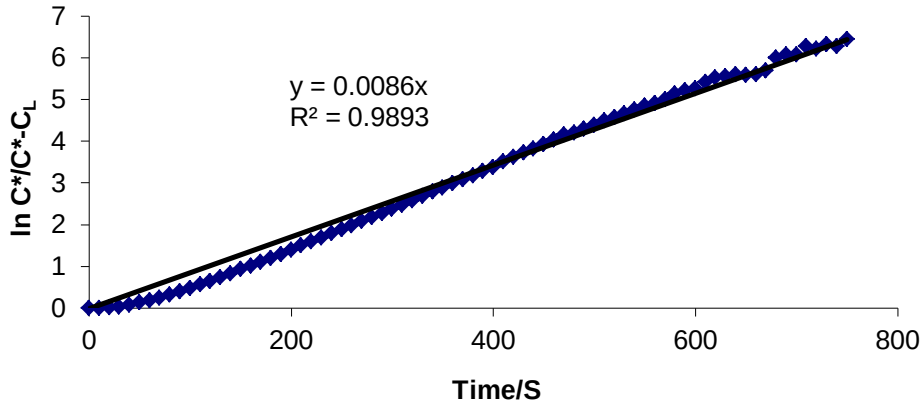

Figure A2: Graph to determine K_La

Figure A2 shows that the gradient is 00086, which shows that for this plot the value of K_La is 0.0086 s^{-1}.

A2 Calculation of Oxygen Transfer in the HBR

The equations and theory behind how oxygen transfer was calculated in the HBR have been presented in chapter 2, section 2.3.4.2. A sample calculation is shown below

For any set of conditions studied within the HBR, two D.O probes were utilised. One was placed upstream of the collector and one downstream. In order to ensure that the same D.O concentration was passed into the rotor, air was bubbled into the holding vessel for 10 minutes until saturation was achieved (7.1 ppm @ 35 ^oC). The values for the D.O concentration upstream and downstream of the rotor were noted and reported in Microsoft Excel as shown in table A2

Table A2: Screenshot from Microsoft Excel for HBR Transfer Calculations

Initial D.O (Calibrated)/ppb	Temperature/°C	Final D.O/ppb	Temp (Final D.O)/ °C
7100	35	1114	30.2
7100	35	1202	29.2
7100	35	1317	29.0
7100	35	1040	30.1
7100	35	1121	30.0
7100	35	1154	30.1
7100	35	997	29.6
7100	35	1087	30.2
7100	35	1113	30.1

The NTU and $K_L a$ values are then calculated via the equations presented in section 2.3.4.2 of chapter 2. As an example of the calculations, the top row in table A2 shows that at the end of the run, D.O concentration was 1114 ppb. The NTU and $K_L a$ values are therefore

$$NTU = ln\frac{C_i}{C_o} = ln\frac{7100}{1114} = 1.85$$

$$K_l a = \frac{NTU.L}{\rho_l \pi (R_0^2 - R_i^2)} = \frac{1.85 * 6.65 * 10^{-3}}{998 * 3.142(0.14^2 - 0.1^2)} = 0.001763\ s^{-1}$$

A3 $K_L a$ Measurement by the Dynamic Gassing Out Method

For the fermentation experiments performed in the BioFlow III with *E.coli* K12, the $K_L a$, OUR and OTR of the system was calculated by the dynamic gassing out method (for theory see Chapter 2, section 2.2.3).

The dynamic aspect of the method is that the respiration rate of the culture is used to calculate the oxygen transfer of the system. The air supply to the fermenter is shut off for a period of time. For the experiments in the current study, this was either for 10 minutes or until the D.O concentration reached 30 % (whichever was sooner). After this period, the air supply was switched back on at the same rate before the supply was cut. A typical D.O concentration profile for this period is shown in figure A3.

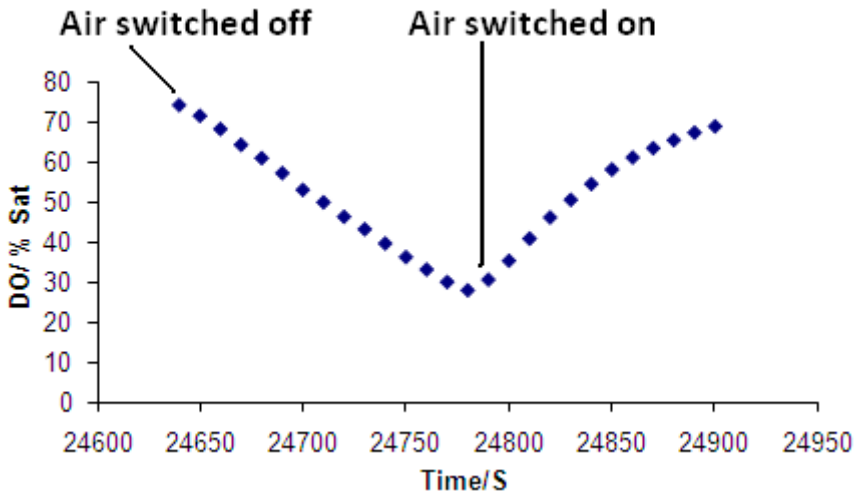

Figure A3: DO concentration profile during determination of K_La

In order to calculate the OUR of the culture, the first half of figure A3 is plotted separately. A linear trend line is then placed on the data, and the equation reveals the gradient which is the OUR for that experiment (shown figure A4)

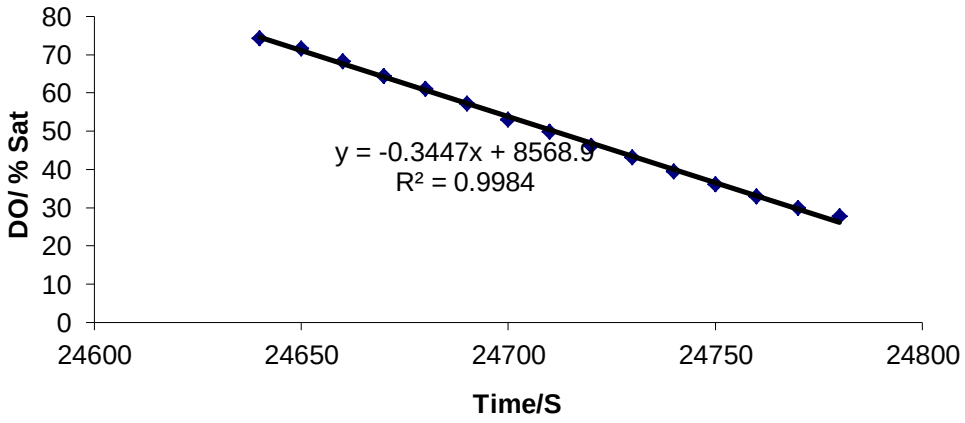

Figure A4: Calculation of OUR

Once the OUR has been determined, the second half of figure A3 is plotted as this aids in calculating the value of K_La (shown figure A5)

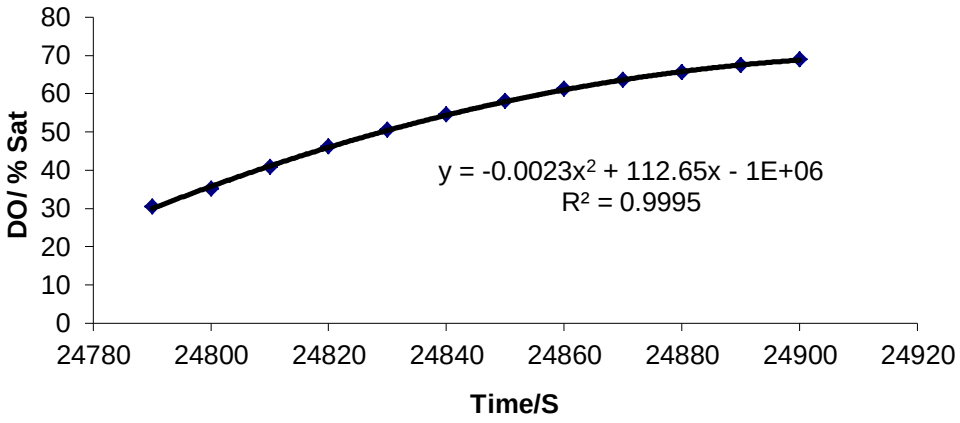

Figure A5: D.O concentration after air supply switched back on

The two values shown in figures A4 and A5 are used to calculate $K_L a$. A plot of D.O against d(DO)/dt + OUR produces a graph with the gradient $-1/K_L a$, from which $K_L a$ can be estimated (figure A6)

Time/s	DO (%)	d(DO)/dt	d(DO)/dt+OUR
24790	30.42	-1.384	-1.0393
24800	35.2	-1.43	-1.0853
24810	40.77	-1.476	-1.1313
24820	46.08	-1.522	-1.1773
24830	50.51	-1.568	-1.2233
24840	54.48	-1.614	-1.2693
24850	58.12	-1.66	-1.3153
24860	61.14	-1.706	-1.3613
24870	63.49	-1.752	-1.4073
24880	65.5	-1.798	-1.4533
24890	67.38	-1.844	-1.4993
24900	68.96	-1.89	-1.5453

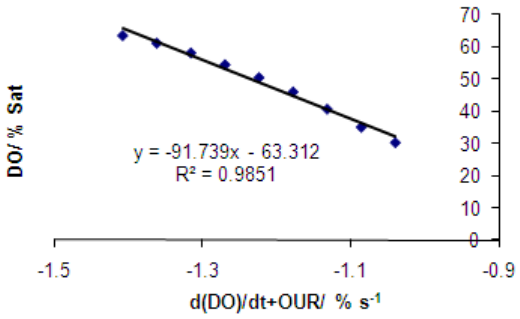

1/kla	91.739	s
kla	0.0109	s^{-1}

Figure A6: Calculation of $K_L a$ for the Dynamic Gassing Out Method

As well as OUR and $K_L a$, the OTR of the system can be calculated also, shown equation A1. dC_L/dt in equation A1 is the OTR, so the OTR for the above example can be calculated as follows:

$$OTR = K_L a(C^* - C_L)$$ (From equation A1)

In the example above, the K_La value is given by figure A6 (0.0109 s^{-1}). C* is the value at the start of the experiment (74.33 % sat), and C_L is final value taken before the air supply was switched back on (27.77 % sat). The OTR can therefore be calculated as

$$OTR = 0.0109(74.33 - 27.77)$$

$$OTR = 0.5075\ \%\ s^{-1}$$

If the fermentation is not to be limited by oxygen transfer then the OTR needs to be at least equal to if not greater than the OUR. In this example the OTR of 0.5075 % s^{-1} is greater than the OUR of 0.3447 % s^{-1}, showing this system is not limited by oxygen transfer.

A3 Calculation of Bubble Diameter using Image J

In sections 4.2 (for the STR) and 4.3.2 (for the HBR) bubble diameters were determined with use of the software Image J. An example (shown for the HBR) below shows how the bubble diameter was arrived at.

The HBR images were taken with a Phantom Miro 4 high speed digital camera on loan from the EPSRC instrument pool. A typical image from the camera is shown in figure A7.

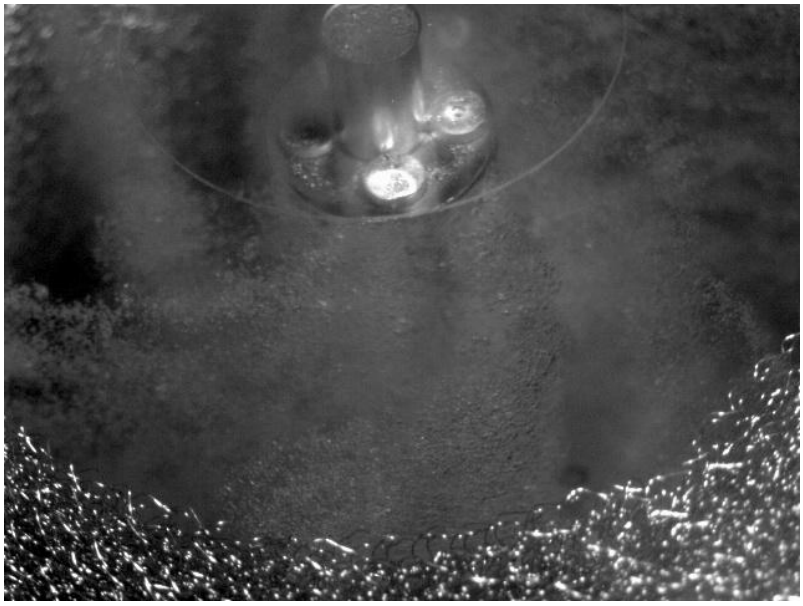

Figure A7: Digital image taken with the Phantom Miro 4 High Speed Digital Camera (picture taken at 1200 rpm, 0.6 l/min liquid flow rate and 15.576 l/min gas flow rate)

Once an image had been opened for analysis, the scale was then set in ImageJ. This was determined by the number of pixels between two points of known distance which was present on every photograph taken. For the HBR this was the top of one of the liquid injectors which

is known to have a diameter of 1 mm. Using ImageJ the coordinates of point 1 and 2 were used to set the scale-shown figure A8.

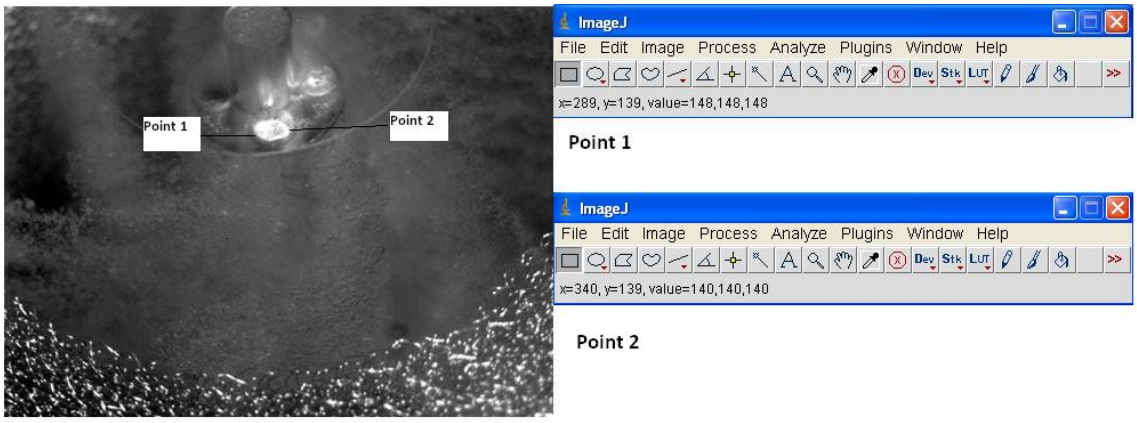

Figure A8: Scale setting in ImageJ

From figure A8, the two x values (340 and 289) reveal the number of pixels per mm-in this instance 340-289 = 51 pixels mm^{-1}. A similar scale system was used for the STR pictures except that the scale was pixels cm^{-1}. This value was then input into ImageJ to set the scale.

Bubble size then was analysed using the elliptical section in ImageJ for 30 random bubbles. The images were then put into Microsoft excel for analysis as shown in Table A3.

Table A3: Partial Screenshot of Excel data

Bubble Number	Observed Bubble area/mm²	Calculated Bubble Diameter/mm	Circularity
1	2.254	1.694	1.000
2	1.646	1.448	0.970
3	1.254	1.264	1.000
4	1.744	1.490	0.998
5	2.038	1.611	1.000
6	1.411	1.340	1.000
7	1.568	1.413	1.000
8	2.038	1.611	1.000
9	1.686	1.465	0.993
10	1.686	1.465	0.993
11	1.999	1.595	0.982
12	2.038	1.611	1.000
13	1.999	1.595	0.982
14	2.195	1.672	0.990
15	1.901	1.556	1.000
16	2.43	1.759	1.000
17	2.43	1.759	1.000
18	2.685	1.849	1.000
19	1.568	1.413	1.000
20	2.038	1.611	1.000
21	2.038	1.611	1.000
22	2.195	1.672	0.990
23	2.254	1.694	1.000
24	2.195	1.672	0.990
25	2.666	1.842	1.000
26	1.901	1.556	1.000
27	2.862	1.909	1.000
28	2.195	1.672	0.990
29	1.686	1.465	0.993
30	2.038	1.611	1.000

The mean bubble diameters for each experiment are then used to plot the graphs shown in chapter 4 (sections 4.2 and 4.3.2).

Appendix B: Hydrodynamic Measurements

The aim of Appendix B is to note some of the hydrodynamic characteristics of the impellers examined and the fluids used for the study. This is useful to relate the viscosity and surface tension of the fluid to the size of the bubble diameter noticed with each impeller (from Chapter 4). This is especially important when coming to investigate the effect of the addition of the antifoam DF204 to the fermentation medium

B1 Impeller Calculations

Tables B1 and B2 show some of the calculations performed for the impeller systems used in the experiments in the STR and RPB

Table B1: STR physical calculations

	6 cm Impellers	11 cm Impellers
Re_m (200 rpm-Water)	1791.27	3283.99
Re_m (500 rpm-Water)	4479.02	8211.54
Re_m (800 rpm-Water)	7166.78	13139.10
Re_m (1000 rpm-Water)	8958.05	16423.09
Re_m (200 rpm-50 % Water-50 % Glycerol)	295.52	541.79
Re_m (200 rpm-50 % Water-50 % Glycerol)	738.94	1354.73
Re_m (200 rpm-50 % Water-50 % Glycerol)	1182.37	2167.67
We_m (200 rpm-Water)	1196.49	7372.84
We_m (500 rpm-Water)	7480.95	46097.86
We_m (800 rpm-Water)	19153.05	118021.80
We_m (1000 rpm-Water)	29923.78	184391.45
We_m (200 rpm-50 % Water-50 % Glycerol)	15557.89	95868.31
We_m (200 rpm-50 % Water-50 % Glycerol)	97273.99	599405.90
We_m (200 rpm-50 % Water-50 % Glycerol)	249045.18	1534625.64

Table B2: RPB physical calculations

	RPB
Re_m (200 rpm-Water)	72844.88
Re_m (400 rpm-Water)	145689.75
Re_m (800 rpm-Water)	182146.98
Re_m (1000 rpm-Water)	364293.95
Re_m (1200 rpm-Water)	437173.61
We_m (200 rpm-Water)	80468570.02
We_m (400 rpm-Water)	321874280.08
We_m (800 rpm-Water)	503120721.79
We_m (1000 rpm-Water)	2012482887.16
We_m (1200 rpm-Water)	2898252099.73

B2 Fluid Calculations

Table B3 notes the different viscosities and surface tensions measured with the different fluids used in the current study

Table B3: Physical measurements of the fluids

Fluid	Viscosity @ 35 oC/mNs m^{-2}	Surface Tension/N m^{-1}
Deionised Water	0.4	0.07900
Water-Glycerol (50 % Mixture by Volume)	4.7	0.06673
SMS Medium	1.0	0.07788
SMS Medium + DF204	6.2	0.02899
M63 Medium	1.4	0.06987
M63 Medium + DF204	6.9	0.02502

Appendix C: Additional Transfer Characterisation and Bubble Study Data

The aim of Appendix D is to present tables of figures behind the transfer and bubble study for the impellers studied, and to present some additional data not included in Chapter 5. The results in this appendix look at the transfer capability and bubble study conducted with the BioFlo III reactor. For a full discussion of these results please see sections 5.1 and 5.2 of Chapter 5

C1 Air/Water Transfer Results

Tables C1-C3 show the results presented for the air/water transfer results as noted in section 5.1.1 in Chapter 5 to illustrate the effects of agitation (rpm) and air flow rate (vvm)

Table C1: Transfer Values for the Rushton impeller for the Air/Water system

	200 rpm	**500 rpm**	**800 rpm**	**1000 rpm**
0.2 vvm	0.006	0.0232	0.0176	0.014
0.6 vvm	0.0086	0.0283	0.0337	0.0274
1.0 vvm	0.0099	0.0294	0.0385	0.0334

Table C2: Transfer Values for the 6 cm Knitted Wire Impeller for the Air/Water system

	200 rpm	**500 rpm**	**800 rpm**	**1000 rpm**
0.2 vvm	0.0026	0.0084	0.0162	0.0215
0.6 vvm	0.0039	0.0107	0.0185	0.0258
1.0 vvm	0.0054	0.0137	0.0213	0.0298

Table C3: Transfer Values for the 11 cm Knitted Wire Impeller for the Air/Water system

	200 rpm	**300 rpm**	**400 rpm**
0.2 vvm	0.0071	0.0141	0.0193
0.6 vvm	0.0104	0.0215	0.0295
1.0 vvm	0.014	0.0259	0.0312

Tables C1-C3 has shown above give rise to figures 5.2 and 5.4 in chapter 5. Figure 5.3 in chapter 5 which illustrates the effect of power consumption on the value of K_La is noted in table C4

Also noted in section 5.1.1 was that the trends presented for 1000 rpm (400 rpm for the 11 cm knitted wire impeller) and 1.0 vvm air flow rate. Figures 51a and b present another set of results for the 3 impellers at a fixed air flow rate of 0.2 vvm (C1a) and a fixed agitation rate of 200 rpm (C1b)

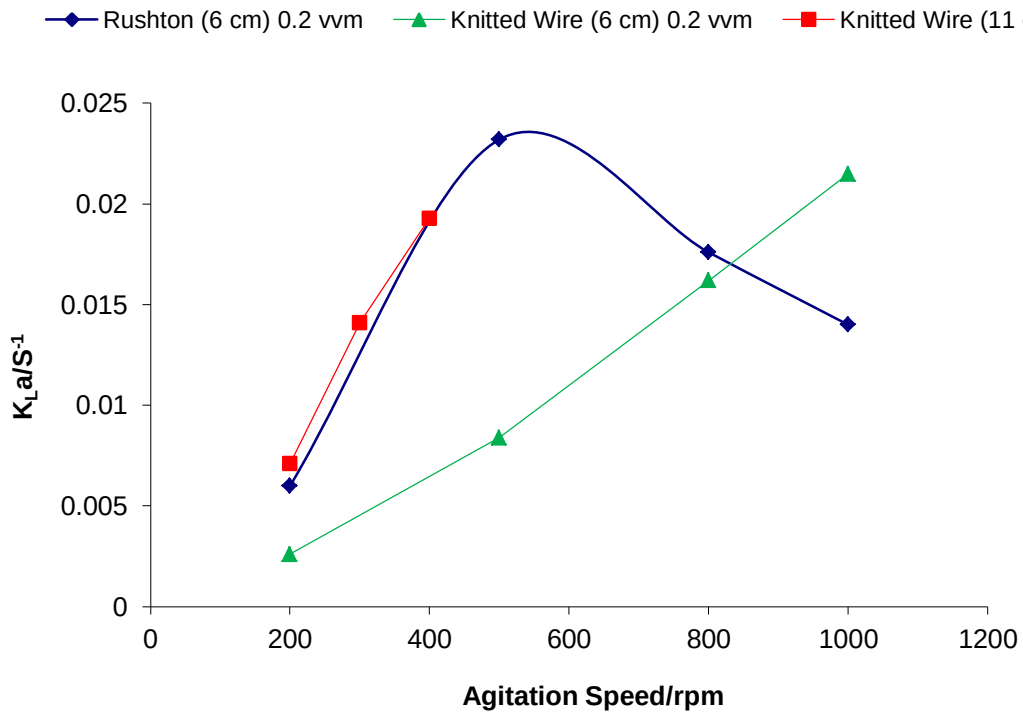

Figure C1a: The effect of agitation on K_La results in the Air/Water system

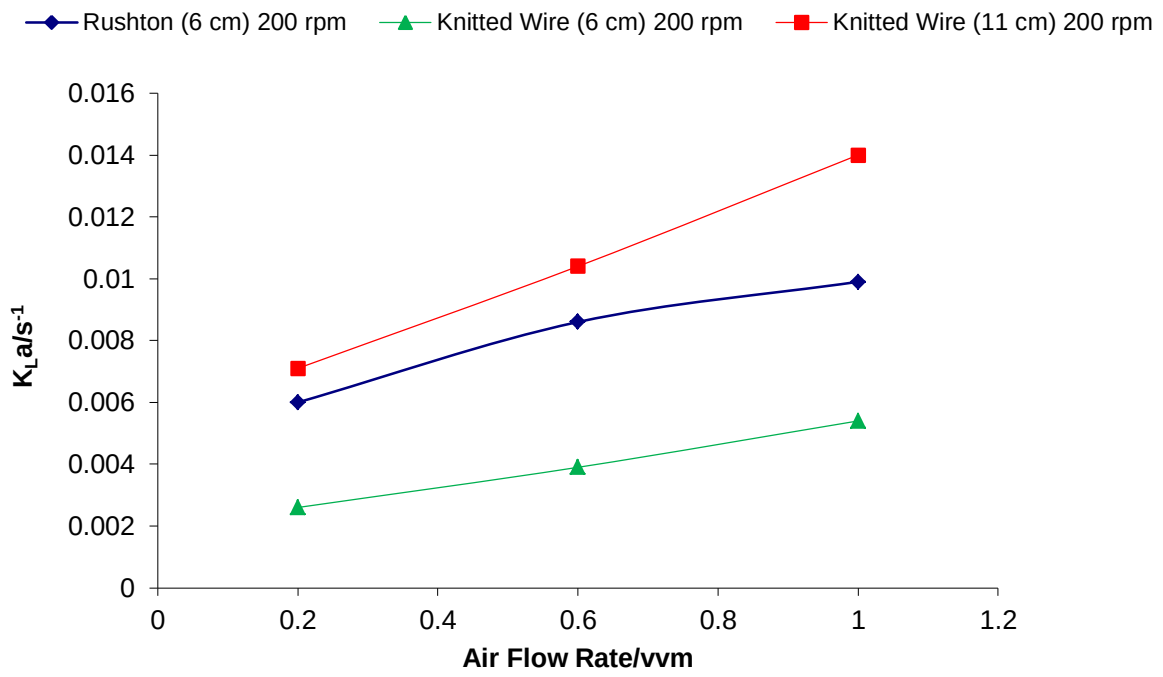

Figure C1b: The effect of air flow rate on K_La results in the Air/Water system

Figures C1 a and b show similar trends to those figures presented in section 5.1.1 in chapter 4, albeit with lower K_La values reflecting the lower agitation and air flow rates plotted. Figure C1b does not show as much crossover in the data as the 1.0 vvm data in figure 5.4. It does show the rough trend that the 11 cm knitted wire impeller produces the highest K_La values and outperforms the Rushton impeller in the lower agitation regions when agitation rate is investigated.

C2 Air/Water-Glycerol Transfer Results

Section 4.1.2 noted the effect of viscosity on the value of K_La observed. Tables C7-C9 show the values recorded that were used to plot figure 5.7

Table C7: Transfer Values for the Rushton impeller for the Air/50 %Water-50 % Glycerol system

	200 rpm	**500 rpm**	**800 rpm**
0.2 vvm	0.0019	0.0111	0.0115
0.6 vvm	0.0024	0.0128	0.0158
1.0 vvm	0.0033	0.0135	0.0195

Table C8: Transfer Values for the 6 cm Knitted Wire impeller for the Air/50 %Water-50 % Glycerol system

	200 rpm	**500 rpm**	**800 rpm**
0.2 vvm	0.0009	0.0031	0.0082
0.6 vvm	0.0014	0.004	0.0085
1.0 vvm	0.0022	0.0043	0.0095

Table C9: Transfer Values for the 11 cm Knitted Wire impeller for the Air/50 %Water-50 % Glycerol system

	200 rpm	**300 rpm**	**400 rpm**
0.2 vvm	0.0034	0.007	0.0107
0.6 vvm	0.0045	0.0077	0.0138
1.0 vvm	0.0052	0.0104	0.0149

As with the Air/Water results presented, the trends noted in section 5.1.2 have been noted with other agitation and air flow rates. These are noted in figures C2a (fixed air flow rate of 0.2 vvm), C2b (fixed agitation rate of 200 rpm), C2c (comparing a 0.2 vvm run for both the water and 50 % water-50 % glycerol systems

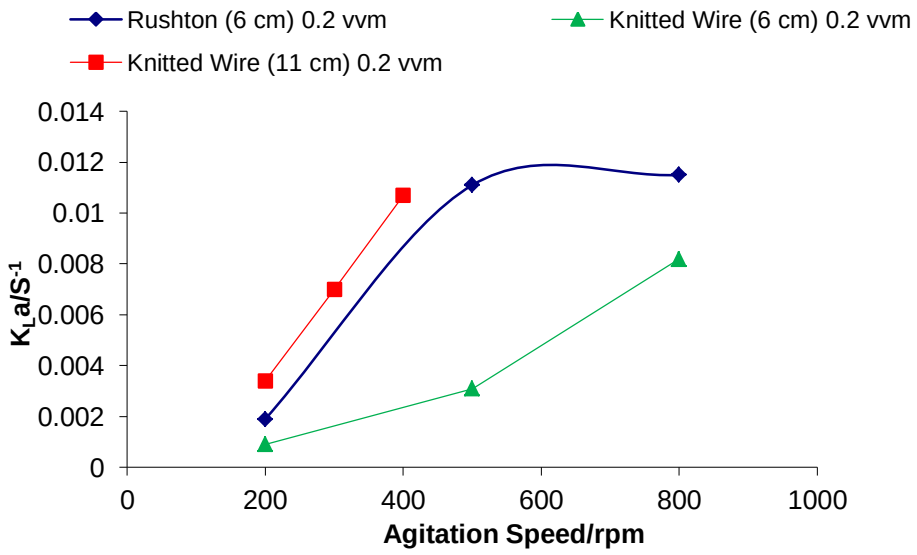

Figure C2a: The effect of agitation speed on K_La results for the 50 % Water-50 % Glycerol system

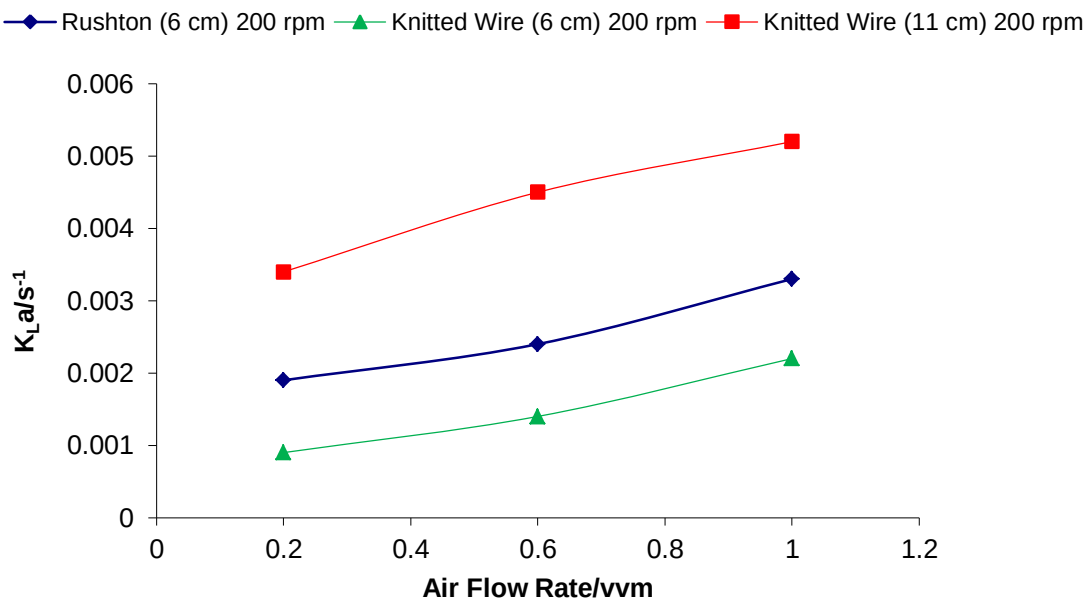

Figure C2b: The effect of air flow rate on K_La results for the 50 % Water-50 % Glycerol system

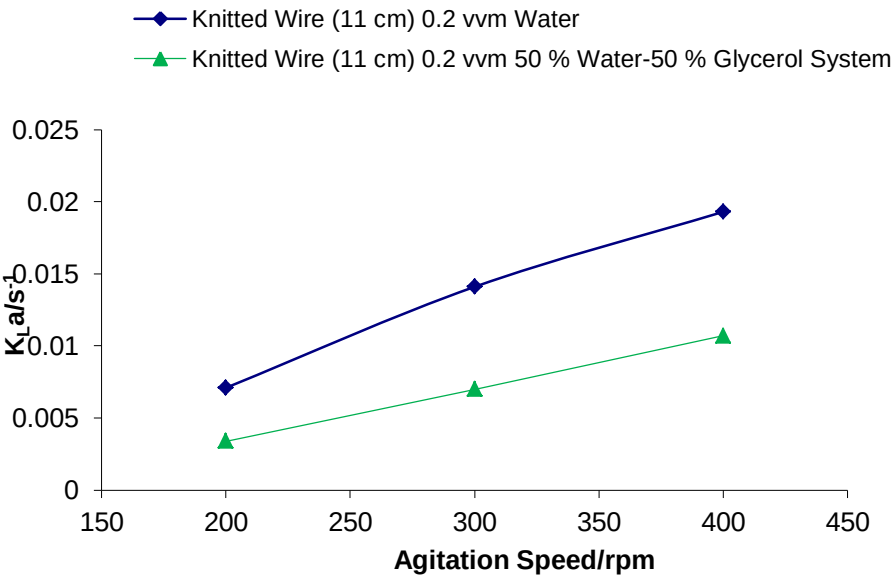

Figure C2c: The effect of viscosity on K_La results for the 11 cm knitted wire mesh impeller (fixed air flow rate of 0.2 vvm, water-glycerol mixture is 50 % of each component by volume).

C3 Air/Water Bubble Results

Section 5.2.1 noted the bubble size produced by each impeller within the air/water system. Tables C10-C12

Table C10: Mean Bubble Size for the Rushton impeller in the Air/Water system

Agitation Rate/rpm	Airflow Rate/vvm	Bubble Size/cm
200	0.2	0.469
200	0.6	0.457
200	1	0.442
500	0.2	0.429
500	0.6	0.413
500	1	0.394
800	0.2	0.340
800	0.6	0.310
800	1	0.286
1000	0.2	0.319
1000	0.6	0.298
1000	1	0.280

Table C11: Mean Bubble Size for the 6 cm Knitted Wire mesh impeller in the Air/Water system

Agitation Rate/rpm	Airflow Rate/vvm	Bubble Size/cm
200	0.2	0.417
200	0.6	0.404
200	1	0.369
500	0.2	0.387
500	0.6	0.373
500	1	0.341
1000	0.2	0.300
1000	0.6	0.269
1000	1	0.248

Table C12: Mean Bubble Size for the 11 cm Knitted Wire mesh impeller in the Air/Water system

Agitation Rate/rpm	Airflow Rate/vvm	Bubble Size/cm
200	0.2	0.283
200	0.6	0.261
200	1	0.241
300	0.2	0.242

300	0.6	0.222
300	1	0.199
400	0.2	0.223
400	0.6	0.178
400	1	0.147

Section 5.2.1 also noted that the trends presented in the main section of chapter also had occurred at other agitation and air flow rates. Figures C3a and b show the mean bubble diameter at 0.2 vvm (C3a) and 500 rpm (C3b)

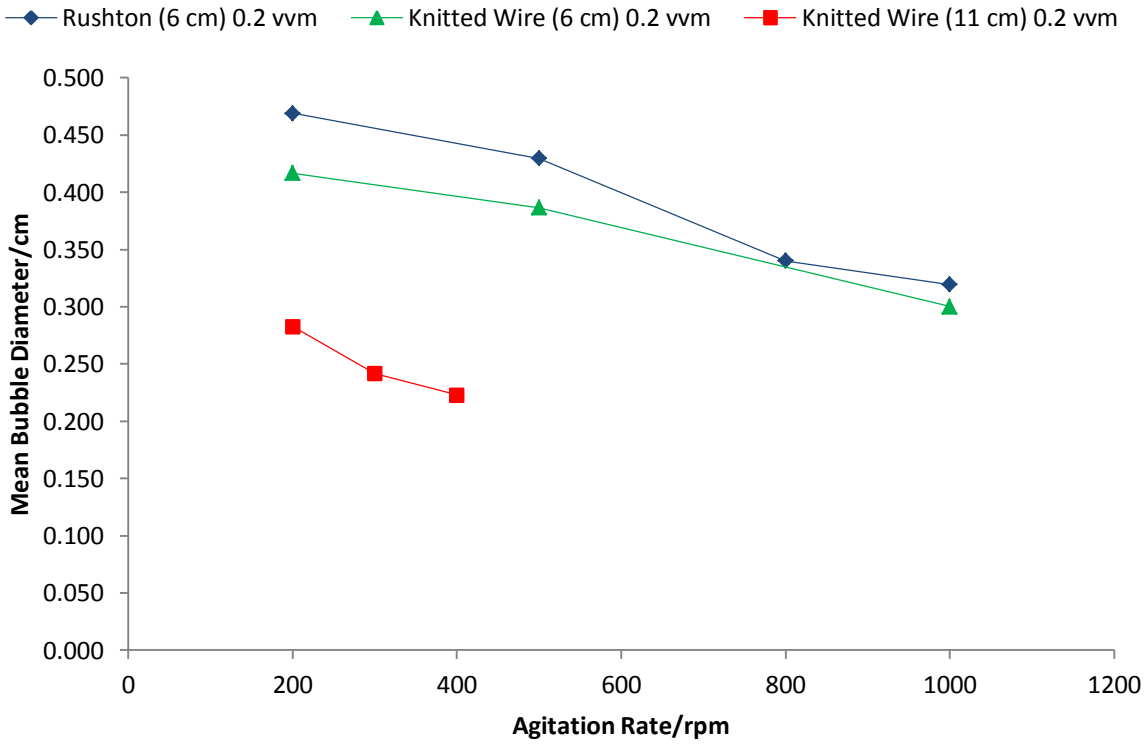

Figure C3a: The effect of agitation rate on Mean Bubble diameter for the Air/Water system

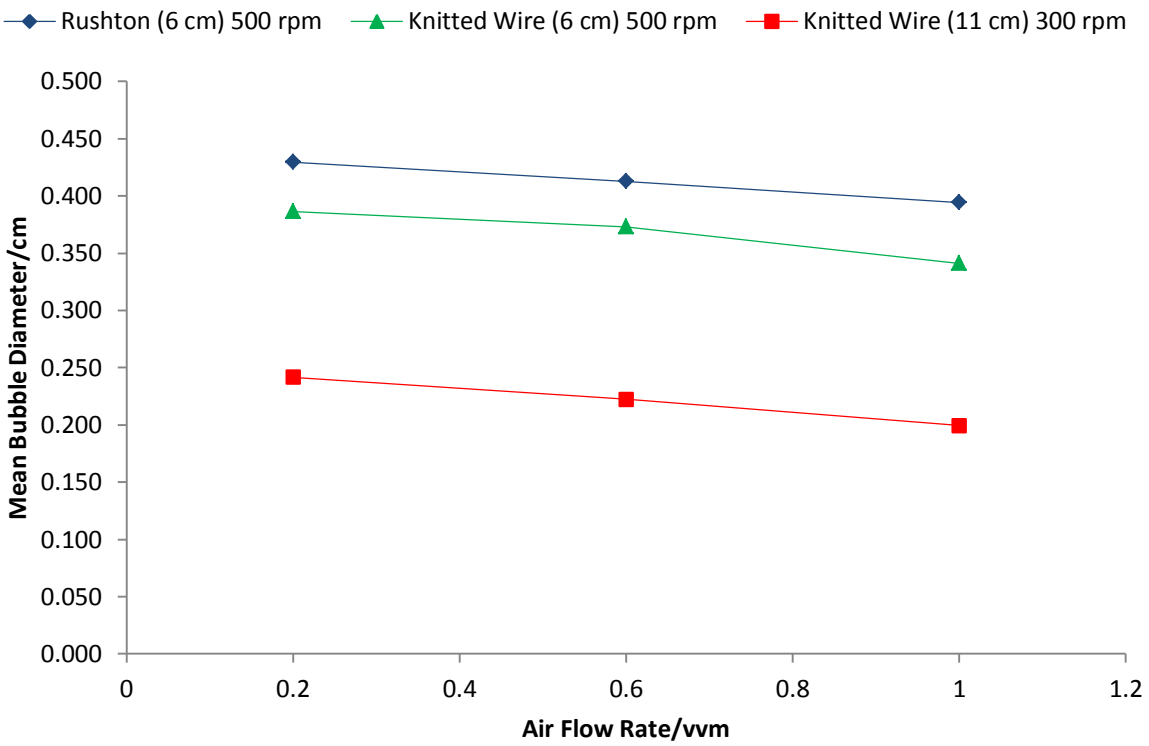

Figure C3b: The effect of air flow rate on Mean Bubble diameter for the Air/Water system

Similar trends are noted in figures C3a and b compared to figures 5.12 and 5.13 in Chapter 5 indicating that the same phenomena is present at the different agitation/air flow rates examined. The comparison to the 11 cm knitted wire impeller is not as robust due to the difference in agitation rates.

C4 Air/Water-Glycerol Bubble Results

As for the transfer results, a bubble study was conducted with the mixed water-glycerol system (50 % of each component by volume). Tables C13-C15 show the results used to generate figures 5.14a and 5.15a

Table C13: Mean Bubble Size for the Rushton impeller in the Air/50 %Water-50 % Glycerol system

Agitation Rate/rpm	Airflow Rate/vvm	Bubble Size/cm
200	0.2	0.333
200	0.6	0.312
200	1	0.258
500	0.2	0.257
500	0.6	0.247
500	1	0.227
800	0.2	0.240
800	0.6	0.224
800	1	0.181

Table C14: Mean Bubble Size for the 6 cm Knitted Wire impeller in the Air/50 %Water-50 % Glycerol system

Agitation Rate/rpm	Airflow Rate/vvm	Bubble Size/cm
200	0.2	0.242
200	0.6	0.224
200	1	0.177
500	0.2	0.217
500	0.6	0.201
500	1	0.167
800	0.2	0.173
800	0.6	0.159
800	1	0.151

Table C15: Mean Bubble Size for the 11 cm Knitted Wire impeller in the Air/50 %Water-50 % Glycerol system

Agitation Rate/rpm	Airflow Rate/vvm	Bubble Size/cm
200	0.2	0.232
200	0.6	0.212
200	1	0.178
300	0.2	0.208
300	0.6	0.177
300	1	0.152
400	0.2	0.148
400	0.6	0.133
400	1	0.104

Section 5.2.2 identified that as agitation rate and air flow rate were increased the mean bubble diameter was seen to decrease. Figures C4a-c note this trend for another air flow rate (0.2 vvm-C4a), agitation rate (500 rpm-C4b) and the effect of viscosity on the 11 cm knitted wire impeller (fixed air flow rate of 0.2 vvm-C4c)

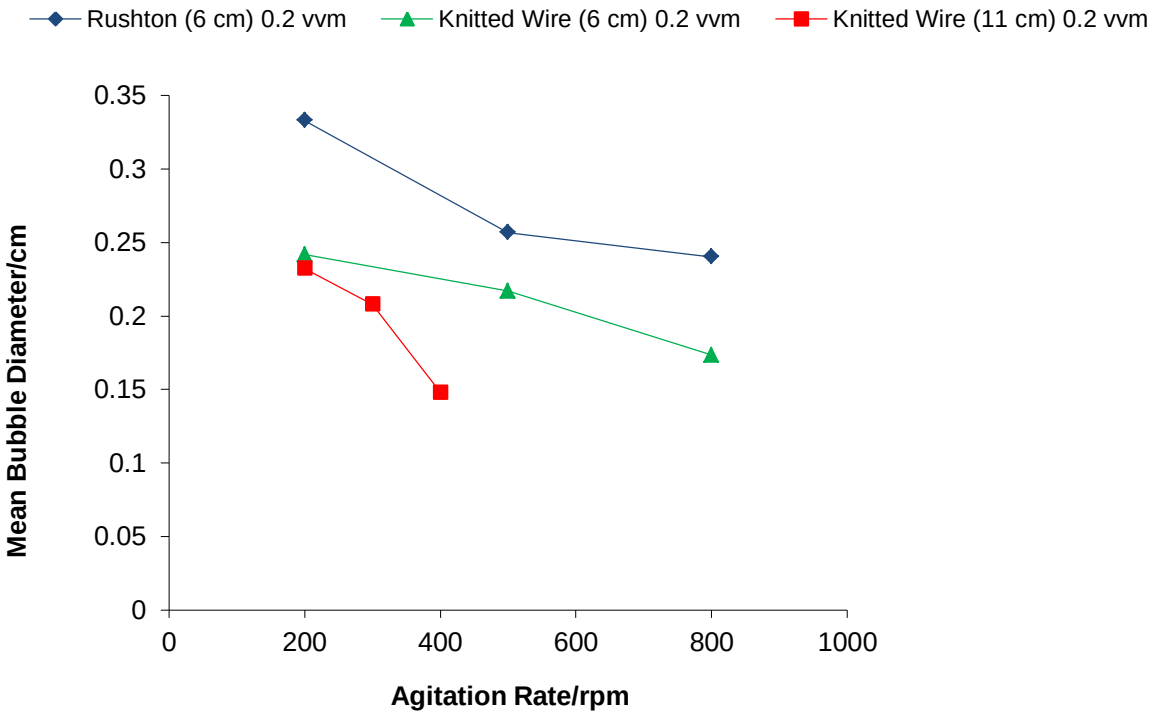

C4a: The effect of agitation rate on Mean Bubble diameter for the Air/50 % Water-50 % Glycerol system

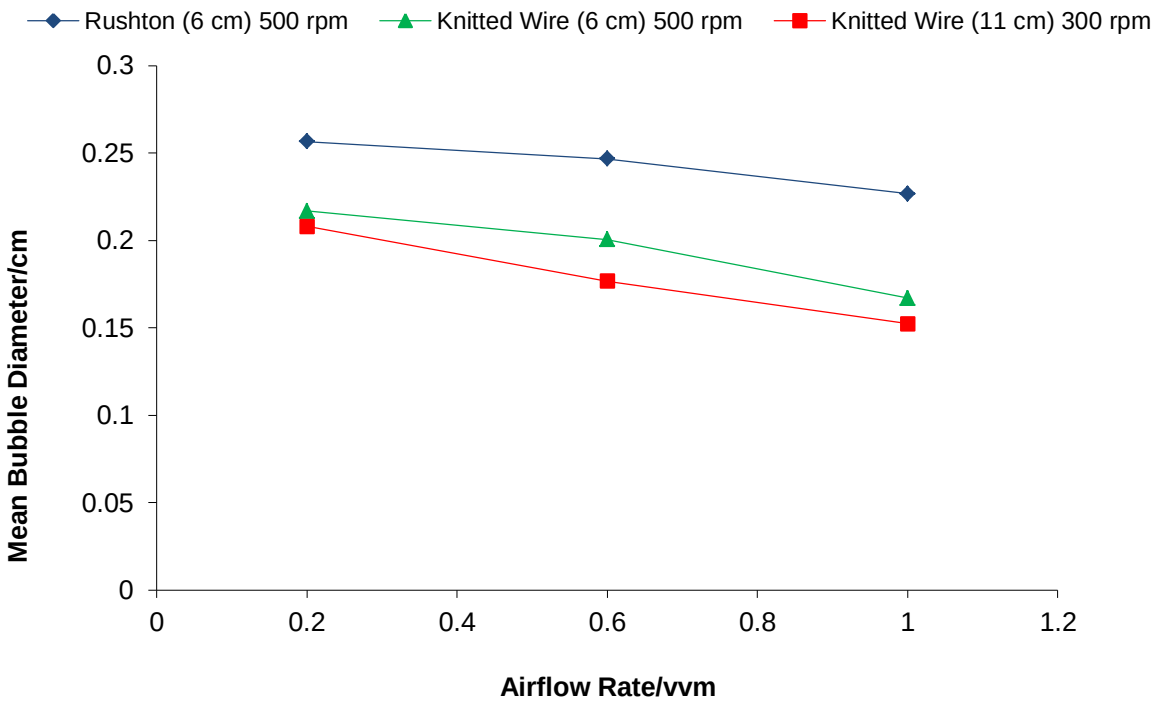

Figure C4b: The effect of air flow rate on Mean Bubble diameter for the Air/50 % Water- 50 % Glycerol system

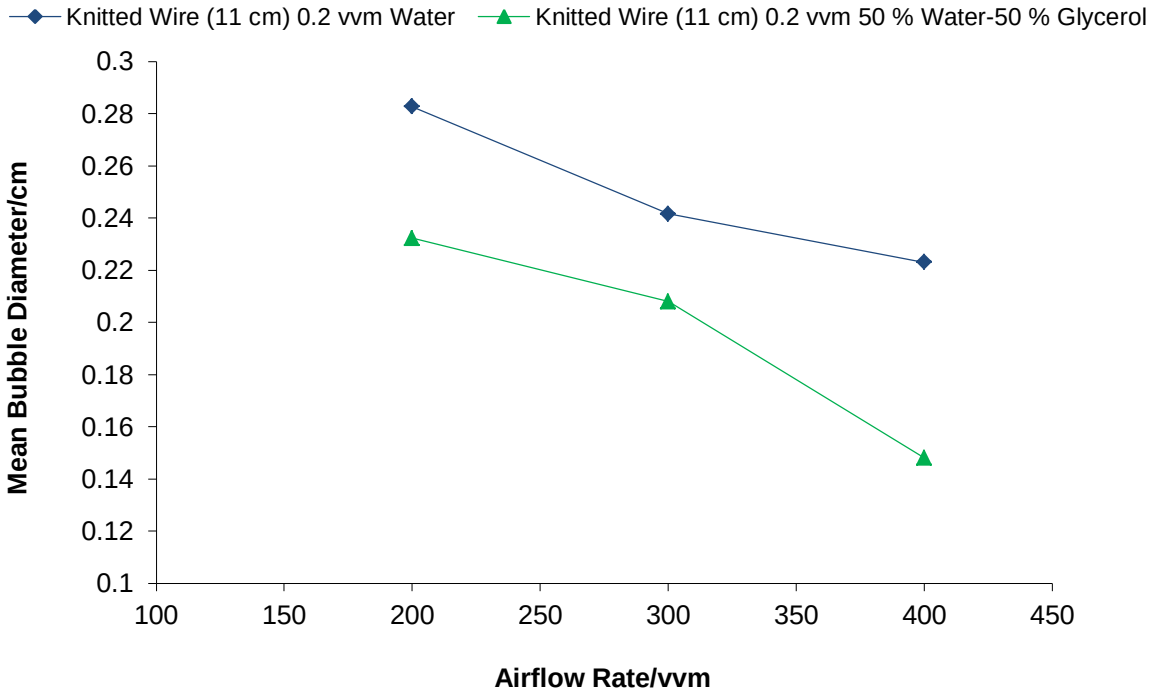

Figure C4c: The effect of viscosity on Mean Bubble diameter for the 11 cm knitted wire impeller (fixed air flow rate of 0.2 vvm, water-glycerol mixture is 50 % by volume of each component).

As with the air/water bubble study the same trends presented here are roughly present in the main results in section 4.2.2. Again the comparison is not as robust due to the difference in agitation rates between the 6 and 11 cm impellers.

C5 SMS Medium Bubble Results

In section 5.2.3 the mean bubble diameter of the SMS medium system was investigated with the Rushton and knitted wire impellers only. This occurred with and without the addition of the antifoam DF204. Tables C16-C18 (without antifoam) and tables C19-C21 (with antifoam) show these results used to produce figures 5.16 and 5.17 in section 4.2.3 of Chapter 4

Table C16: Mean Bubble Size for the 6 cm Rushton impeller in the SMS medium system without antifoam

	0.2 vvm	0.6 vvm	1.0 vvm
200 rpm	0.367	0.334	0.313
300 rpm	0.345	0.321	0.309
400 rpm	0.333	0.312	0.301

Table C17: Mean Bubble Size for the 6 cm Knitted Wire impeller in the in the SMS medium system without antifoam

	0.2 vvm	0.6 vvm	1.0 vvm
200 rpm	0.311	0.295	0.267
300 rpm	0.301	0.286	0.259
400 rpm	0.286	0.267	0.254

Table C18: Mean Bubble Size for the 11 cm Knitted Wire impeller in the in the SMS medium system without antifoam

	0.2	0.6	1
200	0.288	0.263	0.249
300	0.266	0.253	0.232
400	0.244	0.229	0.217

Table C19: Mean Bubble Size for the 6 cm Rushton impeller in the SMS medium system with antifoam

	0.2	0.6	1
200	0.209	0.195	0.188
300	0.199	0.178	0.165
400	0.188	0.165	0.144

Table C20: Mean Bubble Size for the 6 cm Knitted Wire impeller in the in the SMS medium system with antifoam

	0.2	0.6	1
200	0.188	0.176	0.167
300	0.165	0.156	0.144
400	0.159	0.144	0.122

Table C21: Mean Bubble Size for the 11 cm Knitted Wire impeller in the in the SMS medium system with antifoam

	0.2	0.6	1
200	0.162	0.145	0.137
300	0.148	0.132	0.113
400	0.136	0.113	0.107

Appendix D: Additional Fermentation Data

The aim of Appendix D is to present tables of figures behind the *E.coli* and *P.putida* studies, and to present some additional data not included in Chapter 6. The results in this appendix look at the batch *E.coli*, batch *P.putida*, and fed-batch *P.putida* fermentation systems conducted with the BioFlo III reactor. For a full discussion of these results please see sections 6.2, 6.3, and 6.4 of Chapter 6

D1 *E.coli* K12 Batch Fermentation Experiments

Section 6.2.2 presented the biomass concentration analysis for the *E.coli* K12 fermentation runs. The data used for figures 6.2a-c are presented in Tables D1-D3, and figures 6.3a and b are presented in Table D4

Table D1: OD values for the Rushton impeller at 400 rpm/1.5 vvm

Time/Hours	OD @ 600 nm	Mean TVC/CFU	DCW/ g l^{-1}
0	0.0418	n/a	n/a
1	0.101	2.10E+06	0.1
2	0.307	6.50E+06	0.1
3	0.574	2.50E+07	0.2
4	1.734	6.80E+07	0.5
5	3.065	9.60E+07	1
6	4.424	6.50E+08	1.4
7	6.21	9.50E+08	2
8	6.765	3.80E+09	2.2

Table D2: OD values for the 6 cm Knitted Wire impeller at 400 rpm/1.5 vvm

Time/Hours	OD @ 600 nm	Mean TVC/CFU	DCW/ g l^{-1}
0	0.0419	n/a	n/a
1	0.164	8.70E+06	0.1
2	0.355	1.10E+07	0.2
3	1.575	4.10E+07	0.5
4	2.72	8.20E+07	0.8
5	4.734	2.50E+08	1.5
6	6.136	9.80E+08	2
7	7.168	3.50E+09	2.3
8	7.308	6.70E+09	2.4

Table D3: OD values for the 11 cm Knitted Wire impeller at 400 rpm/1.5 vvm

Time/Hours	OD @ 600 nm	Mean TVC/CFU	DCW/ g l^{-1}
0	0.042	n/a	n/a
1	0.199	9.20E+06	0.1
2	0.574	1.21E+08	0.2
3	2.5	2.30E+08	0.8
4	4.59	7.00E+08	1.5
5	6.838	9.80E+08	2.3
6	8.666	4.50E+09	2.9
7	8.722	8.80E+09	2.9
8	8.75	9.50E+09	2.9

Table D4: The effect of agitation on OD values for the 11 cm Knitted Wire Impeller

Time/Hours	OD for 200 rpm/1.5 vvm	OD for 300 rpm/1.5 vvm	OD for 400 rpm/1.5 vvm
0	0.0411	0.0415	0.042
1	0.111	0.129	0.199
2	0.389	0.426	0.574
3	1.042	1.266	2.5
4	1.776	2.34	4.59
5	2.862	3.654	6.838
6	3.912	4.878	8.666
7	5.103	5.88	8.722
8	5.852	7.044	8.75

Table D5: The effect of agitation on OD values for the 11 cm Knitted Wire Impeller

Time/Hours	OD for 400 rpm /1.0 vvm	OD for 400 rpm /1.25 vvm	OD for 400 rpm /1.5 vvm
0	0.0421	0.0422	0.042
1	0.141	0.144	0.199
2	0.444	0.404	0.574
3	1.398	1.866	2.5
4	2.488	2.925	4.59
5	4.151	4.382	6.838
6	5.148	5.607	8.666
7	6.252	7.462	8.722
8	7.202	7.943	8.75

The effect of agitation and air flow rate have been noted at other values and these are shown in figures D1a (for a fixed air flow rate of 1.0 vvm) and D1b (for a fixed agitation rate of 200 rpm)

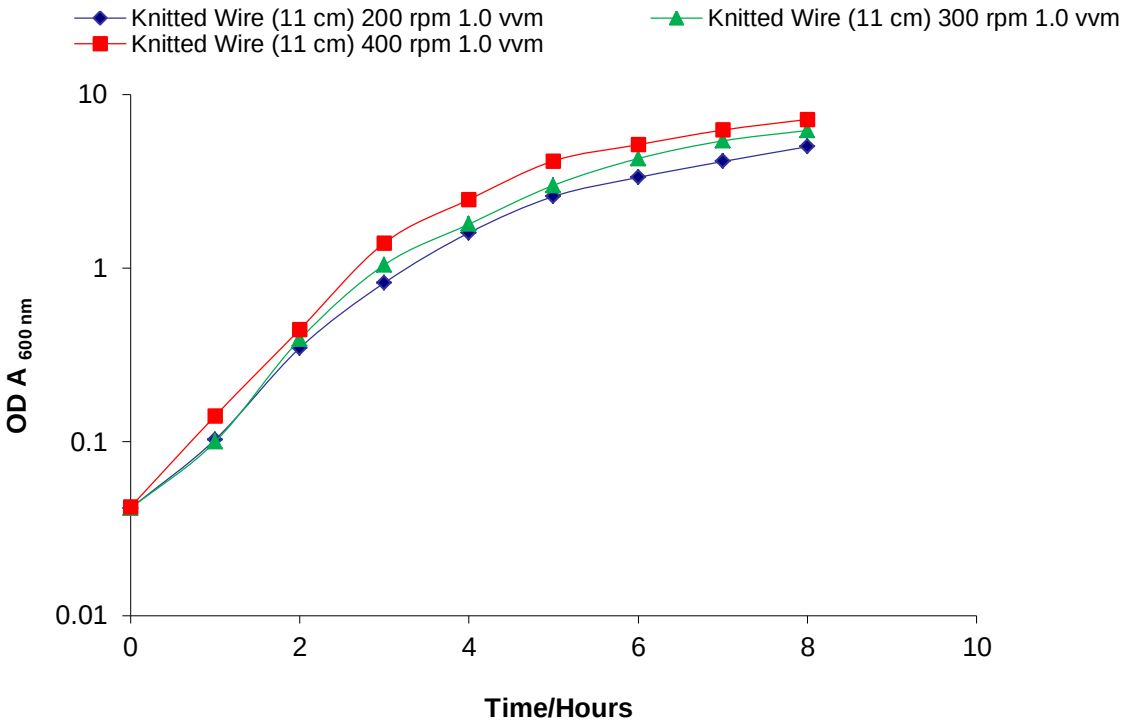

Figure D1a: The effect of agitation rate on OD values for the BioFlo 11 cm Knitted Wire Impeller

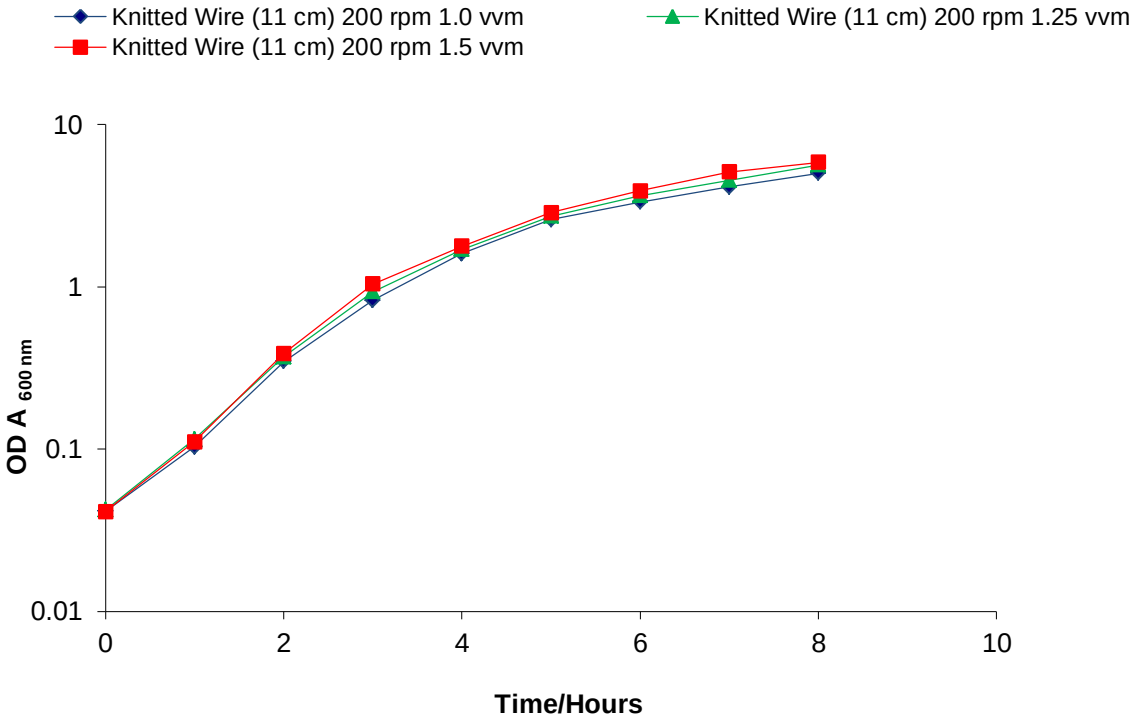

Figure D1b: The effect of airflow rate on OD values for the BioFlo 11 cm Knitted Wire Impeller

The trends noted here are also present in the figures presented in Chapter 6; however these values are smaller reflecting the lower agitation and airflow rates employed.

Section 6.2.3 examined the OUR of each impeller, table E6 notes the results presented in figure 6.4

Table D6: OUR values for all impellers at 400 rpm/1.5 vvm

	OUR Hour 2/% s^{-1}	OUR Hour 4/% s^{-1}	OUR Hour 6/% s^{-1}
Rushton (6 cm)	0.0126	0.2101	
Knitted Wire (6 cm)	0.019	0.2116	
Knitted Wire (11 cm)	0.0608	0.2301	0.3447

Similar trends occur at other agitation and air flow rates which are noted in figure D2a (fixed air flow rate of 1.0 vvm) and D2b (fixed agitation rate of 200 rpm) for the 11 cm knitted wire mesh impeller

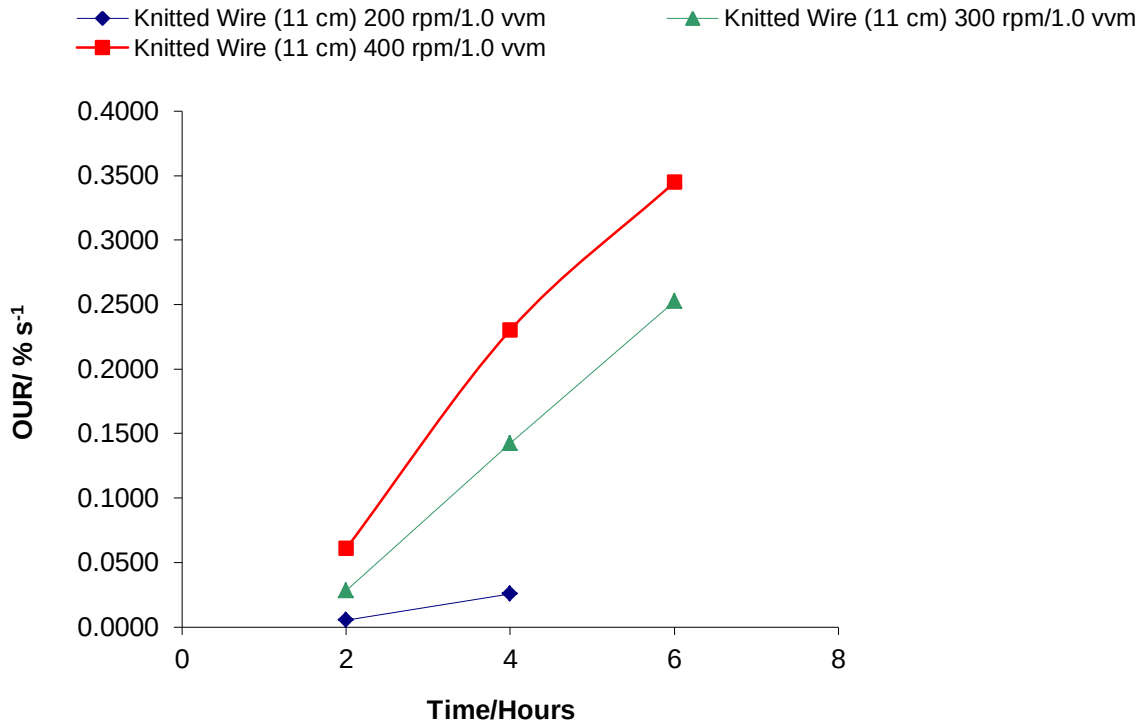

Figure D2a: Effect of agitation rate on OUR values for the 11 cm knitted wire mesh impeller

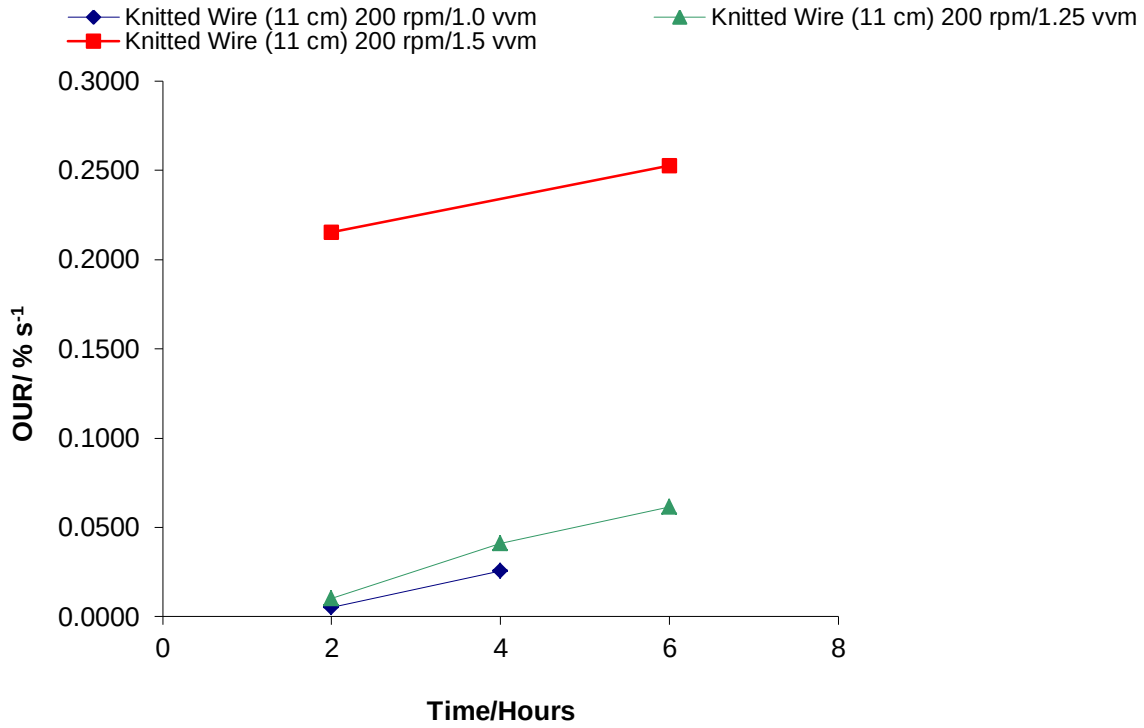

Figure D2b: Effect of air flow rate on OUR values for the 11 cm knitted wire mesh impeller

Similar trends can be seen with the 11 cm knitted wire impeller that a higher agitation and air flow rate produce a higher OUR value. As the age of the fermentation cycle increases, due to the increase in mean TVC noticed, the OUR value is seen to rise as the demand for oxygen intensifies. The main discussion for this is in section 6.3.5 of Chapter 6

Section 6.3.4 investigated the K_La and OTR results produced by the *E.coli* fermentation system. The results for figures 6.5a and b are noted in Tables E7 and E8

Table D7: K_La values for all impellers for a fixed airflow rate of 1.5 vvm

	Rushton (6 cm) K_La /s^{-1}	Knitted Wire (6 cm) K_La /s^{-1}	Knitted Wire (11 cm) K_La /s^{-1}
200 rpm	0.00542123	0.005920313	0.01011061
300 rpm	0.007676954	0.008713078	0.017993055
400 rpm	0.021901007	0.028778635	0.058268267

Table D8: K_La values for all impellers for a fixed agitation rate of 400 rpm

	Rushton (6 cm) K_La/s^{-1}	Knitted Wire (6 cm) K_La/s^{-1}	Knitted Wire (11 cm) K_La/s^{-1}
1.00 vvm	0.004373497	0.013215975	0.016925629
1.25 vvm	0.010489877	0.023759741	0.025363973
1.50 vvm	0.021901007	0.028778635	0.058268267

These experiments have been conducted for other air flow and agitation rates. Figures D3a and b note the effect of agitation and air flow rate at fixed values of 1.0 vvm (D3a) and 200 rpm (D3b)

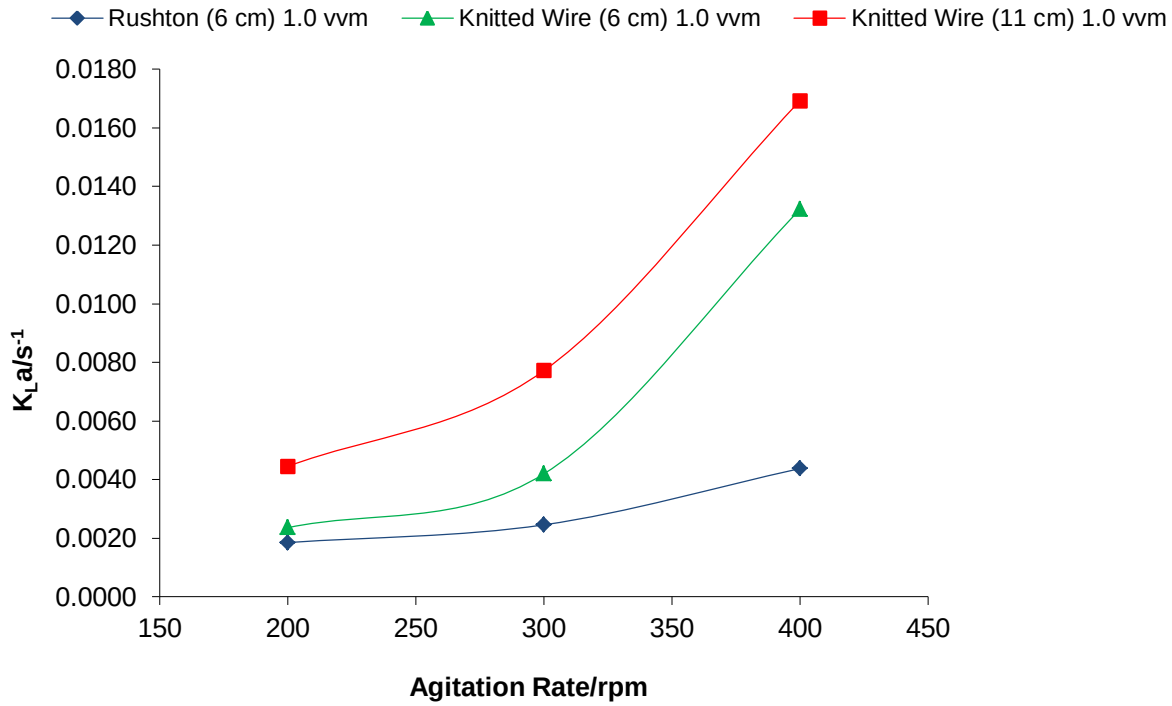

Figure D3a: The effect of agitation rate on K_La values for the all impeller for a fixed airflow rate of 1.0 vvm

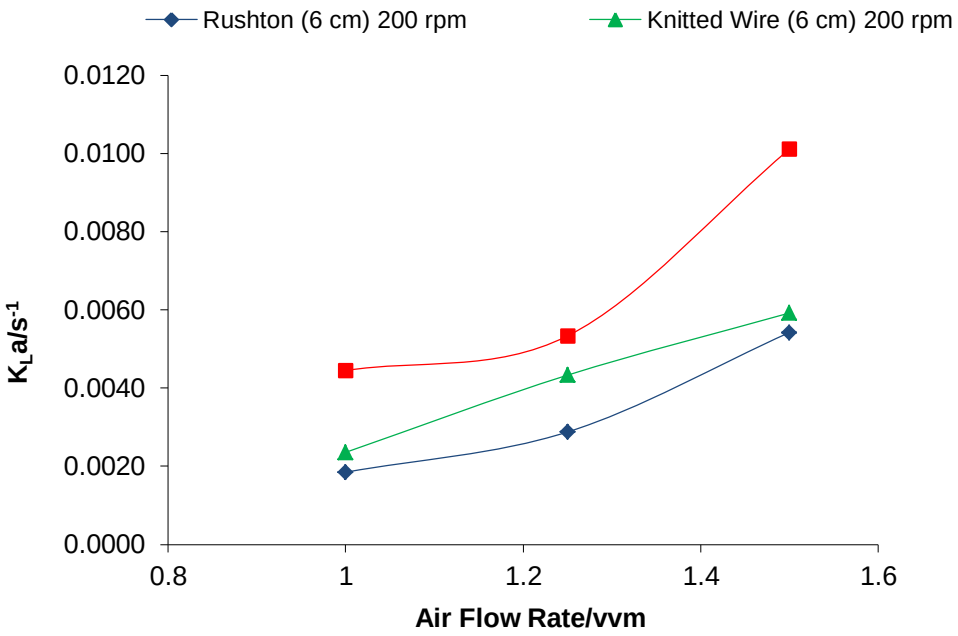

Figure D3b: The effect of air flow rate on K_La values for the all impellers at 200 rpm

When compared to the figures presented in section 6.2.4 it is easy to notice the same trends are prevalent throughout. For a full discussion of these results see section 6.2.5

D2 *P.putida* KT2442 Batch Fermentation Experiments

The results from section 5.3 of Chapter 5 which note the biomass concentration and % yield of the impellers are noted in tables E9-E11

Table D9: Results for the Rushton impeller for the *P.putida* batch fermentation

Time/H	OD @ 600 nm	Dry Cell Weight/DCW g l^{-1}	Mean TVC/CFU
1	0.277	0.1000	5.23E+05
2	0.404	0.2000	9.20E+06
3	0.664	0.2000	2.20E+07
4	1.149	0.4000	5.33E+07
5	1.748	0.6000	1.40E+08
6	2.470	0.9000	4.50E+08
7	2.778	1.2000	8.47E+08
8	3.549	1.5000	2.20E+09
18	3.830	1.5000	4.70E+10
24	3.450	1.5000	4.73E+10

Table D10: Results for the 6 cm Knitted Wire impeller for the *P.putida* batch fermentation

Time/H	OD @ 600 nm	Dry Cell Weight/DCW g l^{-1}	Mean TVC/CFU
1	0.268	0.10	6.40E+05
2	0.422	0.20	1.06E+07
3	0.746	0.30	4.87E+07
4	1.284	0.40	6.53E+07
5	1.928	0.60	2.50E+08
6	2.810	0.90	5.57E+08
7	3.570	1.20	9.10E+09
8	4.568	1.60	3.37E+10
18	4.28	1.70	2.67E+11
24	4.056	1.70	1.60E+11

Table D11: Results for the 11 cm Knitted Wire impeller for the *P.putida* batch fermentation

Time/H	OD @ 600 nm	Dry Cell Weight/DCW g l^{-1}	Mean TVC/CFU
1	0.289	0.10	7.30E+05
2	0.505	0.20	1.09E+07
3	0.978	0.30	5.37E+07
4	1.815	0.50	6.90E+07
5	2.396	0.70	3.77E+08
6	3.636	1.00	5.80E+08
7	4.515	1.30	1.01E+10
8	5.620	1.70	4.93E+10
18	5.274	1.90	6.07E+11
24	4.653	2.00	5.90E+11

D3 *P.putida* KT2442 Fed-Batch Fermentation Experiments

Section 6.4 in Chapter 5 noted the results for the fed-batch fermentation conducted with the BioFlow III reactor. Tables D12-D14 notes these results.

Table D12: Results for the Rushton impeller for the *P.putida* fed batch fermentation

Time/H	OD @ 600 nm	Dry Cell Weight/DCW g l^{-1}	Mean TVC/CFU
1	0.289	0.10	5.03E+05
2	0.516	0.10	9.13E+06
3	0.774	0.20	2.13E+07
4	1.275	0.30	5.60E+07
5	2.008	0.60	1.27E+08
6	3.150	1.00	5.60E+08
7	4.344	1.40	8.70E+08
8	6.479	2.10	2.43E+09
17	7.320	2.40	4.67E+10
18	7.260	2.40	5.23E+10
19	7.080	2.40	5.33E+10
20	6.960	2.30	5.23E+10
21	6.840	2.30	5.40E+10
22	6.760	2.30	5.33E+10
23	6.620	2.20	5.20E+10
24	6.520	2.20	5.13E+10
25	7.740	2.50	7.03E+10
26	8.240	2.70	7.40E+10
27	9.680	3.20	8.90E+10
28	10.120	3.30	9.83E+10
29	11.770	3.90	9.00E+10
30	13.536	4.50	2.00E+11
31	14.404	4.80	2.93E+11
32	15.260	5.00	3.37E+11
33	16.472	5.50	4.40E+11
34	17.220	5.70	6.13E+11
35	18.042	6.00	8.07E+11
36	19.414	6.40	4.33E+11
37	19.992	6.60	1.87E+11
38	20.160	6.70	9.33E+10
39	20.592	6.90	7.90E+10
40	20.979	7.00	5.27E+10
41	21.127	7.00	3.00E+10
42	22.032	7.30	2.33E+10
43	22.230	7.40	8.60E+09
44	22.932	7.60	7.03E+09
45	23.280	7.80	5.37E+09
46	23.840	8.00	4.00E+09
47	24.108	8.00	2.53E+09
48	24.641	8.10	1.07E+09

Table D13: Results for the 6 cm Knitted Wire impeller for the *P.putida* fed batch fermentation

Time/H	OD @ 600 nm	Dry Cell Weight/DCW g l^{-1}	Mean TVC/CFU
1	0.291	0.10	6.30E+05
2	0.506	0.10	1.07E+07
3	0.858	0.30	4.80E+07
4	1.515	0.50	6.30E+07
5	3.606	1.20	2.70E+08
6	5.450	1.80	5.57E+08
7	8.008	2.70	9.07E+09
8	10.268	3.40	3.30E+10
17	11.628	3.80	5.73E+11
18	11.484	3.80	4.93E+11
19	11.084	3.70	4.70E+11
20	10.846	3.60	4.63E+11
21	11.084	3.60	3.50E+11
22	10.744	3.60	3.20E+11
23	10.676	3.60	2.70E+11
24	10.540	3.60	2.73E+11
25	12.096	4.00	6.70E+11
26	13.400	4.40	8.07E+11
27	15.312	5.10	9.63E+11
28	17.300	5.70	1.57E+12
29	18.603	6.20	2.60E+12
30	20.370	6.80	3.20E+12
31	22.638	7.50	4.07E+12
32	23.240	7.70	5.20E+12
33	24.161	8.00	5.53E+12
34	25.567	8.50	6.60E+12
35	26.364	8.80	7.30E+12
36	28.495	9.40	8.20E+12
37	30.285	10.00	9.10E+12
38	32.150	10.70	1.20E+13
39	33.337	11.00	1.57E+13
40	34.272	11.40	1.73E+13
41	36.192	12.00	2.20E+13
42	38.460	12.80	2.23E+13
43	40.383	13.40	2.47E+13
44	42.306	14.10	2.83E+13
45	44.132	14.70	2.90E+13
46	46.620	15.50	2.60E+13
47	48.168	16.00	2.70E+13
48	50.297	16.70	2.90E+13

Table D14: Results for the 11 cm Knitted Wire impeller for the *P.putida* fed batch fermentation

Time/H	OD @ 600 nm	Dry Cell Weight/DCW g l^{-1}	Mean TVC/CFU
1	0.3	0.10	7.37E+05
2	0.589	0.20	1.18E+07
3	1.058	0.40	5.50E+07
4	2.420	0.80	7.17E+07
5	4.792	1.60	4.17E+08
6	8.484	2.80	5.87E+08
7	11.610	3.90	1.05E+10
8	13.240	4.50	5.37E+10
17	14.036	4.60	6.87E+11
18	13.728	4.60	6.07E+11
19	13.650	4.60	5.80E+11
20	13.629	4.50	5.37E+11
21	13.587	4.50	4.77E+11
22	13.503	4.50	4.60E+11
23	13.482	4.50	4.40E+11
24	13.420	4.50	4.63E+11
25	14.872	5.00	9.30E+11
26	16.128	5.40	2.50E+12
27	18.522	6.20	2.93E+12
28	20.280	6.80	3.77E+12
29	23.426	7.80	4.87E+12
30	26.208	8.70	5.83E+12
31	30.184	10.10	7.47E+12
32	32.928	11.00	8.87E+12
33	34.250	11.40	1.83E+13
34	36.146	12.00	2.73E+13
35	38.192	12.70	3.03E+13
36	40.415	13.50	3.20E+13
37	43.338	14.40	4.43E+13
38	45.895	15.30	5.13E+13
39	47.403	15.80	5.00E+13
40	49.536	16.50	4.97E+13
41	50.768	17.00	5.27E+13
42	51.636	17.20	5.37E+13
43	53.053	17.70	5.30E+13
44	54.431	18.10	5.23E+13
45	56.170	18.70	5.17E+13
46	58.735	19.60	5.30E+13
47	60.632	20.20	5.27E+13
48	62.699	21.10	5.30E+13

Appendix E: Additional HBR Data

The aim of Appendix F is to present tables of figures behind the hydrodynamic and fermentation studies with the HBR, and to present some additional data not included in Chapters 4 and 5. The results in this appendix look at the hydrodynamic, transfer capability, and batch *P.putida* systems conducted with the HBR. For a full discussion of these results please see section 5.3 and 5.4 of Chapter 5 (for hydrodynamics and transfer study) and section 5.5 in Chapter 5 (for *P.putida* batch fermentation system).

E1 Bubble Study

Section 5.3.2 considered the capability of the new HBR to produce small bubbles with and without packing. A comprehensive set of experiments conducted produced the results shown in figures 5.20-5.22. The results for figures 4.20 and 4.22 are noted in tables E1-E3 (with packing) and tables E4-E6 (without packing). Note the calculated air flow rates have been rounded to the nearest whole number

Table E1: Mean Bubble Diameter for HBR at 400 rpm (with packing)

	Air Flow Rate @ STP/l min^{-1}		
Liquid Flow Rate/l min^{-1}	9	12	16
0.4	1.597	1.489	1.394
0.5	1.576	1.417	1.302
0.6	1.556	1.322	1.273

Table E2: Mean Bubble Diameter for HBR at 800 rpm (with packing)

	Air Flow Rate @ STP/l min^{-1}		
Liquid Flow Rate/l min^{-1}	9	12	16
0.4	0.902	0.801	0.726
0.5	0.884	0.784	0.701
0.6	0.809	0.761	0.659

Table E3: Mean Bubble Diameter for HBR at 1200 rpm (with packing)

	Air Flow Rate @ STP/l min^{-1}		
Liquid Flow Rate/l min^{-1}	9	12	16
0.4	0.523	0.471	0.420
0.5	0.505	0.452	0.404
0.6	0.488	0.432	0.361

Table E4: Mean Bubble Diameter for HBR at 400 rpm (without packing)

	Air Flow Rate @ STP/l min^{-1}		
Liquid Flow Rate/l min^{-1}	5	9	12
0.4	5.588	5.490	5.242
0.5	5.386	5.259	5.100
0.6	5.267	5.181	4.927

Table E5: Mean Bubble Diameter for HBR at 800 rpm (without packing)

	Air Flow Rate @ STP/l min^{-1}		
Liquid Flow Rate/l min^{-1}	5	9	12
0.4	4.498	4.312	4.156
0.5	4.264	4.064	3.933
0.6	4.062	3.930	3.753

Table E6: Mean Bubble Diameter for HBR at 1200 rpm (without packing)

	Air Flow Rate @ STP/l min^{-1}		
Liquid Flow Rate/l min^{-1}	5	9	12
0.4	3.374	3.170	2.971
0.5	3.183	2.948	2.679
0.6	2.986	2.710	2.497

The effect of rotational speed, gas flow rate, and liquid flow rate were considered in figure 5.20 a and b. Figure E1a and b considers this at different values to note the trends present.

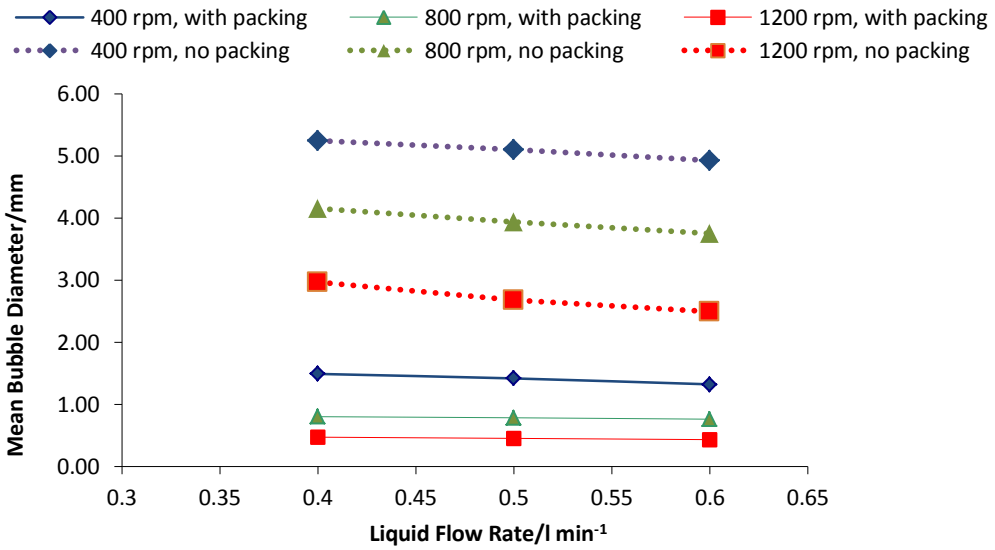

Figure E1a: Effect of Rotational Speed and Liquid Flow Rate on Mean Bubble size in HBR (constant gas flow rate of 12 l min^{-1})

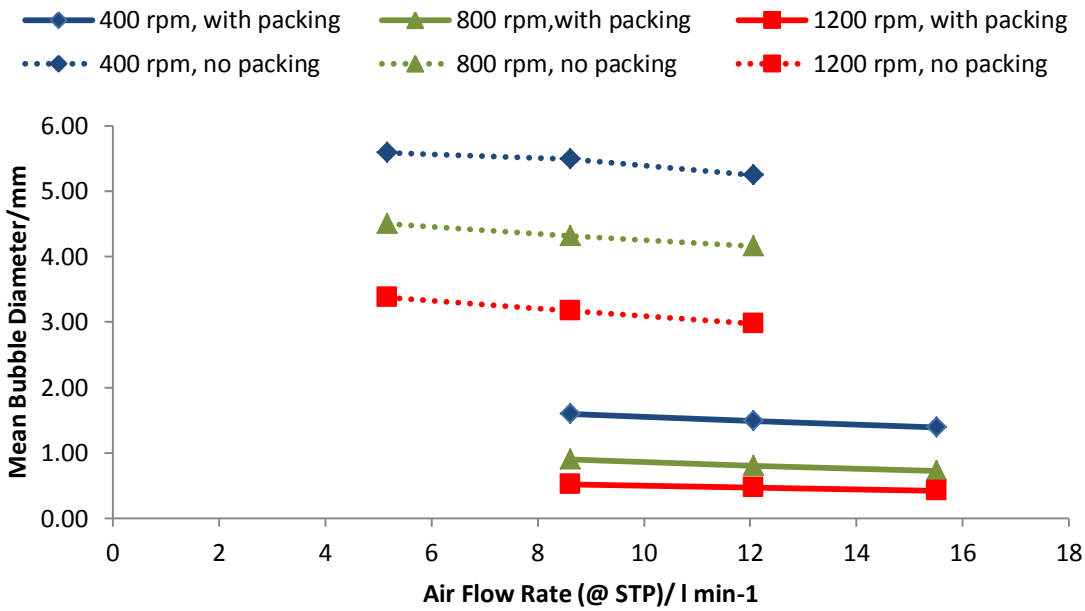

Figure E1b: Effect of Rotational Speed and Air Flow Rate on Mean Bubble size in HBR (constant liquid flow rate of 0.4 l min^{-1})

Despite the use of slightly different gas and liquid flow rates, figures E1 a and b look identical to the plots in figure 5.20 a and b. This clearly shows that the same trends are prevalent for the different parameters used.

Mean bubble size distribution was also investigated, the results for figure 5.21 are noted in table E7

Table E7: Typical Bubble Size Distribution for the HBR (distribution for an operating condition of 800 rpm, 0.4 l min^{-1} liquid flow rate, and 12.068 l min^{-1} gas flow rate)

Mean Bubble Size/mm	Number	%
0.715-0.720	5	16.66667
0.720-0.725	6	20
0.725-0.730	11	36.66667
0.730-0.735	5	16.66667
0.735-0.740	3	10
Total	30	

Rotational speed more than any of the other factors studied has the greatest impact on bubble distribution. Figure E2 notes the bubble distribution at 400 rpm, 0.4 l min^{-1} liquid flow rate, and 12.068 l min^{-1} gas flow rate.

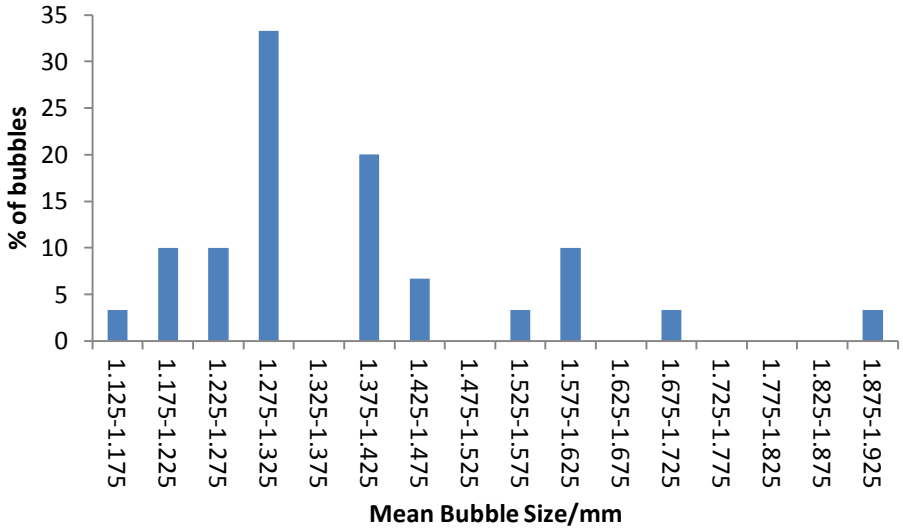

Figure E2: Typical Bubble Size Distribution for the HBR (distribution for an operating condition of 400 rpm, 0.4 l min^{-1} liquid flow rate, and 12.068 l min^{-1} gas flow rate)

Comparing figure E2 to 5.21, there is a difference in the range of bubble data. The data in figure 4.21 shows a normal distribution, the data in figure F2 is slightly skewed.

E2 Transfer Characterisation Study

Section 4.4 investigated the transfer capability of the HBR with and without packing present. This was calculated by NTU and $K_l a$. Tables E8 and E9 present the results plotted in figures 5.24 and 5.25

Table E8: NTU and $K_L a$ values for the HBR (with packing)

Rotational Speed/rpm	Corrected Air Flow Rate/l min^{-1}	Liquid Flow Rate/l min^{-1}	NTU	$K_L a/s^{-1}$
400	8.62	0.4	1.84	1.75E-03
400	8.62	0.5	1.74	2.07E-03
400	8.62	0.6	1.68	2.40E-03
400	12.068	0.4	1.92	1.83E-03
400	12.068	0.5	1.84	2.19E-03
400	12.068	0.6	1.81	2.59E-03
400	15.516	0.4	1.97	1.87E-03
400	15.516	0.5	1.87	2.23E-03
400	15.516	0.6	1.86	2.65E-03
800	8.62	0.4	1.98	1.89E-03
800	8.62	0.5	1.86	2.22E-03
800	8.62	0.6	1.84	2.63E-03
800	12.068	0.4	2.04	1.94E-03
800	12.068	0.5	1.93	2.30E-03
800	12.068	0.6	1.89	2.69E-03
800	15.516	0.4	2.06	1.96E-03
800	15.516	0.5	1.98	2.35E-03
800	15.516	0.6	1.96	2.79E-03
1200	8.62	0.4	2.17	2.06E-03
1200	8.62	0.5	2.11	2.51E-03
1200	8.62	0.6	2.06	2.94E-03
1200	12.068	0.4	2.33	2.21E-03
1200	12.068	0.5	2.18	2.60E-03
1200	12.068	0.6	2.12	3.02E-03
1200	15.516	0.4	2.47	2.35E-03
1200	15.516	0.5	2.26	2.69E-03
1200	15.516	0.6	2.19	3.12E-03

Table E9: NTU and K_La values for the HBR (without packing)

Rotational Speed/rpm	Corrected Air Flow Rate/l min^{-1}	Liquid Flow Rate/l min^{-1}	Average NTU	K_La/s^{-1}
400	5.172	0.4	1.77	1.69E-03
400	5.172	0.5	1.72	2.05E-03
400	5.172	0.6	1.62	2.31E-03
400	8.62	0.4	1.81	1.72E-03
400	8.62	0.5	1.75	2.09E-03
400	8.62	0.6	1.65	2.36E-03
400	12.068	0.4	1.91	1.82E-03
400	12.068	0.5	1.82	2.16E-03
400	12.068	0.6	1.69	2.42E-03
800	5.172	0.4	1.86	1.77E-03
800	5.172	0.5	1.78	2.12E-03
800	5.172	0.6	1.70	2.42E-03
800	8.62	0.4	1.92	1.83E-03
800	8.62	0.5	1.81	2.16E-03
800	8.62	0.6	1.72	2.46E-03
800	12.068	0.4	1.97	1.88E-03
800	12.068	0.5	1.93	2.30E-03
800	12.068	0.6	1.76	2.51E-03
1200	5.172	0.4	1.91	1.82E-03
1200	5.172	0.5	1.85	2.20E-03
1200	5.172	0.6	1.80	2.56E-03
1200	8.62	0.4	1.98	1.88E-03
1200	8.62	0.5	1.94	2.31E-03
1200	8.62	0.6	1.86	2.66E-03
1200	12.068	0.4	2.01	1.91E-03
1200	12.068	0.5	1.96	2.34E-03
1200	12.068	0.6	1.93	2.75E-03

Figures 5.24 and 5.25 investigate the effect of rotational speed, gas flow rate and liquid flow rate on the value of NTU and K_la observed. Figures E3 and E4 present another set of results investigating these factors.

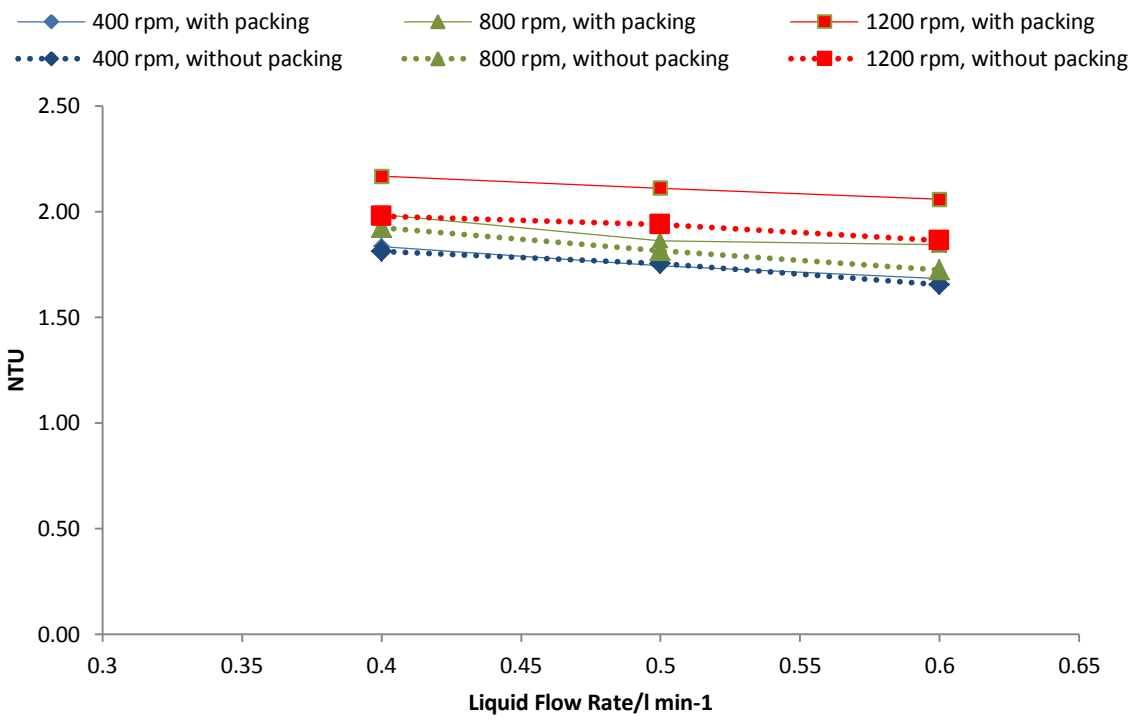

Figure E3a: Effect of Rotational Speed and Liquid Flow Rates on NTU Values for the HBR (fixed gas flow rate of 9 l min^{-1} @ STP).

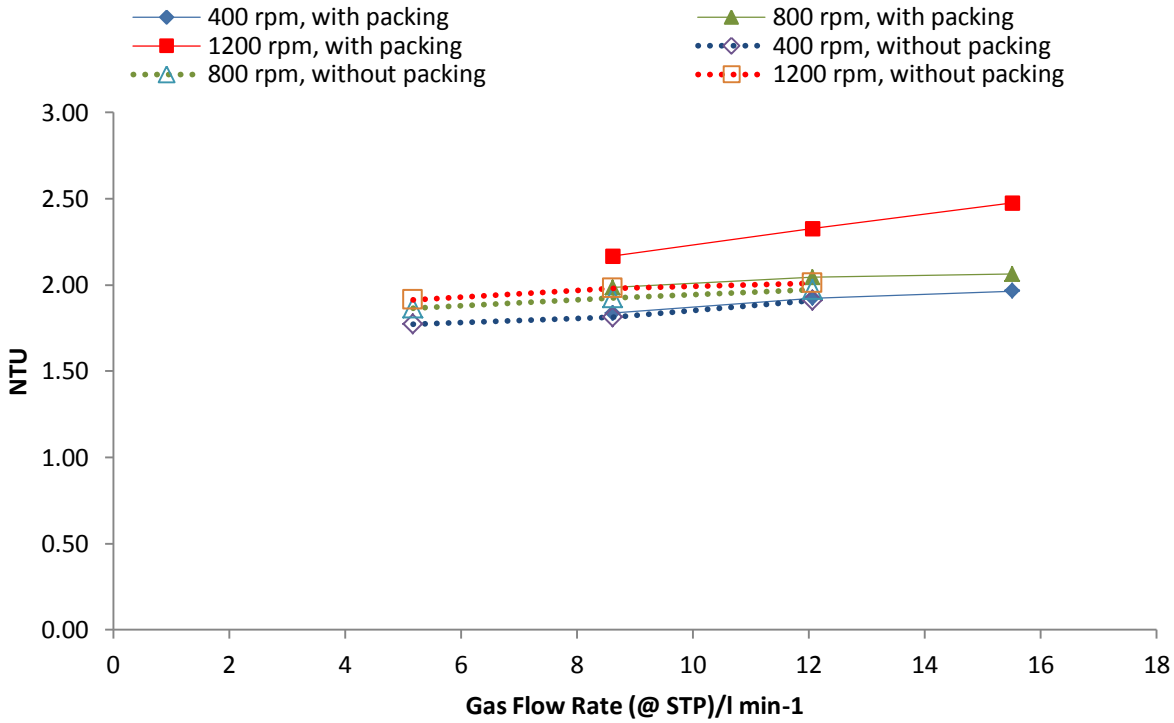

Figure E3b: Effect of Rotational Speed and Gas Flow Rates on NTU Values for the HBR (fixed liquid flow rate of 0.4 l min^{-1}).

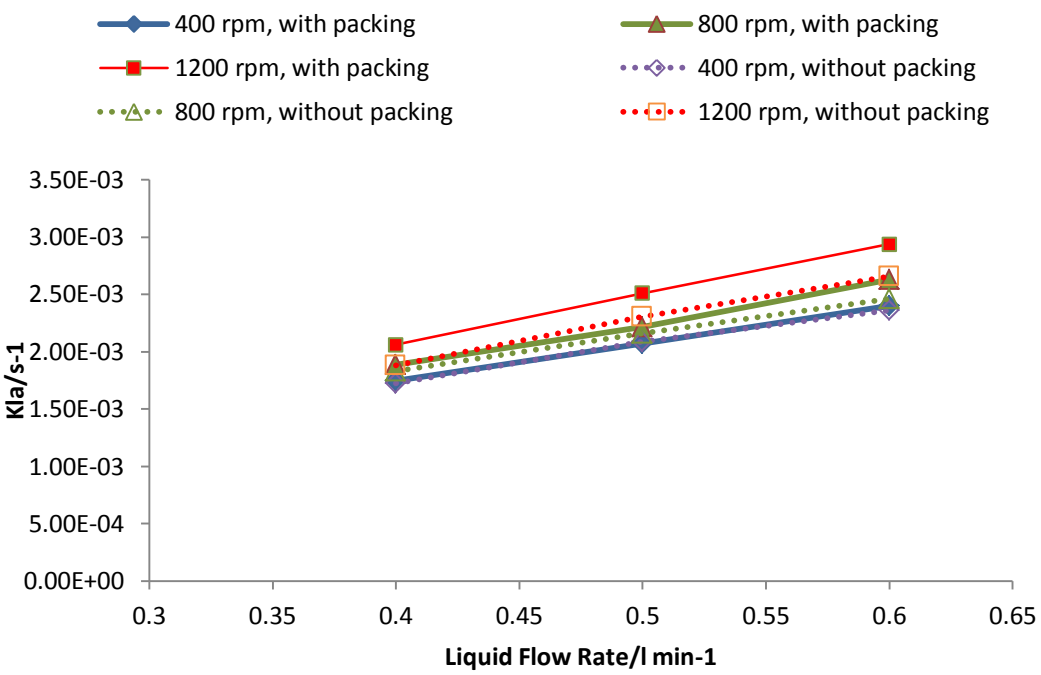

Figure E4a: The effect of rotational speed and liquid flow rate on $K_l a$ for the HBR (fixed gas flow rate of 9 l min^{-1} @ STP).

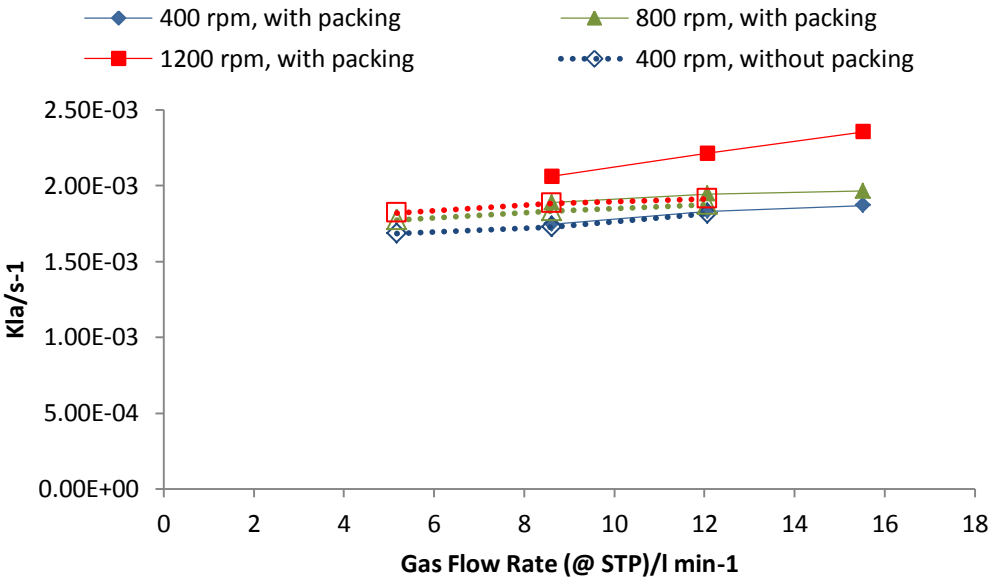

Figure E4b: Effect of Rotational Speed and Gas Flow Rates on $K_l a$ Values for the HBR (fixed liquid flow rate of 0.4 l min^{-1}).

As with the results presented for the bubble study, there is not much to distinguish the two data sets showing that the trends are well established for all the factors studied.

References

Adsul M.G *et al* (2011) "Development of Biocatalysts for Production of Commodity Chemicals from Lignocellulosic Biomass" *Bioresource Technology* **In Press**

Aoune, A. and Ramshaw, C (1999) "Process Intensification: Heat and Mass Transfer Characteristics of Liquid Films on Rotating Discs" *International Journal of Heat and Mass Transfer*, **42**, 2543 (1999)

Anderson A.J and Wynn J.P "*Microbial polyhydroyalkanoates, polysaccharides, and lipids*" in Basic Biotechnology (2001), 2nd Edition Cambridge University Press UK. Pages 325-333

Bailey J E, Ollis D F, (1987) Biochemical Engineering Fundamentals McGraw-Hill (New York) 2nd Edition Pages 457-529

Badino A.C *et al* (2000) "Improving $K_L a$ determination in fungal fermentation, taking into account electrode response time" *J.Chem.Technol.Biotechnol* **75** 469–479.

Bi Y. H, Hill G A, Sumner R J (2005) "Enhancement of the overall volumetric oxygen transfer coefficient in a stirred tank bioreactor using ethanol" *Canadian Journal of Chemical Engineering* **79**:3 Pages 463-467

Blanch Harvey W, Clark Douglas S (1997) Biochemical Engineering Marcel Dekker (New York) Pages 353-415

Bombac A (2006) "Individual impeller flooding in aerated vessel stirred by multiple-Rushton impellers" *Chemical Engineering Journal*, **116** 2 85-95

Boodhoo, K.V.K. *et al.* (2006) "Classical Cationic Polymerization of Styrene in a Spinning Disc Reactor Using Silica-Supported BF_3 Catalyst", *Journal Applied Polymer Science* **101:** 8-19

Boodhoo K.V.K *et al* (2008) "Intensification of gas–liquid mass transfer using a rotating bed of porous packings for application to an *E. coli* batch fermentation process" *Chemical Engineering Journal* **135**:1-2 Pages 141-150

Boodhoo K.V.K (Personal Communication by email, October 2006) Oxygen Mass Transfer

Burns, J.R. and Ramshaw, C. (1996) "Process intensification: Visual study of liquid maldistribution in rotating packed beds", *Chemical Engineering Science* **51:** 1347-1352

Burns J.R *et al* (2000) "Process intensification: operating characteristics of rotating packed beds — determination of liquid hold-up for a high-voidage structured packing" *Chemical Engineering Science* **55** 13 2401-2415

Buwa V, Dewan A, Nassar A.F, Durst F (2006) "Fluid dynamics and mixing of single-phase flow in a stirred vessel with a grid disc impeller: Experimental and numerical investigations" *Chemical Engineering Science* **61** 9 2815-2822.

Cartwright C.D. and Boodhoo, K.V.K. (2008) "Intensification of PHA production by application of porous mesh impellers", *Proceedings of the 2nd Annual Bioproduction Meeting,* Thessaloniki, Greece

Calderbank, P. and Jones, S. (1961) *Trans. IChemE*, **39**, 363

Castilho L.R, Mitchell D.A, Freire D.M.G (2009) "Production of PHAs from waste materials and by products by submerged and solid state fermentation" *Bioresource Technology* **100:** 5996-6009

Chhatre S, Bracewell D, Titcherner-Hooker N (2009) "A microscale approach for predicating the performance of chromatography columns used to recover therapeutic polyclonal antibodies" *Journal of Chromatography A* **In Press**

Chia-Chang L, Yu-Shao C, Hwai-Shen L (2000) "Predicition of liquid hold up in counter current flow roating packed bed reactor" *Trans IChemE* **78:** 397-403

Chisti Y and Moo-Young M (1996) "Bioprocess Intensification through Bioreactor Engineering" *Chemical Engineering Research and Design* **74** A5 575-583.

Chisti Y "Bioreactor Design" in "*Basic Biotechnology*" (2006) Colin Ratledge and Bjørn Kristiansen Editors 3rd Edition Cambridge University Press Cambridge UK Pages 181-200

Conway K *et al* (2002) "Gas–Liquid–Solid Operation of a Vortex-Ingesting Stirred Tank Reactor" *Chemical Engineering Research and Design* **80** 8 839-845

Crueger W (1989) "Biotechnology" 2nd Edition Bayer AG Germany

Deront M *et al* (1998) "Volumetric oxygen mass transfer coefficient in an upflow co current packed-bed bioreactor" *Chemical Engineering Science* **53**:7 Pages 1321-1330

Davidson, J. and Schuler, B. (1960) *Trans. IChemE*, **38**, 335-341

Decker J "The Microbial Growth Curve" [WWW Document] URL http://microvet.arizona.edu/Courses/MIC205/Exams/05Exams/05Ex2key.htm. Accessed January 18th 2011.

Doran, Pauline M (1999) Bioprocess Engineering Principles Academic Press (London) Forth Printing Pages 190-213

Duetz W.A (2007) "Microtitre Plates as mini-bioreactors: miniaturisation of fermentatuion methods" *Trends in Microbiology* **15:** 469-475

Eugenio L.I *et al* (2009) "The turnover of medium-chain-length polyhydroxyalkanoates in *Pseudomonas putida* KT2442 and the fundamental role of PhaZ depolymerase for the metabolic balance**"** *Environmental Microbiology* **In Press**

Ford J J *et al* (2008) "X-ray computed tomography of a gas-sparged stirred-tank reactor" *Chemical Engineering Science* **63** 8 2075-2085

Galaction A.I *et al* (2004) "Enhancement of oxygen mass transfer in stirred bioreactors using oxygen-vectors. 1. Simulated fermentation broths" *Bioprocess and Biosystems Engineering* **26**:4 Pages 231-238.

Galaction A.I *et al* (2005) "Enhancement of oxygen mass transfer in stirred bioreactors using oxygen-vectors 2. *Propionibacterium shermanii* broths" *Bioprocess and Biosystems Engineering* **24**:4 Pages 263-271

Gill N.K *et al* (2008A) "Design and charaterisation of a minature stirred bioreactor system for parallel microbial fermentations" *Biochemical Engineering Journal* **39:** 164-176

Gill N.K *et al* (2008B) "Quantification of Power Consumption and Oxygen Transfer Characterisation of a Stirred Miniature Bioreactor for predicitive Fermentation Scale Up" *Biotechnology and Bioengineering* **100:** 1144-1155

Giovart M *et al* (2010) "Exploring the lag phase and growth initiation of a yeast culture by means of an individual-based model" *Food Microbiology* **In Press**

Gogate P.R, Beenackers A.A.C.M, Pandit A.B (2000) "Multiple impeller systems with a special emphasis on bioreactors: a critical review" *Biochemical Engineering Journal* **6:** 109-144

Grinis L, Kholmer V, Korin E (2004) "Liquid oxygenation improvement by interaction of bubbles and vibration fields" *Chemical Engineering & Technology* **27** 11 1206-1211.

Hallenbeck P.C, Ghosh D "Advances in fermentative biohydrogen production: the way forward?" *Trends in Biotechnology* **27**:5 287-297

Hashemi M *et al* (2011)' "Mathematical modeling of biomass and α-amylase production kinetics by *Bacillus* sp. in solid-state fermentation based on solid dry weight variation" *Biochemical Engineering Journal* **53** 159-16

Jassim, M. (2002) "Process Intensification: Absorption and Desorption of Carbon Dioxide from Monoethanolamine Solutions Using Higee Technology", *PhD thesis,* Newcastle University

Kang *et al* (2010) "A novel strategy for succinate and polyhydroxybutyrate co-production in *Escherichia coli*" *Bioresource Technology* **101** 19 7675-7678

Kelleher, T. and Fair, J.R. (1996) "Distillation Studies in a High-Gravity Contactor", *Industrial Engineering and Chemistry Research* **35:** 4646-4655

Kilonzo P *et al* (2004) "The effects of non-Newtonian fermentation broth viscosity and small bubble segregation on oxygen mass transfer in gas-lift bioreactors: a critical review" *Biochemical Engineering Journal* **17** 1 27-40

Koch V *et al* (1995) "Effect of Antifoam Agents on the Medium and Microbial Cell Properties and Process Performance in Small and Large Reactors" *Process Biochemistry* **30** 5 Pages 435-446

Laakkonen M *et al* (2005) "Local bubble size distributions in agitated vessel: Comparison of Three Experimental Technique" *Trans IChemE*

Lamping S.R *et al* (2003) "Design of a prototype miniature bioreactor for high throughput automated bioprocessing" Chemical *Engineering Science* 58 747–758.

Lee J.M (1992) "Biochemical Engineering" Prentice Hall (Simon and Schuster Company) New Jersey.

Lin J.J *et al* "Osmotic (a_w) effects on growth and ethanol Production of Free and Immobilized *Zymomonas mobilis"* *Process Biochemistry* 26 143-151

Lin C.C *et al* (2007) "Removal of Carbon Dioxide by Absorption in a Rotating Packed Bed" *Ind. Eng. Chem. Res.*, **42**, 2381-2386

Lo Y.M *et al* (2001) "Oxygen transfer characteristics of a centrifugal, packed-bed reactor

Madigan M.T, Martinko J.M (2006) "*Brock: Biology of Microorganisms*" 11th Edition Pearson Prentice Hall Carbondale U.S.A. Pages 941-967.

Madigan M.T, *et al.* (2009) "*Brock: Biology of Microorganisms*" 12th Edition, Pearson Benjamin Cummings

Manginot C *et al* (1998) **"**Nitrogen demand of different yeast strains during alcoholic fermentation. Importance of the stationary phase" *Enzyme and Microbial Technology* **23** 7-8 511-517

Mathure P, Patwardhan A (2005) "Comparison of mass transfer effiency in horizontal rotating packed beds and rotating biological contactors" *Journal of Chemical Technology and Biotechnology* **80:** 413-419

Martin Y, Vermette P (2005) "Bioreactors for tissue mass culture: Design, characterisation and recent advances" *Biomaterials* **26**: 7481-7503

Martin M, Montes F.J, Galan M.A (2008) "On the contribution of the scales of mixing to the oxygen transfer in stirred tanks" *Chemical Engineering Journal* **145**: 232-241

Martinez D.T *et al* (2009) "Hydrodynamic and oxygen mass transfer studies in a three phase (air-water-ionic liquid stirred tank bioreactor" *Biochemical Engineering Journal* **45**: 209-217

McCarthy E.D *et al* (2007) "Application of an intensified narrow channel reactor to the aqueous phase precipitation of Barium Sulfate" *Journal of Colloid and Interface Science* **305:** 72-87

Mercer A.C (1992) "Process Intensification: The UK Programmes to encourage the development and use of intensified heat exchange equipment and technology" *Chemical Engineering Progress* **13** 6 539-545.

Merico A *et al* (2003) "Aerobic sugar metabolism in the spoilage yeast *Zygosaccharomyces bailii*" *FEMS Yeast Research* **4**:3 277-283

Mortimer, C.H. (1956) "The oxygen content of air-saturated fresh waters, and aids in calculating percentage saturation", *International Association Theoretical Applied Communication* **6.**

Nicklin J, Graeme-Cook K, Killington R (2003) "*Instant Notes in Microbiology*" 2nd Edition Garland Science Abingdon UK Pages 93-107

Ni X, Gao S (1996) "Scale up correlation for mass transfer coefficents in pulsed baffled reactors" *The Chemical Engineering Journal* **63:** 157-166

Nielsen J "Microbial Process Kinetics" in "*Basic Biotechnology*" (2006) Colin Ratledge and Bjørn Kristiansen Editors 3rd Edition Cambridge University Press Cambridge UK Pages 155-180

Nikakhtari H, Hill G.A (2005) Paper A "Hydrodynamic and oxygen mass transfer in an external loop airlift bioreactor with a packed bed" *Biochemical Engineering Journal* **27**:2 Pages 138-145

Nikakhtari H, Hill G. A (2005) Paper B "Enhanced oxygen mass transfer in an external loop airlift bioreactor using a packed bed" *Industrial & Engineering Chemistry Research* **44:**4 Pages 1067-1072

Nocentini, M *et al* (1993) "Gas-liquid mass transfer and hold-up in vessels stirred with multiple Rushton turbines and water-glycerol solutions" *Industrial Engineering Chemistry Research* **32** 19-26

Noorman H.J "Mass Transfer" in "*Basic Biotechnology*" (2006) Colin Ratledge and Bjørn Kristiansen Editors 3rd Edition Cambridge University Press Cambridge UK Pages 201-217

Ortiz-Ochoa K *et al* (2005) "A novel method for the measurement of oxygen mass transfer rates in small-scale vessels" *Biochemical Engineering Journal* **25**:1 Pages 63-68.

Ottens M, Wesselingh J.A, Van der Wielen L.A.M (2006) "Downstream Processing" "*Basic Biotechnology*" (2006) Colin Ratledge and Bjørn Kristiansen Editors 3rd Edition Cambridge University Press Cambridge UK.

Papagianni M (2004) "Fungal morphology and metabolite production in submerged mycelia processes" *Biotechnology Advances* **22**189-259

Peel, J.A.R. (1995) "Mass transfer and hydrodynamics in a gas-liquid centrifugal field de-oxygenator", *PhD thesis,* Newcastle University

Peel J, Howarth C Ramshaw C (1998) "Process Intensification: Higee Seawater Deaeration" *Chemical Engineering Research and Design* **76:** 585-593

Postgate J (1995) "*The Outer Reaches of Life"* Canto Press, Cambridge UK

Puthli M *et al* (2005) "Gas-liquid transfer studies with triple impeller system on a laboratory scale bioreactor" *Biochemical Engineering Journal* **23:** 25-30

Mulchandani A and Bassi A.S (1995) "Principles and Applications of Biosensors for Bioprocess Monitoring and Control" *Critical Reviews in Biotechnology* **15:** 105-124

Ramshaw C (1985) "Process Intensification: A Games for n players" *The Chemical Engineer* **1** 1 30-33

Reay D (2008) "The role of process intensification in cutting greenhouse gas emissions" *Applied Thermal Engineering* **28:** 2011-2019

Reay D.A, Ramshaw C, Harvey A.P, "Process Intensification: engineering for Efficiency, Sustainability and Flexibility" (2008) Elsevier

Riberia G.F, Monteoliva-Sanchez M, Ramos-Cormenzana A (2001) "Production of polyhidroxyalkanoates by *Pseudomonas putida* KT2442 harboring pSK2665 in wastewater from olive oil mills (alpechín)" *Electronic Journal of Biotechnology* **4**:2 Pages 116-119

Richardson J.F, Harker J.H, Backhurst J.R (2002) "*Coulson and Richardson's Chemical Engineering: Volume Two- Particle Technology and Separation Processes"* 5th Edition Butterworth Heinemann Oxford UK

Richardson J.F, Peacock D.G (2005) "*Coulson and Richardson's Chemical Engineering: Volume Three-Chemical and Biochemical Reactors and Process Control*" 3rd Edition Butterworth Heinemann Oxford UK

Shuler M.L, Kargi F (2002) "*Bioprocess Engineering: Basic Concepts*" 1st Edition Prentice Hall PTR Upper Saddle River, New Jersey, U.S.A. Pages 1-11, 285-328, and 329-384

Skula V.B *et al* (2001) "Scale up of biotransformation process in stirred tank reactor using dual impeller bioreactor" *Biochemical Engineering Journal* **8:** 19-29

Sonnleitner B "Measurement, Mointoring, Modelling, and Control" in "*Basic Biotechnology*" (2006) Colin Ratledge and Bjørn Kristiansen Editors 3rd Edition Cambridge University Press Cambridge UK Pages 251-270

Stanbury P.F, Whitaker A, Hall S.J (2000)" *Principles of Fermentation Technology*" 2nd Edition, Butterworth Heinemann Oxford U.K. Pages 167-192, 199-209, and 243-272.

Stankiewicz A.J, Mouljin J.A (2000) "Process Intensification: Transforming Chemical Engineering" *Chemical Engineering Progress* **1** 1 22-34.

Stankiewicz A.J (2003) "Reactive Seperations for Process Intensification: An Industrial Perspective" *Chemical Engineering and Processing* **42** 1137-144
Taghavi M (2010) "Experimental and CFD investigation of power consumption in a dual Rushton turbine stirred tank" *Chemical Engineering Research and Design* **In Press**

Tatterson G.B (1991) "*Fluid Mixing and Gas Dispersion in Agitated Tanks"* 1st Edition McGraw-Hill Inc New York USA Pages 4-5

Sun Z *et al* (2007) "Carbon limited fed batch production of medium chain length polyhydroxyalkanoates from nonanoic acid by *Pseudomonas putida* KT2440" *Applied Microbiology Technology* **74:** 69-77

Tortajada, M. *et al.* (2008) "Pilot Scale mcl-Polyalkanoate Production and Purification from *Pseudomonas Putida* KT2442", Proceedings of the 1st Annual Bioproduction Meeting, Poros, Greece

Troeger C.N *et al* (2008) "Intensification of PHA production by application of the Oscillatory Baffled Bioreactor" *Proceedings of the 2nd Annual Bioproduction Meeting,* Thessaloniki, Greece

Tschentscher R *et al* (2009) "Gas-liquid mass transfer in rotating solid foam reactors" *Chemical Engineering Science* **In Press**

Vicevic M, Boodhoo K.V.K, Scott K (2007) "Catalytic isomerisation of α-pienne oxide to campholenic aldehyde using silica supported zinc trifilicate catalysts: II Performance of immobilised catalysts in a continous spinning disc reactor" *Chemical Engineering Journal* **133:** 43-57

Vicevic M, Novakovic K, Boodhoo K.V.K, Morris A.J (2008) "Kinetics of styrene free radical polymerisation in the spinning disc reactor" *Chemical Engineering Journal* **135**:1-2 78-82

Vrabel P, van der Lans R.G. J. M, Luyben K.C. A. M, Boon L, Nienow A.W (2000) "Mixing in large-scale vessels stirred with multiple radial or radial and axial up-pumping impellers: modelling and measurements" *Chemical Engineering Science* **55** 23 5881-5896

Wang G.Q *et al* (2008) "Performance of a new rotating zigzag bed-a new HiGEE" *Chemical Engineering and Processing* **47:** 2131-2139

Weber J, Agblevor F. A (2005) "Microbubble fermentation of Trichoderma reesei for cellulase production" *Process Biochemistry* **40**:2 Pages 669-676

Wise W.S (1951) "The measurement of the aeration of culture media" *Journal of General Microbiology* **5** 167-177

Vidal-Mas J *et al* (2001) "Rapid flow cytometry – Nile red assessment of PHA cellular content and heterogeneity in cultures of *Pseudomonas aeruginosa* 47T2 (NCIB 40044) grown in waste frying oil" *Antonie van Leeuwenhoek* **80:** 57-63

Yang S.T, Lo Y.M, Min D.B (1996) “Xanthan Gum Fermentation by *Xanthomonas campestris* immobilized in a Novel Centrifugal Fibrous-Bed Bioreactor” *Biotechnology Progress* **12** 630-637

Zhang W, Li Z.J, Agblevor F. A (2005) “Microbubble fermentation of recombinant *Pichia pastoris* for human serum albumin production” *Process Biochemistry* **40**:6 Pages 2073-2078.

Zhao H *et al* (2010) “High-gravity process intensification technology and application” *Chemical Engineering Journal* **156** 3 588-593